USE OF PECTIN FOR THE SPRAY DELIVERY OF MESENCHYMAL STROMAL CELLS FOR BRAIN INJURY

Amy Nash

May 2023
Thesis submitted to the University of Nottingham for the degree of Doctor of Philosophy

Abstract

Traumatic brain injury (TBI) occurs as a result of significant impact to the head causing damage to the brain tissue, such as that resulting from traffic collisions and falls, and can lead to long-term disability for affected patients. Current therapies for brain injury aim to limit further damage occurring via secondary injury pathways as a response to the initial trauma. Animal studies have shown improved neurological outcomes after injury following mesenchymal stromal cell (MSC) transplantation (Volkman, 2017) due to the immunomodulatory and pro-regenerative effects of the proteins and extracellular vesicles of the secretome (Pischiutta *et al.*, 2022). Successful delivery of these cells is limited by the delivery route. Cells delivered intravenously show poor migration to the site of injury, resulting in a large loss of therapeutic cells (Harting *et al.*, 2009). Therefore, it was hypothesised that spraying MSCs in a pectin solution would result in retained viability and phenotype of the cells, possibly offering a suitable method for local delivery of MSCs to TBI patients in the future.

Pectin is cross-linkable with calcium, enabling cells to be sprayed in solution. In this thesis, four grades of citrus pectin were selected for evaluation, each with differing degrees of methylation (DM) and amidation (DA). CU-701 and CU-L have 37% and 28% DM respectively and LM-102 and LM-104 have 19% and 20% DM, and 30% and 27% DA respectively. The mechanical and biocompatibility properties of each of these grades was assessed, including viscosity, gelation, and cytotoxicity testing. Each grade demonstrated a viscosity suitable for spraying at 1% w/v in 1xPBS pH 7.4 and gelation with calcium was still observed. Since all grades of pectin (at 1% w/v in 1xPBS pH 7.4) showed low cytotoxicity, all grades were progressed to cell spraying studies.

The mucosal atomisation device (MAD) syringe sprayer was selected for evaluation in the cell spraying experiments. The cell viability after spraying was assessed at a range of cell densities using the 3T3 mouse fibroblasts and the SH-SY5Y human neuroblastoma cell lines. Once viability was established, similar cell viability testing was carried out using primary human MSCs derived from the bone marrow of three separate donors, showing that high viability after spraying could be achieved at all cell densities tested. Studies then progressed to evaluate the viability and surface marker expression (CD90, CD105, CD73,

CD34, CD11b, CD19, CD45, and HLA-DR) by flow cytometry of the hMSCs after spraying in pectin solutions. High viability, comparable to the hMSC seeded by syringe in 1xPBS, was achieved for all pectin grades. The results of the surface marker expression analysis showed CU-701 was the only grade of pectin not to show a significant downregulation of CD90, CD105, and CD73 compared to the control, or significant upregulation of CD34, CD11b, CD19, CD45, and HLA-DR. As a result, CU-701 pectin was taken forward into preliminary differentiation studies and a differential gene analysis. No spontaneous differentiation of the hMSCs into cells of an osteogenic or adipogenic lineage was observed as a result of seeding in CU-701 pectin or spraying. Preliminary data indicated the osteogenic differentiation may be impaired for one of the three donors, however adipogenic differentiation was observed in all conditions tested. Further studies are required to test for chondrogenic differentiation, to further test the osteogenic differentiation potential, and to include the hMSCs from the third donor. Differential gene expression analysis of approximately 30,000 genes was then carried out using cells which had been syringed or spraying in either 1xPBS or CU-701 pectin. This indicated that the process of spraying had very little effect on gene expression, but that the CU-701 pectin and the different donors caused genes to be differentially expressed.

Using the SH-SY5Y cell line, *in vitro* models of oxidative stress and excitotoxicity were optimised and established. Pectin hydrogels were added to the damaged cells in culture, and the LM-102 and CU-701 pectin grades were selected for use in the co-culture model. Human MSCs were added to well inserts by syringe or spray in 1xPBS, LM-102, or CU-701 pectin to understand whether they influenced SH-SY5Y survival or proliferation after damage by glutamate or H_2O_2. No significant differences were observed, suggesting hMSCs may modulate repair following damage via alternative pathways.

Overall, this study has demonstrated that viable hMSCs can be sprayed in different grades of pectin using the MAD syringe sprayer. The CU-701 grade appears to be most suitable for use with hMSCs based on experiments carried out in this thesis. This provides key information for the future development of spraying hMSCs in pectin as a local delivery method for use in TBI.

COVID-19 Impact statement

The work in this thesis was impacted by the restrictions imposed as a result of the COVID-19 pandemic. Work began on this PhD project in May 2019. Progress was interrupted in October 2019 as the cell culture laboratories used by the regenerative medicine and cellular therapies (RMCT) division were moved to the new Biodiscovery Institute building. This move took longer than anticipated and cell culture work was halted until January 2020. In March 2020, all research buildings were closed. Upon reopening in August 2020, strict occupancy limits and restricted working were enforced. The occupancy limits in the laboratories meant fewer experiments could be undertaken, and training on equipment took much longer due to group size restrictions. Very limited office spaces were available, which severely hindered productivity without access to proper working environments and routines. These restrictions remained in place until summer 2021, however the hangover effects of the COVID-19 pandemic continued to affect research for much longer due to shortages in supply chains of many consumables, including plasticwares and cell culture media.

As a result of the restricted access to laboratories and equipment, the original aims of the project were adjusted due to the limited time left to complete experiments once the buildings were reopened. Initial aims had included progressing to *in vivo* studies to understand whether MSC delivery in pectin by spraying was a viable option, however focus was instead shifted to *in vitro* experiments to characterise the hMSCs after spraying and develop and *in vitro* model of TBI.

Acknowledgements

Firstly, I would like to thank my supervisors, Dr Maria Marlow, Dr Lisa White, and Prof. James Phillips. You have all helped to shape me as a researcher and kept me motivated through the toughest of times. Maria, thank you for all your guidance throughout my PhD. Your positivity and enthusiasm about science and my work kept me going in the most difficult periods. Your passionate approach to research never failed to lift my spirits. Lisa, thank you for your keen eye for detail and for never letting my standards slip. Your many questions have kept me on my toes and have improved my critical thinking skills. James, your wealth of experience has been invaluable throughout my PhD. Thank you for continuing to question me in such a way that made me feel like we were all on the same team. I knew that when I was stuck, I could rely on any of you for guidance, so thank you for being a great supervisory team.

A massive thank you to all those on the CDT in Advanced Therapeutics and Nanomedicines. To those who have already left, thank you for welcoming me into the CDT family. A special thank you to Dr Alice Brookes for keeping me going throughout so much of the PhD, but especially during the COVID-19 pandemic. You were a fantastic housemate and an excellent friend. To (soon to be Dr) Chloe Stewart, it takes a truly special kind of friend to agree to run 100km non-stop with me, thank you for being a fellow nutter. I am incredibly grateful to have met both of you through the CDT.

Thank you to everyone who has helped me out in the labs. Joshua Jones, thank you for keeping my cells alive and for all your help with the rheometer. You really are the King of Rheology. To Dr I-Ning Lee, thank you for your guidance with all things cells and for telling me straight if I was about to do something you thought could be done better. Fiona Smith, I have thoroughly enjoyed working on our side projects together. You have broadened my horizons and given me exciting other projects to work on. To Derek Hardie and Isobel Jobson, thank you for making B216 a brighter place to work. Cell culture was always more exciting when you were both around.

To James Mealing, thank you for pushing me to embark on the PhD journey when you could see I needed the next challenge. Thank you also for always

providing a home away from home when I needed a break. Thank you for always sounding interested in my work, and sometimes asking harder questions than my supervisory team! I appreciate everything you have done to help me reach submission day.

An enormous thank you to my partner Alex Abbott. You have been an absolute rock. You have been there for me in the toughest moments and reminded me why I am doing this. Thank you for your continued reassurance that I can reach the end, even when the end seemed so far away. Your support has been massively appreciated and I cannot wait to celebrate the end of this chapter with you.

Finally, to my Dad, there aren't enough words to thank you fully for everything you've done for me. You nurtured my curiosity in the world, taking time to answer my many questions. You've always believed in me and let me know that anything was achievable if I put my mind to it. No problem seemed too big to solve with your help and guidance. You always used to say, "if it were easy, everyone would do it" and "you can't enjoy the downhills without the uphill struggles"; the mental resilience you instilled in me has kept me going. Thank you for all your help in the workshop with the spray devices, it was an enjoyable escape from the labs. Thank you also for offering to help when the RNA extractions were failing, even though I'm fairly confident you aren't sure what RNA stands for! You have made me who I am today and I'm proud to have you as my Dad. Thank you.

Table of Contents

Abstract i

COVID-19 Impact statement iii

Acknowledgements iv

Table of Contents vi

List of figures xii

List of tables xiv

Abbreviations xvi

Chapter 1 Introduction 1

1.1. Traumatic brain injury 1

1.1.1. Cells of the brain 2

1.1.2. Primary injury 3

1.1.3. Secondary injury 5

1.1.4. Current therapies 8

1.2. Developing novel TBI treatments 10

1.2.1. Pharmacological approaches 10

1.2.2. Cell therapies 11

1.3. TBI models 14

1.3.1. *In vitro* models 14

1.3.2. Injury types 19

1.3.3. Animal models 20

1.4. Cell delivery 24

1.5. Materials for cell delivery 27

1.6. Pectin 28

1.6.1. Gelation 32

1.6.2. Past uses 34

1.6.3. Tissue engineering 34

1.7. Thesis hypothesis 36
1.8. Thesis aims and objectives 37
Chapter 2 Materials and methods 38
2.1. Materials 38
2.2. Pectin purification 40
2.2.1. Bicinchoninic acid (BCA) protein assay 40
2.2.2. Fourier-transform infrared spectroscopy 41
2.3. Pectin rheology 42
2.3.1. Qualitative pectin gelation screen 42
2.3.2. Viscosity 43
2.3.3. Amplitude sweep 43
2.3.4. Young's modulus measurement 43
2.4. Cell culture and passaging 44
2.4.1. NIH 3T3 mouse fibroblasts 44
2.4.2. SH-SY5Y human neuroblastoma cells 44
2.4.3. Human mesenchymal stem cells 44
2.5. Cell counting and health/viability testing 46
2.5.1. Cell counting 46
2.5.2. PrestoBlue metabolic activity assay 46
2.5.3. Lactate dehydrogenase (LDH) assay 47
2.5.4. Live/Dead staining 48
2.6. Imaging and image analysis using FIJI 48
2.7. Cytotoxicity testing 49
2.7.1. Extraction test 49
2.7.2. Direct test 50
2.8. Cell spraying 50
2.8.1. Cells in media/PBS 50

2.8.2. Cells in pectin 51
2.9. Cell retention within spray device 51
2.10. Flow cytometry 52
2.11. hMSC differentiation 56
2.12. Transcriptome analysis 58
2.12.1. Sample preparation 58
2.12.2. RNA extraction 58
2.12.3. RNA library preparation and sequencing 59
2.13. SH-SY5Y damage model optimisation – 96-well plate 61
2.13.1. Excitotoxicity model 61
2.13.2. Oxidative stress model 61
2.14. SH-SY5Y damage model optimisation – 24-well plate 62
2.14.1. Excitotoxicity model 62
2.14.2. Oxidative stress model 62
2.15. SH-SY5Y damage model – effect of pectin gels alone 63
2.16. SH-SY5Y damage model – hMSC co-culture 63
2.17. Statistical testing 66
Chapter 3 Pectin characterisation 67
3.1. Introduction 67
3.1.1. Extraction 67
3.1.2. Pectin Purification 68
3.1.3. Pectin gelation 69
3.1.4. Pectin functionalisation 69
3.1.5. Pectin viscosity & pectin gel mechanical strength – Rheological measurements 70
3.1.6. Cytotoxicity testing 73
3.2. Hypothesis, aims, and objectives 75

3.2.1. Hypothesis 75
3.2.2. Aims 75
3.2.3. Objectives 75
3.3. Method design 76
3.3.1. Calculations for viscosity testing 76
3.3.2. Cytotoxicity testing 77
3.4. Results 78
3.4.1. Purification – Protein content of pectin samples 78
3.4.2. Purification – FTIR spectra of pectin samples 79
3.4.3. Gelation screen – Pipetted pectin solutions 80
3.4.4. Gelation screen – Sprayed pectin solutions 82
3.4.5. Rheology – Viscosity of pectin solutions 84
3.4.6. Rheology – Amplitude sweep of pectin gels 86
3.4.7. Young's modulus of pectin gels 87
3.4.8. Cytotoxicity testing – Pectin gels in direct contact with SH-SY5Y cells 88
3.4.9. Cytotoxicity testing – Pectin gel conditioned media on SH-SY5Y cells 90
3.5. Discussion 92
3.5.1. Purification 92
3.5.2. Characterisation of pectin solutions and gelation 93
3.6. Conclusions 97
Chapter 4 Cell spraying 99
4.1. Introduction 99
4.1.1. Spray delivery of cells 99
4.1.2. Spraying of MSCs 101
4.1.3. Spray delivery materials 102
4.1.4. Properties of MSCs 104

4.1.5. MSC secretome 105
4.1.6. Transcriptome analysis 107
4.2. Hypothesis, aims, and objectives 111
4.2.1. Hypothesis: 111
4.2.2. Aims: 111
4.2.3. Objectives: 111
4.3. Method design 112
4.3.1. Spray device 112
4.3.2. Cell spraying 113
4.4. Results 116
4.4.1. Cell retention within spray device 116
4.4.2. Metabolic activity of 3T3 mouse fibroblasts after spraying 117
4.4.3. Metabolic activity and LDH release from SH-SY5Y cells after spraying 118
4.4.4. Viability of hMSCs after spraying 120
4.4.5. hMSC viability after spraying in pectin 122
4.4.6. Flow cytometry analysis on hMSCs after spray or syringe seeding 124
4.4.7. Differentiation of hMSCs 133
4.4.8. Differential gene expression of hMSCs 135
4.5. Discussion 143
4.6. Future work 150
4.6.1. Spray device development 150
4.7. Conclusions 154
Chapter 5 *In vitro* TBI modelling 156
5.1. Introduction 156
5.2. Hypothesis, aims, and objectives 160
5.2.1. Hypothesis: 160

5.2.2. Aims 160
5.2.3. Objectives 160
5.3. Method design 161
5.4. Results 163
5.4.1. SH-SY5Y damage model development 163
5.4.2. SH-SY5Y damage model development in 24-well tissue culture plates 165
5.4.3. Pectin hydrogel addition to SH-SY5Y damage models 167
5.4.4. hMSC in PBS/pectin co-culture SH-SY5Y damage models 169
5.5. Discussion 171
5.6. Conclusions 176
Chapter 6 Discussion, future work, and conclusions 177
6.1. Discussion 177
6.1.1. Pectin characterisation 178
6.1.2. Optimisation of cell spraying in pectin 179
6.1.3. In vitro modelling of TBI 181
6.1.4. Summary 182
6.2. Future work 183
6.3. Conclusions 185
References 186

List of figures

Figure 1.1 – Major structures found within the brain 1
Figure 1.2 – Neuron structure, including the synapse 2
Figure 1.3 – Meningeal layers surrounding the brain in humans 4
Figure 1.4 – The secondary injury cascades in TBI 6
Figure 1.5 – The structure of rhamnogalacturonan-I, homogalacturonan and rhamnogalacturonan-II 30
Figure 1.6 – Galacturonic acid structure of pectin..... 31
Figure 1.7 – Schematic of the 'egg box' structure of LMP 32
Figure 1.8 – Schematic of the β-elimination reaction..... 33
Figure 2.1 – The reduction of resazurin to resorufin – PrestoBlue..... 47
Figure 2.2 – Schematic of the reaction taking place in the presence of LDH . 48
Figure 2.3 – The MAD spray device 50
Figure 2.4 – Flow cytometry Kaluza analysis gating 55
Figure 2.5 – Schematic showing the co-culture damage models – 1 hour 64
Figure 2.6 – Schematic showing the co-culture damage models – 24 hours... 64
Figure 3.1 – Schematic showing the pectin extraction process 68
Figure 3.2 – Schematic showing the amplitude sweep tests..... 71
Figure 3.3 – Schematic showing the Young's modulus test..... 72
Figure 3.4 – Protein content of pectin samples..... 78
Figure 3.5 – FTIR spectra of the different grades of pectin powder..... 79
Figure 3.6 – Strength of different grades of pipetted pectin gels 80
Figure 3.7 – Strength of different grades of sprayed pectin gels..... 82
Figure 3.8 – Viscosity of 1% w/v purified pectin solutions 84
Figure 3.9 – Storage (G') and loss (G'') modulus of purified pectin 86
Figure 3.10 – Linear region of the stress-strain curves..... 87
Figure 3.11 – Direct cytotoxicity testing of purified pectin hydrogels..... 88
Figure 3.12 – Elution cytotoxicity testing of purified pectin hydrogels..... 90
Figure 4.1 – Schematics of three different spray nozzles 99
Figure 4.2 – Schematic showingRNA-seq library preparation..... 109
Figure 4.3 – The MAD sprayer..... 112
Figure 4.4 – Images of the turbine labelled "FIG 22" 113
Figure 4.5 – SH-SY5Y cell count..... 116

Figure 4.6 – Short-term assessment of the effect of spraying 3T3 cells..... 117
Figure 4.7 – Short-term assessment of the effect of sprayingSH-SY5Ys 118
Figure 4.8 – Short-term assessment of the effect of spraying hMSCs 120
Figure 4.9 – Viability of hMSCs sprayed or syringed in pectin or 1xPBS ... 122
Figure 4.10 – Graphical representation of flow cytometry data 125
Figure 4.11 – CD90 FITC flow cytometry overlay analysis 127
Figure 4.12 – CD105 PerCP-Cy5.5™ flow cytometry overlay analysis..... 128
Figure 4.13 – CD73 APC flow cytometry overlay analysis 129
Figure 4.14 – PE CD35, CD11b, CD19, CD45, and HLA-DR flow cytometry overlay analysis 130
Figure 4.15 – CD105 PerCP-Cy5.5™ flow cytometry overlay with isotype 131
Figure 4.16 – Principal component analysis RNA-seq..... 136
Figure 4.17 – Three bottle pump spray actuators 150
Figure 4.18 – The AptarPharma standard actuator attached to a syringe for spraying..... 151
Figure 4.19 – Spray pattern of water and food dye, and pectin..... 151
Figure 4.20 – Syringe device design..... 152
Figure 4.21 – The V-notch modified device from Figure 4.20..... 153
Figure 4.22 – Possible design option to optimise pectin and cell spraying... 153
Figure 5.1 – 96-well plate damage model optimisation..... 163
Figure 5.2 – 24-well plate damage model optimisation..... 165
Figure 5.3 – Pectin hydrogel on damage models..... 167
Figure 5.4 – Damage model co-cultures..... 169

List of tables

Table 1.1 – Cell lines used to model TBI 16
Table 1.2 – A summary of the commonly used animal models of TBI 22
Table 1.3 – Summary of the applications of pectin over time 29
Table 2.1 – Materials and equipment, and the supplier 38
Table 2.2 – Supplier for each grade of pectin used 40
Table 2.3 – Dilution scheme for BCA assay microplate protocol 41
Table 2.4 – Calcium chloride concentrations in solution and in pectin gels ... 42
Table 2.5 – Donor number, age, and sex of donors of hMSCs 45
Table 2.6 – The antibody contents in each vialfor flow cytometry 53
Table 2.7 – Cell samples and antibody added for flow cytometry 53
Table 2.8 – Samples prepared and added to well inserts for the damage model co-culture experiment 65
Table 3.1 – Values when calculating the shear stress on a fluid when expelling it from the MAD sprayer 77
Table 3.2 – Summary of the LVER limit and the G′ value at 1% strain 86
Table 3.3 – Young's modulus of purified pectin gels 87
Table 4.1 – Spray device name and nozzle category of devices studied for use in cell delivery 100
Table 4.2 – Summary of a selection of the devices, cell types, carrier material for spraying 103
Table 4.3 – The percentage of positive cells and the SD – flow cytometry .. 124
Table 4.4 – Differentiation images of hMSCs 133
Table 4.5 – Differential gene expression analysis summary 135
Table 4.6 – Top 20 up and down regulated genes comparing PBS spray versus PBS syringe 137
Table 4.7 – Top 20 up and down regulated genes comparing CU-701 spray versus CU-701 syringe 138
Table 4.8 – Top 20 up and down regulated genes comparing CU-701 syringe versus PBS syringe 139
Table 4.9 – Top 20 up and down regulated genes comparing CU-701 spray versus PBS spray 140

Table 4.10 – Log_2 fold change (LFC) and adjusted P-value (Padj) of selected genes in the listed contrasts 141
Table 5.1 – Glutamate model conditions as reported in current literature..... 158
Table 5.2 – H_2O_2 model conditions as reported in current literature..... 158

Abbreviations

µg	Microgram
µL	Microlitre
µM	Micromolar
µm	Micrometre
3T3	Mouse fibroblast cell line
AMPA	α-amino-3-hydroxyl-5-methyl-4-isoxazole-propionate
ANOVA	Analysis of variance
APC	Allophycocyanin
ATP	Adenosine triphosphate
ATR	Attenuated total reflection
BBB	Blood brain barrier
BCA	Bicinchoninic acid
BDNF	Brain derived neurotrophic factor
BSA	Bovine serum albumin
CCI	Controlled cortical impact
CD	Cluster of differentiation
CNS	Central nervous system
CSF	Cerebral spinal fluid
CT	Computerised tomography
DA	Degree of amidation
DAI	Diffuse axonal injury
DAMP	Damage-associated molecular pattern
DC	Decompressive craniotomy
DM	Degree of methylation
DMEM	Dulbecco's modified eagle medium
DMSO	Dimethyl sulphoxide
DNA	Deoxyribonucleic acid
ECM	Extracellular matrix
EDTA	Ethylenediaminetetraacetic acid
EU	Endotoxin unit
FAO	Food and agriculture organisation
FBS	Foetal bovine serum
FDA	Food and drug administration
FITC	Fluorescein isothiocyanate
FPI	Fluid percussion injury
FSC	Forward scatter
FTIR	Fourier-transform infrared spectroscopy
GCS	Glasgow coma scale
GDNF	Glial cell line-derived neurotrophic factor
GFAP	Glial fibrillary acidic protein
HG	Homogalacturonan
HGF	Hepatocyte growth factor
HLA-DR	Human Leukocyte Antigen – DR isotype
HMP	High methyl pectin
ICP	Intracranial pressure
IMS	Industrially methylated spirits

ISCT	International society for cell therapies
ISO	International standards organisation
LAL	Litmus amoeba lysate
LDH	Lactate dehydrogenase
LMP	Low methyl pectin
LPS	Lipopolysaccharide
LVER	Linear viscoelastic range
MAD	Mucosal atomisation device
MEM	Minimum essential media
mg	Milligrams
mL	Millilitre
mM	Millimolar
MSC	Mesenchymal stromal cell
MTT	3-(4,5-dimethylthiazol-2-yl)-2,5-diphenyltetrazolium bromide
ng	Nanogram
NGF	Neural growth factor
nm	Nanometer
NMDA	N-methyl-D-aspartate
NSC	Neural stem cell
PBBI	Penetrating ballistic brain injury
PBS	Phosphate buffered saline
PCR	Polymerase chain reaction
PE	Phycoerythrin
PEG	Poly-ethylene glycol
PerCP	Peridinin-Chlorophyll-protein
PSC	Pluripotent stem cell
RFU	Relative fluorescence units
RG	Rhamnogalacturonan
RGD	Arginylglycylaspartic acid
RNA	Ribonucleic acid
ROS	Reactive oxygen species
SH-SY5Y	Human neuroblastoma cell line
SSC	Side scatter
TBI	Traumatic brain injury
TE	Trypsin/EDTA
TNF-α	Tumour necrosis factor-α
VEGF	Vascular endothelial growth factor
w/v	Weight/volume
WHO	World health organisation

Chapter 1 Introduction

1.1. Traumatic brain injury

Traumatic brain injuries (TBI) occur as a result of impact to the head which affects the normal function of the brain. The brain is a highly interconnected organ which controls everything in the body from unconscious, essential functions such as digestion, to movement and cognition. The severity of injury and recovery by the patient are affected by many different factors, including the mechanism of injury, immediate care following the injury, and the environment in which the patient recovers (Ponsford *et al.*, 2000, Prins *et al.*, 2013). The different mechanisms of injury can lead to different structures of the brain being affected, which are shown in Figure 1.1.

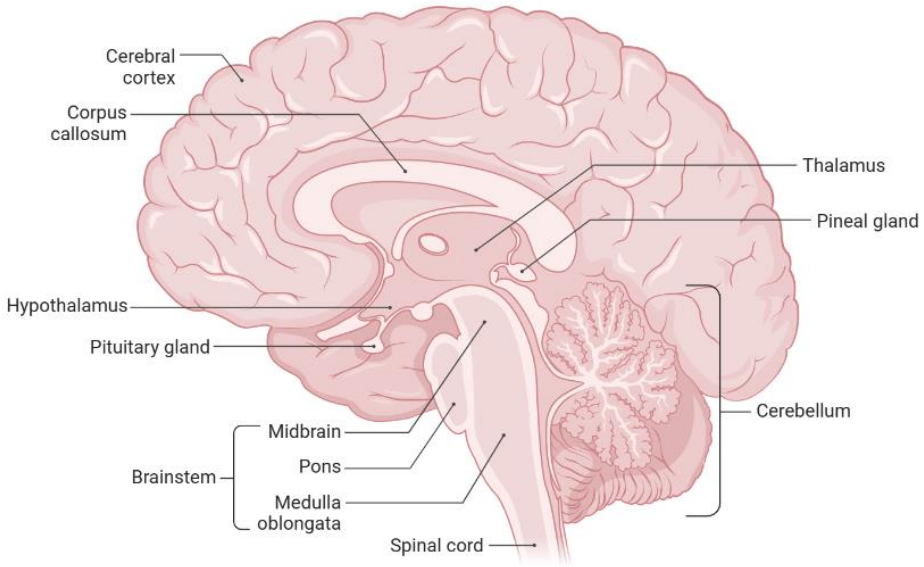


Figure 1.1 – Major structures found within the brain. Image adapted from a BioRender template.

The brain functions to coordinate movement, reflexes, essential body functions, conscious thought, learning, emotion, and language. The cerebral cortex is the largest structure within the brain and is responsible for many of the conscious functions (thought, emotion, learning, etc.) (Javed, 2022). Nerves from the spinal cord run into the brain via the brainstem. The pituitary and pineal gland act in conjunction with the hypothalamus to regulate homeostasis within the body. The

cerebellum functions to refine signals for movements, therefore aiding with balance and fine motor control.

1.1.1. Cells of the brain

There are four main cell types within the brain: neuron, microglia, oligodendrocyte, and astrocyte.

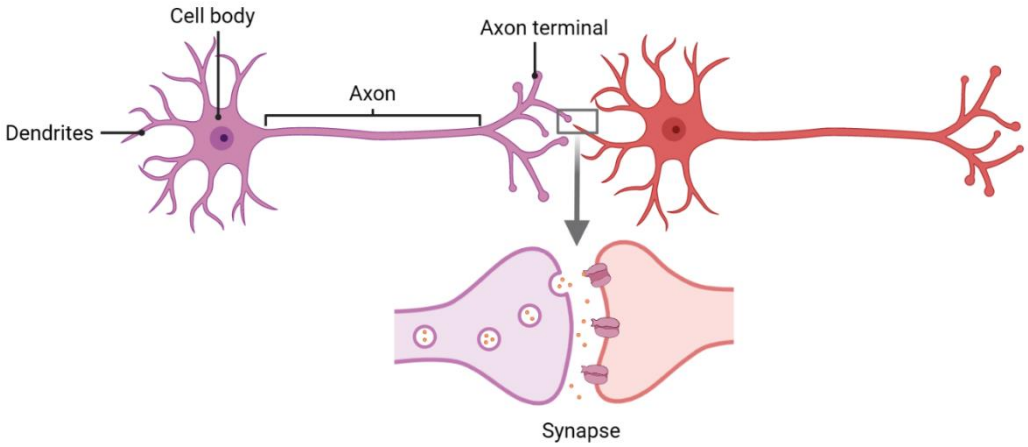


Figure 1.2 – Neuron structure, including the synapse. The left neuron (pink) passes information to the right neuron (red) via the synapse between the axon terminal of the left, and the dendrite of the right. The process of neurotransmitter release is highlighted in the bottom image. Figure made in BioRender.

Shown in Figure 1.2, neurons have a cell body containing the nucleus, an axon, and dendrites. The cell body carries out the metabolic functions within the cell. The axon carries electrical impulses as action potentials, and the dendrites receive information. When the action potential reaches the end of an axon, where the synapse is found, the electrical impulse cannot bridge the gap. Here, neurotransmitters are released to pass the signal on, depicted in Figure 1.2. The neurotransmitters are released in vesicles via exocytosis, triggered by local increases in Ca^{2+} concentration in response to the action potential. These neurotransmitters then bridge the gap and bind to receptors on the cell membrane of the neighbouring neuron (Fon *et al.*, 2001).

The central nervous system (CNS) is broadly broken down into grey and white matter, named based on their appearance. The grey matter has a higher abundance of neural cell bodies, dendrites, and synapses, and tends to be located more superficially (closer to the skull or internal ventricles). The white matter

has a higher proportion of axons and myelinating cells and tends to be found in deeper regions of the brain (Köhler *et al.*, 2021).

Microglia are essentially the immune cells of the brain. They use fine filipodia to sense the microenvironment and detect damage or infection in the CNS. Microglia then act as phagocytes to clear dead cells and debris (Jäkel *et al.*, 2017). Microglia also have functions in neurogenesis and the assembly of neural networks. They help to regulate synaptic plasticity, phagocytosing unneeded dendrites and synapses (Colonna, 2017). Microglia can also respond to protect neurons from N-methyl-D-aspartate (NMDA)-induced excitotoxicity (Colonna, 2017).

Oligodendrocytes are the myelinating cells of the CNS. They wrap around the axons of neurons to insulate them, speeding up impulse propagation. Oligodendrocytes also offer metabolic support to the axons of neurons (Bradl and Lassmann, 2010, Moore *et al.*, 2020).

Astrocytes are the most abundant cell type found in the brain. They are closely associated with synapses and the blood-brain barrier (BBB) to regulate permeability, and function to maintain extracellular concentrations of ions, water, neurotransmitters, and other small molecules (Siracusa *et al.*, 2019). In response to injury, astrocytes become reactive, containing the injury through the formation of a glial scar. A feature of neuroinflammation is astrocyte swelling, associated with their ion homeostasis function (Kim *et al.*, 2019).

1.1.2. Primary injury

TBI is broadly broken down into two stages: primary and secondary. Primary injury describes the initial impact, such as a blunt force, penetrating, or acceleration/deceleration injury. The injury can directly cause tearing of blood vessels, damage to the neurons, microglia, astrocytes, and oligodendrocytes, and can cause the deformation of tissue. This results in necrotic cell death and lesions within the brain, with cellular contents and debris released into the brain tissue (Kaur and Sharma, 2018). Damage to the brain tissue can lead to loss of functions and connectivity between neurons, resulting in wide ranging symptoms such as memory loss, loss of movement, seizures, and chronic neurodegenerative disorders such as early-onset Alzheimer’s disease.

After injury occurs, TBI can be classed as mild, moderate, or severe, and is often scored using the Glasgow Coma Scale (GCS). This assesses visual, verbal, and motor responses to stimuli to generate a score between 3-15, with higher numbers equating to a less severe injury (Jain and Iverson, 2020). Each case of TBI is unique due to variation in the mechanism of injury, force, site of impact, patient's genetics and age, and the quality of the immediate care given (Prins *et al.*, 2013).

Primary injury can result in a range of injuries to the brain. Figure 1.3 shows the meningeal layers surrounding the brain to highlight the location of the different intracranial haematomas briefly summarised below.

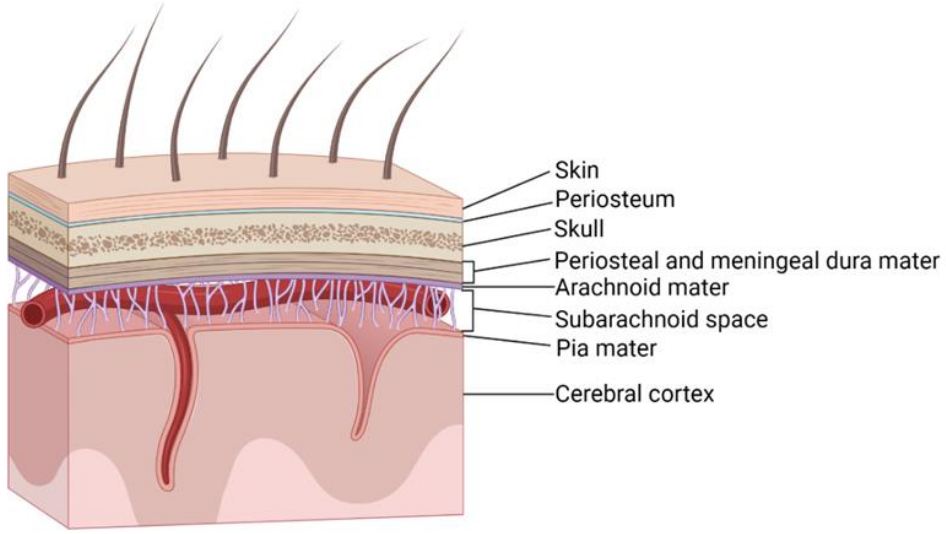


Figure 1.3 – Meningeal layers surrounding the brain in humans.

Intracranial haematomas are bleeding in or around the brain and can be sub-categorised based on the location in relation to the meningeal layers shown in Figure 1.3. They result from damage to blood vessels and can cause an increase in pressure within the skull, leading to further, and potentially fatal, damage to the brain tissue. Epidural haematomas are bleeding between the meningeal dura mater and the skull. These are commonly caused by damage to the middle meningeal artery resulting from fractures to the temporal bone (Kaur and Sharma, 2018). These tend to have a rapid onset due to arterial bleeding but are less common. Subdural haematomas are bleeds between the dura and the arachnoid mater. These results from damage to veins in the subdural space. They are slower to form but tend to be more serious and have a higher mortality rate (Parikh *et al.*, 2007). Intraparenchymal haemorrhage describes bleeding from a

region in the brain as a result of damage to blood vessels. These commonly have a non-traumatic cause, but can be caused by a penetrating injury, such as a gunshot wound (Tenny, 2022).

Skull fractures can be depressed or non-depressed and indicate that significant force was involved in causing the injury. Non-depressed fractures are lower risk, whereas depressed fractures have a high chance of tearing the dura and damaging the cerebral cortex (Parikh *et al.*, 2007). They are associated with a high risk of causing haematomas, especially when the fracture occurs to the temporal bone and damages the middle meningeal artery, causing epidural haematomas (Parikh *et al.*, 2007).

Contusions are areas of bleeding within the brain tissue and are often associated with a force causing the movement of the brain within the skull (Adatia *et al.*, 2021). Contusions can be classed as coup, contrecoup, or coup-contrecoup injuries. Coup lesions occur at the impact site, commonly when the head is stationary, and the object is moving. Contrecoup lesions occur distal to the impact site, commonly when the head is moving and hits a stationary object. Coup-contrecoup lesions have damage sites both where the impact occurred and distal to it (El Sayed *et al.*, 2008).

Diffuse axonal injury (DAI) describes damage to axonal fibres resulting from shear stresses when the brain accelerates and decelerates. DAI is commonly seen in moderate to severe closed-head injuries (without penetration from an object or skull fracture) (Frati *et al.*, 2017). Historically, this was classed as a very severe form of injury as imaging would only pick up severe cases. However, advances in imaging have demonstrated this form of injury is present in mild TBI such as concussion, like those commonly seen in contact sport athletes (Laskowitz and Grant, 2016). As the axons are essential for carrying electrical impulses to neighbouring neurons or other effectors, DAI can affect their ability to relay information within the brain.

1.1.3. Secondary injury

The secondary injury follows within minutes of the primary, and can continue to affect patients decades later with the onset of Alzheimer's disease and other forms of dementia (Wilson *et al.*, 2017).

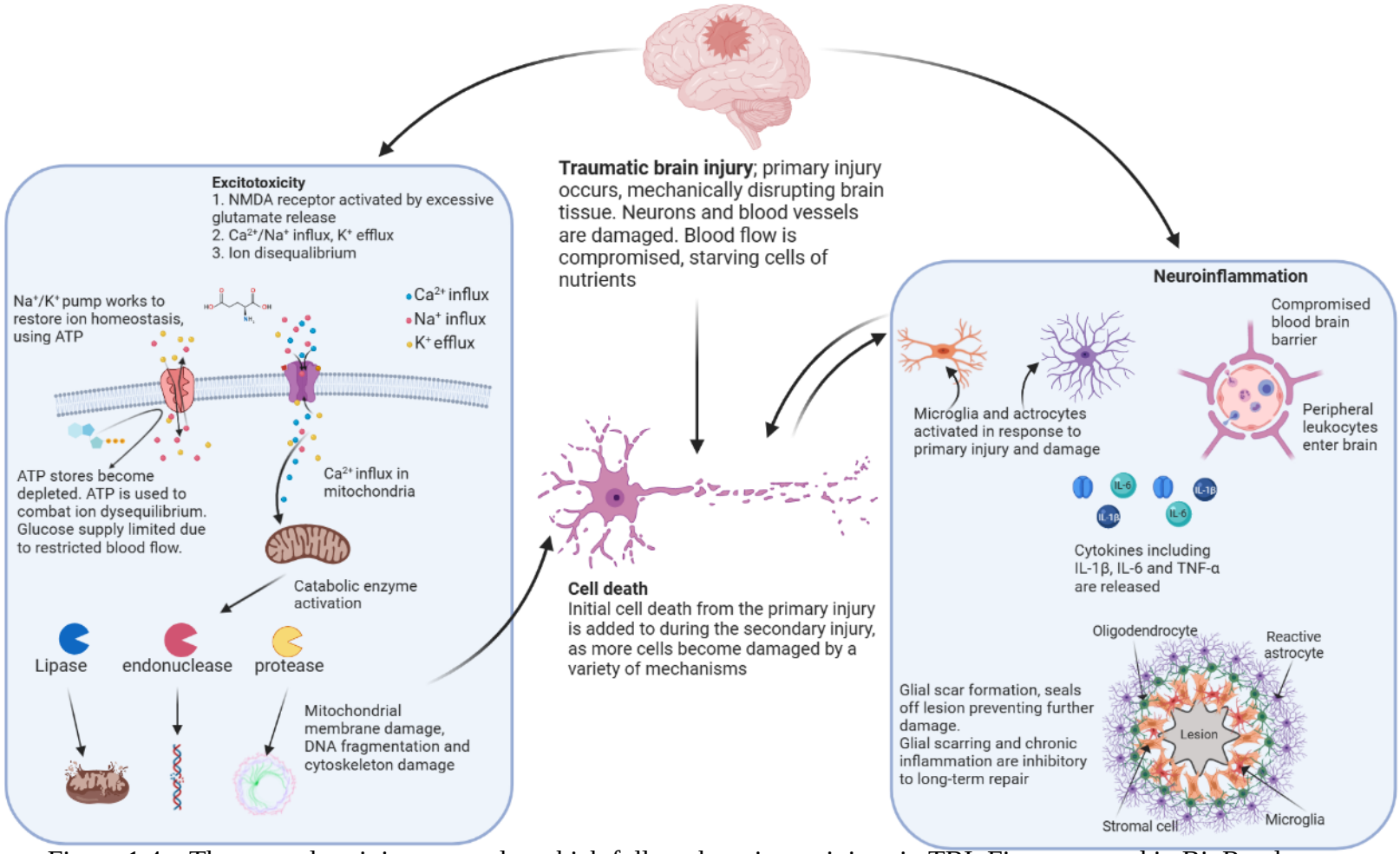


Figure 1.4 – The secondary injury cascades which follow the primary injury in TBI. Figure created in BioRender.

Many of the secondary injury pathways are interlinked, shown in Figure 1.4. When the primary injury occurs, the cell membranes are stretched, leading to a flux of ions, including K^+, Na^+, and Ca^{2+} (Pearn *et al.*, 2017). This ionic imbalance causes an osmotic imbalance, which can lead to water retention in the brain, oedema formation, and an increase in intracranial pressure (ICP) causing further damage (Werner, 2007). The Na^+/K^+ ATPase pumps work to restore the balance of K^+ and Na^+, consuming large amounts of the cellular ATP (Kaur and Sharma, 2018). The dysregulation of Ca^{2+} can impact the mitochondria, causing swelling, loss of function, and can trigger oxidative stress and apoptotic pathways to contribute to further cell death (Greve *et al.*, 2009).

Excitotoxicity is a key feature of secondary injury, caused by high glutamate levels following the initial injury, which can remain so for up to 48 hours (Ladak *et al.*, 2019). This can lead to excitotoxicity due to prolonged activation of NMDA or α-amino-3-hydroxy-5-methyl-4-isoxazolepropionic acid (AMPA) receptors, resulting in an influx of Ca^{2+}, further exacerbating the effects on the mitochondria (Greve *et al.*, 2009).

Glucose metabolism is impaired following TBI, with a transient initial period of rapid glucose uptake, suggested to be due to the demand of the ion transporters working to restore the ionic imbalance, followed by a period of glucose metabolism depression (Prins *et al.*, 2013). Following TBI, more glucose is used anaerobically, and the utilisation of lactate as a metabolic substrate also increases (Jalloh *et al.*, 2015). Ultimately, if the metabolism within cells cannot match the energy demands, cell death can occur as a result of this impairment.

Another consequence of impaired metabolism after injury is an increase in the production of reactive oxygen species (ROS) such as superoxide (O_2^-), hydrogen peroxide (H_2O_2), and hydroxyl radicals (•OH), in the brain (Fesharaki-Zadeh, 2022). ROS are also a consequence of neuroinflammation following injury, and can react with lipids, nucleic acids, and proteins. This can lead to membrane damage, including the mitochondrial membrane, as well as protein inactivation, including ion channels. These all lead to further cell injury and death (Lozano *et al.*, 2017).

The intermediate phase of the secondary injury includes responses from the immune system. Resident microglia and astrocytes become activated and reactive. Due to the primary injury and cell membrane damage, the BBB becomes compromised, allowing for the recruitment of peripheral leukocytes (Lozano *et al.*, 2017). An initial immune response is essential in the early phases of recovery to remove cellular debris and contain damaged areas (Kim *et al.*, 2019). Part of this response is known as glial scarring, thought to serve as a protective mechanism to contain injury and prevent the damage of surrounding tissues due to the presence of the lesion. Longer term however, this mechanism prevents the regeneration of axons, remyelination of cells, and integration of new neurons. Chronic inflammation contributes to a lack of regeneration and restoration of neural pathways, and has been linked to the development of neurodegenerative diseases long-term (Xiong *et al.*, 2018b).

1.1.4. Current therapies

Current therapies are unable to repair damage caused by the primary injury, and instead aim to prevent further damage from occurring. If damage to blood vessels has occurred, bleeding or oedema can cause the ICP to increase (Namjoshi *et al.*, 2013). Brain tissue cannot be compressed, and the skull cannot stretch to accommodate increases in pressure, so this can rapidly cause more damage for the patient (Galgano *et al.*, 2017). ICP can be monitored invasively, by inserting pressure sensors directly into the intracranial space. This can be carried out in a few different ways, most commonly in either the intraventricular space to measure the fluid pressure, or by using an intraparenchymal sensor (Zhang *et al.*, 2017).

Medical management of increasing ICP involves elevating the head, delivering hypertonic saline to draw water away from the brain, or delivering mannitol to reduce blood viscosity and create an osmolar gradient similar to the mechanisms of saline (Berger Pelletier *et al.*, 2014, Galgano *et al.*, 2017). In severe cases of TBI, breathing can be impaired so the patient may be placed into an induced coma to ensure continuous breathing. This also reduces the metabolic demand from the brain, reducing the impact of impaired metabolism seen in the secondary injury pathway (Galgano *et al.*, 2017). However, poor airway management during the period of induced coma can increase the injury and lead

to a worse outcome for the patient. Hypoventilation results in an accumulation of CO_2 and an increase in ICP, whilst hyperventilation increases the risk of vasoconstriction in the brain (Dash and Chavali, 2018). A slight hyperventilation is favourable when managing the airway.

Hypothermic cooling of patients with TBI has been used as a treatment, working on the hypothesis that cooling patients will decrease the ICP, reduce the metabolic demand on the brain, and reduce the inflammation (Khellaf *et al.*, 2019). However, clinical trials comparing this treatment to no cooling have often shown little long-term benefits, with some showing a worse outcome resulting in early termination of trials (Andrews *et al.*, 2015).

There are some pharmacological treatments available to patients to manage the symptoms post-TBI. Anti-epileptic medication can be given to manage seizures, which are common following severe TBI (Wat *et al.*, 2019). An altered mental state is often reported in patients after suffering a TBI, therefore, to treat the symptoms of depression and lack of alertness, anti-depressant and stimulant medication can be given (Robert, 2020).

Some patients will require surgical interventions during their TBI care. When an epidural haematoma is detected on a CT scan and measured to be >30 cm^3 it will require surgical evacuation (Li *et al.*, 2010b). Similarly, if a subdural haematoma is detected with >10 mm thickness with a midline shift >5 mm, surgical evacuation will be carried out (Bullock *et al.*, 2006). These often require the removal of a bone flap to gain access to the haematoma for removal, which will then be replaced upon completion of the surgery.

Patients with high ICP due to diffuse brain swelling which cannot be managed medically may require a decompressive craniotomy (DC). The procedure involves the removal of a bone flap to allow more space for the swollen brain. The bone flap may not be immediately replaced, in which case the patient will require a secondary surgery once the swelling has subsided (Adams *et al.*, 2016). This is a lifesaving surgery which prevents herniation of the brainstem, however patients who have received a DC show poorer recovery and increased disability long-term (Dash and Chavali, 2018). Studies are often retrospective due to the difficulty in setting up randomised trials to understand the effects of DC, and the

outcome of that particular study is potentially due to a high severity injury causing the requirement of a DC.

In TBI with a skull fracture, surgery may be required to repair and realign the damaged bones. These are carried out to reduce the risk of infection, prevent increases in ICP, and to prevent longer-term cosmetic problems (Adams *et al.*, 2016). Many of these surgeries described lead to the exposure of the brain, which presents an opportunity to locally deliver additive therapies, overcoming some of the migration issues presenting when using alternative delivery methods.

1.2. Developing novel TBI treatments

TBI can leave patients with long term disability and symptoms, with an increased risk of neurodegenerative disorders later in life. Even if TBI sustained earlier in life was only classed as mild, repeated injury such as that seen in American football, rugby, or other contact sports, has been linked to the onset of neurodegenerative diseases (Wilson *et al.*, 2017). As a result, there is ongoing research to find more effective treatments for preventing further secondary injury from occurring, as well as treatments that are neurorestorative.

1.2.1. Pharmacological approaches

Neuroinflammation is linked to a lack of regeneration following TBI, which is associated with function, memory, and attention deficits in patients (Pearn *et al.*, 2017). Many anti-inflammatory drugs have been evaluated in pre-clinical animal models and shown promise, but translation to humans is poor with detrimental effects often shown (Crupi *et al.*, 2020). Minocycline is an example; in animal TBI models it has been shown to reduce microglial activation and improve recovery, however it has been shown to be detrimental with chronic dosing in clinical trials (Celorrio *et al.*, 2022). Similarly, corticosteroids and progesterone have shown promise in pre-clinical animal models of TBI, which has not translated to positive outcomes in clinical trials (Khellaf *et al.*, 2019).

As calcium is linked to many detrimental effects seen in secondary injury, many different methods of either mopping up excess intracellular Ca^{2+} or blocking transport channels have been evaluated in animal models. These include nimodipine, ziconotide and S100B protein (Galgano *et al.*, 2017). NMDA receptor antagonists such as amantadine have also been investigated to limit

excitotoxicity (Galgano *et al.,* 2017). Again, promising initial results led to clinical trials, however no positive outcomes were recorded in human TBI patients (Ghalaenovi *et al.*, 2018).

1.2.2. Cell therapies

Due to their ability to interact with damaged tissues and secrete trophic factors to aid in repair in response to stimuli (Wei *et al.*, 2013), cell therapies may have advantages over pharmacological approaches. Different strategies to investigate cell therapy for TBI have been researched over the years and are summarised in the following sections.

Pluripotent stem cells, including embryonic and induced pluripotent stem cells, are able to differentiate into any somatic cell type. Therapeutically, these offer the most potential to integrate into the damaged tissue and replace lost cells. Efficacy has been demonstrated in neurological damage, but these have been overshadowed by excessive growth, incomplete differentiation, and tumour formation in some cases (Boltze, 2015). The unlimited proliferative potential of pluripotent stem cells is highly useful when division is tightly controlled and directed, as it is during embryonic development, but can be dangerous with tumorigenic potential when cells are delivered to an adult (Yamanaka, 2020).

Neural stem cells (NSC) are found endogenously in the brain in the subventricular zones and dentate gyrus (Zhang *et al.*, 2016). The response to trauma is insufficient for significant repair, despite their potential to differentiate into a variety of brain cell types (Kim, 2009). Efficacy of NSC transplant has been shown in rodent models, where restoration of cognition was demonstrated, however there was no change in lesion size. This suggests that the therapeutic effect is due to the secretion of factors, rather than the replacement of lost cells (Haus *et al.*, 2016). Similarly, efficacy was shown in another rat TBI model where they demonstrated neuroplasticity was due to brain-derived neurotrophic factor (BDNF) from NSCs (Xiong *et al.*, 2018a).

Mesenchymal stromal cells (MSC) are found endogenously in several niches. In adults they can be obtained from the bone marrow, adipose tissue, dental tissue, peripheral blood, salivary glands, and skin, offering an autologous source for

transplantation. MSCs can also be obtained from amniotic tissues, the placenta, the umbilical cord, and Wharton's jelly (Ullah *et al.*, 2015b).

To be classed as a MSC there are a set of criteria the MSCs must meet. According to the International Society for Cellular Therapy (ISCT) Mesenchymal and Tissue Stem Cell Committee, cells must be plastic-adherent, express CD90, CD105, and CD73 surface markers, and not express CD45, CD34, CD14, CD11b, CD79α, CD19, or HLA-DR, and be able to differentiate into osteogenic, adipogenic, and chondrogenic cells (Dominici *et al.*, 2006). MSCs have received attention for their potential in the treatment of neurodegenerative diseases and CNS injury (Volkman, 2017). It has been demonstrated that MSCs are able differentiate into neuronal-like cells *in vitro* given the correct stimuli (Luo *et al.*, 2019). Some animals that have been administered MSCs following TBI have shown some engraftment of the MSCs to the injury site and marker expression such as NeuN and GFAP, indicative of early stages of differentiation (Lu *et al.*, 2001). However, neurological improvement without MSC engraftment has been observed, suggesting trophic factors play a role in recovery following TBI in animal models (Madrigal *et al.*, 2014).

Many clinical trials have demonstrated the safety of MSCs for use in a range of indications, including those of an allogenic source, and the number of clinical trials being registered/beginning each year is increasing (Wright *et al.*, 2021). NSC-like cells derived from bone marrow MSCs have demonstrated safety in a phase I trial in humans carried out by Wang *et al.* (2017) on 10 patients at the First People's Hospital of Jingmen (Jingmen, China) between January 2012 and June 2013. Patients did not appear to have any detrimental side effects following intravenous or intrathecal injection. The authors measured higher neurotropic factors such as BDNF in patient plasma following cell delivery and hypothesised that this may be a possible mechanism of action (Wang *et al.*, 2017).

Umbilical cord (UC)-MSCs have been delivered by lumbar puncture to patients with severe TBI, with some improvements seen in upper limb, lower limb, and sensation scores (Wang *et al.*, 2013). Overall, neurological function improvements were recorded over the 6-month study period and safety demonstrated and Wang *et al.* (2013), suggestions were made that the effects

were due to trophic support or environmental manipulation to stimulate endogenous repair. A clinical trial is active in America at time of writing investigating the safety and efficacy of autologous MSCs for the treatment of TBI (Cox, 2023) (Clinicaltrials.gov – NCT04063215). Another is investigating the safety and efficacy of intravenous allogenic UC-MSCs (AlloRX) for the treatment of TBI in Antigua and Barbuda (Prodromos, 2023) (Clinicaltrials.gov – NCT05018832).

MSCs are under investigation for other neurological indications. Some clinical trials investigating efficacy and safety of MSCs for use in Parkinson's disease have been reviewed by Mendes Filho *et al.* (2018). Studies have shown some positive outcomes, however there are still obstacles to overcome such as the cell number and route of administration to achieve the best outcomes (Mendes Filho *et al.*, 2018). Athersys Inc. are currently undertaking a phase 3 trial into the intravenous delivery of their bone marrow stem cell product MultiStem® for use in the treatment of stroke (Mays, 2023a) (Clinicaltrials.gov – NCT03545607). This follows a successful phase 2 clinical trial which showed positive outcomes in patients after a 12 month follow up (Mays, 2023b) (Clinicaltrials.gov – NCT01436487).

To date, only one MSC therapy has been approved for use in European markets, but not for use in neurological disease or damage. Alofisel® (darvadstrocel) uses adipose derived MSCs as a last resort treatment for complex anal fistulas in adults with Crohn's disease which is unresponsive to the standard biological treatments. The treatment is the local injection of two vials, each containing 3×10^7 cells (European Medicines Agency, 2018).

MSCs have been shown to secrete various growth factors such as vascular endothelial growth factor (VEGF), BDNF, glial cell line-derived neurotrophic factor (GDNF), and nerve growth factor (NGF) (Schepici *et al.*, 2020). These factors have demonstrated neuroprotective effects in various models of brain pathology (Baez-Jurado *et al.*, 2019). MSCs also demonstrate anti-inflammatory and immunomodulatory effects in the damaged brain by the secretion of factors such as transforming growth factor (TGF)-β, indoleamine 2,3-dioxygenase (IDO), IL-10 and hepatocyte growth factor (HGF) (González-González *et al.*,

2020). The secretion of these factors have been shown to reduce the activation of astrocytes and microglia, which is a feature of neuroinflammation following TBI (Andrzejewska *et al.*, 2021). The secretion of immunomodulatory factors such as IL-10 from MSCs has been implicated in the shift of both microglia and macrophages from a pro-inflammatory M1 to an anti-inflammatory M2 state (Andrzejewska *et al.*, 2021, González-González *et al.*, 2020). Exosomes are secreted by MSCs, which contain mRNA, microRNA, and proteins. When isolated and delivered to rats following induced TBI, angiogenesis, neurogenesis, and overall functional recovery is observed (Zhang *et al.*, 2015). Therefore, whilst MSCs may not engraft and differentiate in the injured brain, they may promote angiogenesis, neurogenesis, and reduce the inflammatory response from infiltrating leukocytes, promoting an environment within the injured brain which is more conducive to repair (Adugna *et al.*, 2022, Ludwig *et al.*, 2018, Schepici *et al.*, 2020, Mashkouri *et al.*, 2016).

1.3. TBI models

1.3.1. In vitro models

The use of *in vitro* models is valuable for screening potential therapies and understanding molecular mechanisms (Duval *et al.*, 2017). TBI is complex and difficult to model completely *in vitro.* A range of cell models have been established and published, but there is no single model that offers a complete picture of the TBI mechanisms and efficacy of a potential new treatment. However, *in vitro* models can benefit from the ability to study isolated mechanisms of injury and their effect on different cell types.

A simple and well-established method of culturing cells is to culture single cell types in plates or flasks on plastic. These are often simple to set up and optimise and allow for convenient and high-throughput screening of novel treatments. 2D environments are limited in that they are not representative of the highly complicated and interconnected network that different cells form in the brain. *In vivo*, cells are found within an extracellular matrix (ECM) made up of various different components including proteins and sugars. The mechanical and chemical properties of the ECM, as well as chemical cues from other cells, influence the survival, growth, and behaviour of cells found within the tissue

(Yue, 2014). Removing cells from this environment can alter the effects of potential therapies. Simple 2D models and well-characterised cell lines still have their place in TBI research as early screening tools.

Depending on the complexity required, a range of cell types can be used to study particular injury pathways and cellular responses observed in TBI. Human induced pluripotent stem cells (hiPSC) are induced from somatic human cells, such as fibroblasts, and behave like embryonic stem cells; they can be differentiated into many cell types when given the correct cues (Park *et al.*, 2008). Therefore, hiPSCs can be differentiated into brain cells such as neurons, and injury has been modelled by stretching the cells cultured on elastic surfaces (Sherman *et al.*, 2016). Differentiated hiPSCs have also been used to form co-culture models of the BBB, astrocytes, and neurons, enabling the study of these without the need for primary human or animal cells (Canfield *et al.*, 2017).

Cell lines have been used for many years in biological and medical research as a tool to understand cellular processes, design screening tools for novel therapies, and establish *in vitro* models for disease and injury (Sarntivijai *et al.*, 2014, Bairoch, 2018). 2D cell lines are relatively simple to culture compared to primary cells, inexpensive, and grow readily, enabling high-throughput screening assays to be established (Duval *et al.*, 2017). Whilst there are advantages to the use of cell lines, they are not without their drawbacks. Many can be passaged numerous times due to immortalisation of the cells. This is an advantage in terms of ease of culture, but the genetic makeup of the cells is altered as a result (Kaur, 2012). When considering human cell lines such as the SH-SY5Y cell line described in Table 1.1, they have 47 chromosomes (ATCC, 2023b), one more than would be found in their healthy counterparts. Despite this, cell lines are commonly used in early research to understand cellular processes occurring as a result of TBI, and to screen novel therapies for TBI. These are summarised in Table 1.1

Table 1.1 – Cell lines used to model TBI. The cell lines included have relevance to cells found in the brain and have been used to study mechanisms of TBI injury.

Cell type	Origin	Relevance to TBI	TBI model use
PC-12	Pheochromocytoma of the rat adrenal gland (Wiatrak *et al.*, 2020).	Neurite-like processes extend from the cell body. Cells have ion channels, neurotransmitter receptors, and neurotransmitter secretion (Wiatrak *et al.*, 2020).	Oxidative stress has been modelled with H_2O_2 to study potential neuroprotective effects of compounds (Li *et al.*, 2022, Zheng *et al.*, 2014).
SH-SY5Y	Human neuroblastoma from a metastatic bone tumour. Subclone of the SK-N-SH cell line (ATCC, 2023b).	Neurite-like extensions from adherent cells. The cells can be used differentiated or undifferentiated (Kovalevich and Langford, 2013, Shipley *et al.*, 2016).	Models of ischaemia, excitotoxicity, and oxidative stress, using oxygen and glucose deprivation, glutamate, and H_2O_2 respectively (Liu *et al.*, 2018). Mechanical injury by stretching cells grown on elastic substrates (Skotak *et al.*, 2012).
NG108-15	Hybrid of mouse neuroblastoma N18TG-2 cells and rat glioma C6 BV-1 cells (Merck, 2023).	Neurite extensions and acetylcholine expression (Daniels, 1974). Cells can be differentiated to lead to the presence of action potentials in the cells (Liu *et al.*, 2012).	Cells have been used to model blast TBI using pressure to damage the cells when cultured in well plates (Arun *et al.*, 2011).
bEnd.3	Endothelial cells derived from the brain of a mouse with endothelioma (ATCC, 2023a).	Used to model the endothelium of the BBB. Can be used in isolation (Berrout *et al.*, 2012), or in combination with other cells to form a more complex model of the BBB, for example bEnd.3 cells have been co-cultured with primary astrocytes (Michinaga *et al.*, 2021).	Stretch injury to understand Ca^{2+} and the relevant transporters in BBB damage (Berrout *et al.*, 2012). bEnd.3 cells and primary astrocytes in co-culture, damaged by fluid percussion, has been studied to understand endothelin-1 and sonic hedgehog protein in BBB damage (Michinaga *et al.*, 2021).
BV-2	Derived from primary mouse microglial cells, immortalised with the J2 retrovirus.	Cells have markers associated with microglial cells and are used to study neuroinflammation (Timmerman *et al.*, 2018).	Cells have been stimulated with lipopolysaccharide to study molecules for downregulation of inflammatory responses (Kumar *et al.*, 2017).
HT22	Mouse hippocampal neuronal cell line.	Cells expresses acetylcholine receptors and have neurite outgrowths (Liu *et al.*, 2009).	Stretch models to mimic neurite damage to screen novel treatments for their effects on neural outgrowth recovery (Rachmany *et al.*, 2017).

Of the six cell lines described, four are derived from mice, one from rat, and one from human. When considering that the animal models used are often mice or rat, using a cell line derived from the same species as these models may offer advantages in terms of translation to the animal models. However, developing treatments for human TBI is the end goal for many of the studies, therefore a cell line of human origin, expressing human genes, may offer advantages in translation to human patients (Dumont *et al.*, 2016).

The selection of the appropriate cell line also depends on the mechanism by which the novel therapy is thought to have an effect. The bEnd.3 cell line is used to model the BBB and the effects of injury on cellular mechanisms within the cells. Using bEnd.3 cells, the transient receptor potential channels TRPC1 and TRPP2, responsible for Ca^{2+} transport in response to mechanical signalling, have been implicated in injury sensitivity following stretch injury (Berrout *et al.*, 2012). Increased BBB permeability can result from TBI and can lead to impaired fluid homeostasis, aggravating the issue of increased intracranial pressure and causing further damage (McKee and Daneshvar, 2015). Understanding the molecular pathways involved can lead to the identification of novel therapeutic targets.

The PC-12, SH-SY5Y, NG108-15, and HT-22 cell lines all have neurite-like outgrowths from the cell body, similar to those observed in primary neurons. These can be used as a measure of cellular recovery following injury in response to novel treatments, in addition to assessing their viability or metabolic activity. Both PC-12 and SH-SY5Y cells have been subjected to damage by oxidative stress to model one component of secondary injury, with the effect of therapeutic molecules subsequently studied (Zheng *et al.*, 2014, Feng *et al.*, 2016). Mechanical injury to SH-SY5Y, NG108-15, and HT-22 cells has also been carried out, modelling the primary injury and the effect on neuronal cells. The effects of exendin-4 on HT-22 cells damaged following stretch injury was studied, with administration demonstrating both increased cell viability and neurite outgrowth after injury (Rachmany *et al.*, 2017). SH-SY5Y and NG-108 cells were both damaged by a pulse of pressure to mimic blast injury to study the cellular effects on both cell types, and their sensitivity to blast. In that particular study, SH-SY5Y cells were shown to be more sensitive to injury than

the NG108-15 cells, determined by 3-(4,5-dimethylthiazol-2-yl)-2,5-diphenyl tetrazolium bromide (MTT) assay (Arun *et al.*, 2011).

Primary cells can also be used to model injury pathways present in TBI. These are closer to the cell types *in vivo* as they are not immortalised to form cell lines (Kaur, 2012), however, they require the sacrifice of animals to obtain *ex vivo* tissue to extract the cells. Cells are therefore less abundant and require ethical considerations before use. To form these cultures, tissue is digested to remove the ECM, and cells placed in culture. Astrocytes, glial cells, and neurons are the most abundant cell types derived from *ex vivo* tissue. All three of these cell types dissociated from the *ex vivo* tissue can be used to form co-culture models formed to study the effect of injury or novel therapeutics on the different cell types (Goshi *et al.*, 2020).

Organotypic cultures in the context of TBI use thin slices of CNS tissue maintained in culture to model injury. These slices have been used to study neural circuits in whole brain slices, monitoring the interaction of the different cell types in response to injury stimuli, as well as changes in metabolism and phenotype of the cells (Humpel, 2015). Blast and stretch injuries have been simulated directly on organotypic cultures (Hamilton and Santhakumar, 2020, Morrison *et al.*, 2006). A limitation of this culture method is that younger animals are used for the preparation of the tissue slices, which can lead to developmental bias in the results of the studies (Morrison *et al.*, 2011). The preparation of the CNS slices also causes damage to the tissue, which can lead to exaggerated results.

1.3.2. Injury types

Mechanical injury occurs as the primary injury in TBI and can be modelled in a few different ways using cells in culture. Stretch models take cells cultured on a flexible basement membrane and apply stretch to non-fatally damage them. This simulates damage to axons seen when mechanical disruption to the brain results in shearing and loss of connections. Commonly, the aim is to assess cellular effects to identify potential therapeutic targets, or to assess novel therapeutics for their ability to support the regrowth of neurites and reestablishment of neural connections (Morrison *et al.*, 2006).

Models have been established using organotypic cultures (Morrison *et al.*, 2006), where membranes supporting hippocampal slices were stretched over an "indenter" to cause damage. SH-SY5Y cells have also been used in a similar stretch model; cells were cultured on an elastic membrane and the stretch was obtained using compressed air (Skotak *et al.,* 2012). Damage can be measured by loss of axons or neurites, cell death, or expression of damage markers.

Blast injury can be modelled by exposing cells in culture to gas pressure, or liquid pressure. Both aim to increase pressure on the cells for a brief time period, exposing them to similar membrane damaging forces to those experienced by TBI patients (Hanna and Pfister, 2023). Zander *et al.* has simulated blast injuries on both PC12 (Zander *et al.*, 2015) and SH-SY5Y (Zander *et al.*, 2016) cells using pressure increases to model the blast. The pressure increases caused increased membrane permeability in both cell lines, indicative of membrane damage. Blast injuries have also been induced on organotypic cultures, with injury severity similarly measured by detecting increases in membrane permeability across experimental cultures (Campos-Pires *et al.*, 2018).

Compression models directly compress cells in culture to cause damage, and often aims to mimic the controlled cortical impact (CCI) and weight-drop animal models (Hanna and Pfister, 2023) described in Table 1.2. 2D cultures are essentially incompressible, therefore 3D cultures lend themselves better to model compression injuries. The compression of the cultures leads to shear stress being placed on cells as the 3D culture moves under pressure. Primary neuronal cells in collagen gels have been subjected to controlled compression to study the

effect on the cells in the following 24 hours to understand the morphological changes to cells (Bar-Kochba *et al.*, 2016). Human iPSCs forming cerebral organoids within gelatine and agarose were subjected to a modified CCI within a phantom brain in a mouse skull. This was compared to the injury carried out in live mice. Reponses were comparable, although not all cell types within the brain were present in the cerebral organoids (Ramirez *et al.*, 2021). The development of these models may reduce the reliance on animal studies to advance the understanding of mechanisms in TBI.

Chemical damage models aim to simulate aspects of the secondary injury pathway in TBI resulting from the primary injury. The SH-SY5Y cell line is popular for use due to the ease of culture and neuron-like phenotype (Liu *et al.*, 2018). These models offer a simple tool to screen potential therapies against damage due to particular mechanisms, before moving on to alternative models. Oxygen and glucose deprivation models studying the effect of hypoxia and reoxygenation in the presence or absence of glucose have been established, concluding that the presence of glucose results in higher levels of apoptosis in cells when oxygen is reintroduced (Serra-Prez *et al.*, 2008). Hypoxia models were also used to determine the effect of the presence of glutamate on reoxygenation (Piccirillo *et al.*, 2018).

SH-SY5Y cells are sensitive to damage by glutamate, and therefore offer a simple model of excitotoxicity which can be used prior to animal investigations. Extendin-4 was screened for protective effects in a glutamate SH-SY5Y model, in which the cells were not differentiated. A protective effect was seen, which translated into enhanced recovery when delivered to rats with a fluid percussion injury (FPI) TBI (Eakin *et al.*, 2013). Oxidative stress can be modelled using SH-SY5Y cells with the addition of H_2O_2. Severity can be modelled based on the concentration of H_2O_2 added, with many opting for a concentration of less than 200 µM and a milder injury (Liu *et al.*, 2018).

1.3.3. Animal models

Due to the heterogeneity of TBIs, many animal models exist aiming to replicate different injury pathways. Many of the models were initially developed in larger animals such as pigs, cats, sheep, and dogs, but were later adapted for use with

rodents (Xiong, 2013). This minimises the cost of housing the animals and makes handling easier for researchers.

Testing in animal models is vital and offers the most complete view of efficacy and safety before moving to human clinical trials, however many models are severe and place suffering on animals, therefore their use needs to be carefully considered. Some of the commonly used models are described in Table 1.2. Each of the models aims to simulate human TBI caused by different mechanisms. The blast induced TBI, seen in many military personnel, is caused by acceleration and deceleration of the brain within the skull as a result of air pressure waves, and may also be caused by ischaemia resulting from thorax injury (Bryden *et al.*, 2019). In contrast, penetrating injury causes tearing of tissue and blood vessels within the cerebral cortex, resulting in a lesion containing dead cells and bleeding (Xiong, 2013). In addition to the type of primary injury observed in TBI differing with the different mechanisms of injury, the treatment will also differ. When the injury causes haematoma reaching the critical sizes detailed in section 1.1.4, surgery is required to remove and repair the damaged blood vessels (Adams *et al.*, 2016). Whereas if generalised oedema is present, resulting from disruption to water and ion homeostasis as cells are damaged, ICP monitoring and medical interventions to reduce pressure such as delivery of mannitol may be more applicable (Galgano *et al.*, 2017).

Some cell therapies incorporate the use of a scaffold to aid the repair of a lesion. Guan *et al.* (2013) developed collagen scaffold for the delivery of MSCs and used a CCI model as the impact to the exposed dura results in a localised lesion which may benefit from the use of a scaffold to bridge the newly formed gap (Guan *et al.*, 2013). In contrast, the Marmarou weight drop model described results in a diffuse injury, therefore a scaffold may not be necessary in the absence of a lesion (Marmarou *et al.*, 2009).

Table 1.2 – A summary of the commonly used animal models of TBI, a brief outline of the model protocol, their relevance to injuries seen in humans, and whether MSC have been investigated as a treatment using each model, including the outcome.

Model	Description	Human relevance	Use of MSCs
Fluid percussion injury (FPI)	Fluid under pressure is used to compress the brain. Saline reservoirs struck with a pendulum cause pulses of pressure to the expose dura of the animal (Lifshitz, 2009).	The model can be used to cause a midline or a lateral injury (Kabadi *et al.*, 2010) with similar characteristic to haemorrhage and diffuse damage in humans (Lyeth, 2016).	UC-MSCs have been delivered locally to the injured brain by injection. This allowed Th17 T-cells to differentiate into T-reg cells, reducing inflammation and improving recovery (Chen *et al.*, 2022).
Controlled cortical impact (CCI)	A mechanical device is used to cause injury to the exposed dura. The size of the device, velocity and impact depth are all measured, allowing for more control over the injury (Osier *et al.*, 2015).	Originally developed to model road traffic collision TBIs. Is now more broadly used as a standardised model with controlled variables (Osier and Dixon, 2016).	UC-MSCs have been delivered intracerebrally to mice following a CCI. Mice showed an early neurological improvement compared to no treatment, and this improvement over the control group was seen one month following injury (Zanier *et al.*, 2011).
Penetrating ballistic-like brain injury model (PBBI)	Injury is caused by penetration of a projectile, forming a cavity (Xiong, 2013).	The model is used to cause an injury similar to that seen in humans resulting from a gunshot or other penetrating object (Williams *et al.*, 2006).	To the best of our knowledge, no studies to investigate the use of MSCs in PBBI. NSCs have been transplanted into rat PBBI models, with engraftment of cells demonstrated (Spurlock *et al.*, 2017).
Weight drop – Marmarou	A stainless-steel disc is placed on the exposed skull of the animal, and a weight dropped onto this (Marmarou *et al.*, 2009).	Aims to mimic the sort of injuries seen in patients following a vehicle collision or a fall, causing a more diffuse injury (Marmarou *et al.*, 2009).	Intravenous bone marrow (BM)-MSCs demonstrated migration to the injured brain and improved functional recovery over the control after 14 days (Anbari *et al.*, 2014).
Weight drop – Maryland	Two offset rods attached to a cylinder are secured to the rodent's head to dissipate impact. A steel ball weight is dropped along a track, which will impact the front of the cylinder (Hayman *et al.*, 2018).	Aims to model the frontal impact with rotational forces to more accurately reproduce the sort of injury seen following vehicle collisions (Hayman *et al.*, 2018).	The Maryland model was developed fairly recently (2018) and therefore, to our knowledge, has yet to be used to model recovery following MSC delivery.

Weight drop – Feeny's	A craniotomy is performed to expose the dura and a weight dropped directly onto this to cause contusions (Feeney *et al.*, 1981).	Feeny's weight drop method causes a more localised injury with a much smaller injury area, more representative of injury resulting from a smaller impact area in humans.	UC-MSCs were delivered locally within an alginate/hyaluronic acid scaffold to injured rats. An improved outcome was demonstrated, which was enhanced in the presence of the scaffold (Zhang *et al.*, 2018).
Weight drop – Shohami's	The skull is exposed, but no craniotomy performed. A weight is then dropped onto the skull to cause injury (Flierl *et al.*, 2009).	Aims to model a focal closed head injury (Khalin *et al.*, 2016).	To our knowledge, there have been no studies to investigate the delivery of MSCs to animals injured using Shohami's weight drop model.
Blast TBI model	Uses shock tubes to subject the animal to shockwaves resulting from explosive detonation. Often the animals are equipped with a Kevlar® vest to protect the thorax from the blast (Xiong, 2013).	Injury in humans result from pressure waves impacting the body and head. It is thought damage can occur directly to the brain as a result of acceleration/deceleration of the brain within the skull, and as a result of absorption of some of the energy of the shockwave (Bryden *et al.*, 2019).	To our knowledge, there have been no studies investigating the delivery of MSCs to animals injured using the blast TBI model. However, the secretome and conditioned media from has been delivered to injured mice and shown positive effects on retinal inflammation and visual deficits (Jha *et al.*, 2018).

Many of the animal models summarised in Table 1.2 have been tested with the delivery of MSCs with positive outcomes measured. The cells are commonly via intravenous delivery or local injection (Schepici *et al.*, 2020), however there are other cell delivery routes available.

1.4. Cell delivery

Delivery of cells is often a trade-off between how invasive the process is, and delivering cells locally to the site of injury, especially in the context of brain injury. The BBB in the healthy state prevents the entry of many molecules and cells into the brain (Daneman, 2015). Whilst essential for brain function, it presents a large pharmacological barrier and can result in the costly loss of many therapeutic cells if they fail to migrate into the brain.

Cell therapies require large numbers of cells, which require preparation in sterile environments. Some applications present opportunities to use autologous cell sources, or potentially an off-the-shelf source of cryopreserved cells, otherwise a donor is required as a cell source (Hipp, 2008). The preparation of the cells is an expensive process, therefore any opportunity to minimise the number of cells required for the therapy should be exploited. Local delivery maximises the number of cells delivered to the required site, thus minimising the number of cells required, however safety and practicality must also be considered when selecting the delivery route.

Safety has been demonstrated in animals and human trials for TBI, stroke, and Parkinson's disease using both NSCs and MSCs (Kabu *et al.*, 2015). Intravenously delivered cells are subject to pulmonary sequestration as they become trapped in the narrow capillaries. It is estimated approximately 80% of delivered cells become trapped in the lungs (Zhang *et al.*, 2020). Therefore, whilst MSCs have been shown to migrate to the brain, only a small proportion will do so (Harting *et al.*, 2009, Sohni and Verfaillie, 2013). Estimations vary: Harting *et al.* (2009) estimated only 0.0005% of the intravenously delivered labelled MSCs reached the rat brain (most became trapped in the pulmonary capillaries) (Harting *et al.*, 2009) whereas Jackson *et al.* (2010) estimated that around 8% of the cells delivered intravenously reached the lesion (Jackson *et al.*, 2010), and Yoon *et al.* (2010) gave an estimate of 1.4% (Yoon *et al.*, 2010).

Therefore, the cell delivery method requires optimisation to avoid wasting therapeutic cells and avoid the risk of pulmonary oedema associated with the accumulation of cells in the lungs.

In terms of the number of cells delivered to the injury site, intraarterial has been shown to be superior to intravenous delivery. However, in animals such as rats, an increased morbidity is seen due to arterial blockages (Li *et al.*, 2010a, Walker *et al.*, 2009). The safety concerns render this delivery route inappropriate for human use.

Intrathecal delivery is also superior to intravenous in terms of the number of cells delivered to the injury site. It is less invasive than local delivery, but still carries more risk than intravenous delivery. This route is also limited by a high cerebral spinal fluid (CSF) turnover rate and problems with cells settling in the subarachnoid space (Boltze, 2015). Safety has been demonstrated using intrathecal MSC delivery in human clinical trials with TBI patients (Wang *et al.*, 2013, Wang *et al.*, 2017), but this route still relies on cell migration to the brain.

Intranasal delivery has been investigated in animal models by pipetting cells into the nasal passage of rats. From there, they migrated through the cribriform plate to the olfactory neural pathway and into the brain and CSF (Danielyan *et al.*, 2009). A high number of cells were trapped at the back of the nasal passage, but some migrated and provided therapeutic benefit (Danielyan *et al.*, 2009). BM-MSCs labelled with green fluorescent protein delivered intranasally to mice with brain lesions were found to neither survive nor migrate within the 7 day test period (Chartoff *et al.*, 2011). However, a study investigating the intranasal delivery of NSCs to mice with experimentally induced autoimmune encephalomyelitis did demonstrate positive therapeutic effects with migration of the intranasally delivered cells (Wu, 2013). Intranasal delivery was compared to intravenous, and in the latter group, very little migration or engraftment of cells was observed. This delivery route may have issues arise from tolerability as many cells may be lost if the patient were to sneeze. Dosing of cells would be highly variable as a result.

Delivering cells directly to the site of injury has advantages in minimising cell loss and wastage. This route is highly invasive for brain injury, however, it is

estimated the around 10% of severely injured TBI patients will require some form of surgery (Fong *et al.*, 2017), presenting an opportunity for therapeutic cells to be delivered. Cell transplantation for use in Parkinson's disease relies on the engraftment of delivered cells to replace degenerated dopaminergic neurons to alleviate symptoms (Jang *et al.*, 2020). Cells are directly injected into the brain, with clinical trials showing some improvements in patient outcomes, particularly in mild cases with a shorter disease duration (Jang *et al.*, 2020). However, injecting cells into the brain parenchyma can cause localised damage and inflammation. Additionally, as MSCs act via the secretome rather than via direct engraftment, topical application may be preferential. This has been investigated using fibrin to retain cells at the delivery site, and beneficial effects were seen in the rats with a TBI (Lam *et al.*, 2013). Local delivery of cells to the brain within hydrogel materials has also been investigated for the repair of stroke lesions, with promising results shown (Lam *et al.*, 2014, Zhong *et al.*, 2010). Using hydrogel materials to retain cells at the delivery site and to protect those cells from the inflammatory environment may enhance the proportion of cells delivered which can then be therapeutically beneficial.

Spray delivery of cells has been investigated, primarily for wound care and lung delivery. Veazey *et al.* (2005) investigated an aerosol device for spraying bovine fibroblasts, showing that a higher pressure and smaller nozzle size correlated with lower cell viability (Veazey *et al.*, 2005). Zhang *et al.* (2022) showed the same correlation using UC-MSC, and also demonstrated that the cells retained their capacity to differentiate into chondrocytes and adipocytes following spraying (Zhang *et al.*, 2022). Both of these studies used air pressure devices to generate a spray, whereas the ReCell® spray kit uses a syringe-based device (Wood *et al.*, 2012). The kit aims to take skin from a patient donor, digest the sample to obtain a cell suspension to spray onto the wound site to facilitate repair. Only a 6% reduction in cell viability (75% to 69%) was observed following spraying, showing the device could be used to deliver cells (Wood *et al.*, 2012). Mixed results in terms of efficacy have been published in clinical trials, with some demonstrating enhanced recovery, and others not reaching clinical trial emdpoints (Manning *et al.*, 2022, Peirce and Carolan-Rees, 2019).

Beneke *et al.* (2018) investigated the use of hyperosmolar solutions to shrink cells prior to spraying from a pump spray device to maximise cell viability, showing macrophages could be shrunk and viability and functionality retained (Beneke *et al.*, 2018). MSCs have also been investigated for lung delivery via an endoscopic aerosolization device, with cells maintaining their MSC phenotype and viability (Thiebes *et al.*, 2021). These experiments show that spraying viable cells can be achieved using a range of different spray devices.

Delivering therapeutic cells by spraying may also be suitable for local delivery of cells to the injured brain. However, due to the uneven surface of the brain and the likelihood of sprayed droplets of cells running across the surface of the brain leading to a heterogeneous distribution, a carrier material may be necessary to retain cells at the site of injury.

1.5. Materials for cell delivery

Hydrogels are attractive for use in cell delivery, tissue engineering, and 3D cell culture. They are 3D polymeric networks with a significant proportion of water in the structure (Ahmed, 2015). Numerous materials have been investigated as scaffolds to aid recovery in TBI (Collins *et al.*, 2022), for example transplanting cells within collagen hydrogels has demonstrated superior neurological outcomes in an ischemic rat model (Yu *et al.*, 2010), and cells transplanted within a hyaluronan and heparin based hydrogel showed enhanced survival of the therapeutic cells and a reduction in inflammation, in an ischemic rat model (Zhong *et al.*, 2010). However, to be suitable for cell delivery by spraying (for use in this thesis), the material must demonstrate properties such as shear-thinning or *in situ* gelation to have a low enough viscosity to be sprayed. Therefore, an extensive review of materials investigated for TBI is not provided here but is discussed by Collins *et al.* (2022).

The Tisseel device combines fibrinogen and thrombin to form fibrin (which must be kept separate to prevent premature gel formation) and can be applied by spraying. This has been investigated in combination with cells for possible wound healing applications. Using human adipose stromal vascular cells, differentiation and proliferative potential of the cells was retained after spraying with the Tisseel device (Zimmerlin *et al.*, 2013). Keratinocytes have been

sprayed using this fibrin system, demonstrating viability and proliferation of cells (Harkin *et al.*, 2006), and wound healing has also been demonstrated when MSCs are sprayed with fibrin onto human wounds (Falanga *et al.*, 2007).

A sprayable gellan-based material for the spray delivery of fibroblasts to the skin was studied for retention of the cells at the delivery site. A slight reduction in cell viability was seen following spraying, but this was not statistically significant compared to the not sprayed control, showing that spraying within a material is an option to prevent droplets running away from the delivery site (ter Horst *et al.*, 2019). Thermo-responsive hydrogels with a sol-gel temperature of 37 °C, such as some polyethylene glycol (PEG) gels (Klouda *et al.*, 2008) may be suitable for spraying. However, they could also present issues when using cells maintained in culture at 37 °C, as if the temperature is not tightly controlled, blockage of the spray device could occur.

Alginate is commonly used in regenerative medicine and as a scaffold for 3D cell culture as it demonstrates biocompatibility (Szekalska *et al.*, 2016). Alginate gels with the addition of divalent Ca^{2+} ions (Andersen *et al.*, 2015), and forms a solution prior to gelation, presenting the opportunity for it to be sprayed. Pectin is similar to alginate in terms of the structure and gelation by Ca^{2+} (Cao *et al.*, 2020), however pectin is more sensitive to gelation by Ca^{2+} (Zhang *et al.*, 2019). Calcium is found endogenously in the brain, which could be sufficient to induce gelation *in situ*. Pectin has a history of biocompatibility (Hartman, 1943), including in the brain (McCrorie *et al.*, 2020). In addition, pectin has demonstrated some anti-inflammatory properties (Hu *et al.*, 2020a) which could aid in the treatment of TBI.

1.6. Pectin

Pectin is a naturally occurring saccharide-based polymer obtained from fruits. It forms a network within the cell walls of plants and plays a role in modulating the physiology, growth, development and defence functions within plants (Willats *et al.*, 2001). Pectin is extracted from fruits, most commonly citrus and apple, which can be obtained from the waste of the juicing industry. Pectin has been used for a number of years in a range of industries and applications. Some of these are summarised in Table 1.3.

Table 1.3 – Summary of the applications of pectin over time.

Field of use	Application	Reference
Food and drink production	Used as a thickener in many food and drink products, most notably in jam.	(Olsen, 1933, Olsen, 1939)
Diarrhoea treatment	Investigated and used to treat cases of infant diarrhoea.	(Winters, 1939)
Wound treatment	Believed to prevent infection and enhance healing of wounds.	(Maclay *et al.*, 1944, Olsen, 1940)
Haemorrhagic shock	Used as a blood substitute to prevent death from catastrophic blood loss.	(Hartman *et al.*, 1941, Hartman, 1943, Hartman, 1951)
Drug delivery	Many investigations for drug delivery applications, including colon targeting, buccal delivery, microparticle formulation, and an excipient in tablets.	(Joseph, 1995, Munjeri *et al.*, 1997, Watts and Smith, 2009)
Weight management	Used to satiate patients and investigated for stabilising blood sugar.	(Tiwary *et al.*, 1997, Doherty and Jackson, 1992)
Tissue engineering and cell delivery	Cell encapsulation studies for cell delivery and bone regeneration have been carried out, showing pectin could be a viable material.	Encapsulation: (Neves *et al.*, 2015, Gentilini *et al.*, 2018) Tissue engineering: (Murugan Sumathra *et al.*, 2017, Zhao, 2016, Prasanna Mallick *et al.*, 2018)

The exact chemical structure of pectin is dependent on the fruit source, fruit age, extraction method, and post-extraction processing (Gawkowska *et al.*, 2018). Galacturonic acid is the most abundant sugar found within pectin; to be classed as pectin, it must contain at least 65% galacturonic acid according to the Joint FAO/WHO Expert Committee on Food Additives and the European Commission (Commission, 2012). This distinguishes pectin from other polysaccharide substances found in certain fruit cell walls, such as proto-pectin, amylopectin, or cellulose (Voragen *et al.*, 2009).

Homogalaturonan (HG), rhamnogalaturonan-I (RG-I) and rhamnogalatuonan-II (RG-II) are the three most abundant domains found in pectin (shown in Figure 1.5). HG accounts for approximately 60% of the structure of pectin (Lara-Espinoza *et al.*, 2018). Other domains are found in lesser amounts including xylogalacturonan containing xylose residue side chains, arabinan with arabinose side chains, arabinogalactan-I, and arabinogalactan-II, both containing galactose residue side chains (Voragen *et al.*, 2009).

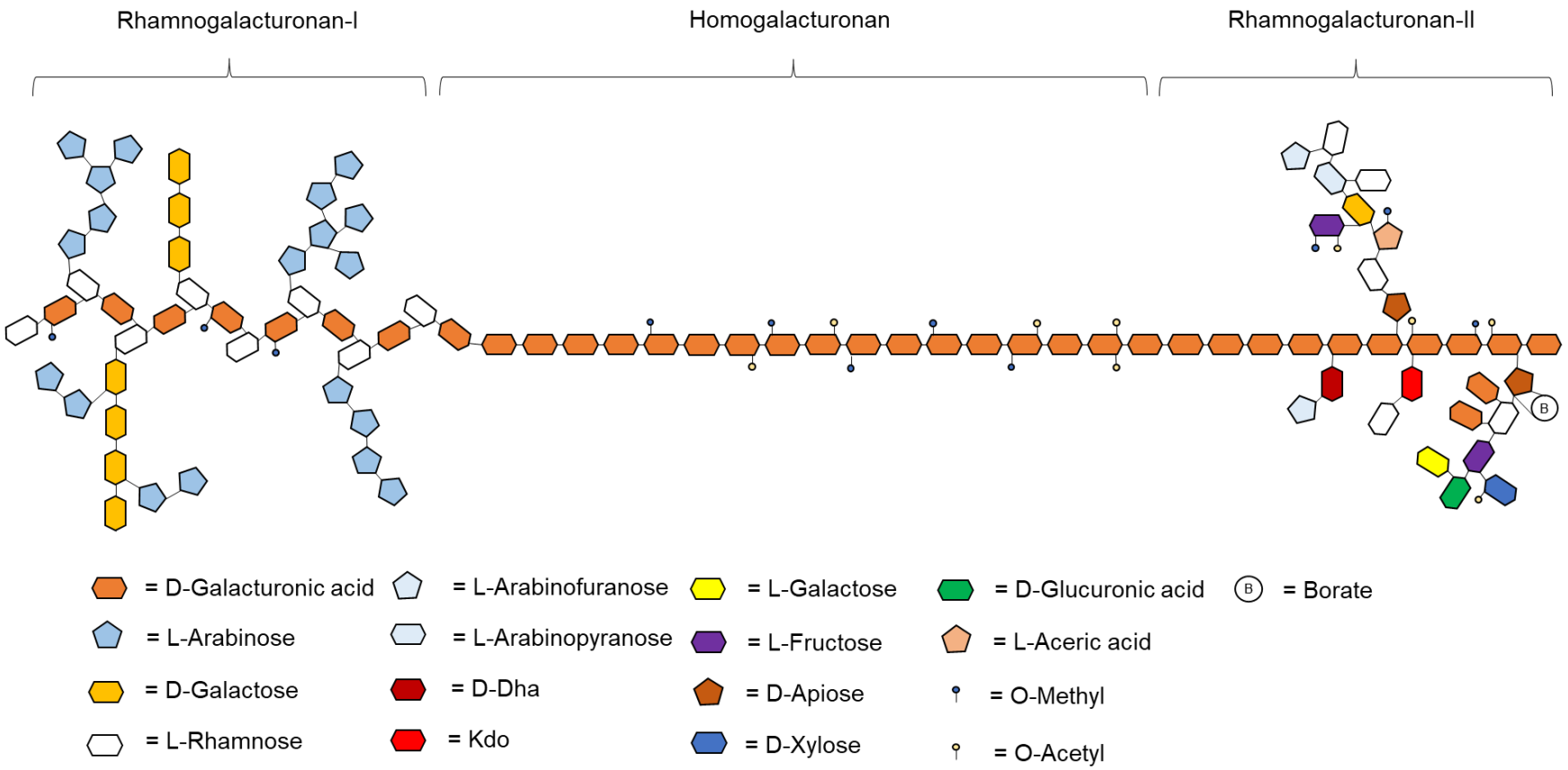


Figure 1.5 – The structure of rhamnogalacturonan-I, homogalacturonan and rhamnogalacturonan-II. Adapted from (Minzanova *et al.*, 2018) and (Gawkowska *et al.*, 2018).

RG-I is made up of repeating units of α-1,2-L-rhamnose-α-1,4-D-galacturonic acid. RG-I is branched as the L-rhamnose can be substituted on the O-4 position by neutral sugars such as arabinose and galactose, enabling side chain formation shown in Figure 1.5 (Lara-Espinoza *et al.*, 2018). RG-II is highly conserved in the plant kingdom and has the most complex structure of all the domains within pectin (Voragen *et al.*, 2009). It contains four branches with a total of 13 different glycosyl residues with over 22 glycosidic linkages (Bar-Peled *et al.*, 2012). Homogalacturonan is a linear, unbranched chain consisting of α-1,4-linked D-galacturonic acid.

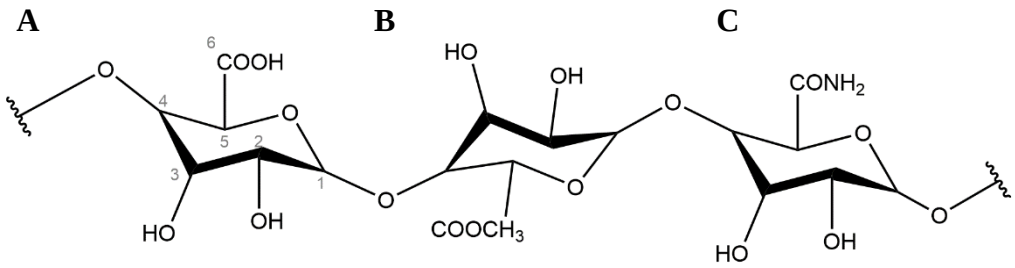


Figure 1.6 – Galacturonic acid structure of pectin without methyl esterification or amidation **A**, with methyl esterification **B**, and with amidation **C**. Residues are linked by an α-1,4-glycosidic link.

Residues can be methyl esterified or amidated at C-6 (shown in Figure 1.6B and C respectively) (Noreen *et al.*, 2017). The number of galacturonic acid residues that have been methyl esterified on the C-6 position (shown in Figure 1.6B) is measured as the degree of methylation (DM) and shown as the percentage of these -$COOCH_3$ groups relative to -COOH (Claude H. Hills, 1945, Sriamornsak, 2003). Broadly, pectin is classed as high methoxyl pectin (HMP) with >50% methylation and low methoxyl pectin (LMP) with <50% methylation (D. May, 1990). The degree of amidation (DA) is also shown as a percentage of amidation at the C-6 position. Both modifications are shown in Figure 1.6 and have implications for the gelation properties (Gawkowska *et al.*, 2018).

1.6.1. Gelation

As mentioned, hydrogels are 3D polymeric networks of chemically (covalent bonds) or physically (non-covalent interactions) cross-linked polymeric chains containing at least 70% (but can be over 99%) water (Li and Mooney, 2016). Physical hydrogels can be cross-linked by a range of interactions such as hydrogen bonds, Van der Waals forces, and electrostatic interactions. Formation of such hydrogels is often triggered by temperature, pH or ionic interactions and can be reversed (Ullah *et al.*, 2015a).

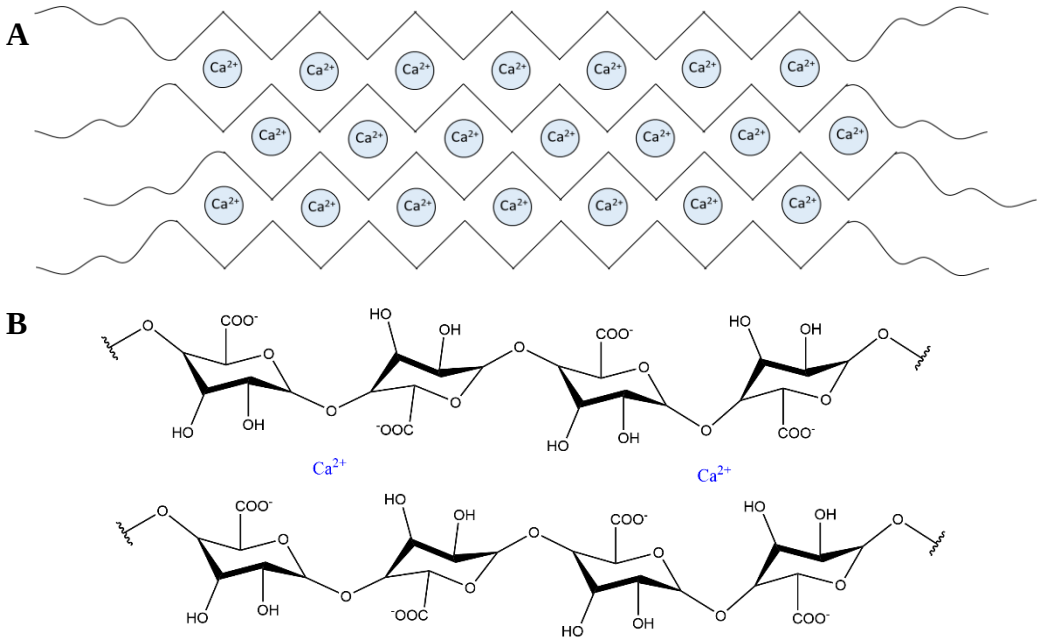


Figure 1.7 – Schematic of the 'egg box' structure with LMP chain interactions with calcium **A** and the specific interactions with the carboxylic acid groups on galacturonic acid residues and calcium ions **B**.

Pectin forms a physically cross-linked hydrogel, however the gelation method of HMPs and LMPs are different due to the differing degree of free carboxylic acid groups. LMP forms a hydrogel in the presence of divalent cations, such as calcium, due to the higher availability of carboxylic acid groups. These groups on the galacturonic acid chains interact due to opposite charges with calcium ions, forming an 'egg box' structure of cross-linked chains shown in Figure 1.7. This was determined by Grant *et al.* in 1973 (Grant, 1973). This gelation method may be more useful for tissue engineering, cell delivery, and drug delivery uses. HMP does not cross-link in the presence of calcium but is temperature sensitive and requires >50% soluble solids (such as sugar) present for gelation to occur.

For this reason, HMP is largely used in the food and drink industry as a thickener or gelling agent.

The DA has an impact on the stiffness and resistance to degradation of the gel formed, particularly in LMPs. A higher DA allows for more hydrogen bonds to form which cross-link the chains, reducing the requirement for divalent cations (Guillotin *et al.*, 2007). A higher DA also increases the solubility of the pectin, allowing for quicker dissolution (Belkheiri *et al.*, 2021). When considering the breakdown of pectin hydrogels, pectin gels can begin to dissolve, and pectin chains can degrade non-enzymatically by β-elimination. This occurs more readily at higher pH (>6) and is shown in Figure 1.8 (Diaz *et al.*, 2007).

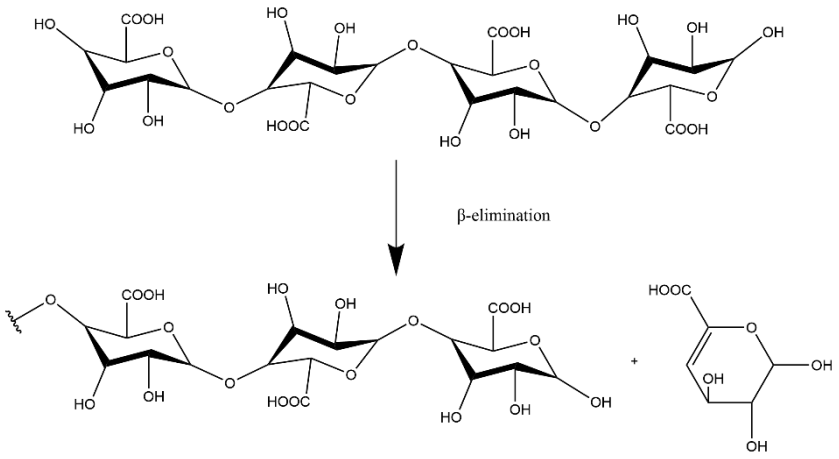


Figure 1.8 – Schematic of the β-elimination reaction which results in the breaking of the α 1,4-glycosidic link between galacturonic acid residues, depolymerising pectin.

The properties of LMP gels are not only influenced by the DA and DM (influenced by fruit age and source), but also the molecular weight. A higher molecular weight results in a more viscous pectin solution and stiffer gel formation due to more cross-linking interactions between pectin chains. MW is largely determined by the selection of fruit from which pectin is extracted (Gawkowska *et al.*, 2018). Banana peel pectin ranges from 87-248 kDa, whilst lime citrus pectin is 342.7 kDa (Dranca and Oroian, 2018). Citrus fruit and apples are the most abundantly used sources, providing a high yield and high galacturonic acid content. The DM usually obtained immediately following extraction using citrus fruit is around 70%, due to both the esterification of pectin natively within the plant cells as fruit ripens and the extraction process itself. Other fruits and the age of the fruit will influence the DM.

1.6.2. Past uses

During the Second World War, due to the increased incidence of traumatic injury, pectin was investigated for use as a plasma expander to treat haemorrhagic shock. Pectin was proposed as a blood substitute as it was believed to be non-antigenic, osmotically balanced, and large enough to be retained in the circulation. Hartman investigated the use in a total of eight animal studies, demonstrating excretion in the urine, no retention in the liver, and efficacy in a blood loss model (Hartman *et al.*, 1941). The first human patient, a female receiving treatment for breast metastases, demonstrated safety and efficacy. Blood pressure was elevated or maintained in all subsequent patients included in the study, so pectin was deemed a suitable treatment for haemorrhagic shock (Hartman, 1943). The uptake of material by Kupffer cells of the liver, endothelial cells of the spleen, glomerular cells of the kidney, and alveolar cells of the lungs following intravenous pectin injections was later demonstrated. It was not deemed to be toxic to cells and was excreted renally (Popper, 1945). Studies demonstrated that autoclaving to shorten pectin chain lengths reduced retention in cells (Hartman, 1951), but ultimately blood banking meant pectin was no longer used as a plasma expander. However, it is important to note that the application of pectin as a plasma expander provided valuable toxicity knowledge.

1.6.3. Tissue engineering

Pectin demonstrates biocompatibility, simple conditions for hydrogel formation, and groups such as carboxylic acid which can be modified to alter the properties, making it a promising material for tissue engineering and cell delivery.

The selection of pectin grades (amidated or non-amidated, degree of methylation, and fruit source) can influence the resistance of pectin hydrogels to degradation, and the strength of the gel formed (Gawkowska *et al.*, 2018). It is known these can be influenced by both the pectin concentration and calcium concentration, however, less seems to be known about the effect of amidation and methylation (beyond the classification as LMP) on degradation profile and gel strength in the context of tissue engineering. Very few studies have been conducted on pectin alone as a hydrogel for tissue engineering as it has no attachment sites for cells. To overcome this, two studies have investigated

carbodiimide chemistry to attach an RGD (arginine-glycine-aspartate) peptide to the pectin, to enable cell adherence. The first (Munarin *et al.*, 2012a) showed viability using a MC3T3-E1 preosteoblast cell line. The second (Neves *et al.*, 2015) demonstrated viability of MSCs in unmodified pectin, however their phenotype was more rounded than in the RGD-pectin. This study used $CaCO_3$ as the calcium source to form a gel as the calcium is released more slowly, leading to a more homogeneous gel forming.

The $CaCO_3$ method of gelation was also used by Gentilini *et al.* (2018) when they studied the effect of adding glucose and glutamine to the pectin hydrogels (without RGD functionalisation) when used with L929 mouse fibroblasts. Gentilini *et al.* found 90-98% viability over 7 days in all the pectin formulations, with softer gels more resistant to degradation forming in the presence of glucose and glutamine (Gentilini *et al.*, 2018).

The addition of pectin into a formulation used to encapsulate islet cells designed for transplant into diabetic patients showed a reduction in damage associated molecular patterns (DAMP)-induced toll-like receptor-2 mediated immune response following the addition of LMP into the microcapsule formulations. The islets showed long-term survival and efficacy in diabetic mice (Hu *et al.*, 2020b). Others have also reported anti-inflammatory effects of pectin, with a reduction in the secretion of pro-inflammatory cytokines observed following pectin administration to peripheral blood cells in culture (Hertzel Salman *et al.*, 2008). When given as a dietary supplement to mice, both local and systemic inflammatory responses were lessened, which was more pronounced when LMP was used (Popov *et al.*, 2013, Lim *et al.*, 2003).

1.7. Thesis hypothesis

It was hypothesised that pectin is a suitable material for human MSC delivery for TBI treatment, and that spraying cells suspended in a pectin solution is a suitable local delivery method. As pectin gels in the presence of calcium, which is found endogenously in the brain, it could be sprayed as a solution and form a gel when in contact with the brain parenchyma. As dysregulation of calcium homeostasis is a feature of secondary injury in TBI, pectin may have beneficial effects on reducing the extracellular calcium and restoring homeostasis. Pectin has also demonstrated anti-inflammatory properties, which may enhance the anti-inflammatory effects seen by the delivery of MSCs.

1.8. Thesis aims and objectives

The aim of this project was to evaluate the effect of spraying within pectin solutions on human MSCs and determine if this could be a suitable method for local delivery of cells. Different grades of pectin were tested to determine suitability for use in spray delivery. Spray delivery was optimised first with the 3T3 mouse fibroblast and SH-SY5Y human neuroblastoma cell lines, before spraying human MSCs in pectin and characterising the effect of spraying on their phenotype and gene expression.

The project objectives were as follows:

- Characterise the physical properties of four grades of pectin, including viscosity, gelation in various diluents, and biocompatibility (Chapter 3)
- Characterise the effect of spraying cells in pectin by measuring impacts on cell viability, phenotype, and gene expression (Chapter 4)
- Assess the effect of MSCs sprayed in pectin on simple *in vitro* TBI damage models (Chapter 5)

Chapter 2 Materials and methods

2.1. Materials

Table 2.1 – Materials and equipment, and the supplier.

Materials and equipment	Supplier
0.1M sodium hydroxide solution	Sigma Aldrich, 1310-73-2
1 mL syringe	Hanke Sass Wolf
5kg load cell for Texture Analyser	Stable Micro Systems
Accutase®	Sigma Aldrich, A6964-100ML
Anton Paar Modular Compact Rheometer 302	Anton Paar
BD Plastipak™ 1 mL Leur Slip Syringe	Fisher Scientific, 15489199
Calcium chloride anhydrous	Scientific Laboratory Supplies
CyQUANT™ LDH Cytotoxicity Assay	ThermoFisher Scientific, Invitrogen C20301
Dulbecco's Modified Eagle Medium	Gibco, 11965092
Dulbecco's phosphate buffered saline	Sigma Aldrich, D8537-1L
Dimethyl sulphoxide (DMSO)	Sigma Aldrich
Eppendorf centrifuge	Eppindorf 5430
Flow cytometer	Beckman Coulter, CytoFLEX S
Foetal bovine serum	Sigma Aldrich, F9665
Fourier-transform infrared spectrophotometer	Agilent Cary 630 FTIR Spectrophotometer
Freeze drier	Biopharma
Gentamicin	Sigma Aldrich, G1397
Ham's F12 Nutrient Mix	Gibco, 11765054
Industrially methylated spirit	Fisher Scientific
LIVE/DEAD™ Viability/Cytotoxicity Kit, for mammalian cells	ThermoFisher Scientific, Invitrogen L3224
MAD Nasal™ Intranasal Mucosal Atomization Device	Teleflex
Mesenchymal Stem Cell Adipogenic Differentiation Medium	PromoCell, C-28016
Mesenchymal Stem Cell Growth Medium 2	PromoCell, C-28009
Mesenchymal Stem Cell Osteogenic Differentiation Medium	PromoCell, C-28013
Minimum Essential Medium Eagle	Gibco, 11095080
MSCGM™ Mesenchymal Stem Cell Growth Medium BulletKit™	Lonza, PT-3001
NanoDrop™ spectrophotometer	ThermoFisher Scientific

NIH 3T3 mouse fibroblasts	Kindly gifted from RMCT division, School of Pharmacy
Non-essential amino acids	Gibco, 11140035
Norit SX Plus CAT activated charcoal	Sigma Aldrich, 7440-44-0
Pectin Classic CU-701	Herbstreith and Fox
Pectin Classic CU-L 094/19	Herbstreith and Fox
Pectin GENU LM 102 AS	CP Kelco
Pectin GENU LM 104 AS	CP Kelco
Penacillin/streptomycin	Gibco, 15070063
Phosphate buffered saline tablets	Sigma Aldrich, P4417
Pierce™ BCA protein assay kit	ThermoFisher Scientific, 23227
Pierce™ Chromogenic Endotoxin Quant Kit	ThermoFisher Scientific, A39552
PrestoBlue™ HS Cell Viability Reagent	ThermoFisher Scientific, Invitrogen P50200
Primary human mesenchymal stem cells	Lonza, PT-2501
Rheometer 25 mm measuring cone	Anton Paar, part #79038, serial #12205
Rheometer 25 mm measuring parallel plate	Anton Paar, part #79044, serial #37100
RNeasy® plus mini kit	Qiagen, 74134
SH-SY5Y human neuroblastoma cells	European Collection of Authenticated Cell Cultures, 94030304
Sodium Chloride	Sigma Aldrich, S9888
Sterile cell strainer (0.7 µm)	Fisherbrand, Fisher Scientifc
Syringe Filter (0.22 and 0.45 µm) Merck Millex™ PES	Fisher Scientific
TA HD Plus Texture Analyser	Stable Micro Systems
Tecan infinite 200Pro plate reader	Tecan
Tecan Spark 10M plate reader	Tecan
Trypsin/EDTA	Gibco, 11590626

2.2. Pectin purification

The following grades of pectin were used and kindly gifted from the suppliers stated.

Table 2.2 – Supplier for each grade of pectin used, the degree of methylation (DM), the degree of amidation (DA) and the pH of pectin dissolved in water at concentrations stated.

Supplier	Grade	DM	DA	pH
Herbstreith and Fox	Classic CU-701	37%	-	3.4 (1% solution)
	Classic CU-L 094/19	28%	-	~4 (1% solution)
CP Kelco	GENU LM 102 AS	30%	19%	4-5 (1% solution)
	GENU LM 104 AS	27%	20%	4-5 (1% solution)

Pectin was added to deionised H_2O to form a 1% w/v solution. Pectin was stirred using a magnetic stir bar and hot plate set to 70 °C at 400 rpm until observed to be fully dissolved. The solution pH was adjusted to ~6 using 0.1 M NaOH (Sigma). Once cool, 2% w/v activated charcoal (Norit SX Plus Cat, Sigma) was added and stirred at 400 rpm for 1 hour at room temperature. Pectin solution was added to microcentrifuge tubes (1.7 mL) and spun at 19,500 g for 45 minutes. The supernatant was removed and pooled, before being added to microcentrifuge tubes and spun again at 19,500 g for 30 minutes. Supernatant was removed and filtered through 0.22 (LM-102, LM-104 and CU-L) or 0.45 µm (CU-701) syringe filters before being freeze dried. Pectin was stored at -20 °C until use.

2.2.1. Bicinchoninic acid (BCA) protein assay

Samples were prepared by dissolving pectin (0.5% w/v) in 1xPBS. The protein assay was carried out using the Pierce™ BCA protein assay kit (ThermoFisher Scientific) following the microplate protocol. The working reagent was prepared by mixing 50 parts reagent A with 1 part reagent B. The bovine serum albumin (BSA) standard curve was prepared using the recommended dilutions as follows:

Table 2.3 – Dilution scheme for microplate protocol (working range 20-2,000 µg/mL)

Vial	Volume of diluent (1xPBS) (µL)	Volume and source of BSA (µL)	Final concentration (µg/mL)
A	0	300 of stock	2000
B	125	375 of stock	1500
C	325	325 of stock	1000
D	175	175 of vial B	750
E	325	325 of vial C	500
F	325	325 of vial E	250
G	325	325 of vial F	125
H	400	100 of vial G	25
I	400	0	0 = Blank

25 µL of each standard or sample was pipetted into a 96-well plate (Costar 96 flat transparent) in duplicate. 200 µL of working reagent was added to each well and the plate was mixed by tapping for 30 seconds. The plate was then covered and incubated at 37 °C for 30 minutes. The absorbance was read at 562 nm, as per the manufacturers protocol (Tecan Spark 10M, application SparkControl). To calculate the protein content of each sample, the blank reading was subtracted from each standard or sample. Absorbance was plotted against BSA concentration (R^2 >0.99), and the line gradient used to calculate sample protein content. Protein concentration was converted to µg/mg of pectin. The pectin concentration was 0.5% w/v or 5 mg/mL, therefore calculated values were divided by 5. The working range of the standard curve was converted from 25-2000 µg/mL to 5-400 µg/mg of pectin.

2.2.2. Fourier-transform infrared spectroscopy

Fourier-transform infrared spectroscopy (FTIR) was carried out using the Agilent Cary 630 FTIR Spectrophotometer. Solid samples were placed on the clean crystal and a full spectrum scan from 650-4000 cm^{-1} was carried out in attenuated total reflectance (ATR) mode. Results were plotted with the transmittance on the y-axis.

2.3. Pectin rheology

2.3.1. Qualitative pectin gelation screen

Pectin solutions were prepared at 2%, 1.5% or 1% w/v concentrations in dH_2O, 1xPBS or 0.9% NaCl. pH of 1xPBS and 0.9% NaCl pectin solutions were measured. Solutions were then split in half, and half were adjusted to pH 7.4 with 0.1 M NaOH. 50 µL of each solution was pipetted onto a glass microscope slide with 10 µL of varying concentrations of $CaCl_2$ solution on to induce gelation. Gel strength was physically assessed using a pipette tip and inversion, then scored on a scale of 0 to 5, as follows:

0 = No gel

1 = Increased viscosity, no gel formed

2 = Some gelation but will not hold shape

3 = Weak gel

4 = Soft gel

5 = Firm gel

The effect of different diluents and pH on gel strength were also assessed. Pectin solutions were then sprayed using the MAD sprayer onto microscope slides with 10 µL $CaCl_2$ on, and gel strength was assessed and scored again.

The concentrations of calcium chloride solutions were as follows and corresponds to a final calcium concentration as stated.

Table 2.4 – Calcium chloride concentrations in solution and in pectin gels.

Calcium chloride solution concentration (mM)	Final calcium chloride concentration after pectin addition (mM)
1	0.17
2	0.33
5	0.83
10	1.67
25	4.17
50	8.33

2.3.2. Viscosity

The cone and plate measurement system were used on the Anton Paar Modular Compact Rheometer 302. The plate was set to 25 °C for measurements, and a 25 mm cone used (part #79038, serial #12205, 24.972 mm diameter, angle 1.002 °).

25 readings were taken with measurement times ranging from 1-25 s. These measurement times increased logarithmically. The measurement gap between the plate and cone was set to 0.051 mm. RheoCompass™ software was used to set the measurement parameters and record data. Pectin solutions were prepared in 1xPBS and adjusted to approximately pH 7.4 at 1% w/v.

2.3.3. Amplitude sweep

The parallel plate measurement system was used on the Anton Paar Modular Compact Rheometer 302. The plate was set to 37 °C for measurements and gel preparation. 25 mm parallel plate was used (part #79044, serial #37100, diameter 24.981 mm). Measurements were set to ramp logarithmically from 0.01% to 100% strain with 25 measurements recorded at a frequency of 10 rad/s. The measurement gap was set to 0.525 mm.

Before measurements, gels were formed on the plate by adding 60 µL of 50 mM $CaCl_2$ solution and spreading it to cover the entire measurement area. Next, 300 µL pectin solutions were added (final concentration of 1% w/v dissolved in 1xPBS, $CaCl_2$ concentration following pectin addition was 8.33 mM). Parallel plates were moved to the set measurement gap and a 3-minute hold preceded measurements to equilibrate gel temperature.

2.3.4. Young's modulus measurement

Young's modulus was measured using the texture analyser (Trevor, TA HD+, Stable Microsystems). Pre-test speed was set to 2 mm/s, with the trigger force set to 0.25 N. The test speed was 0.5 mm/s, and the target was 50% strain.

2.4. Cell culture and passaging

2.4.1. NIH 3T3 mouse fibroblasts

NIH 3T3 mouse fibroblasts were cultured in Dulbecco's Modified Eagle Medium (DMEM) supplemented with 10% foetal bovine serum (FBS) and 1% antibiotic/antimycotic. Cells were incubated at 37 °C with 5% CO_2 in T75 tissue culture treated flasks.

Cells were passaged when they reached approximately 80% confluency. Media was removed, cells were washed with 1xPBS and 3 mL trypsin/EDTA (TE) was added to remove cells from the flask. Cells were incubated for 5 minutes at 37 °C, before neutralising TE with 7 mL media. The cell suspension was transferred to a 15 mL falcon tube and spun at 200 xg for 5 minutes. Supernatant was removed and the pellet was resuspended in 10 mL fresh media. 1 mL of the cell suspension was transferred into a new T75 flask containing 9 mL of pre-warmed media for a 1:10 split. This was carried out every 3-4 days.

2.4.2. SH-SY5Y human neuroblastoma cells

SH-SY5Y human neuroblastoma cells were cultured in Minimum Essential Media (MEM):Ham's F12 Nutrient Mix (1:1) supplemented with 10% FBS, 1% non-essential amino acids, and 1% antibiotic/antimycotic. Cells were incubated at 37 °C with 5% CO_2 in T75/T225 tissue culture treated flasks.

Cells were passaged when they reached approximately 80-90% confluency. Media was removed, cells were washed with 1xPBS and 3 mL trypsin/EDTA (TE) was added to remove cells from the flask. Cells were incubated for 3 minutes at 37 °C, before neutralising TE with 7 mL media. The cell suspension was transferred to a 15 mL falcon tube and spun at 200 xg for 3 minutes. Supernatant was removed and the pellet was resuspended in 10 mL fresh media. 1 mL of the cell suspension was transferred into a new T75 flask containing 9 mL of pre-warmed media for a 1:10 split. This was carried out every 7 days.

2.4.3. Human mesenchymal stem cells

Mesenchymal stem cells were purchased from Lonza and supplied at passage 2. Biological repeats in experiments were carried out using three separate human

cell donors of different ages and sex. Cell donor information supplied by Lonza is shown in Table 2.5.

Table 2.5 – Donor number, age, and sex of donors of hMSCs.

Donor number:	Age:	Sex:
26000	20	Male
27519	21	Female
33357	28	Male

Cells were thawed into the MSCGM™ Mesenchymal Stem Cell Growth Medium BulletKit™ from Lonza, containing foetal bovine serum, L-Glutamine, and gentamycin (GA-1000). To thaw the MSCs, 10 mL basal media was added to a T75 flask and allowed to reach 37 °C in the incubator for 30 minutes. The vial of cells, containing >750,000 cells, was removed from liquid nitrogen and rapidly thawed in the water bath set to 37 °C. When only a sliver of ice remained in the vial, the outside was wiped down with 70% IMS and the entire contents was added to the pre-warmed flask of media. The cells were incubated at 37 °C with 5% CO_2 in T75 tissue culture treated flasks. The media was changed after 24-hours to remove any residual freezing media. A cell stock was prepared at passage 3 when cells reached 90% confluency. For subsequent culture, PromoCell Mesenchymal Stem Cell Growth Medium 2 was used.

Cells were passaged when they reached approximately 80% confluency. Media was removed, cells were washed with 1xPBS and 3 mL trypsin/EDTA (TE) or 3 mL Accutase was added to remove cells from the flask. Cells were incubated for 5 minutes at 37 °C before checking cells were detached. If cells were >90% detached, TE was neutralised with 7 mL media. If cells were <90% detached, they were left for a further 3 minutes before checking again. This was repeated until >90% cells were detached but the total time cells were in contact with TE did not exceed 15 minutes. If using Accutase, once cells had detached, 7 mL 1xPBS was added to the flask to dilute. The cell suspension was transferred to a 15 mL falcon tube and spun at 450 xg for 5 minutes. Supernatant was removed and the pellet was resuspended in 2 mL fresh media. Cells were counted on a haemocytometer to determine cell density. Cells were then reseeded in a fresh T75 flask between 300,000-500,000 cells/mL. Media was changed every 2-3 days between passaging. Cells did not exceed passage 6 before use for syringing and spraying experiments.

Cell stocks were prepared by removing the supernatant from the cell pellet and adding freezing media. Freezing media was prepared by adding 10% DMSO to cell culture media. Cells were frozen at 300,000-500,000 cells per vial. After the addition of freezing media, vials were added to insulated freezer containers and placed in a -80 °C freezer for >24 hours, before adding the cells to the liquid nitrogen storage.

2.5. Cell counting and health/viability testing

2.5.1. Cell counting

Cell density was calculated following counting using a haemocytometer. 10 µL of cells were loaded under the coverslip on a haemocytometer. Cells were counted in the four corner sections and the following formula used to calculate approximate cell density:

$$Cell\ density\ (cells/mL) = \frac{total\ cell\ count}{4} \times 10{,}000$$

2.5.2. PrestoBlue metabolic activity assay

PrestoBlue (Invitrogen, ThermoFisher Scientific) metabolic activity assays were carried out according to the manufacturers protocol. 10x PrestoBlue solution was diluted 1:10 PrestoBlue:media. Media was then removed from test wells, and diluted PrestoBlue added, including a blank well containing no cells.

Plates were incubated for approximately 60 minutes at 37 °C. After incubation, a minimum of 75 µL of media was transferred in triplicate to black 96-well plates (Costar 96 Flat Bottom Black Polystyrene Cat. No.: 3991/3650/3916/3915/3925) for fluorescence reading (Tecan infinite 200Pro plate reader), excitation 550 nm, emission 590 nm.

The average relative fluorescent unit (RFU) readings for no-cell (media) control wells were subtracted from test well values. Values were then normalised to the untreated control wells using the following calculation to work out the metabolic activity as a percentage of the controls:

$$Metabolic\ activity\ \% = \frac{Test\ well\ RFU}{Untreated\ control\ well\ RFU} \times 100$$

The PrestoBlue assay is not a true measure of viability, instead being an indirect indicator based on the metabolic activity of the treatment cells compared to the control cells. PrestoBlue is a resazurin based dye. When cells are metabolically active, as they are when still alive, they are able to reduce the dye, causing the following reaction:

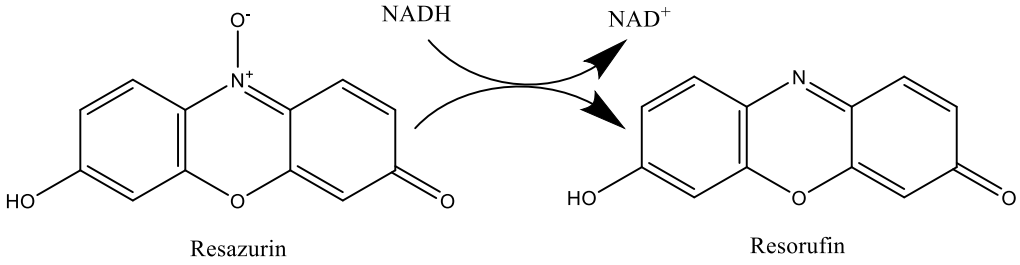


Figure 2.1 – The reduction of resazurin to resorufin, the vital dye found in PrestoBlue.

Resorufin is fluorescent and can therefore be measured and quantified. The metabolic activity can be calculated as a relative percentage of the control and indicates the health of the cells.

2.5.3. Lactate dehydrogenase (LDH) assay

CyQUANT™ LDH Cytotoxicity Assay (Invitrogen, ThermoFisher Scientific) was carried out according to the manufacturers protocol. Cells were plated as follows in triplicate: spontaneous LDH activity cells were left untreated to measure the spontaneous release of LDH from cells. Maximum LDH activity cells were incubated overnight, then 10x lysis buffer to well 45 minutes before sampling wells for assay (10 µL to 100 µL well volume). The treated sample wells were the test cells, either sprayed into the wells, or treated with pectin gels.

At the desired timepoint, 50 µL was transferred into 96-well flat-bottomed plates. 50 µL of the Reaction Mixture (containing the reaction components shown in Figure 2.2) was added to each sample, and the plate incubated at room temperature for 30 minutes protected from the light. 50 µL of Stop Solution (containing acetic acid) was then added and the absorbance measured at 490 nm and 680 nm.

If LDH is present, the following reaction will occur to form formazan.

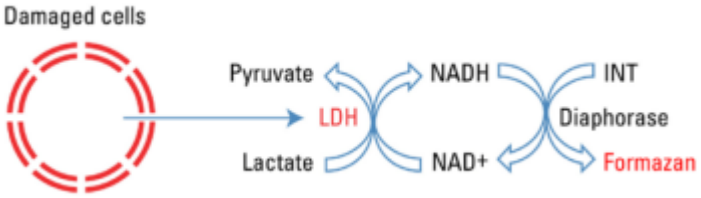


Figure 2.2 – Schematic of the reaction taking place in the presence of LDH (Invitrogen, 2023).

The LDH activity was determined by subtracting the 680 nm absorbance reading from the 490 nm reading for each sample. The % cytotoxicity was calculated using the following formula:

$$\%\ cytotoxicity\ = \frac{Treated\ sample\ well - Spontaneous\ LDH\ activity}{Maximum\ LDH\ activity - Spontaneous\ LDH\ activity} \times 100$$

2.5.4. Live/Dead staining

Live/Dead staining of cells was carried out using the LIVE/DEAD Viability/Cytotoxicity Kit for Mammalian Cells (Invitrogen, ThermoFisher). Stain was prepared by adding calcein AM at a dilution of 1/5000, and ethidium homodimer-1 at a dilution of 1/1000 to DPBS. NucBlue™ Live ReadyProbes™ Reagent (Hoechst 33342) (ThermoFisher) was also added at a concentration of 1 drop per mL to stain DNA. The plate of cells being analysed was then spun down at 100 xg for 1 minute, and the media carefully removed to retain detached dead cells. Stain was then added to wells at an equal volume to the volume of media (eg. 100 µL per well in 96-well plate). The plate was incubated at room temperature for 10 minutes before imaging.

2.6. Imaging and image analysis using FIJI

An image of a representative area of the well was taken on the 4x magnification lens using brightfield, and the DAPI, GFP, and Tomato fluorescent channels. Exposure time was kept constant whilst imaging.

The number of dead cells and total cells (based on DNA stain) was analysed using FIJI (Schindelin *et al.*, 2012). Images were opened in separate channels. The image background was subtracted: Process>Subtract background>rolling ball radius = 50 pixels>OK. The image was adjusted to set the threshold: Image>Adjust>Threshold left threshold set to between 20-30. The cell number

(dead and total cells) was then calculated: Analyze>Analyze particles> size 0-infinity, circularity 0-1, select Display results, Clear results, and Summarize. The number of particles were then transcribed into an Excel workbook. Live cell counts were not recorded in 2D cultures if many of the cells were touching. Live cell number would be calculated based on the total number of cells minus the number of dead cells.

2.7. Cytotoxicity testing

Extraction and direct cytotoxicity tests were carried out using the international standard for biological evaluation of medical devices, ISO 10993-5 and -12, as a guide. The standards do not fit perfectly with testing hydrogel materials, but the protocol was adapted and followed as closely as possible. Volume ratios were calculated in line with section 10.3.3. table 1 (found in ISO 10993-12), irregularly shaped solids. The table states 0.2 g of material is used per mL for extraction media. For direct testing, the material should cover approximately 10% of the surface area of the cells. Cells used were the SH-SY5Y human neuroblastoma cell line, maintained and seeded as described in 2.4.2.

2.7.1. Extraction test

Pectin gels were prepared by adding 10 µL of 25, 50 or 100 mM $CaCl_2$ into 24-well plates, followed by 100 µL of 1% w/v pectin solutions (final $CaCl_2$ concentrations after pectin addition were 2.27, 4.55, or 9.09 mM). This gave gels with approximate mass of 100 mg. To these, 500 µL of SH-SY5Y cell culture media was added and plates were incubated for 24 hours at 37 °C to form the extraction test media.

SH-SY5Y cells were seeded into 48-well plates at a density of 50,000 cells/mL (25,000 cells/well) and allowed to grow for 24 hours.

After 24 hours, media was replaced with either fresh complete media, extraction test media, or media containing 50% DMSO or 5% triton-X. This was left on the cells for 24 hours before carrying out a PrestoBlue assay to determine the metabolic activity of the test wells.

2.7.2. Direct test

SH-SY5Y cells were seeded into 12-well plates (growth surface area 3.5 cm^2) at a density of 50,000 cells/mL and allowed to grow for 24 hours.

Pectin gels were prepared by adding 10 µL of 25, 50 or 100 mM $CaCl_2$ into 96-well plates (final $CaCl_2$ concentrations after pectin addition were 2.27, 4.55, or 9.09 mM), followed by 100 µL of 1% w/v pectin solutions to give gels with approximately 0.32 cm^2 base surface area (approximately 10% of the growth surface area of the 12-well plates). These were placed into wells containing cells and incubated for 24 hours before carrying out a PrestoBlue assay to determine the metabolic activity of the test wells.

2.8. Cell spraying

The Mucosal Atomisation Device (Teleflex) attached to a 1 mL syringe (Henke Sass Wolf) was used for cell spraying experiments. The nasal shield was removed as it was not required. The device set-up was as follows:



Figure 2.3 – The MAD spray device (Teleflex) with the nasal shield removed, attached to a 1 mL syringe (Henke Sass Wolf).

For experiments using cells, the device was cleaned using 1% distel initially, followed by 70% IMS. The device was stored in a sterile container between experiments. Before starting work, 5 mL 70% IMS was sprayed through the device, followed by 5 mL 1xPBS. Between conditions in an experiment, 3 mL 1xPBS was sprayed through the device to clear any residual cells.

2.8.1. Cells in media/PBS

Cells for spraying were detached from flasks using the same method as passaging above (2.4). Cell density was determined using a haemocytometer, and cell suspensions of desired density were prepared in media or 1xPBS. The desired volume of cell suspension was sprayed into the wells using the syringe, and spraying was carried out from the top edge of the well to keep spraying

height consistent. The spraying speed was approximately 4 seconds per mL. Control wells were included in experiments by adding cell suspensions to wells by syringe. Basal growth media was added to wells in equal volume to the cell volume (e.g., 500 µL cell suspension + 500 µL basal growth media) Plates were incubated at 37 °C with 5% CO_2 for desired length of time before determining metabolic activity by PrestoBlue assay, LDH assay and/or Live/Dead staining.

2.8.2. Cells in pectin

Pectin solutions were prepared by dissolving 1% w/v of pure lyophilised pectin (formed following protocol in 0) in 1xPBS on a heated magnetic stirrer plate set at 70 °C. Solutions were stirred for a minimum amount of time for solids to completely dissolve. Solutions were cooled and the pH adjusted to 7.4 using 0.1 M NaOH. Pectin solutions were passed through a 0.22 µm syringe filter in a class II microbiological safety cabinet before use. $CaCl_2$ solutions were also passed through a 0.22 µm syringe filter before use.

Cells were detached using trypsin or Accutase (for hMSCs), spun down and the pellet resuspended in 1 mL of 1xPBS. Cells were then counted using a haemocytometer (2.5.1). This cell suspension was then used to prepare the pectin and cell suspensions at the desired densities.

$CaCl_2$ solutions were added to well plates at 10% of the volume of pectin desired (e.g., 10 µL $CaCl_2$ with 100 µL pectin used). Following the addition of pectin, media was carefully added to wells. Media was added to pectin in a 1:1 ratio. Cells were left for the desired length of time before carrying out further experiments.

2.9. Cell retention within spray device

To determine whether cells would be trapped within the spray device, SH-SY5Y cell suspensions were prepared as previously described at a density of 100,000 or 200,000 cells/mL. These were then sprayed, syringed, or pipetted into 1.7 mL tubes. They were counted immediately after using a haemocytometer. Three repeats were carried out in triplicate.

2.10. Flow cytometry

Flow cytometry was carried out to determine whether hMSC were still positive for CD90, CD105, and CD73, and negative for CD34, CD11b, CD19, CD45, and HLA-DR, as they should be to be classed as MSCs (Dominici *et al.*, 2006). Flow cytometry is carried out by adding fluorescently labelled antibodies specific to the cell surface proteins of interest. If the surface markers are present on the cells, the antibodies bind, and the fluorescent label detected by the flow cytometer. Blank cells are tested to determine whether the cells have any level of autofluorescence at the wavelengths tested. Isotype controls are also run and used for later analysis. The isotype controls are antibodies which are fluorescently labelled with the relevant fluorophore, but which will not bind to the cells. This is used to determine the level of non-specific binding to the cells.

Cells were prepared for flow cytometry by spraying in 1xPBS, syringing in 1xPBS, spraying in pectin, or syringing in pectin as previously described at a density of 100,000 cells/mL (2.8). 12-well plates were used. Cells were left for 24 hours before being detached and suspended in 1xPBS. For those cells being grown in pectin, 1xPBS pH 7.4 was used to dissolve the pectin. This was carried out by adding 500 µL 1xPBS, pipetting up and down 5 times to disrupt the gel structure. Liquid was removed and added to a 50 mL falcon tube with a 70 µm cell strainer on top. 500 µL 1xPBS was added to the well and pipetted up and down 3 times to disrupt any remaining gel structure and to wash the well. This was added to the falcon tube. 250 µL Accutase was added to the wells to remove any adherent cells. This was incubated for 5 minutes, then 500 µL 1xPBS added to the well, then all liquid removed and added to the falcon tube. Wells were checked for any remaining cells and the process repeated if needed. Cells were then spun at 300 xg for 5 minutes, supernatant removed, and the cell pellet was resuspended in BD Pharmingen™ Stain Buffer (Cat. No. 554656).

500 µL of cell suspension was added to each flow cytometry tube. The human MSC analysis kit from BD Biosciences (Cat. No. 562245) was used containing fluorescently labelled antibodies to the cell surface markers of interest. The cocktail contents are outlined below.

Table 2.6 – The antibody contents in each vial and the fluorophore each antibody is labelled with. All isotype antibodies are mouse and not specific to the desired surface markers. All positive and negative cocktail antibodies are mouse antibodies raised against the human surface markers listed.

BD hMSC kit vial description:	Antibody contents (antibody specificity, fluorophore)
hMSC Positive Isotype Control Cocktail	mIgG1, κ FITC mIgG1, κ PerCP-Cy5.5 mIgG1, κ APC
PE hMSC Negative Isotype Control Cocktail	mIgG1, κ PE mIgG2a, κ PE
hMSC Positive Cocktail	CD90, FITC CD105, PerCP-Cy5.5 CD73, APC
PE hMSC Negative Cocktail	CD34, PE CD11b, PE CD19, PE CD45, PE HLA-DR, PE

Cell samples and stains were added as follows:

Table 2.7 – Cell samples and the fluorescently labelled antibody added. DAPI was added to all flow cytometry tubes containing the hMSC positive/negative cocktails.

Cell sample	BD hMSC kit vial/antibody added to the flow cytometry tube with the cell sample (antibody specificity, fluorophore)	Volume of fluorophore labelled antibody
PBS syringe	CD90, FITC	5 µL
	CD44, PE	5 µL
	CD105, PerCP-Cy™5.5	5 µL
	CD73, APC	5 µL
	Blank	0 µL
	hMSC Positive Isotype Control Cocktail PE hMSC Negative Isotype Control Cocktail	10 µL
	hMSC Positive Cocktail PE hMSC Negative Cocktail	10 µL
PBS spray	hMSC Positive Isotype Control Cocktail PE hMSC Negative Isotype Control Cocktail	10 µL
	hMSC Positive Cocktail PE hMSC Negative Cocktail	10 µL
CU-701 syringe	hMSC Positive Isotype Control Cocktail	10 µL

	PE hMSC Negative Isotype Control Cocktail	
	hMSC Positive Cocktail PE hMSC Negative Cocktail	10 µL
CU-701 spray	hMSC Positive Isotype Control Cocktail PE hMSC Negative Isotype Control Cocktail	10 µL
	hMSC Positive Cocktail PE hMSC Negative Cocktail	10 µL
CU-L syringe	hMSC Positive Isotype Control Cocktail PE hMSC Negative Isotype Control Cocktail	10 µL
	hMSC Positive Cocktail PE hMSC Negative Cocktail	10 µL
CU-L spray	hMSC Positive Isotype Control Cocktail PE hMSC Negative Isotype Control Cocktail	10 µL
	hMSC Positive Cocktail PE hMSC Negative Cocktail	10 µL
LM-102 syringe	hMSC Positive Isotype Control Cocktail PE hMSC Negative Isotype Control Cocktail	10 µL
	hMSC Positive Cocktail PE hMSC Negative Cocktail	10 µL
LM-102 spray	hMSC Positive Isotype Control Cocktail PE hMSC Negative Isotype Control Cocktail	10 µL
	hMSC Positive Cocktail PE hMSC Negative Cocktail	10 µL
LM-104 syringe	hMSC Positive Isotype Control Cocktail PE hMSC Negative Isotype Control Cocktail	10 µL
	hMSC Positive Cocktail PE hMSC Negative Cocktail	10 µL
LM-104 spray	hMSC Positive Isotype Control Cocktail PE hMSC Negative Isotype Control Cocktail	10 µL
	hMSC Positive Cocktail PE hMSC Negative Cocktail	10 µL

The PBS syringe samples were used as the controls. For the analysis, compensation controls were set up by Dr David Onion in the flow cytometry

suite in the Queens Medical Centre at the University of Nottingham. Compensation control parameters are required when using multiple fluorophores in one cell sample, as is the case when using the positive and negative cocktails in the BD hMSC analysis kit. When set up correctly, the compensation will correct for any fluorescence being detected in any of the channels other than the intended one, so there is no interference from the other fluorophores (Roederer, 2002).

CytoFLEX S flow cytometer was set up to record 10,000 events within the gated parameters (single cell events), or run for 90 seconds, which ever came sooner.

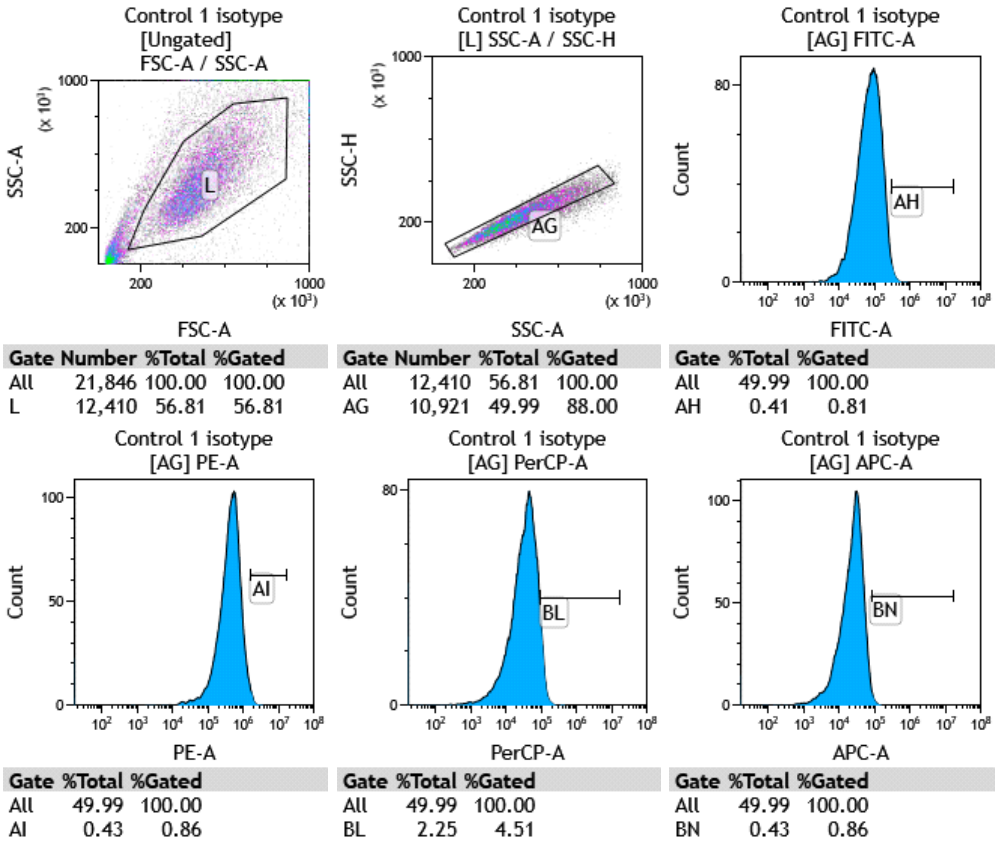


Figure 2.4 – Kaluza analysis gating shown using the PBS syringe isotype sample for hMSC donor #26000, which should be negative for each fluorophore with non-specific antibodies. The first gate selects for cells and eliminates debris using the forward (FSC) vs side (SSC) scatter plot. The second selects for single cell events, eliminating any doublet or triplet cells. The subsequent gates (one for each fluorophore detector FITC, PE, PerCP, and APC) were set against the negative population of cells to select for the positive population if it were present in the cocktail samples. These gates were copy and pasted onto the cell samples containing the specific antibody cocktails.

Data analysis was carried out using the Kaluza software (Beckman Coulter). The graphs showing an example of the gating protocol is shown in Figure 2.4. Gates were first set on the forward scatter-area (FSC-A) vs side scatter-area (SSC-A) plot to select for cells and disregard debris. From that, gates were set on the SSC-A vs SSC-H plot to select for single cell events. This gate was then used to set the gate to select for DAPI negative only, if applicable. Using this gate for live, single cells only, histograms showing the marker vs the cell count were set for the isotype control samples. Using these, gates were set as follows:

CD90 FITC: >0.8%, <1%

CD105 PerCP-Cy5.5: >4.5%, <5%

APC CD73: >0.8%, <1%

PE negative cocktail: >0.8%, <1%

The gates set for each marker on the isotype control samples from the PBS syringe cells were then copy and pasted onto the histograms for the positive and negative cocktail samples for each marker to identify the population positive for each. The isotype control samples for each pectin cell condition were not used to set gates to maintain consistency.

2.11. hMSC differentiation

The hMSC differentiation study was carried out to determine whether hMSCs retain their capacity to differentiate into osteogenic and adipogenic cells following spraying in 1xPBS and pectin. It was also carried out to determine whether cells spontaneously differentiate following spraying in 1xPBS and pectin. Each condition was carried out in duplicate, and two cell donors were used (#33357 and #27519) (N=2, n=2).

Cells were prepared for the differentiation study by spraying in 1xPBS, syringing in 1xPBS, spraying in pectin, or syringing in pectin as previously described at a density of 100,000 cells/mL (2.8). 12-well plates were used. Cells were left for 24 hours before being detached and suspended in 1xPBS. For those cells being grown in pectin, 1xPBS pH 7.4 was used to dissolve the pectin. This was carried out by adding 500 µL 1xPBS, pipetting up and down 5 times to disrupt the gel

structure. Liquid was removed and added to a 50 mL falcon tube with a 70 µm cell strainer on top. 500 µL 1xPBS was added to the well and pipetted up and down 3 times to disrupt any remaining gel structure and to wash the well. This was added to the falcon tube. TE was used to remove any remaining adherent cells.

For cells grown in 1xPBS, TE was used to detach adherent cells. Media was removed, wells washed with 1xPBS, then TE added until cells detached (maximum 15 minutes).

Cell suspensions obtained from each condition were used to seed plates for the differentiation study. 20,000 cells/well were seeded in 24 well plates. Cells were allowed to grow for 48 hours in basal growth media, before media was changed for control or differentiation media.

For the wells testing for spontaneous differentiation, hMSC basal growth media (Lonza) was used. For the wells testing for differentiation, adipogenic or osteogenic differentiation media (PromoCell) was used. Media was changed every 3-4 days for 14 days.

Staining and imaging were carried out by Dr I-Ning Lee, RMCT division, School of Pharmacy, University of Nottingham:

> On the 14th day, the wells testing for spontaneous or induced osteogenic differentiation were fixed with 4% PFA for 30 minutes at room temperature. These were washed with dH_2O, then 1% Alizarin Red S stain was added for 30 minutes. Wells were then washed with dH_2O and imaged.
>
> The wells testing for induced or spontaneous adipogenic differentiation were fixed with 4% PFA for 30 minutes at room temperature. These were washed with 60% isopropanol and left to dry. Oil Red O stain was then added for 10 minutes. Wells were then washed with dH_2O and counterstained for 5 minutes in haematoxylin. Wells were washed with dH_2O and imaged.

2.12. Transcriptome analysis

2.12.1. Sample preparation

hMSCs were prepared for RNA extraction by spraying in 1xPBS, syringing in 1xPBS, spraying in CU-701 pectin, or syringing in CU-701 pectin as previously described. 12-well plates were used, and cells were seeded at 100,000 cells/mL. Cells were left for 24 hours before being detached and suspended in 1xPBS. For those cells being grown in pectin, TE was added to chelate Ca^{2+} and detach cells. This was carried out by adding 500 µL TE, pipetting up and down 5 times to disrupt the gel structure. Liquid was removed and added to a 50 mL falcon tube with a 70 µm cell strainer on top. 500 µL 1xPBS was added to the well and pipetted up and down 3 times to disrupt any remaining gel structure and to wash the well. This was added to the falcon tube. 250 µL Accutase was added to the wells to remove any adherent cells. This was incubated for 5 minutes, then 500 µL 1xPBS added to the well, then all liquid removed and added to the falcon tube. Wells were checked for any remaining cells and the process repeated if needed. Cells were then spun at 300 xg for 5 minutes, supernatant removed. The cell pellet for cells grown without pellet was then placed on ice. The pellet obtained from cells grown in pectin was resuspended in 1xPBS, then spun again at 300 xg for 5 minutes to wash residual pectin off the cells. The supernatant was then removed, and the tube placed on ice. This was repeated three times using a separate donor each time.

2.12.2. RNA extraction

RNA extraction was carried out using the Qiagen RNeasy® mini kit following the manufacturers protocol. 350 µL lysis buffer (buffer RLT) was added to the cell pellets. This was pipetted up and down to homogenise, then transferred to a gDNA eliminator spin column. This was spun for 30s at 9,000 xg. 350 µL 70% ethanol was added to the flow through, and the total volume was added to a RNeasy spin column in a collection tube. This was spun for 15s at 9,000 xg. Flow through was discarded and 700 µL of buffer RW1 (wash buffer) was added. This was spun and the flow through discarded. 500 µL buffer RPE was added, spun for 15s at 9,000 xg, flow through discarded. 500 µL buffer RPE was added again, spun for 2 minutes at 9,000 xg, flow through discarded. The RNeasy spin

column was transferred to a clean collection tube and spun again for 1 minute at 9,000 xg. The spin column was then transferred to a clean 1.5 mL collection tube. 30 µL of nuclease free dH_2O was added, left for 1 minute, then spun for 1 minute at 9,000 xg to elute the RNA. The concentration of RNA was measured using the NanoDrop™ (ThermoFisher Scientific) blanked with the same water used to elute the RNA.

2.12.3. RNA library preparation and sequencing

Quality assurance, RNA library preparation, sequencing, and differential gene expression analysis was carried out by the DeepSeq department located in the Queens Medical Centre at the University of Nottingham. Their protocol is as follows:

> The Qubit Fluorometer and Qubit RNA BR assay kit (ThermoFisher Scientific, Q10211) were used to determine RNA concentration. The Agilent TapeStation 4200 and Agilent RNA ScreenTape Assay Kit (Agilent, 5067-5576 and 5067-5577) was used to determine the RNA integrity number. 100 ng of extracted RNA was then used to make a cDNA library for sequencing using the QuantSeq 3' mRNA-Seq library prep kit for Illumina (FWD) (Lexogen, 015.96). These were indexed using the Lexogen i7 6nt Index Set (Lexogen, P04496). 14 cycles of PCR were carried out for all samples.
>
> Libraries were quantified using the Qubit Fluorometer and the Qubit dsDNA HS Kit (ThermoFisher Scientific, Q32854). Library fragment-length distributions were analysed using the Agilent TapeStation 4200 and the Agilent High Sensitivity D1000 ScreenTape Assay (Agilent, 5067-5584 and 5067-5585).
>
> Libraries were pooled in equimolar amounts and final library quantification was performed using the KAPA Library Quantification Kit for Illumina (Roche, KK4824). Library pool sequenced on the Illumina NextSeq 500 platform, on a NextSeq 500/550 Mid Output v2.5 150 cycle kit (Illumina, 20024904), to generate approximately 5 million 75bp single end reads per sample. Data was converted to FastQ format

using ‘bcl2fastq2’, part of the Illumina Secondary Analysis Software (v1.37.0).

All data analysis was performed using the Lexogen QuantSeq workflow; a pipeline developed specifically for data generated from the QuantSeq 3’ mRNA-Seq library prep kit for Illumina (FWD). The workflow is as follows:

During the Lexogen QuantSeq workflow, raw reads were trimmed of polyA tails and Illumina NextSeq adapters using Cutadapt (Martin, 2011). Resulting fragments of <20 bp were removed. Trimmed reads were aligned to the human reference genome (Homo sapiens GRCh38_emsembl_release_107_ERCC_SIRV) using the STAR aligner (Dobin *et al.*, 2013). Aligned reads were passed to ‘featureCounts’ (Liao *et al.*, 2014) in order to classify and count each alignment against the reference, using the appropriate annotation data.

For differential gene analysis, comparisons were drawn between the various contrasts specified above and analysed using the ‘R’ package ‘DESeq2’, (Love *et al.*, 2014). Each contrast was assessed for significantly differentially expressed genes (adjusted p-value <0.1).

Differential gene expression analysis carried out using the following comparisons:

- PBS spray vs PBS syringe
- CU-701 spray vs CU-701 syringe
- CU-701 spray vs PBS spray
- CU-701 spray vs PBS syringe
- CU-701 syringe vs PBS spray
- CU-701 syringe vs PBS syringe

2.13. SH-SY5Y damage model optimisation – 96-well plate

SH-SY5Y human neuroblastoma cells were cultured as described above (2.4.2). Initial optimisation work was carried out in 96-well tissue culture treated polystyrene plates to minimise waste, with cells seeded at a density of 50,000 cells/mL (100 µL per well), equating to approximately 15,600 cells/cm^2. Cells were left to adhere for 12-24 hours before use.

The aim of the optimisation work was to find a concentration of glutamate and H_2O_2 which results in approximately a 50% reduction in metabolic activity of the population of cells. The aim was also to demonstrate that high concentrations of both glutamate and H_2O_2 can result in the death of the cell population, demonstrated by recording a lack of metabolic activity.

2.13.1. Excitotoxicity model

Glutamate spiked media at concentrations ranging from 10 – 400 mM were prepared from a 1 M glutamate stock prepared in SH-SY5Y complete media, which was filtered through a 0.22 µm syringe filter before use. Media was removed from the wells, and 100 µL of glutamate spiked media at various concentrations was added in triplicate. Plates were incubated with glutamate for 1 hour at 37 °C with 5% CO_2 before wells were gently washed with 1xPBS, and fresh complete media added. Plates were incubated for 24 hours, before carrying out a PrestoBlue assay to assess the extent of the damage. Metabolic activity was calculated as a percentage of the undamaged control, which underwent washing and media changes at the same timepoints without the presence of glutamate.

2.13.2. Oxidative stress model

Two time periods using hydrogen peroxide were investigated. Hydrogen peroxide spiked media was prepared from a 3% stock bottle. This was used to prepare a 100 mM stock in media, which was used to prepare H_2O_2 spiked media at various concentrations ranging from 10 – 1000 µM.

For the 1-hour model, H_2O_2 spiked media at various concentrations was added to wells in triplicate. Plates were incubated for 1 hour at 37 °C with 5% CO_2 before wells were gently washed with 1xPBS, and fresh complete media was added. Plates were incubated for 24 hours before carrying out a PrestoBlue

assay. Metabolic activity was calculated as a percentage of the undamaged control, which underwent washing and media changes at the same timepoints without the presence of H_2O_2.

For the 24-hour model, H_2O_2 spiked media at various concentrations was added to wells in triplicate. Plates were incubated for 24 hours at 37 °C with 5% CO_2, before carrying out a PrestoBlue assay. Metabolic activity was calculated as a percentage of the undamaged control, which underwent washing and media changes at the same timepoints without the presence of H_2O_2.

2.14. SH-SY5Y damage model optimisation – 24-well plate

SH-SY5Y human neuroblastoma cells were cultured as previously described. Cells were seeded at a density of 50,000 cells/mL. 600 µL were seeded per well in a 24-well plate to give approximately 15,700 cells/cm^2, to be comparable with the 96-well plate model development. Cells were left to adhere for 12-24 hours before use.

Further optimisation was required to determine whether the change in plate size from 96-well to 24-well would affect the metabolic activity measured by PrestoBlue in the wells with cells damaged at different concentrations of the damaging media. Well inserts for the co-culture model require the use of 24-well plates.

2.14.1. Excitotoxicity model

As before, 1 M stock prepared in SH-SY5Y complete media, which was filtered through a 0.22 µm syringe filter before use. Glutamate spiked media at concentrations ranging from 10-1000 mM were prepared from this. Damaging media was added in triplicate following the same protocol was followed as the 96-well plate optimisation, with metabolic activity once again calculated as a percentage of the undamaged control wells.

2.14.2. Oxidative stress model

As before, two time periods for the oxidative stress models were used. 100 mM H_2O_2 spiked media was prepared, and this was used to prepare H_2O_2 spiked media at various concentrations ranging from 10 – 400 µM. Damaging media

was added in triplicate following the same protocol as the 96-well plate optimisation for both the 1-hour and 24-hour models, with metabolic activity once again calculated as a percentage of the undamaged control wells.

2.15. SH-SY5Y damage model – effect of pectin gels alone

The excitotoxicity model and the two time periods for the oxidative stress model were used to test the effect of pectin hydrogels alone on damaged cells. Concentrations of damaging media were chosen to give approximately 50% loss of metabolic activity. For the excitotoxicity model, this was 250 mM glutamate. For the oxidative stress model, this was 25 µM H_2O_2 for both the 1-hour and 24-hour models. 1% w/v pectin solutions were used to form hydrogels. 100 µL gels were formed by adding pectin solutions to wells in a 96-well plate containing 10 µL of 100 mM $CaCl_2$ solution.

For the 1-hour models, damaging media was added, plates were incubated for 1 hour, media was then removed, wells gently washed with 1xPBS, and fresh media was added. Pectin hydrogels were then added, using a spatula to remove the gels from the 96-well plate. For the 24-hour model, pectin hydrogels were added immediately after the damaging media. Hydrogels were placed directly on the cells in culture. Plates were then incubated for 24 hours, before carrying out a PrestoBlue assay. Any remaining gel was removed from the wells, as well as media. This was replaced with 400 µL complete SH-SY5Y media containing 1x PrestoBlue. Plates were incubated for 1-2 hours before transferring media to a black 96-well plate for reading by fluorescence.

2.16. SH-SY5Y damage model – hMSC co-culture

As before, concentrations of damaging media were selected to give approximately a 50% reduction in metabolic activity: 250 mM glutamate and 25 µM H_2O_2.

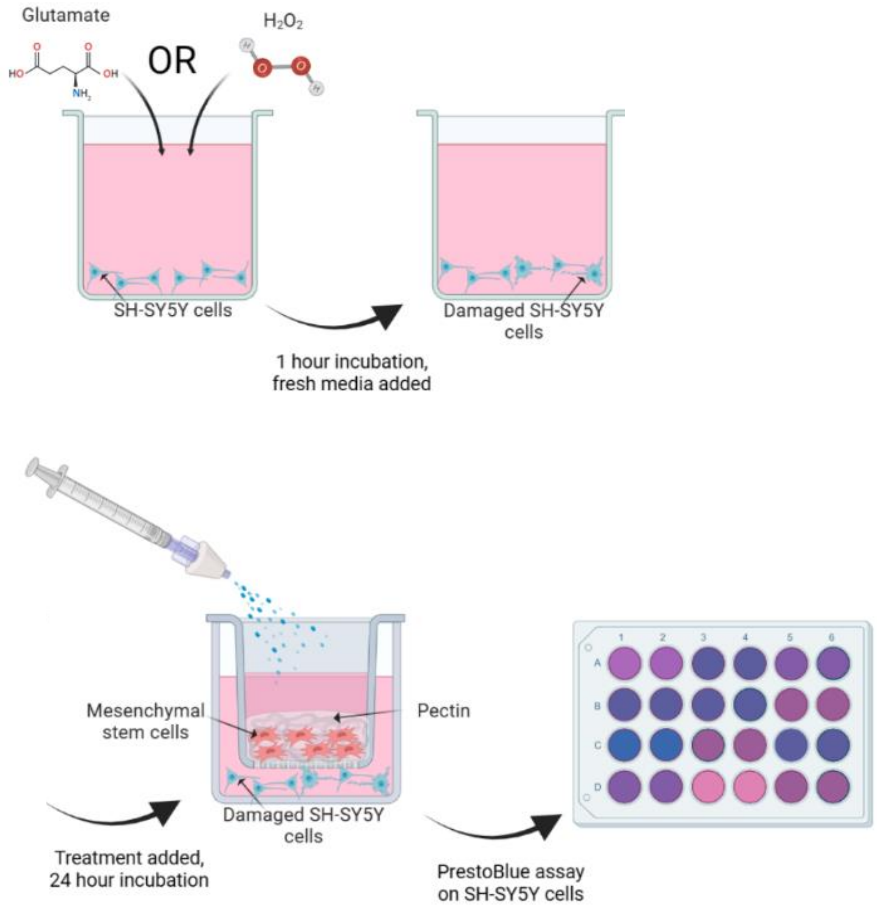


Figure 2.5 – Schematic showing the method used for the co-culture damage models which add the treatment after a 1-hour incubation with the glutamate or H_2O_2 spiked media. Plates are then incubated for 24-hours, before carrying out a PrestoBlue assay on the SH-SY5Y cells.

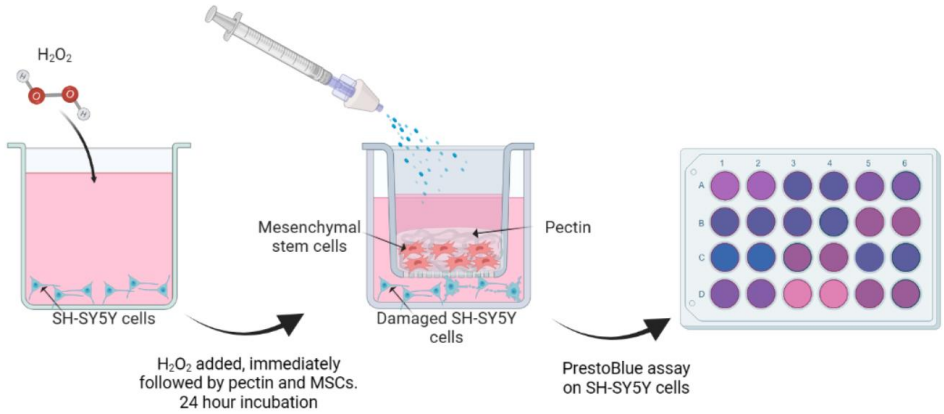


Figure 2.6 – Schematic showing the method used for the co-culture damage model which adds the treatments immediately after the addition of H_2O_2, followed by a 24-hour incubation. A PrestoBlue assay is then carried out on the SH-SY5Y cells.

Well inserts for 24-well plates were used with a surface area equivalent to that of a 96-well plate. hMSCs were prepared at a seeding density of 100,000 cells/mL, resulting in 10,000 cells/well. Well inserts had a pore size of 1 µm, chosen primarily due to stock availability, but to also guarantee cells would not migrate through to the wells containing SH-SY5Y cells. The following conditions were tested on damaged cells, all prepared in well inserts (all pectin conditions were gelled with 10 µL 100 mM $CaCl_2$ solution, which was added to well inserts first). After seeding cells, 100 µL media was added to each well. Pectin grades used described in Table 2.2.

Table 2.8 – Samples prepared and added to well inserts for the co-culture experiment. Syringe seeded method indicates cells are added to wells using a 1 mL syringe. Spray seeding method indicated cells are added to wells using a 1 mL syringe with the MAD sprayer attached (shown in Figure 2.3).

Condition ID	Cell suspension (100 µL)	Seeding method
hMSC media	Blank PBS	Syringe
hMSC syringed	PBS + hMSCs	Syringe
hMSC sprayed	PBS + hMSCs	Spray
CU-701 syringed	CU-701 + hMSCs	Syringe
CU-701 sprayed	CU-701 + hMSCs	Spray
LM-102 syringed	LM-102 + hMSCs	Syringe
LM-102 sprayed	LM-102 + hMSCs	Spray

Glial cell line-derived neurotrophic factor (GDNF) at a concentration of 50 ng/mL was also used as a positive control, as it has previously demonstrated efficacy against glutamate damage in SH-SY5Y cells (Wang *et al.*, 2016). All conditions were tested in duplicate. Experiments were carried out on three occasions using different cell donors for the hMSCs each time (N=3, n=2).

Cells were damaged as previously described. In the models requiring a 1-hour incubation, well inserts were prepared during the incubation and transferred into 24-well plates containing the damaged SH-SY5Y cells immediately after the addition of fresh media. In the 24-hour model plates, well inserts were prepared and added to wells immediately following the addition of H_2O_2 spiked media.

Plates were incubated for 24 hours, before carrying out a PrestoBlue assay to determine metabolic activity of cells. Well inserts were removed; media was removed and 400 µL complete media containing 1x PrestoBlue was added. Plates were incubated for 1-2 hours before media was transferred to a black 96-well plate for reading by fluorescence.

2.17. Statistical testing

In each experiment, three biological replicates were carried out, unless stated otherwise. Biological replicates in the case of cell lines were experiments carried out at different time points using cells at a different passage. Biological repeats (shown by N) in the case of the hMSCs were carried out using separate cell donors, details of which are shown in Table 2.5. Three technical repeats (shown by n) were carried out in each experiment, (unless stated otherwise) to allow for variability in the samples and measurements. The mean was calculated, and the mean of each biological repeat used to calculate statistical significance. Normal distribution for the data was assumed for all experiments. Ideally, more biological repeats would have been carried out to give more statistical power, but this was inhibited by cost of hMSCs from Lonza, and time constraints.

The flowchart from the Nishimura Lab group was initially used to guide the statistical test selection (Nishimura, 2023). The data obtained from the cell experiments was continuous (the data obtained can be any value, not only discrete values). When two groups were compared, a T-test was carried out. As cells for each condition of an experiment were from the same flask of cells, grown together in the same conditions, a paired T-test was selected. When there were multiple groups of paired samples, a multiple paired T-test was carried out. The P value for statistical significance was set to 0.05, and the Holm-Šídák method was used to correct for multiple comparisons (GraphPad, 2023a). When there were more than two test groups, a one-way ANOVA was carried out. A Dunnett's post-test is a test used to determine statistical significance between each experimental test group and a control condition by comparing the mean values of these groups (GraphPad, 2023b).

Chapter 3 Pectin characterisation

3.1. Introduction

As discussed in Chapter 1, pectin was selected due to previously demonstrated biocompatibility and mucoadhesive properties, including when delivered directly to the rat brain (McCrorie *et al.*, 2020). Low methoxyl pectin (LMP) forms a gel when it comes into contact with calcium ions (Gawkowska *et al.*, 2018), therefore, as calcium is found endogenously in the brain, pectin solutions containing cells could be sprayed as a liquid and gel *in situ*. Some studies have investigated the use of pectin for cell encapsulation (Munarin *et al.*, 2012b), including for use with hMSCs (Neves *et al.*, 2015), showing the cells remain viable when encapsulated.

3.1.1. Extraction

Pectin is extracted from the cell walls of fruits and vegetables. Pectin extracted from citrus peel and apple pomace has dominated the market since the 1940s and continues to be the most popular source of pectin today due to the ease and low cost of obtaining it from the waste of the juicing industry (Rodríguez Robledo and Castro Vázquez, 2020). Pectin is acidic, soluble in water, but insoluble in alcohol (Fremy, 1840); this forms the basis for extraction.

Chemical extraction of pectin using acid is the most common method and has been used since the early 1900s (Baker, 1935). It is carried out by treating the raw material with hot mineral acid (such as hydrochloric acid) at pH 2.0, filtering the extract and precipitating the crude pectin with alcohol. The precipitate is then washed, dried, and milled to produce a pectin powder (Rodríguez Robledo and Castro Vázquez, 2020). This process is outlined in Figure 3.1. Chemical extraction has been extensively used and researched, particularly for use in extracting citrus and apple pectin which make up >99% of the pectin market (Rodríguez Robledo and Castro Vázquez, 2020).

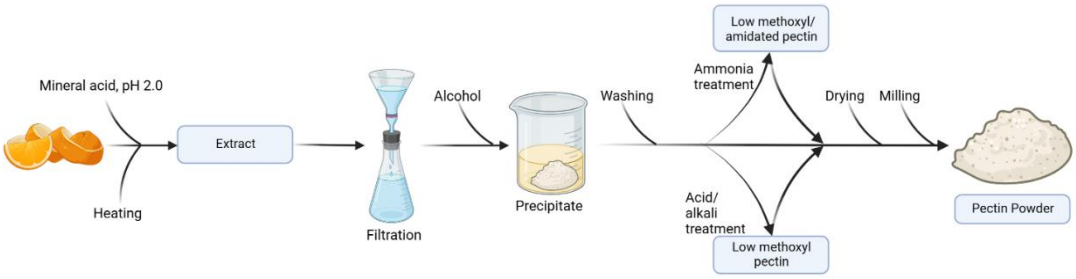


Figure 3.1 – A schematic showing the extraction process using hot mineral acid. Pectin obtained by this method typically has a degree of methylation (DM) of 70%, however de-esterification (defined as the removal of -CH_3 groups at the C6 position on GalA residues) can be carried out by acid or alkali treatment, or ammonia treatment to obtain an amidated LMP, indicated in the flow diagram.

Due to the strong acid and alcohol used in this process, pectin obtained should be free from contamination from microbes associated with the fruit from which it is obtained. However, following the drying and milling, pectin is not stored in sterile conditions or containers as the primary use of pectin is in the food and drink industry (Rodríguez Robledo and Castro Vázquez, 2020). As a result, purification and sterilisation methods require investigation for the use of pectin in cell delivery.

3.1.2. Pectin Purification

The use of pectin in the food and drink industry is extensively documented, as well as many uses in industry pharmaceutical, with interest increasing for the use of pectin in regenerative medicine (Lara-Espinoza *et al.*, 2018). For delivery to humans, materials must be sterile and free from contamination with antigenic substances such as proteins or endotoxins (Li and Boraschi, 2016). Endotoxins are released from the surface of bacterial cell walls in the form of lipopolysaccharides (LPS) and are known to cause inflammatory responses in cells (Weiss and Barker, 2018). Materials used as medical devices are required to have less than a specified endotoxin unit (EU) per mL; 0.5 EU/mL for general devices, and less than 0.06 EU/mL if that device or material will come into contact with cerebral spinal fluid (FDA, 2012).

One possible method of purification of pectin described by Munarin *et al.* (2011) involved three stages of ethanol washes: 10 g of pectin was washed in 100 mL of 50% ethanol for 30 minutes, filtered, rinsed with 75 mL of 50% ethanol, then

50 mL of 95% ethanol before being dried (Munarin *et al.*, 2011). No criteria for successful purification were described.

A second method described by Neves *et al.* (2015) used charcoal. This method was based on a patented purification method used for alginate (Bender, 2013). A pectin solution at 1% w/v was prepared in ultrapure water, and the pH adjusted to 6.0. 2% w/v activated charcoal was added and stirred for 1 hour at room temperature. The mix was centrifuged at 27,000 xg for 1 hour, supernatant removed, and the charcoal pellet discarded. The supernatant containing pectin was stirred for 30 minutes, centrifuged again at 27,000 xg for 1 hour, and then freeze dried. Protein concentration, endotoxin levels, and polyphenol quantification was carried out to validate the purification protocol, however no level was detailed on acceptable levels of these (Neves *et al.*, 2015).

3.1.3. Pectin gelation

Cross-linking of LMP occurs due to ionic interactions between the positive calcium ions and the negative charge on the carboxylic acid group on the pectin chains (Grant, 1973). Pectin is acidic, however for use in cell delivery, pectin solutions are required to have a physiological pH of 7.4 as any deviation from this can denature cellular proteins and lead to cell death (Mackenzie *et al.*, 1961). This adjustment in pH can alter the ionic charges found on the pectin chains, which has been shown to alter some of the hydrogel properties, such as calcium sensitivity and stiffness (Fraeye *et al.*, 2010).

Much of the research carried out on pectin involved dissolving it in water, however for use in tissue culture, the pectin solution is required to be isotonic to the cells. In some tissue engineering research, pectin is dissolved in 0.9% w/v NaCl solution (Neves *et al.*, 2015, Birch *et al.*, 2015, Gentilini *et al.*, 2018), or phosphate buffered saline solutions (1xPBS) (Takei *et al.*, 2010). Due to the presence of ions such as Na^+, it is feasible that some charge shielding, or charge interactions occur, which may cause premature gelation, precipitation, or no gelation.

3.1.4. Pectin functionalisation

Pectin has no sites within the structure for mammalian cells to adhere to. Therefore, the addition of a peptide for cells to recognise and bind to has been

investigated (Munarin *et al.*, 2011, Munarin *et al.*, 2012b). The sequence arginine-glycine-aspartate (RGD) is recognised by integrins and facilitates cell binding, therefore this ligand has been used in material functionalisation (Pierschbacher and Ruoslahti, 1984). There is limited work currently on the functionalisation of pectin and that work has been based on work to functionalise alginate by carbodiimide chemistry (Rowley *et al.*, 1999). They used the sequence GRGDY and showed cell adherence using mouse skeletal myoblasts.

Evangelista et al. (2007) investigated the differentiation of MC3T3-E1 cells into bone cells using a peptide sequence G_4RGDSP to functionalise alginate, using parameters outlined by Rowley et al. (1999). They showed that cells were more osteoblast-like when encapsulated in RGD-functionalised alginate, compared to unmodified alginate (Evangelista *et al.*, 2007). Like alginate, pectin is a polysaccharide which cross-links with divalent cations. It has carboxylic acid groups available for this cross-linking, but which can also be modified with carbodiimide chemistry. The reaction conditions used by Munarin *et al.* (2011) were again based on the work by Rowley *et al.* (1999). MC3T3-E1 cells were once again used and similar results were observed in terms of differentiation when compared to unfunctionalized pectin (Munarin *et al.*, 2011). These studies demonstrated cells could be encapsulated in pectin for tissue engineering. Neves *et al.* (2015) used RGD pectin to encapsulate mesenchymal stromal cells. Cells demonstrated an elongated phenotype in the RGD pectin, and whilst still viable, cells were rounded in the unfunctionalized pectin (Neves *et al.*, 2015).

3.1.5. Pectin viscosity & pectin gel mechanical strength – Rheological measurements

Rheology is the study of the flow of liquids and the deformation of solids (Mezger, 2014). Here, rheological measurements provide information on the viscoelastic properties of solids and the viscosity of liquids (Mezger, 2014).

Material viscosity will influence the suitability of the material for spraying. If a material is too viscous, it will not pass through a spray nozzle or it will cause cell death as increased viscosity of a solution is correlated with a lower cell viability when used to spray cells (Hendriks *et al.*, 2015). Therefore, it is important to understand the behaviour of the pectin solutions when subjected to the stress of spraying. Liquids can be broadly classed as Newtonian, or Non-

Newtonian. With the former, the viscosity remains unaltered by stress placed on it, and can be said to have no shear thinning or shear thickening properties. However, with Non-Newtonian fluids, the viscosity is dependent on the forces placed upon it and can either thicken (increase in viscosity) or thin (decrease in viscosity) in response to increased shear stress (Sedaghat, 2017). During the spraying process, the solution being sprayed will be subject to high shear stress upon leaving the spray device. To accurately determine the parameters for the rheological viscosity measurements, the shear stress should be calculated for the application of the material (Fernando *et al.*, 2000).

Rheological measurements can be used to give information on whether a material can be classed as a gel, and the gel properties. Amplitude sweeps can be carried out to determine the limit of the linear viscoelastic range (LVER) of a material and the point at which it is no longer a gel (Paar, 2023).

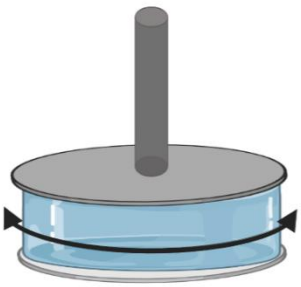


Figure 3.2 – Schematic showing the direction of force applied to hydrogel samples on a rheometer when carrying out amplitude sweep tests. Gel is shown in blue; schematic shows the parallel plate method.

For these tests, the frequency of the oscillation is kept constant, but the distance travelled by the upper plate increases, indicated by the arrows in Figure 3.2. The storage modulus (G′) is a measure of the deformation energy or elastic energy stored by the test material. The loss modulus (G″) is a measure of the deformation energy used by the test material when sheared and is a measure of the viscous properties of the material (Mezger, 2014).

If G′ > G″ then the material is considered to be a gel or solid. If G″ > G′ then the material is a liquid, and the point at which G′ = G″ is the gelation point, or the point at which the material changes state due to the strain applied on it (Stojkov *et al.*, 2021). The region plotted where G′ and G″ are parallel is considered the LVER. When the limit of the LVER is reached, G′ begins to decrease rapidly. This limit is essential when carrying out further tests, such as oscillatory tests,

however, for the purposes of this study, an amplitude sweep was carried out to confirm pectin forms a gel and to give an indication of the stiffness of the gels formed (Mezger, 2014).

Measuring the Young's modulus (E) involves placing tension or compressional stress on a material to determine the elastic properties and the point at which it permanently deforms, shown in Figure 3.3 (Britannica, 2022).

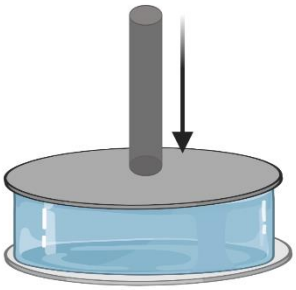


Figure 3.3 – Schematic showing the direction of force applied when testing the Young's modulus on a texture analyser by compressing the material until it breaks. Gel is shown in blue.

It is measured as E = stress/strain and provides information on how easily materials can be deformed or stretched. It is calculated by dividing stress by strain on the linear region on the plot from the texture analyser. Brittle materials tend to be able to withstand a lot of stress (are very strong) but will deform suddenly, whereas plastic materials will stretch, and therefore can withstand a higher strain before deforming.

In terms of characterising hydrogel materials for cell delivery purposes, measuring the G′, G″, and Young's modulus can be informative on whether a particular material will match the properties of the tissue/region of the body it is intended for, and to confirm gelation of the pectin in response to Ca^{2+}. The storage modulus and Young's modulus values are useful as cells are responsive to the mechanical properties of the environment within which they are cultured (Discher, 2005, Janmey *et al.*, 2019). This includes material stiffness, but also the elastic properties and topography. The properties of the environment are also an important consideration for cell division and stem cell differentiation, as many factors including the mechanical properties influence this (McMurray *et al.*, 2015). Altering the stiffness of the environment also influences the organisation of the cytoskeleton within cells, which changes the morphology of cells (Doss *et al.*, 2020).

3.1.6. Cytotoxicity testing

Cytotoxicity testing is carried out on medical devices to ensure the materials they are made out of is not going to cause harm when used by patients (Li *et al.*, 2015). International Organisation of Standardization (ISO) standards are in place to ensure consistent, and quality assured testing. ISO 10993 is in place for the biological evaluation of medical devices. Most relevant for the study using pectin was "ISO 10993-5, Biological evaluation of medical devices — Part 5: Tests for in vitro cytotoxicity" ([ISO], 2009) and "ISO 10993-12, Biological evaluation of medical devices — Part 12: Sample preparation and reference materials" ([ISO], 2012).

ISO 10993-5 details the protocol for *in vitro* cytotoxicity testing, including specifications for culture vessels, cell lines on which to test materials, extraction vehicles for extraction testing, length of times, and the parameters for determining whether a material is deemed to be cytotoxic. A quantitative indication of cell viability is preferred, and one method includes the reduction of a vital dye. PrestoBlue is a resazurin-based assay, relying on the penetration of the dye into the cell and reduction if the cell is metabolically active. As metabolism is essential for cell survival, PrestoBlue assays are an indicator of cell viability (Xu *et al.*, 2015).

ISO 10993-12 details the parameters for sample preparation; the best match should be selected depending on the sample type. Within the ISO document, there is a table detailing the extraction ratio to be used depending on the material size and shape, reproduced below ([ISO], 2012):

Thickness (mm)	**Extraction ratio (surface area or mass/volume)**	**Examples of forms of materials**
<0.5	6 cm^2/mL	Film, sheet, tubing wall
0.5 to 1.0	3 cm^2/mL	Tubing wall, slab, small, moulded items
>1.0	3 cm^2/mL	Larger moulded items
>1.0	1.25 cm^2/mL	Elastomeric closures
Irregularly shaped solid devices	0.2 g/mL	Powder, pellets, foam, non-absorbent moulded items
Irregularly shaped porous devices (low-density materials)	0.1 g/mL	Membranes, textiles

As a hydrogel, pectin does not ideally fit any of the example forms of materials detailed, however the row for irregularly shaped solid devices was selected. The suggested extraction ratio was 0.2 g/mL extraction vehicle.

3.2. Hypothesis, aims, and objectives

3.2.1. Hypothesis

- Pectin has suitable mechanical and biocompatibility characteristics for cell delivery to the brain.

3.2.2. Aims

- Evaluate the effectiveness of the activated charcoal method for the purification of pectin.
- Screen diluents, pectin grades, pectin concentrations and calcium concentrations for appropriateness for forming hydrogels for use in cell delivery.
- Evaluate mechanical properties of pectin hydrogels formed.
- Evaluate cytotoxicity of pectin hydrogels.

3.2.3. Objectives

- Determine the levels of protein in the pectin samples before and after purification as a measure of the efficacy of pectin purification.
- Assess the hydrogels formed when pectin is dissolved in water, 1xPBS, 0.9% NaCl, when the pH has been adjusted to 7.4 and using a range of calcium concentrations.
- Measure the viscosity of pectin solutions at shear rates relevant to spraying using the chosen spray device, the mucosal atomisation device (MAD) syringe sprayer.
- Measure the G′, G″ and Young's modulus of pectin hydrogels made using conditions selected from qualitative gelation screen.
- Assess the metabolic activity of SH-SY5Y cells following the addition of either pectin hydrogels, or cell culture media incubated with pectin hydrogels.

3.3. Method design

Four pharmaceutical grades of pectin were supplied for this work by Herbstreith and Fox (CU-701 and CU-L), and CP Kelco (LM-102 and LM-104). These were not cell grades of pectin therefore; an activated charcoal purification method was used to remove unwanted contamination from the pectin. FTIR spectroscopy and a BCA protein assay were carried out on the purified pectin to determine any structural changes and the reduction in protein content. Once purified, a qualitative gelation screen was carried out to determine the effect of dissolving pectin in isotonic and pH adjusted diluents on calcium-induced gelation. This was repeated by spraying the pectin before gelling to ensure the pectin solutions could be sprayed and still form gels. Gelation of pectin and mechanical strength was testing using an amplitude sweep and texture analyser to determine the LVER and Young's modulus of pectin gels. This concentration reflects the calcium concentration that gave the best cell viability in the cytotoxicity testing (100 mM); concentrations tested in cytotoxicity testing were 25, 50, and 100 mM.

3.3.1. Calculations for viscosity testing

Viscosity measurements were taken between shear rates 100-10,000 1/s to represent the higher shear rates experienced during spraying. The selection of this shear rate range was confirmed with the following equations and calculations:

$$\gamma = \frac{v}{h}$$

Equation 1

Where v = velocity (m/s) and h = distance (m), therefore the unit for shear rate (γ) is inverse seconds.

To calculate the velocity of a fluid, the following equation is used:

$$v = \frac{Q}{A}$$

Equation 2

Where Q = flow rate (m^3/s) and A = the cross-sectional area, in this case the area of the hole in the spray device.

The values shown in Table 3.1 were specifically measured and calculated based on the dimensions and flow rate of the MAD sprayer.

Table 3.1 – Values when calculating the shear stress on a fluid when expelling it from the MAD sprayer.

$Q = 2.5 \times 10^{-7}\ m^3/s$	1 mL of fluid is expelled through the spray device in 4 seconds
$A = 3.14 \times 10^{-8}\ m^2$	Spray device ejection hole is 0.2 mm in diameter
$v = 7.958\ m/s$	$2.5 \times 10^{-7} / 3.14 \times 10^{-8}$
$h = 0.0001\ m$	Distance travelled through the ejection hole in spray device
$\gamma = 7{,}958\ 1/s$	Shear rate based on calculated velocity and distance through spray device hole

3.3.2. Cytotoxicity testing

The cytotoxicity was carried out using the ISO 10993-5 and -12 to guide the experiment. The SH-SY5Y cell line was selected as it fulfils the requirement of being a well-characterised cell line, and is of human origin, the same species as the hMSCs being sprayed and delivery to humans is the intended final goal for the development of this sprayed cell and pectin therapy.

3.4. Results

The aim was to evaluate how effective the activated charcoal method is for pectin purification, adapted from the method described by Neves *et al.* (2015). The results of protein content analysis and FTIR are summarised below. The results of the gelation screen, mechanical strength and viscosity testing, and the cytotoxicity tests to evaluate the suitability of pectin for cell delivery, are also summarised below.

3.4.1. Purification – Protein content of pectin samples

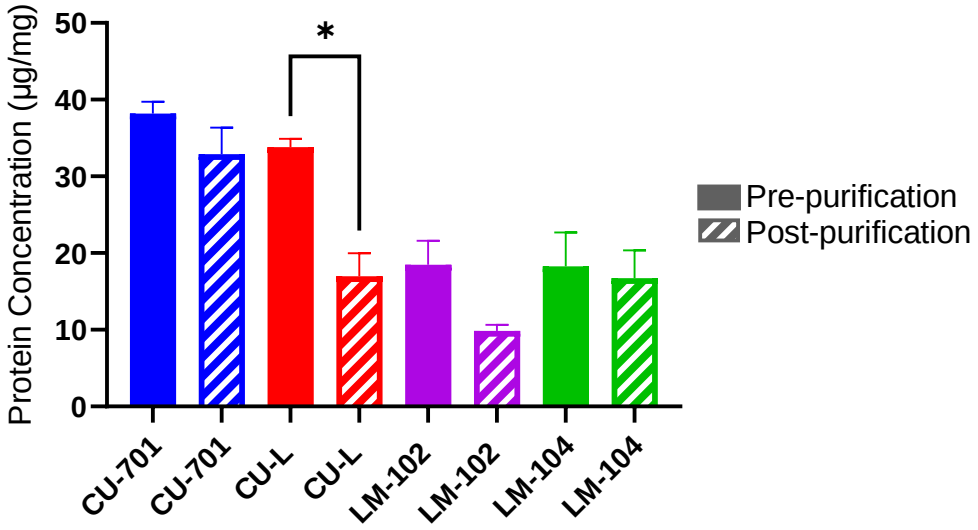


Figure 3.4 – Protein content of pectin samples (0.5% w/v in 1xPBS): pre and post purification using activated charcoal method; protein determined by BCA protein assay. BCA assay standard curve was used to determine protein content values for pectin samples. Samples were tested in duplicate (n) on using three batches (N) (N=3, n=2). Error bars show standard error of the mean (SEM). Paired T-test was used to determine statistical significance of each pectin grade before and after purification. * show $P < 0.05$.

Figure 3.4 shows the results of the BCA protein assay carried out on the four grades of pectin samples before and after purification. Samples were prepared at 0.5% w/v concentrations in 1xPBS. A standard curve was prepared, and this was used to calculate the protein content in pectin as µg/mL, which was converted to µg/mg of pectin.

In all grades of pectin, there is a reduction in the protein content after purification. However, CU-L is the only grade that demonstrates a statistically significant reduction.

3.4.2. Purification – FTIR spectra of pectin samples

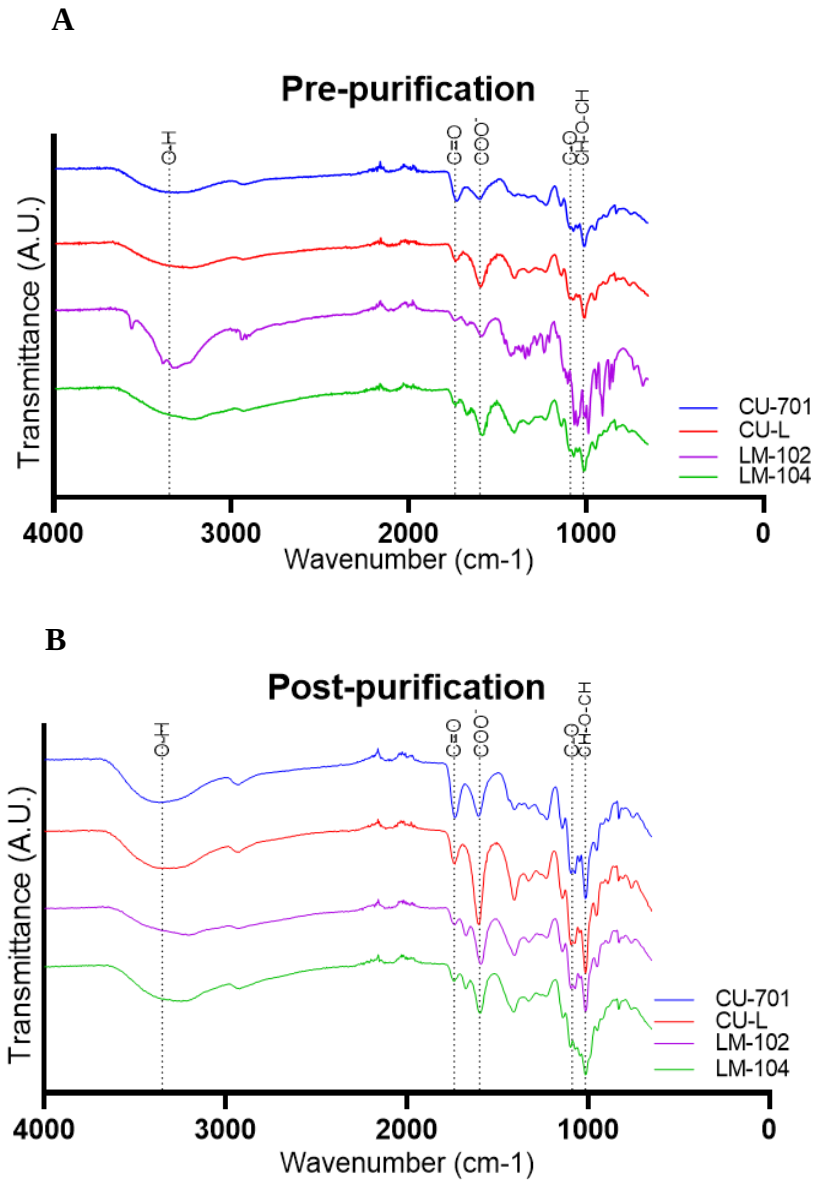


Figure 3.5 – FTIR spectra of the different grades of pectin powder. **A** pre- and **B** post-purification by activated charcoal. Relevant peaks to the pectin structure and wavelengths are as follows: O-H 3350 nm, C=O 1740 nm, COO^- 1600 nm, C-O 1090 nm, CH-O-CH 1017 nm.

Figure 3.5 shows the FTIR spectra of pectin samples before and after purification. The highlighted peaks are those associated with the structure of pectin (ThermoScientific, 2015, Kozioł *et al.*, 2022). In all grades of pectin, the highlighted peaks were retained after purification. A reduction in the intensity of the -OH peak is observed in the LM-102 pectin grade. The LM-102 spectra also appeared more uniform with the other grades following purification, suggesting there were small amounts of contaminants removed.

3.4.3. Gelation screen – Pipetted pectin solutions

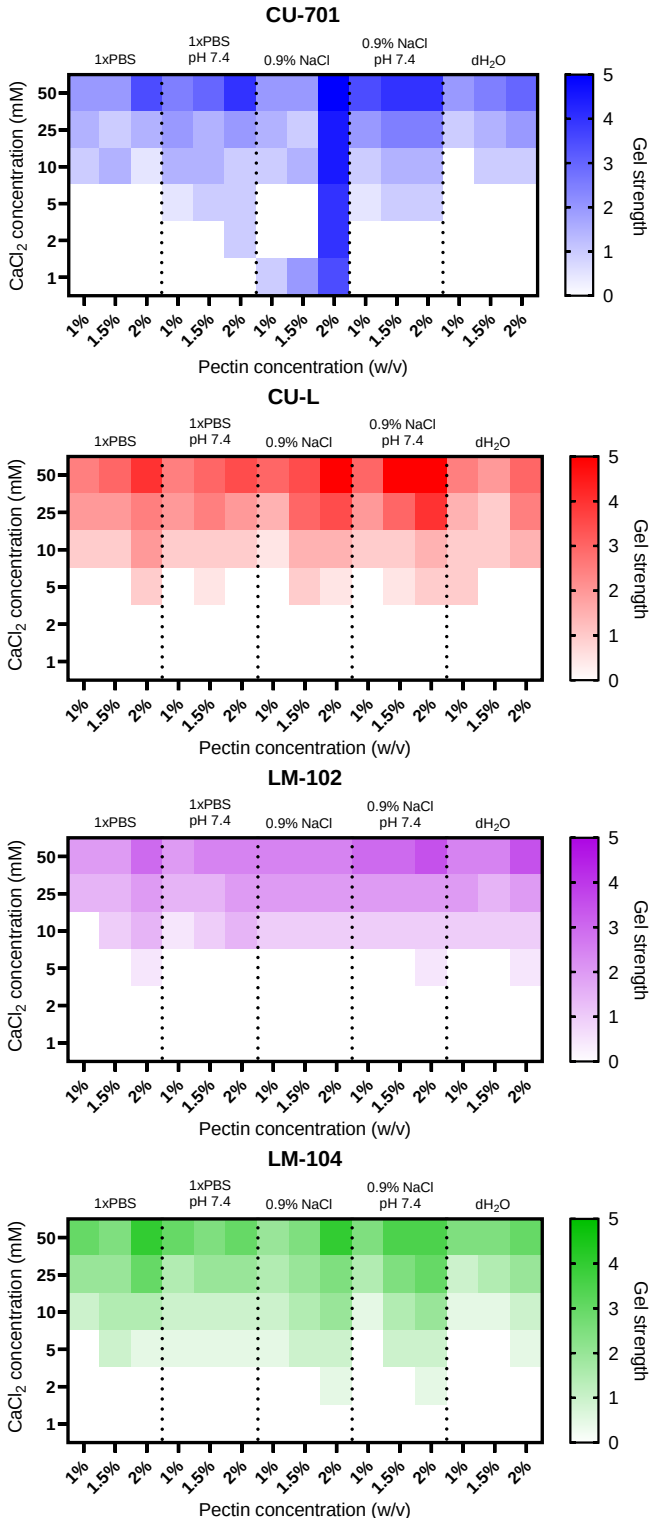


Figure 3.6 – Strength of different grades of pipetted pectin gels formed at different % w/v concentrations, in different diluents, with pH adjusted to 7.4, using varied concentrations of calcium. Calcium concentrations shown are the concentrations of solution used to form gels. Gels were ranked from 0 (no gelation) to 5 (firm gel that can be handled without breaking). Gels were allowed for form for 60s before images were collected to confirm consistent scoring. N=2, all samples were scored in one batch to reduce variability.

Gels formed with all pectin grades and in all diluents and pH values that were tested with higher calcium concentrations. In almost all conditions, a correlation was seen between increasing pectin concentration or calcium concentration and an increase in observed gel strength. The use of isotonic diluents (0.9% NaCl and 1xPBS) did not result in weaker gels in the pectin grades CU-701, CU-L or LM-104 compared to dH_2O. LM-102 saw a slight reduction in the strength of gels formed in 1 and 2% w/v in 1xPBS pH 7.4 and 2% w/v in 0.9% NaCl. In all pectin grades, the strongest, or equal strongest, gel was formed with 0.9% NaCl at pH 7.4 as the diluent. A possible explanation for the difference in gel strength between gels formed in 0.9% NaCl and 1xPBS is a reaction between sodium phosphate (Na_2HPO_4) found in 1xPBS, and $CaCl_2$ used to induce gelation. This reaction results in the formation of tricalcium phosphate ($Ca_3(PO_4)_2$), a precipitate which would reduce the amount of calcium ions available for crosslinking of the pectin chains, leading to the formation of weaker gels.

CU-701 in 0.9% NaCl at 2% w/v formed a gel without the addition of $CaCl_2$ which was strengthened with the addition of >2 mM $CaCl_2$. This gelation was reversed when NaOH was added to increase the pH to 7.4. LM-104 had the greatest sensitivity to calcium chloride overall as gelation occurred with the lowest concentrations of calcium. Concentrations of calcium below 10 mM were not sufficient to form self-supporting gels in any of the grades of pectin tested. At the highest concentration of calcium tested (50 mM), the observed gel strength correlated with the DM; LM-104 and CU-L had the lowest DM and formed the strongest gels.

3.4.4. Gelation screen – Sprayed pectin solutions

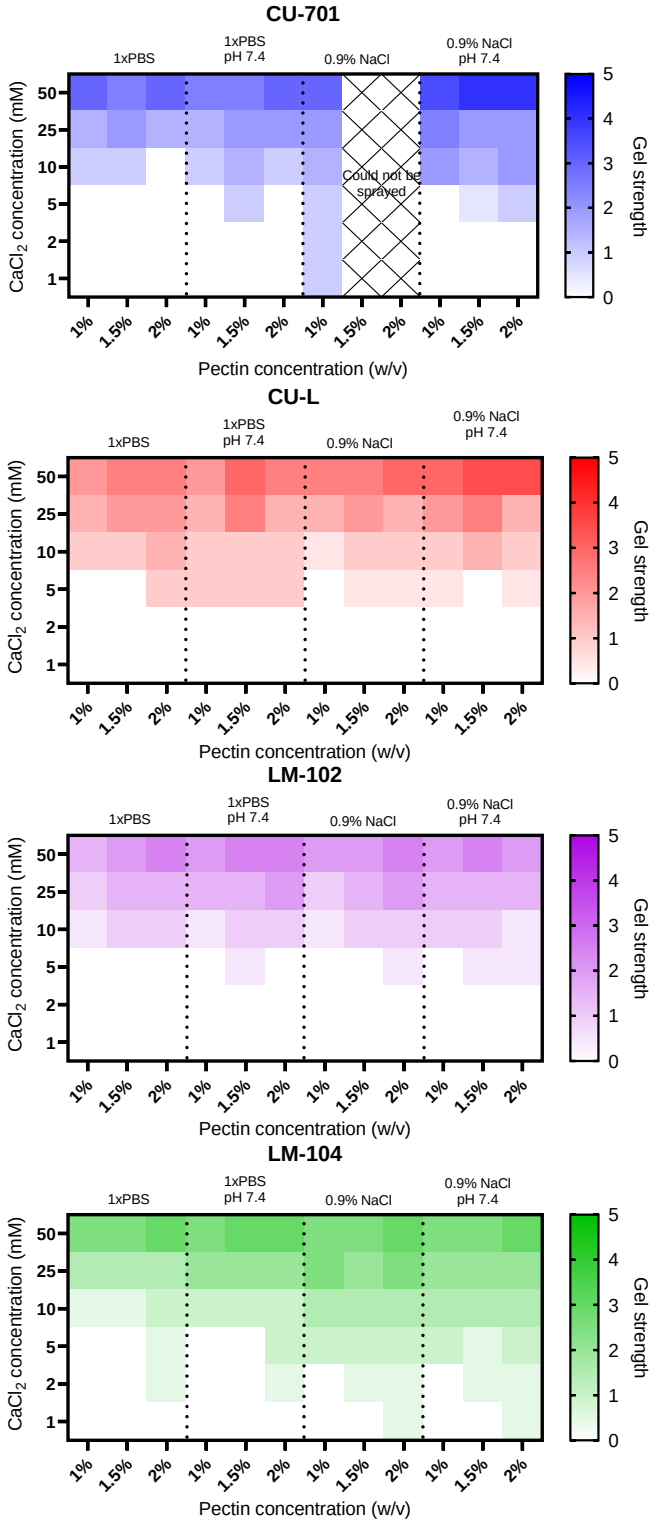


Figure 3.7 – Strength of different grades of sprayed pectin gels. Formed at different % w/v concentrations, in different diluents, with pH adjusted to 7.4, using varied concentrations of calcium. Calcium concentrations shown are the concentrations of solution used to form gels. Gels were ranked from 0 (no gelation) to 5 (firm gel that can be handled without breaking). Gels were allowed for form for 60s before images were collected to confirm consistent scoring. N=2, all samples were scored in one batch to reduce variability.

Gels formed in all diluents and pectin concentrations that were tested with higher calcium concentrations. CU-701 at 1.5 and 2% w/v could not be tested as they were too viscous to pass through the spray device. At 50 mM $CaCl_2$ concentration, a weaker gel formed in the sprayed condition compared to the pipette condition in some of the diluents for all grades of pectin. Self-supporting gels were not formed when calcium concentrations were below 10 mM, however some increases in perceived viscosity were observed when imaging. This was most evident in the LM-104 grade of pectin, which began forming gels at the lowest concentrations of calcium compared to the other grades. The concentration of calcium required to increase the viscosity was also reduced when comparing the sprayed pectin to the pipetted pectin. This was especially evident for LM-104, which scored a 1 on the qualitative score with a pectin concentration of 2% w/v and 1 mM $CaCl_2$.

3.4.5. Rheology – Viscosity of pectin solutions

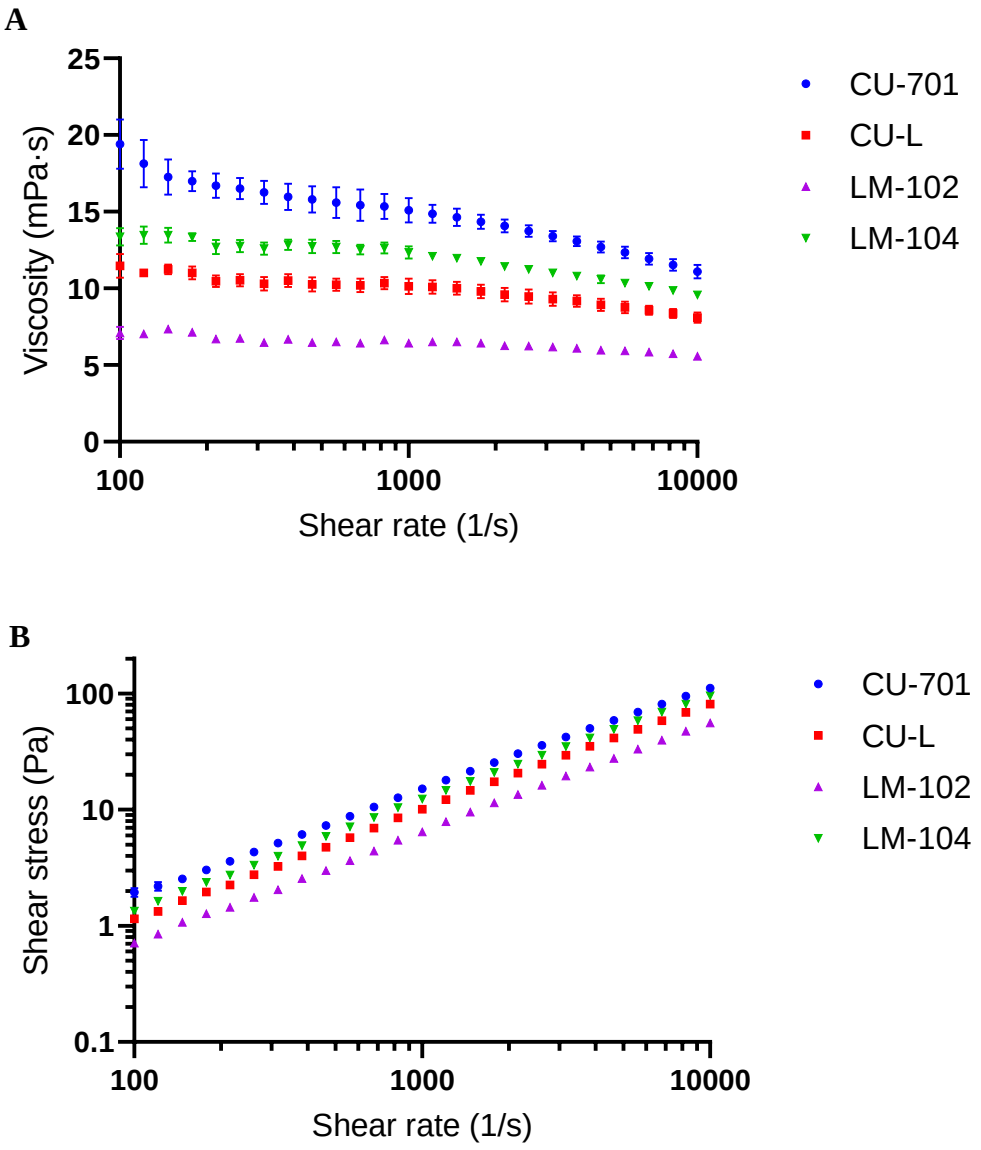


Figure 3.8 – Viscosity of 1% w/v purified pectin solutions made in 1xPBS. Viscosity measurements were carried out using a cone-and-plate instrument set up. 25 measurements were taken logarithmically from 100-10,000 1/s, with measurement times ranging from 1-25 s with a logarithmic ramp. the plate was set to 25 °C. Error bars show the standard deviation, n=3. Shear rate vs viscosity is shown in **A**, and shear rate vs shear stress is shown in **B**.

Figure 3.8 shows the viscosity of 1% w/v pectin solutions. The cone-and-plate measurement set up was used as pectin samples do not show edge drying during the measurement time (Mezger, 2014). The shear rate was increased logarithmically from 100-10,000 1/s, with 25 measurements taken within that range.

Samples demonstrated some slight shear thinning properties over the measured range, with viscosity decreasing from 19.4 mPa·s to 11.1 mPa·s in CU-701, 13.4 mPa·s to 9.6 mPa·s in LM-104, 11.5 mPa·s to 8.1 mPa·s in CU-L, and 7.1 mPa·s to 5.6 mPa·s in LM-102. The linear relationship between shear stress and strain shown in Figure 3.8B demonstrates the shear thinning properties observed in Figure 3.8A are only minor overall.

3.4.6. Rheology – Amplitude sweep of pectin gels

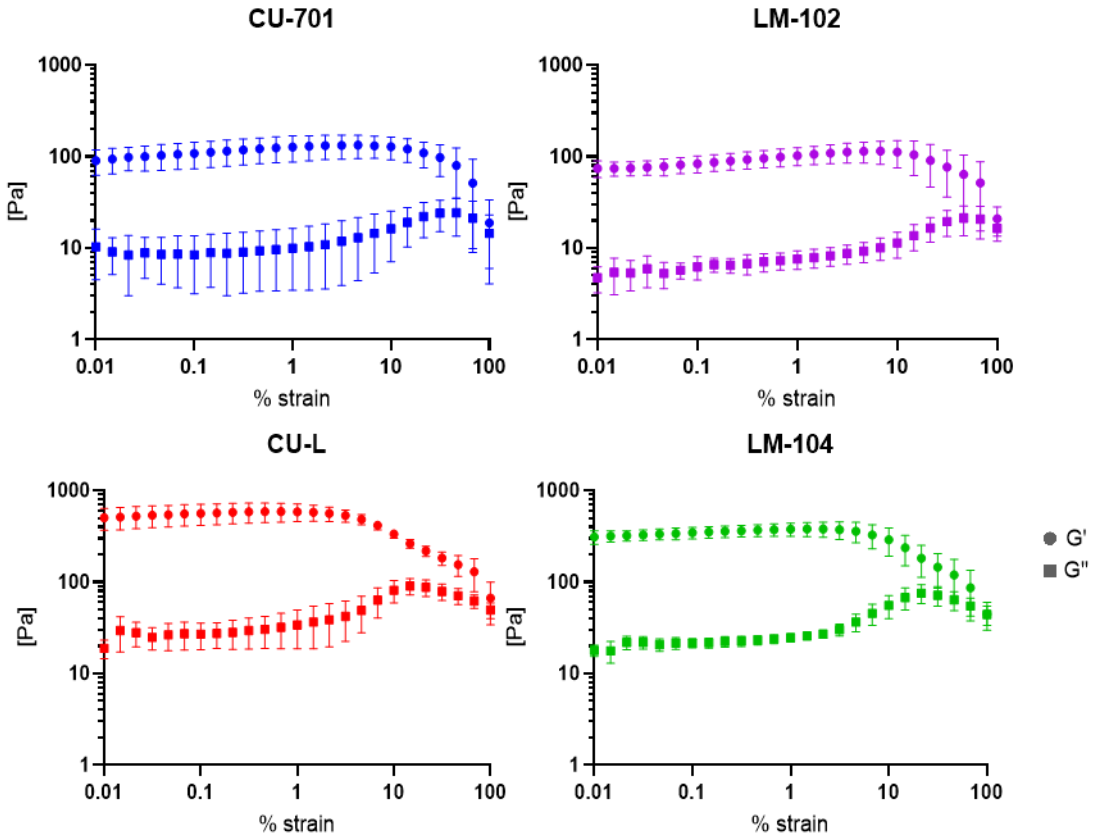


Figure 3.9 – Storage (G') and loss (G'') modulus of purified pectin (1 % w/v in 1xPBS) gels. Formed using 50 mM $CaCl_2$ (final concentration 8.33 mM) using the different grades shown. Gels were allowed to form for 3 minutes on the plate, set at 37 °C prior to measuring. 25 measurements were taken using 25 mm parallel plates, between 0.01-100 % strain at 10 rad/s, increasing the strain logarithmically. Samples were tested in duplicate on three separate occasions with fresh pectin solutions on each occasion (N=3, n=2). Error bars show the standard deviation.

Figure 3.9 shows the viscoelastic measurements for the four grades of pectin gelled with $CaCl_2$. Gels were formed directly on the plate for 3 minutes at 37 °C before measurements were taken. The plots demonstrate that all four grades of pectin formed gels as the storage modulus is higher than the loss modulus for all but the higher strain rates. At this point, the structure of the gels had broken down. The limit of the LVER for all four grades of pectin, and the storage modulus at 1% strain is shown in Table 3.2.

Table 3.2 – Summary of the LVER limit and the G′ value at 1% strain.

Pectin grade	LVER limit (strain %)	G′ value at 1% strain (Pa)
CU-701	10	127.8
CU-L	3.16	487.5
LM-102	14.7	102.6
LM-104	6.8	379.0

3.4.7. Young's modulus of pectin gels

Table 3.3 – Young's modulus of purified pectin gels. Formed with 1% w/v pectin in 1xPBS and 100 mM $CaCl_2$ solution (final concentration of 9 mM). Measurements were taken in triplicate.

Grade	Young's modulus (Pa)
CU-701	100.08
CU-L	152.09
LM-102	110.21
LM-104	153.06

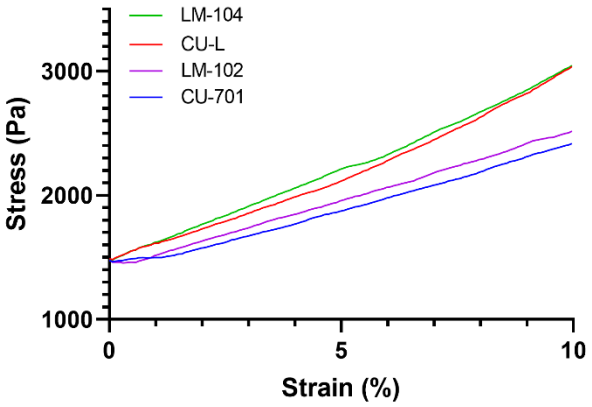


Figure 3.10 – Linear region of the stress-strain curves used to calculate the Young's modulus of the 1% w/v pectin hydrogels shown in Table 3.3.

Table 3.3 shows the Young's modulus for the four grades of pectin as determined by applying a uniaxial strain by compression using a texture analyser. Figure 3.10 shows the linear region of the stress train plots obtained from the texture analyser and used to calculate the Young's modulus. LM-104 and CU-L have the highest values, and LM-102 and CU-701 have the lowest values.

3.4.8. Cytotoxicity testing – Pectin gels in direct contact with SH-SY5Y cells

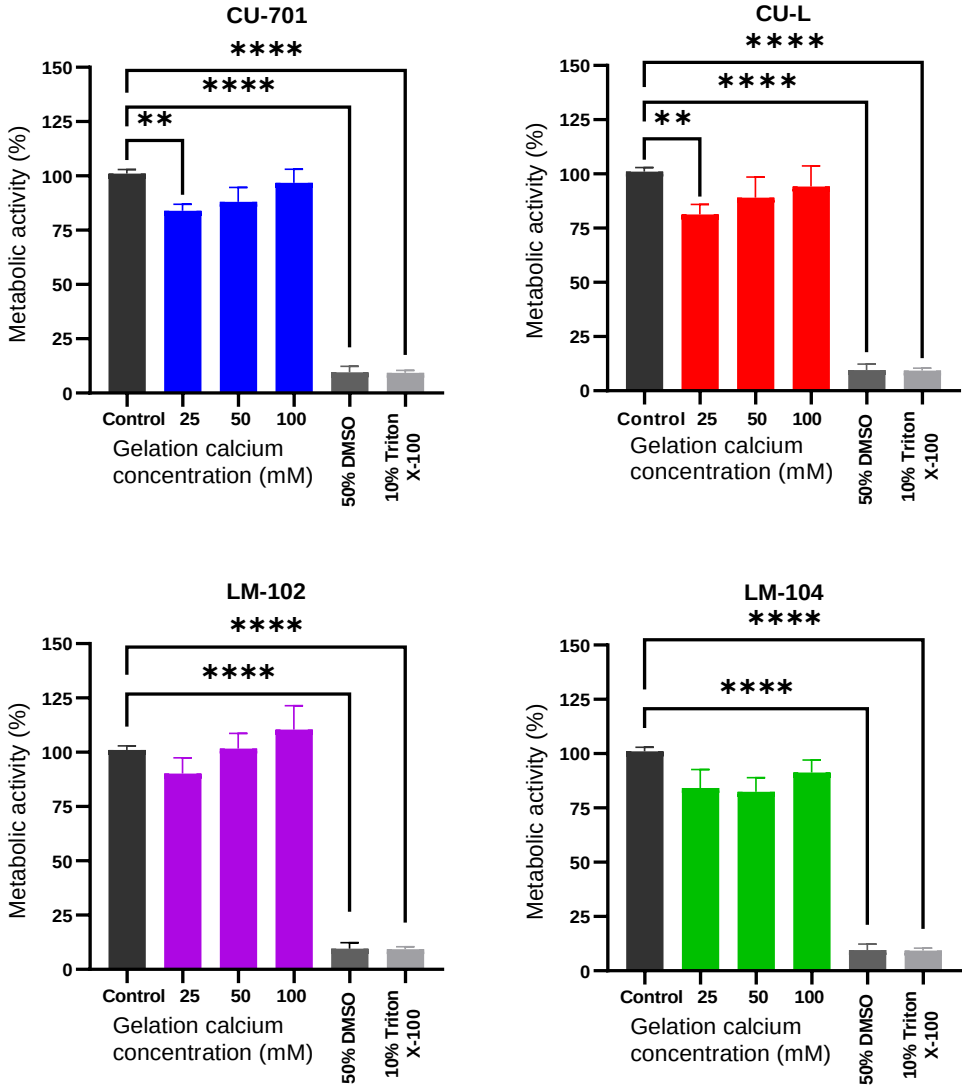


Figure 3.11 – Direct cytotoxicity testing of purified pectin hydrogels (1% w/v). Pectin hydrogels were formed with varying concentrations of calcium. 100 µL of pectin solutions were added to 10 µL of calcium at concentrations stated to induce gelation. Pectin hydrogels were placed onto confluent SH-SY5Y cells in culture for 24 hours. Metabolic activity was assessed using a PrestoBlue assay. Experimental conditions were run in triplicate on three separate occasions, using cells from different passage numbers on different days (N=3, n=3). Error bars show standard error of the mean. One-way ANOVA with a Dunnett's post-test was carried out to determine statistical significance between tested hydrogels and an untreated control. ** shows P<0.01, **** shows P<0.0001.

Figure 3.11 shows the results of the direct cytotoxicity testing using the four grades of pectin to form gels at three different concentrations of $CaCl_2$. There were no statisitically significant differences in the metabolic acitivity of cells in

direct contact with any of the amidated pectin gels (LM-102 or LM-104). Both non-amidated pectin gels (CU-701 and CU-L) formed with 25 mM $CaCl_2$ showed a statistically significant reduction in the metabolic activity compared to the control. Across the four grades of pectin, there was a correlation between a higher $CaCl_2$ concentration used to form the gels, and a higher metabolic activity of the cells compared to the control.

3.4.9. Cytotoxicity testing – Pectin gel conditioned media on SH-SY5Y cells

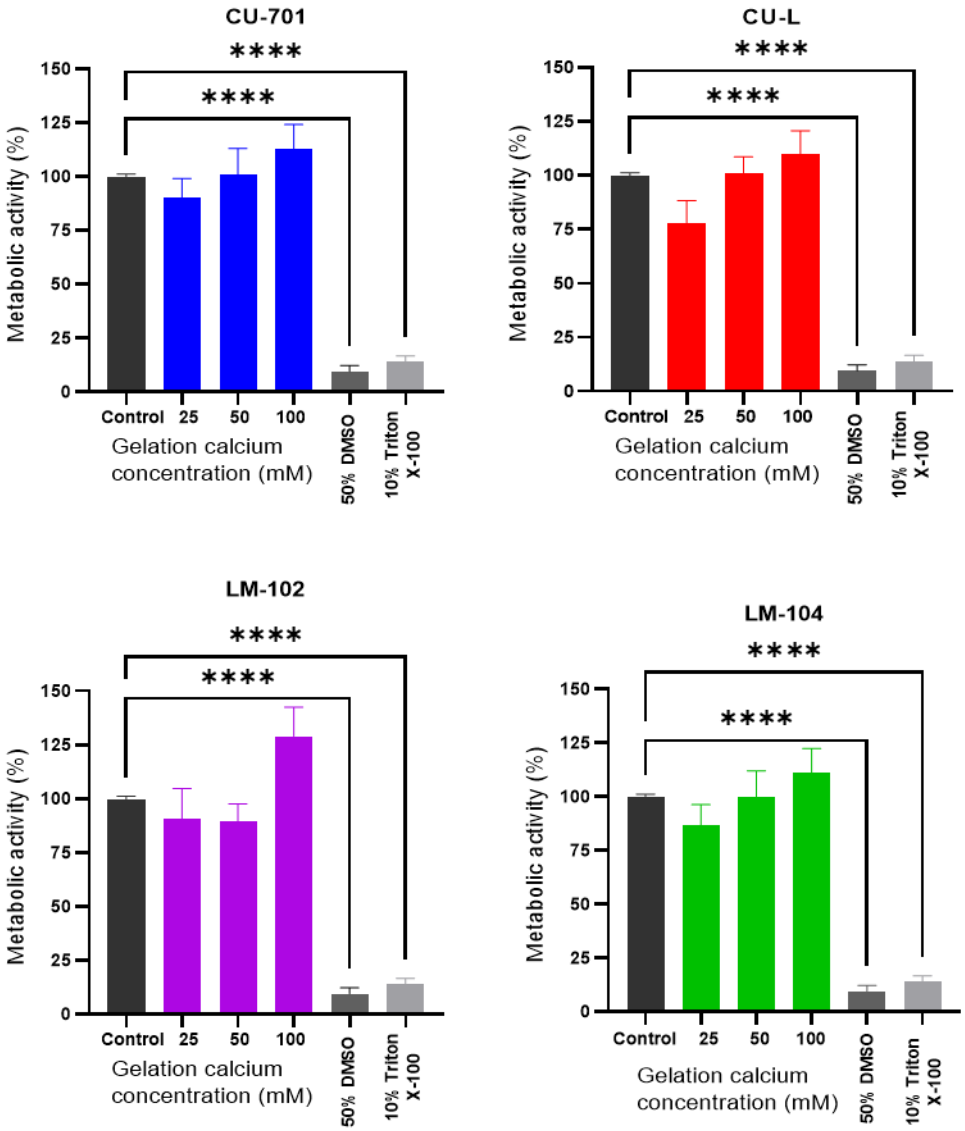


Figure 3.12 – Elution cytotoxicity testing of purified pectin hydrogels (1% w/v). Formed with varying concentrations of calcium. 100 µL of pectin solutions were added to 10 µL of calcium at concentrations stated to induce gelation. Pectin hydrogels were incubated in cell culture media for 24 hours, before the media was transferred onto confluent SH-SY5Y cells in culture. Metabolic activity was assessed using a PrestoBlue assay. Experimental conditions were run in triplicate on three separate occasions, using cells from different passage numbers on different days (N=3, n=3). Error bars show standard error of the mean. One-way ANOVA with a Dunnett's post-test was carried out to determine statistical significance between tested hydrogels and an untreated control. **** shows P<0.0001.

cells

Figure 3.12 shows the results of the elution cytotoxicity testing of the pectin hydrogels. There were no statistically significant differences between the pectin elution test conditions and the control. An increased $CaCl_2$ concentration used to form the gels correlated with an increase in metabolic activity of the cells; all grades of pectin the highest metabolic activity was observed when 100 mM $CaCl_2$ was used to form the pectin hydrogels.

3.5. Discussion

Four grades of low-methyl (LM) citrus pectin were evaluated for their purification, gelation, viscosity, and cytotoxicity. They differed in the degree of methylation (DM) and the degree of amidation (DA), and were from two different suppliers, summarised in Table 2.2. Both pectin grades supplied by CP Kelco were amidated (LM-102 and LM-104), and both from Herbstreith and Fox were non-amidated (CU-701 and CU-L).

3.5.1. Purification

Some investigations into pectin for cell delivery employ a pectin purification step. Munarin *et al.* opted for a two-step ethanol wash, followed by activated charcoal after functionalisation (Munarin *et al.*, 2011, Munarin *et al.*, 2012a). Neves *et al.* (2015) opted for activated charcoal. Both methods were trialled early on in this work, however activated charcoal was chosen as the product of the ethanol wash was difficult to handle and the process resulted in a larger loss of pectin than the activated charcoal method.

Following purification, efforts were made to analyse the products using the same techniques used by Neves *et al.* (2015). Little detail was given on the method used to analyse polyphenol contamination; therefore, this could not be replicated. As the pectin grades demonstrated biocompatibility in the cytotoxicity testing, in the interest of time, other methods of polyphenol quantification were not explored. In the paper, endotoxin analysis was outsourced to an external company. Due to the number of samples here, a litmus amoeba lysate (LAL) chromogenic endotoxin kit was purchased to carry out the analysis in house, however highly variable results were observed, and no reliable conclusion could be drawn from the results. Again, due to time constraints and biocompatibility demonstrated, further testing was not undertaken.

The BCA protein assay used was validated to ensure the pectin samples were not interfering with the results. The BSA (bovine serum albumin) standard was spiked into the pectin samples at known concentrations and analysed following the assay protocol. The concentration spiked into samples corresponded with the concentration detected. The paper by Neves *et al.* (2015) used only the CU-701 and quoted a 70% reduction in protein content following the purification. In this

thesis, a 13.88% reduction in protein content was seen after purification using the CU-701 grade, implying the purification protocol when carried out here was less effective than that in the 2015 paper. The percentage reduction seen for CU-L was 48.84%, for LM-102 was 46.53% and for LM-104 was 8.48%, again implying the purification protocol was less effective on all grades of pectin studied here compared to the 2015 paper. Despite the lower reduction in protein content, the physical appearance of the pectin changed from pale yellow in colour, to white. Solutions made using the purified pectin were colourless, compared to yellow using the pectin before purification, indicating the removal of contaminants.

To ensure only unwanted contaminants such as protein were removed, and the structure of the pectin was not lost, FTIR spectra were compared before and after purification. The peaks associated with the structure of pectin are all still present after purification, suggesting the structure of pectin is unaltered. The bonds highlighted in Figure 3.5 are all found in or between the GalA sugar residues in the pectin chains.

3.5.2. Characterisation of pectin solutions and gelation

Following the results of the purification, all further work was carried out on pectin purified using the activated charcoal method, including the characterisation of the solutions and gels. To be classed as a gel, or a viscoelastic solid, a material must not relax or flow under mechanical stress. There are a variety of table-top rheology methods that can be employed to determine whether this is the case. Often chosen is the vial inversion test, whereby a material is deemed to be a gel if it does not flow when inverted (Raghavan and Cipriano, 2006). However, an alternative method was used here to compare the effect of spraying pectin to pipetting pectin on gel strength, and assess the effect of different diluents, pH, calcium concentrations, and pectin concentrations due to easier use with spraying. In addition to being easier to use and less time consuming, the glass slide method minimised consumable waste.

The conditions chosen for the study were to determine the effect of an increase in pH, and the presence of salts in the diluent on gelation. Monovalent cations can bind to, and shield the charges on pectin chains, preventing interactions with Ca^{2+}, thereby preventing cross-linking of the chains and gelation (Fan *et al.*,

2021). However, these salts are essential for pectin solutions to be isotonic and compatible with the encapsulation of cells (Arango *et al.*, 2013).

Overall, changing the diluent and adjusting the pH to 7.4 did not prevent the gelation of the pectin grades using Ca^{2+}. Changing the diluent to 0.9% NaCl did present an issue in the grade CU-701 at 2% w/v pectin. This grade has the highest degree of methylation, of 37%. High methyl (HM) pectin, (with a DM >50%) has a different gelation mechanism to LM pectin. Due to the higher abundance of methyl groups and fewer carboxylic acid groups, HM pectin is less water soluble, and gelation occurs due to hydrophobic interactions. This gelation is strengthened when the solution is acidified, due to carboxylic acid groups becoming deionised, reducing their water solubility. The presence of sugars or salts reduces the water solubility further, stabilising the hydrophobic interactions and causing gelation (Sriamornsak, 2003).

As CU-701 has the highest DM and the lowest pH in solution, it may be possible that there is some gelation occurring as a result of the HM pectin gelation mechanism. Alternatively, the presence of the sodium and chloride ions may reduce the solubility of pectin when at the higher 2% w/v, and therefore the gelation is actually precipitation of the pectin. However, the ionic strength of both 0.9% NaCl and 1xPBs is very similar: 0.154 M and 0.152 M respectively. Therefore, if this is seen with 0.9% NaCl, it would also be expected with 1xPBS. Adjusting the pH of the 2% w/v CU-701 pectin sample in 0.9% NaCl reversed the gelation observed at a lower pH, suggesting the mechanism may be due to charge shielding as described above.

Despite stronger gels forming with 0.9% NaCl, 1xPBS was chosen to move forward with as it is buffered and therefore it was much easier to adjust the pH of the pectin solutions. When dissolved in 0.9% NaCl, the pectin solutions were very susceptible to large changes in pH with a small addition of NaOH due to the lack of buffer.

Spraying the pectin solutions, compared to pipetting, tended to increase the sensitivity of the grades to calcium, but reduced the strength at the higher concentrations of calcium. This may be due to the gel formed being thinner when sprayed and therefore the perceived strength is weaker. It may also be due to the

pectin forming droplets as it is sprayed, which may have formed small gel droplets when hitting the calcium covered microscope slide. These droplets may not be cross-linked as effectively as the bulk pectin gel formed by pipetting therefore, the gel appears weaker. The small droplets resulting from spraying may have enhanced the sensitivity to calcium at the lower concentrations as droplets have a larger surface area to volume ratio than the pipetted pectin, and therefore a higher surface area was available to cross-link with calcium ions. 1% w/v pectin solutions were chosen for progression to viscosity measurements as they appeared less viscous and passed through the spray device more easily with fewer blockages during the gelation screen.

1% w/v pectin was also chosen as viscosity is an important consideration for the spray delivery of cells, as published data suggests a lower viscosity correlates with a higher viability of delivered cells (Hendriks *et al.*, 2015). For that reason, ideally a pectin solution would show shear thinning properties, or behave as a Newtonian fluid. Shear thickening would be problematic, as an increased viscosity may result in inconsistent spraying, blockage of spray devices, and inconsistent cell viability and delivery. For viscosity data as shown in Figure 3.8, there is a linear relationship between the shear rate and shear stress, indicating the solutions are behaving as Newtonian fluids. For viscosity versus the shear rate, there is a slight decrease in viscosity at higher shear rates, suggesting there are slight shear thinning properties in all four grades of pectin. This is consistent with published data using low concentration solutions of pectin (Chen *et al.*, 2020a, Peighambardoust *et al.*, 2021). Amidation of pectin increases the solubility of pectin, allowing for more hydrogen bonding between water and pectin chains (Belkheiri *et al.*, 2021), however this did not clearly affect the viscosity of the pectin grades. This hydrogen bonding of amide groups has also been suggested to stabilise cross-linking during gelation, therefore increasing the stiffness of pectin gels. This is more applicable to gels formed at a low pH (Fraeye *et al.*, 2010) and was not observed during the amplitude sweep or Young's modulus tests carried out.

The storage modulus and the Young's modulus can give an indication of the stiffness of gels formed by the different grades, using the same concentration of pectin and calcium. CU-L and LM-104 had higher storage moduli and Young's

moduli than CU-701 and LM-102. This suggests, at least for these four grades, the presence of amide groups does not result in stronger or weaker gels. The viscosity of the pectin in solution did not seem to correlate with an increased stiffness of the gel.

CU-L and LM-104 have the lower degrees of methylation of the four grades, with 28% and 27% respectively, and this correlated with a higher gel stiffness. Gels form due to the ionic interactions of the negatively charges carboxylic acid groups (COO^-) and divalent cations, most commonly (and used throughout in these studies) is calcium. The lower the DM, the higher the number of free carboxylic acid groups are present and available to interact with Ca^{2+}, therefore, more cross-linking between pectin chains occurs.

Brain tissue has a relatively low stiffness when compared to other tissues in the body. Values measured in the literature vary depending on the species of the tissue and the method used, however values for the Young's modulus (E) of the whole organ tends to be around 0.5 kPa (Saha *et al.*, 2008). All pectin grades tested had a Young's modulus below 0.5 kPa when formed with 100 mM calcium.

Having established during the gelation screen that gels formed with a calcium concentration >25 mM could be handled, these were able to be used in the cytotoxicity testing carried out. Tests were carried out on SH-SY5Y human neuroblastoma cells. Whilst originally derived from bone neuroblastoma, they have a neuron-like appearance when grown in culture and are often used in simplistic *in vitro* models of neuropathology (Liu *et al.*, 2018). They fit the ISO requirement of using a well-characterised cell line, and are a relevant cell type, being both human and neuron-like in phenotype. Testing was carried out using the direct contact, and extract method described in ISO 10993-5. The direct test is carried out by placing the material directly on the cells in culture, with the material having a surface area in contact with the cells equivalent to approximately 10% of the growth surface area. The material is in contact with cells for 24 hours before measuring viability. Extract testing was carried out by incubating the material in culture media for 24 hours at 37 °C; the conditioned media was then added to cells for 24 hours before viability assessment. The

PrestoBlue assay was used as a suitable method of determining cell viability and cytotoxicity according to ISO 10993-5.

There were no statistically significant differences between the metabolic activity of the untreated control cells and the cells treated with the extraction media from all grades of pectin formed with all concentrations of pectin. However, there was a trend observed which showed a higher metabolic activity in cells incubated with extract media from pectin gels formed with higher concentrations of calcium. This trend of increasing metabolic activity with increasing concentrations of calcium was also observed in the direct method testing. There was a statistically significant reduction between the metabolic activity of control cells and those in direct contact with CU-701 and CU-L pectin gels formed using 25 mM $CaCl_2$ solution, where the metabolic activity of the cell population was reduced by 16% and 19% respectively. Based on ISO 10993-5, the reduction is not enough for the material to be classed as cytotoxic; a reduction greater than 30% by qualitative testing is considered cytotoxic.

Pectin solutions and pastes have a history of biocompatibility in humans as a plasma expander (Hartman *et al.*, 1941, Popper, 1945) and wound dressings (Maclay *et al.*, 1944), therefore biocompatibility in the cytotoxicity testing was expected. The trend shown here of decreased Ca^{2+} concentration correlating to decreased metabolic activity is the inverse of what has been shown in published data for alginate, (also cross-linked with Ca^{2+}), whereby increasing Ca^{2+} concentration correlated with decreasing viability (Cao *et al.*, 2012). However, pectin is more sensitive to Ca^{2+} gelation, therefore it may sequester calcium from the cell culture media, a hypothesis put forward in a recent study showing pectin to be biocompatible in *in vitro* testing on the U87 glioblastoma cell line and human astrocytes (McCrorie *et al.*, 2020). This could explain the trend observed between lower calcium concentration and a reduction in metabolic activity. Due to the lowest metabolic activity in all cytotoxicity tests being in the 25 mM calcium pectin gels, and the highest being in the 100 mM calcium pectin gels, this higher concentration was taken forward into further studies.

3.6. Conclusions

The activated charcoal purification method did not change the structure of pectin, however only limited protein removal was seen, and endotoxin removal

could not be quantified. Calcium induced gelation was observed with all pectin grades dissolved in both 0.9% NaCl and 1xPBS, and when pH was adjusted. 1xPBS at pH 7.4 was the diluent taken forward, and amplitude sweep tests confirmed gelation in all pectin grades. This demonstrates that isotonic pectin gels with appropriate pH can be formed for the purpose of cell delivery to the brain. Gels formed were not deemed to be cytotoxic when tested using the ISO 10993 for guidance. Gels formed with 100 mM $CaCl_2$ solutions demonstrated the highest metabolic activity in all pectin grades, so this concentration was used in the cell delivery in pectin studies, reported in Chapter 4.

Chapter 4 Cell spraying

4.1. Introduction

4.1.1. Spray delivery of cells

As discussed in Chapter 1, spraying of therapeutic cells has been investigated for a range of indications. The spray devices commonly studied were airbrush devices which used pressurised air to generate the aerosol (Veazey *et al.*, 2005, De Windt *et al.*, 2015), or less commonly they used pressurised liquid through a spray nozzle attached to a syringe (Peirce and Carolan-Rees, 2019).

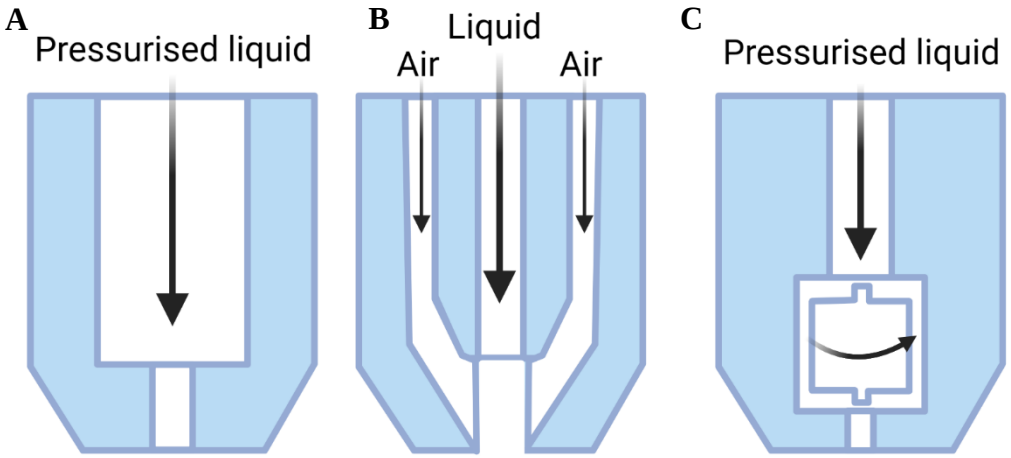


Figure 4.1 – Schematics of three different spray nozzles, **A** simple liquid pressure nozzle, **B** air atomising nozzle, and **C** a turbulent liquid pressure nozzle. Figure created in BioRender.

In the simple liquid pressure nozzle, high liquid pressure generates a spray, which is possibly too high for cells to survive, and will more commonly generate a jet of liquid. In the air atomising spray nozzle devices, pressurised air breaks the stream of liquid into smaller droplets which are then expelled from the device through a narrow orifice (Andrade *et al.*, 2012). Air pressure and orifice size can be controlled, which in turn will control droplet size. The turbine spray device has a vane within the nozzle which spins when a stream of liquid passes through. This disrupts the stream of liquid, forming droplets as it leaves through the orifice, and is the basis for generating a spray in the mucosal atomisation device (MAD) chosen for this study (Denton, 2022).

Table 4.1 – Spray device name and nozzle category of devices studied for use in cell delivery.

Spray device name	Spray device nozzle category	Reference
Mucosal atomisation device (MAD)	Turbulent liquid pressure	(Denton, 2022)
MicroSprayer® Aerosolizer	Liquid pressure with undisclosed aerosol generating components at tip	(Kardia *et al.*, 2014, Kim *et al.*, 2016)
Airbrush spray	Air atomising nozzle	(Pehlivaner Kara and Ekenseair, 2016, Schwartz *et al.*, 2017, Veazey *et al.*, 2005)
Tissomat™ spray kit	Air atomising nozzle	(Harkin *et al.*, 2006, Zimmerlin *et al.*, 2013, Falanga *et al.*, 2007)
Pneumatically assisted atomisation device (PAAD)	Air atomising nozzle	(Zhang *et al.*, 2022)
ReCell® kit	Liquid pressure nozzle	(Wood *et al.*, 2012)
Endoscopic pressure atomisation device	Liquid pressure nozzle	(Thiebes *et al.*, 2021)
Endoscopic air atomisation device	Air atomising nozzle	(Thiebes *et al.*, 2021)
LMA MADgic	Turbulent liquid pressure	(Kim *et al.*, 2016)

Table 4.1 shows the names of the devices, spray nozzle category, and reference in which the nozzle is used for cell delivery. When spraying cells, to ensure a possibility of cell viability being maintained, the droplet size needs to be larger than the cell size, or the membrane of the cell will be disrupted, and the cell killed when it leaves the device (Kardia *et al.*, 2014). It was hypothesised that this was the case with the MicroSprayer® Aerosolizer, a syringe sprayer used to spray both fibroblasts and HeLa cells. The droplet size (25-30 µm droplet) from the device was too small for HeLa cells (~30 µm diameter) which had poor survival, however the smaller fibroblasts (~15 µm diameter) survived the spraying process (Kardia *et al.*, 2014).

In addition to droplet size, high shear stress within the device also carries the possibility of disrupting the cell membrane, therefore this needs to be considered when selecting the spray device. This has been demonstrated numerous times using pressurised air devices; a higher air pressure correlates with a lower cell viability (Pehlivaner Kara and Ekenseair, 2016, Schwartz *et al.*, 2017, Harkin *et al.*, 2006), and a smaller nozzle orifice correlates with a lower cell viability

(Veazey *et al.*, 2005, Zhang *et al.*, 2022). When a lower air pressure is used, the pressurised air atomising devices may be optimal for applications requiring a large surface area coverage, such as cell delivery to burns, as the cell suspensions can be loaded into a large volume hopper and a continuous air supply allows for a continuous spray to be generated. However, for applications requiring smaller cell volumes, a syringe-based spray device may offer an easier alternative, with less equipment and fewer components to sterilise.

Some different syringe-based spray devices have been investigated for cell delivery. The ReCell® kit, designed to harvest and deliver autologous skin cells for wound treatment, uses a syringe-based device to deliver cells (Peirce and Carolan-Rees, 2019). Cells demonstrated 69% viability following spraying, which was only slightly reduced from 75% viability measured before spraying (Wood *et al.*, 2012). The MicroSprayer® Aerosolizer mentioned above was investigated for delivery of airway epithelial cells which enhanced recovery in rabbits with tracheal injury (Kardia *et al.*, 2018).

It has been shown softer surfaces onto which sprayed cells land improved cell viability (Hendriks *et al.*, 2015). Also, lower viscosity of the medium that cells are suspended within for spraying, as well as droplets travelling with a lower velocity after spraying, both correlated with a better cell viability due to smaller forces being exerted on the cells (Hendriks *et al.*, 2015).

4.1.2. Spraying of MSCs

The immunomodulation effects make MSCs an interesting candidate for regenerative medicine. Thiebes *et al.* (2021) compared two different endoscopic spray devices for lung delivery of MSCs. One device used air pressure, and the other liquid pressure, to generate a spray. Both devices delivered viable cells at a range of cell densities, and cells retained the MSC surface markers and trilineage differentiation potential following spraying (Thiebes *et al.*, 2021). Kim *et al.* (2016) compared two liquid pressure devices designed for airway delivery, the MicroSprayer® Aerosolizer and the LMA MADgic device (produced by the same manufacturers as the MAD sprayer chosen for this project). They saw >80% viability in the sprayed cell population, and carried out further characterisation using the LMA MADgic device (Kim *et al.*, 2016). The results

of both these studies suggested pressurised liquid devices can be used for the spray delivery of viable MSCs.

4.1.3. Spray delivery materials

To prevent cells dripping off or away from the delivery site, materials can be used to aid retention at the delivery site. Spraying biomaterials can be particularly useful to aid delivery to uneven topographies and hard-to-reach areas (Moakes *et al.*, 2022). The Tisseel fibrin spray by Baxter is already used (acellular), and was developed to control bleeding and for wound closure in surgery and wound care settings (Macgillivray, 2003). The device combines fibrinogen and thrombin to form a fibrin clot to aid with wound closure and has medical approval already (Macgillivray, 2003). For this reason, many groups have investigated the addition of a variety of cells, including MSCs, into the system to aid recovery of wounds. Using the Tisseel fibrin spray system (Tissomat™), retention of viability and differentiation potential has been demonstrated using adipose derived MSCs (Zimmerlin *et al.*, 2013), and accelerated wound closure has been demonstrated in a trial using human patients (Falanga *et al.*, 2007). Therefore, the Tisseel fibrin spray has been investigated for cell delivery for wound healing in several studies outlined in Table 4.2.

Table 4.2 – Summary of a selection of the devices, cell types, carrier material for spraying, intended indication, and measured outcomes of studies investigating the used of materials for cell delivery by spraying.

Spray device	Cell type	Carrier material	Indication	Outcome	Reference
Tissomat™ - air pressure device	Keratinocytes	Fibrinogen and thrombin to form fibrin (Tisseel)	Wound healing	10 psi resulted in no reduction in viability and slight reduction in metabolic activity. The fibrinogen and thrombin components were diluted, but still prevented run-off from the sprayed surface.	(Harkin *et al.*, 2006)
Tissomat™ - air pressure device	BM-MSCs	Fibrinogen and thrombin to form fibrin (Tisseel)	Wound healing	Wound healing was compared in mice and humans, with a higher cell number correlating with more wound closure. Cells retained their surface markers and ability to differentiate after spraying. Viability data was not shown.	(Falanga *et al.*, 2007)
Tissomat™ - air pressure device	Stromal vascular cells including MSCs	Fibrinogen and thrombin to form fibrin (Tisseel)	Wound healing	Cell viability was not measured; however, cells retained their ability to proliferate and differentiate.	(Zimmerlin *et al.*, 2013)
Airbrush spray device	MC3T3-E1	Alginate	Cell printing	Cell viability of 84% was achieved using a 240 µm nozzle.	(Ahn *et al.*, 2012)
Airbrush spray device	Rat fibroblasts	Polyamidoamine (PAMAM) and N-isopropylacrylamide (NiPAAm)-co-glycidyl methacrylate (GMA) gels	Intestinal delivery	The lowest pressure tested (0.5 bar) demonstrated the highest cell viability (75%). Generally, the higher the viscosity, the lower the cell viability. The single stream spray method resulted in total cell death. The dual stream method was better suited using this material.	(Pehlivaner Kara and Ekenseair, 2016)
Airbrush spray device	Human dermal fibroblasts	Gellan fluid gel	Wound healing	No significant difference in cell viability was seen in sprayed vs not sprayed cells using the gellan fluid gel. The gel prevented run off from the surface of the skin.	(ter Horst *et al.*, 2019)
Airbrush spray device	Rat dermal fibroblasts	Dextran to increase viscosity	Cell printing/modelling	Increasing viscosity and pressure correlated with poor cell viability. The model developed correlated with the measured results.	(Hendriks *et al.*, 2015)

Materials other than fibrin have also been used to aid the spray delivery of cells, including PAMAM:NiPAAm-GMA gel (Pehlivaner Kara and Ekenseair, 2016), alginate (Ahn *et al.*, 2012), and a gellan fluid gel (ter Horst *et al.*, 2019). As discussed in Chapter 1, to be a suitable material for spraying, it must show shear thinning properties, or be liquid during the spraying process. Viscosity is an important factor to consider when using a material to aid the delivery of cells by spraying. As mentioned, a high viscosity can negatively affect the viability of the cells (Hendriks *et al.*, 2015). The viscosity of the PAMAM:NiPAAm-GMA gel was too high to achieve suitable cell viability when cells were sprayed within the material, therefore a dual-spray system was established whereby the cell suspension was sprayed through one nozzle, and the gel material sprayed through a separate nozzle at the same time (Pehlivaner Kara and Ekenseair, 2016). Alginate (which is cross-linked with Ca^{2+}), used for a spray-based cell laden scaffold printing application, demonstrated 86% cell viability when incorporated $CaCl_2$ concentrations were lowest (0.5% w/v), therefore viscosity was lowest, and the scaffolds were stabilised after spraying by addition of more $CaCl_2$ (Ahn *et al.*, 2012). The gellan fluid gel investigated by ter Horst *et al.* (2019) for cell delivery to the skin demonstrated shear thinning properties, with a greatly reduced viscosity at high shear rates. The shear thinning property meant dermal fibroblast viability was maintained during spraying, and a gel formed after the gellan and cells had been sprayed (ter Horst *et al.*, 2019).

The sprayed material and the spraying process may also affect the phenotype of the cells, which may in turn affect their therapeutic potential. If the MSCs are no longer expressing particular proteins and other components of the secretome, this could reduce their regenerative, protective, and anti-inflammatory potential as the secretome is key to the biological effects of MSCs in regenerative medicine (Han *et al.*, 2022).

4.1.4. Properties of MSCs

MSCs have been investigated for a range of regenerative medicine purposes, including bone, cartilage, and muscle repair, as well as for neurological diseases and injuries (Han *et al.*, 2019). As mentioned in Chapter 1, to be designated as MSC, cells must be plastic adherent, positive for CD90, CD105, and CD73 surface markers, and not express CD45, CD34, CD14, CD11b, CD79α, CD19,

or HLA-DR, and be able to differentiate into osteogenic, adipogenic, and chondrogenic lineages (Dominici *et al.*, 2006). CD90 is a cell adhesion molecule which has functions in inflammation and wound healing (Kisselbach *et al.*, 2009). CD105 (also known as endoglin) is part of the transforming growth factor-β (TGF-β) receptor complex and has roles in promoting angiogenesis (Mark *et al.*, 2013). CD73 (also known as ecto-5′-nucleotidase) dephosphorylates AMP to form adenosine, although the function does depend on the cell type and tissue, as CD73 also has functions in binding to components of the extracellular matrix (Minor *et al.*, 2019). One study has shown $CD73^+$ populations of MSCs have more stemness than their negative counterparts, and that they promote fracture healing *in vivo* (Kimura *et al.*, 2021), suggesting important functions in regeneration and repair. Stemness refers to the proliferative and differentiation potential of a population of cells, and specifically to the undifferentiated state when considering MSCs (Kuhn and Tuan, 2010). Where the MSCs are being used to aid repair and modulate inflammation, the differentiation of those cells may not be necessary, such as in the case of TBI (Andrzejewska *et al.*, 2021). Any process that negatively affects stemness of the MSCs could negatively affect the potential of those cells in regenerative medicine (Kimura *et al.*, 2021).

4.1.5. MSC secretome

It was initially thought that once delivered, cells may be able to integrate and differentiate within injured tissues for repair, however studies tracking hMSCs delivered to rats with induced TBI have shown repair without cell integration (Mahmood *et al.*, 2003). It is now generally accepted that the mechanism of action for MSCs is via paracrine signalling and the secretion of growth factors, cytokines, and extracellular vesicles (which comprise the secretome) which are involved in immunomodulation, regeneration, and angiogenesis (Jovic *et al.*, 2022, Fontaine *et al.*, 2016).

MSCs are able to migrate to the injury site in response to inflammation (English, 2013). One study investigating MSC migration induced an inflammatory lesion using LPS on one side of a rat's brain and delivered MSCs on the other. MSCs only migrated away from the delivery site in response to the inflammation at the lesion; MSCs in rats with no inflammatory lesion remained localised at the

delivery site (Jackson *et al.*, 2010). This homing capacity is due to the ability of cells to tether to the vasculature, become activated in response to inflammatory markers, then migrate through vasculature and tissue to the site of damage in response to chemotactic signals (Ullah *et al.*, 2019).

MSCs have been shown to secrete many factors, including growth factors such as vascular endothelial growth factor (VEGF) with pro-angiogenic effects, hepatocyte growth factor (HGF) with pro-regenerative effects, and brain derived growth factor (BDGF), nerve growth factor (NGF), and glial cell line-derived neurotropic factor (GDNF), for neuroprotective effects (Baez-Jurado *et al.*, 2019). MSCs have also been shown to secrete anti-inflammatory factors such as TGF-β, interleukin-10 (IL-10), and indoleamine 2,3-dioxygenase (IDO), which have anti-inflammatory and immunomodulatory properties (Ferreira *et al.*, 2018, Baez-Jurado *et al.*, 2019). MSCs have been shown *in vitro* to suppress T-cell activation and shift macrophages from an M1 pro-inflammatory phenotype towards an M2 anti-inflammatory phenotype (Margiana *et al.*, 2022).

In the context of TBI, MSCs have been shown to modulate inflammation via the secretome, showing reduced neutrophil infiltration, reduced BBB permeability, reduced apoptosis of cells, and increased phagocytosis (Pischiutta *et al.*, 2022). The secretome includes extracellular vesicles or exosomes, and when these have been isolated from MSCs, these have been shown to improve functional recovery in rat models of TBI, having promoted angiogenesis and neurogenesis after delivery (Zhang *et al.*, 2015). A proteomic analysis of the secretome of human BM-MSCs has found 315 different proteins, including growth factors and cytokines linked to wound healing and immunomodulation (Baberg *et al.*, 2019). These have a positive effect on TBI outcome, as well as other neuropathologies including stroke and disease (Baez-Jurado *et al.*, 2019).

This immunomodulatory phenotype is enhanced by preconditioning of MSCs using soluble factors such as interferon-γ (IFN-γ), tumour necrosis factor-α (TNF-α), IL-1β (Rodriguez *et al.*, 2019), and IL-17A (Sivanathan *et al.*, 2017). MSCs cultured in the presence of INF-γ, TNF-α, and IL-1β upregulate their production of IL-10 and IL-1RA, particularly when the cells are then challenged with lipopolysaccharide (Rodriguez *et al.*, 2019). Hypoxia is another pre-conditioning method currently under investigation, with the hypothesis being

that MSCs are often found endogenously within low-oxygen areas, therefore culturing them with low oxygen could enhance their regenerative potential; efficacy in a variety of animal models has been demonstrated (Ferreira *et al.*, 2018).

3D culture of MSCs is environmentally closer to endogenous conditions and investigations have found that pre-conditioning cells by culturing them in 3D prior to transplant enhances their therapeutic behaviour (Wobma *et al.*, 2018). Culturing the cells as spheroids promotes stemness, with increased expression of transcription factors including Oct4, Nanog, and Sox2 (Pennock *et al.*, 2015). Spheroid cultured MSCs showed superior engraftment following intramuscular injection into the hindlimb of mice (Cheng *et al.*, 2012).

Whilst harnessing the secretome seems promising as an option for a cell-free therapy (González-González *et al.*, 2020), the transfer of mitochondria between MSCs and mouse neurons damaged by H_2O_2 has been implicated in protection and recovery, which occurs via direct cell-cell contact (Tseng *et al.*, 2021). Therefore, the use of MSCs over the secretome alone may still be beneficial for regenerative purposes.

4.1.6. Transcriptome analysis

To investigate specific proteins secreted from MSCs, enzyme-linked immunosorbent assays (ELISAs) can be used to directly detect proteins (Arnold, 2000b). Alternatively, polymerase chain reaction (PCR) experiments can be undertaken to detect the mRNA responsible for the synthesis of the protein of interest (Arnold, 2000a). Providing the ELISAs and PCRs are optimised adequately, both methods are highly effective at quantifying levels of a particular molecule expressed and secreted by cells. However, the methods are limited by the number of molecules that can be realistically analysed as they both detect one molecule at a time (Di Gaspero *et al.*, 2022). In addition, both methods are biased by experimental design; the proteins of interest are selected, whereas transcriptome analysis will sequence all extracted RNA (Wang *et al.*, 2009). Transcriptome analysis is a technique that analyses all genes transcribed into mRNA, therefore overcoming this selection bias. This technique is powerful and was enabled by the development of Next Generation Sequencing of DNA (Schuster, 2008).

To carry out transcriptome analysis, RNA is extracted from the sample of cells or tissue, and a cDNA library is generated from the RNA. The cDNA is then sequenced to determine expression levels of each transcript (Ma *et al.*, 2019). The expression levels can then be compared to a control sample to determine whether a particular treatment has affected the expression levels of genes (Blumenberg, 2019). There are a number of different methods to prepare libraries from the extracted RNA. Many methods utilise the poly-A (adenine) tail found at the 3′ end of mRNA to separate it from other unwanted RNA (Ura *et al.*, 2022). This can be carried out by using magnetic beads with a poly-T (thymine) sequence on to extract the mRNA. This mRNA is fragmented, and reverse transcribed into cDNA, which is turned into double stranded cDNA for sequencing. Alternatively, the poly-A tail on the mRNA can be used as a binding site for a complementary poly-T primer to generate the first cDNA strand, followed by random primers to bind to the cDNA to form a double cDNA strand for sequencing (Hrdlickova *et al.*, 2017). These steps are shown in Figure 4.2.

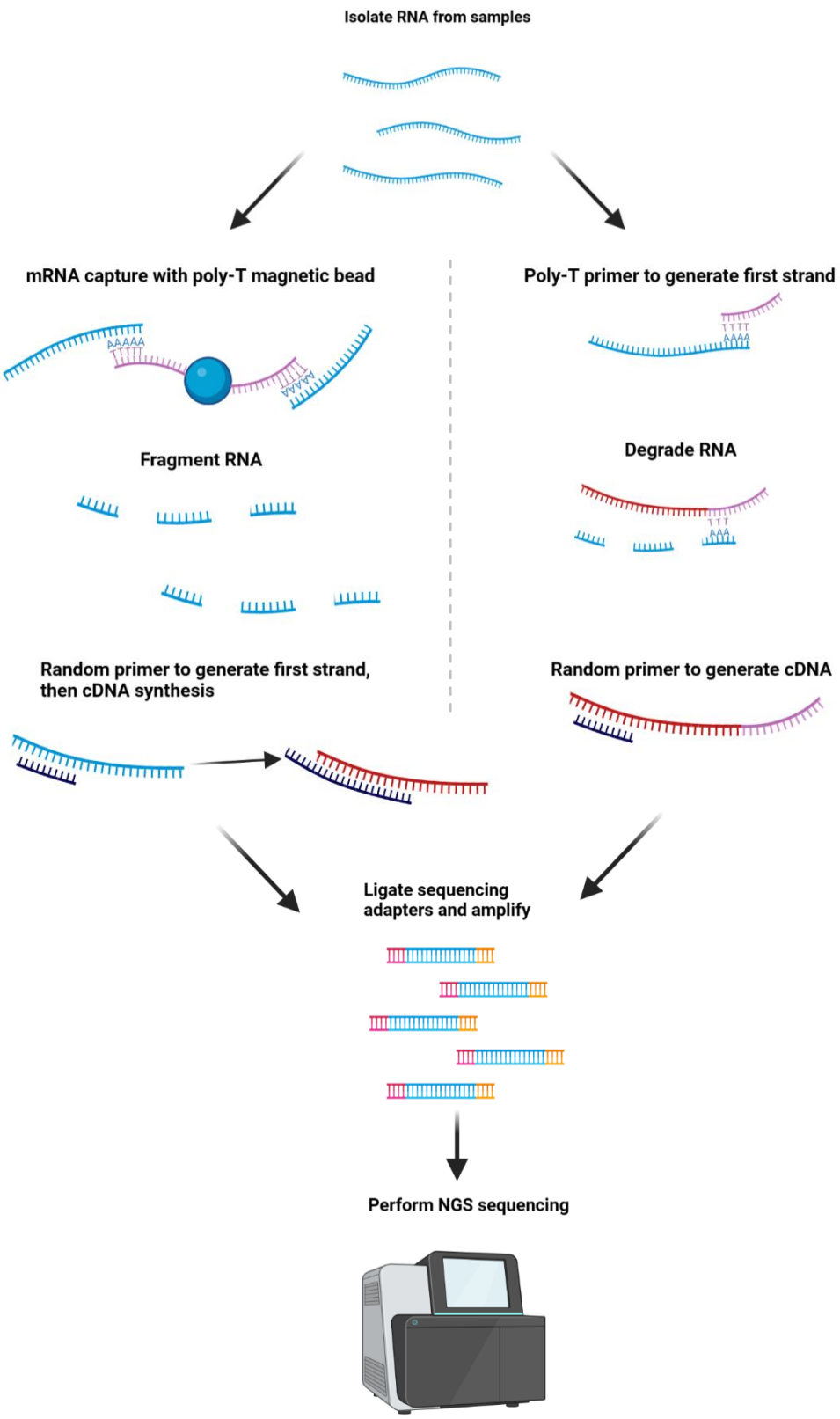


Figure 4.2 – Schematic showing a summary of library preparation using poly-T magnetic beads to capture mRNA (left), or poly-T primers (right) to go on to generate the cDNA library for sequencing. Figure prepared in BioRender and adapted from Ma *et al.* (2019).

Both the bead extraction and the 3′ method have advantages and disadvantages. The bead isolation method fragments the mRNA, therefore generates a bias towards longer transcripts. These longer transcripts form more fragments, therefore appear to have higher expression levels than shorter transcripts (Ma *et al.*, 2019). The 3′ method truly generates just one cDNA molecule per transcript prior to the amplification step, as it requires no fragmentation due to using the 3′ end to bind the primer. The expression levels measured do not show transcript length bias, however, a drawback of this method is enrichment at the 3′ end; the library preparation does not detect different splice variants of genes, particularly if the variants tend towards the 5′ end (Ma *et al.*, 2019). Cost is another factor to consider, the 3′ method libraries are cheaper per sample to prepare, making it more accessible to researchers (Naphade *et al.*, 2022).

Transcriptome analysis has been used to understand the effect of various different factors on gene regulation in hMSCs. The secretome can be affected by pre-treatment of cells with soluble inflammatory markers (Rodriguez *et al.*, 2019). Differential gene expression analysis has highlighted that pre-treatment with IFN-γ leads to upregulation of genes involved in the immune response, whereas pre-treatment with IL-17A leads to the upregulation of genes such as matrix metalloproteinases (MMPs) for chemotaxis and immunosuppression (Sivanathan *et al.*, 2017). The differential expression of >4000 genes was identified following treatment of hMSCs with nanosilicates, including genes related to stress-responsive and surface receptors, for example those in the MAPK pathway and osteogenic differentiation (Carrow *et al.*, 2018). A meta-analysis of hMSC microarrays to understand the effect of donor sex on processes involved in stemness, inflammation, and differentiation concluded sex is a variable influencing expression of key genes involved in these processes, and therefore could affect their therapeutic potential (Bianconi *et al.*, 2020). Undertaking these analyses to understand the effect of treatments or variables can lead to the identification of pathways involved in responses to treatments and the generation of more hypotheses for future work (Blumenberg, 2019).

4.2. Hypothesis, aims, and objectives

4.2.1. Hypothesis:

- Spraying in pectin solutions, using the MAD sprayer, is an appropriate delivery method for cells.

4.2.2. Aims:

- To determine whether viable cells can be sprayed through a pressurised liquid turbine syringe-based device (MAD sprayer).
- To determine whether pectin is suitable to spray cells in and select the best grade for this purpose.

4.2.3. Objectives:

- Assess the viability of 3T3 mouse fibroblasts, and SH-SY5Y human neuroblastoma cells after being sprayed through the MAD syringe-based device using prestoBlue. Use a range of cell densities to assess whether this affects survival.
- Assess the viability of primary hMSCs after being sprayed through the MAD syringe-based device using prestoBlue, LDH, and Live/Dead staining. Further, assess the viability of the hMSCs after being sprayed through the MAD syringe-based device in pectin solutions using Live/Dead staining.
- Measure the effect of spraying or syringing of hMSCs in pectin solutions on the expression of CD90, CD105, CD73, CD34, CD11b, CD19, CD45, and HLA-DR by flow cytometry.
- Assess the effect of spraying and pectin on the potential of the hMSCs to differentiate down an adipogenic or osteogenic lineage. Assess whether spraying or pectin induces spontaneous differentiation of the down an adipogenic or osteogenic lineage when cultured in basal growth media.
- Carry out RNA-seq on sprayed and syringed cells in pectin and 1xPBS:
    a. Determine whether there is a change in the expression levels of proteins of the secretome implicated in immunomodulation and pro-regenerative properties.
    b. Analyse the effect of pectin and spraying on the differential expression of genes.

4.3. Method design

4.3.1. Spray device

As discussed, the desired spray device was a syringe-based device. This has advantages for use with cells as there is very little sterilisation of equipment required and they are simple and easy to use. The device selected was the Mucosal Atomisation Device (MAD) which attaches to both standard and Luer-loc end syringes. The MAD is a patented device principally designed for nasal drug delivery (Denton, 2022).

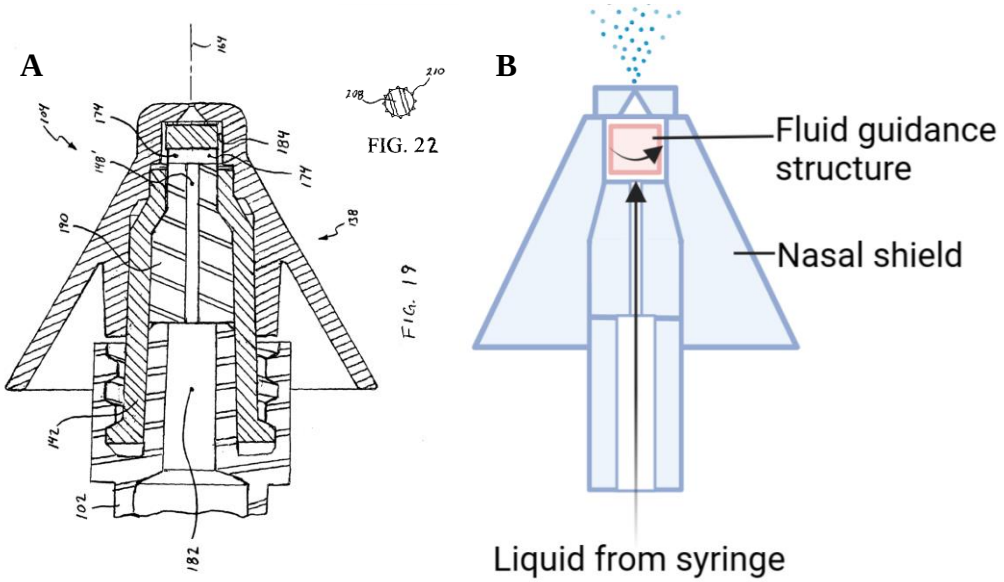


Figure 4.3 – The MAD sprayer. **A** shows figures from the patent application document referenced above. The image labelled "FIG 19" is a cross-sectional view of the device. The image labelled "FIG 22" is the turbine fluid guidance structure. **B** shows a schematic of the MAD sprayer with fluid path shown. Image created in BioRender.

For experiments with cells, the nasal shield was removed from the device as it was not required and is otherwise an additional part requiring sterilisation. The device claimed to have an increased efficiency as there is very little dead space internally, shown in the part labelled "FIG 19". This feature was useful for cell delivery as it had the potential to minimise cells lost within the device. The part labelled "FIG 22" is a turbine which guided fluid down the ribs (labelled "210") to generate the spray as fluid left the device. This was removed from the spray device and imaged, along with the outer casing to obtain dimension (used in Chapter 3 to calculate shear stress). The outer casing was damaged when removing the internal turbine, but the hole through which fluid exits is still visible.

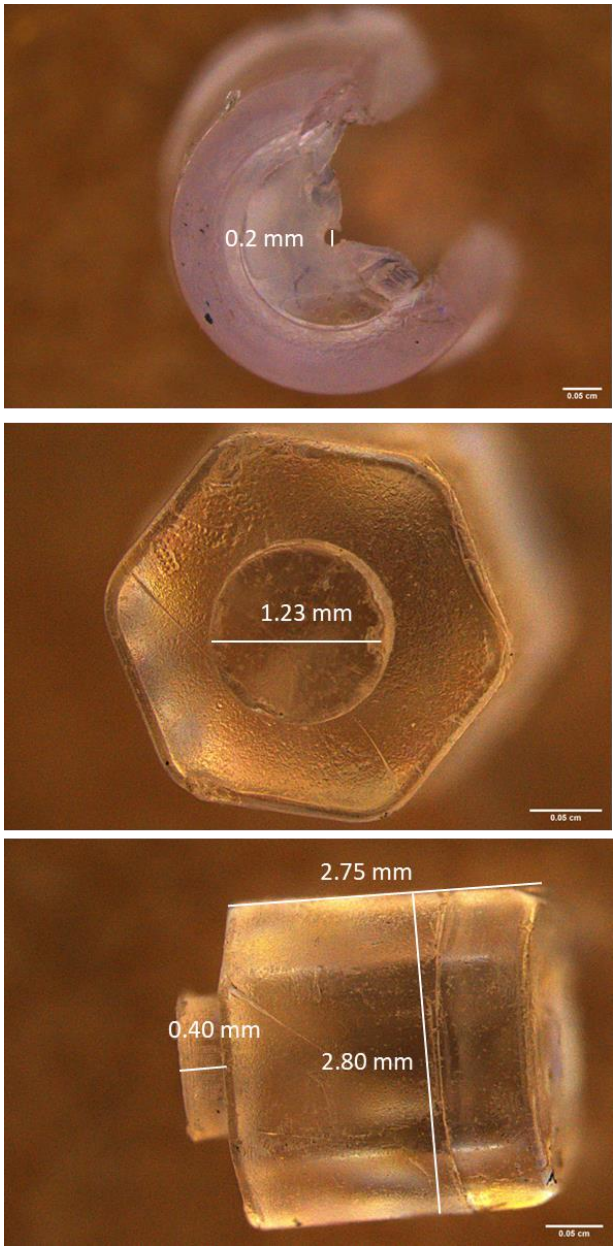


Figure 4.4 – Images of the turbine labelled “FIG 22” in Figure 4.3 and the outer casing which contains the turbine and the fluid exit hole. Imaged using the Leica M205A microscope. Dimensions were measured in FIJI.

4.3.2. Cell spraying

To test the patent claim for the reduced dead space in the MAD sprayer, which should therefore result in fewer cells being retained within the device, cells were counted before and after delivery by pipetting, syringing, and spraying. SH-SY5Y cells were used for this test to understand whether any cells were lost and whether this would affect the prestoBlue and LDH assays.

After assessing cell retention within the device, SH-SY5Y cells and 3T3 mouse fibroblasts were used in initial optimisation studies where the metabolic activity and LDH release 24 hours after seeding was measured to understand the effect of spraying and the cell density on the cells. This minimised the use of expensive primary hMSCs.

Following optimisation with cell lines, primary bone marrow (BM) derived hMSCs were used with the spray device and the viability, metabolic activity, and LDH release were measured. hMSCs were used from three separate human donors, details of which are listed in 2.4.3. The cells were then suspended in pectin and the viability measured by Live/Dead staining and confocal microscopy. The metabolic activity and LDH release could not be measured due to pectin interfering with the assays. Following this, the effect of the pectin and spraying on the phenotype was analysed by flow cytometry to measure whether the cells are still positive for CD90, CD105, and CD73, and negative for CD35, CD11b, CD19, CD45, and HLA-DR. Osteogenic and adipogenic differentiation potential was assessed using two of the three donors and using CU-701 pectin. Each condition was tested for differentiation potential using differentiation-inducing media, and for spontaneous differentiation using control basal growth media.

Additionally, to understand the effect of spraying and pectin on the gene expression of the hMSCs, transcriptome analysis was carried out. CU-701 pectin only was selected for this analysis (sprayed and syringed) based on the flow cytometry results. The QuantSeq 3′ mRNA-Seq library prep kit from Lexogen was selected to prepare the library for sequencing. The 3′ method does not give information on splice variants but can give more accurate information on differential gene expression. The cells were analysed 24 hours after seeding by syringe or spraying. This time point was chosen to remain consistent with the timepoints tested for flow cytometry and viability, and because any change in gene expression in response to the stress of spraying should be detectable (Blumenberg, 2019).

The purpose of carrying out the transcriptome analysis was to understand whether there was any up or down regulation of genes in response to the process of spraying. Any changes in the differential gene expression analysis for the PBS

spray versus PBS syringe, and the CU-701 spray versus CU-701 syringe comparisons would inform of any changes in response to the spraying process. Comparing those changes in gene expression in PBS or CU-701 pectin would in turn inform of whether the cells respond differently to being sprayed in PBS compared to pectin. The second purpose was to understand whether the pectin had an effect on gene expression, independent of the spraying. The CU-701 spray vs PBS spray, and the CU-701 syringe vs PBS syringe differential gene expression analysis would be informative of any changes that occur. As mentioned above, the expression of various growth factors and cytokines with pro-regenerative and anti-inflammatory effects can be upregulated for hMSCs in 3D when compared to hMSCs cultured in 2D on tissue culture plastic (Rodriguez *et al.*, 2019). The following genes were searched for in the list of significantly up or down regulated genes in the differential expression analysis, based on their implication in pro-regenerative and anti-inflammatory effects: TGFB1, IGF1, VEGF, HGF, GDNF, BDNF, NGF, IDO, IL1RN, Oct4, and Sox2.

4.4. Results

4.4.1. Cell retention within spray device

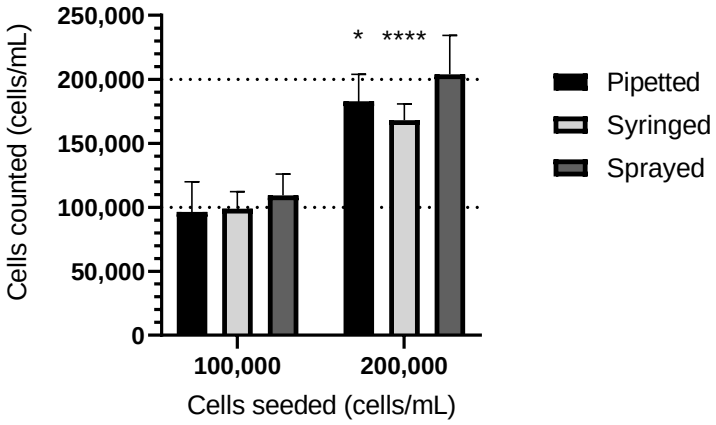


Figure 4.5 – SH-SY5Y cells counted following pipetting, syringing, or spraying (using the MAD sprayer) at 100,000 or 200,000 cells/mL using a haemocytometer. Three repeats were carried out in triplicate (N=3, n=3). Error bars show standard deviation. A one sample t-test was carried out to compare the mean of each group to the theoretical cell count (100,000 or 200,000). * Shows P≤0.05, **** shows P≤0.0001.

To determine whether cells were retained within the chosen spray device, cell counts using the SH-SY5Y cells were carried out. The results shown in Figure 4.5 indicate the spray device does not retain cells at either density tested. Cells seeded by pipette, syringe, or spray at a cell density of 100,000 cells/mL showed no statistical difference between the starting density and the measured density after seeded. In groups where cells were seeded by pipette, syringe, or spray at a density of 200,000 cells/mL, the sprayed cells showed no statistical difference, whereas the pipetted and syringed cells did, with the means of both groups below 200,000 cells/mL. This indicated that cells were not retained within the spray device, but did show, particularly at the higher cell density, that counted cells after syringe and pipette were lower than expected.

4.4.2. Metabolic activity of 3T3 mouse fibroblasts after spraying

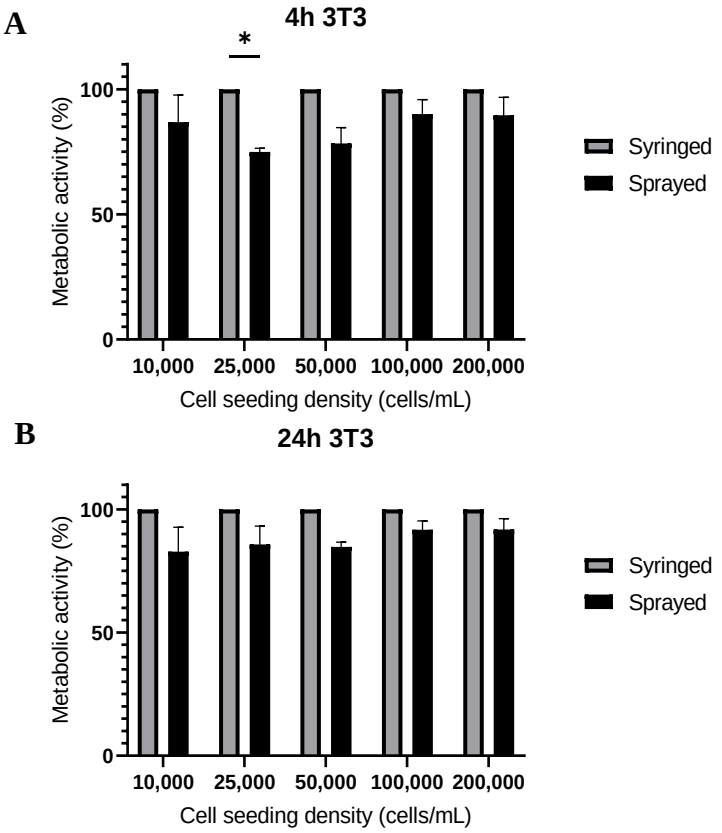


Figure 4.6 – Short-term assessment of the effect of spraying on the metabolic activity of the mouse 3T3 fibroblast cell line. Cells were added to 24-well plates by either spraying through the MAD or added via syringe (500 µL). Metabolic activity was assessed **A** 4- or **B** 24-hours after seeding by PrestoBlue assay. Metabolic activity is shown as a percentage of each syringed control at each seeding density. Three repeats were carried out in triplicate (N=3, n=3). Error bars show standard error of the mean. Multiple paired t-tests (normal distribution) were carried out to determine statistical significance between each syringe and spray conditions. P value set to 0.05 with Holm-Šídák correction. * Shows $P \leq 0.05$.

After confirming cells were not retained within the spray device, prestoBlue assays after spraying were carried out to measure the metabolic activity of the cells after spraying as an indirect measure of viability, first using 3T3 cells. This enabled optimisation of the spraying conditions using inexpensive cell lines. Results shown in Figure 4.6 suggest there is a reduction in metabolic activity of the 3T3 cells after spraying, however this reduction is not statistically significant in all conditions and timepoints, except with a seeding density of 25,000 cells/mL tested 4 hours after seeding where there was a 25% reduction in metabolic activity. After 24 hours, the maximum reduction in metabolic activity compared to the syringe control was approximately 18%.

4.4.3. Metabolic activity and LDH release from SH-SY5Y cells after spraying

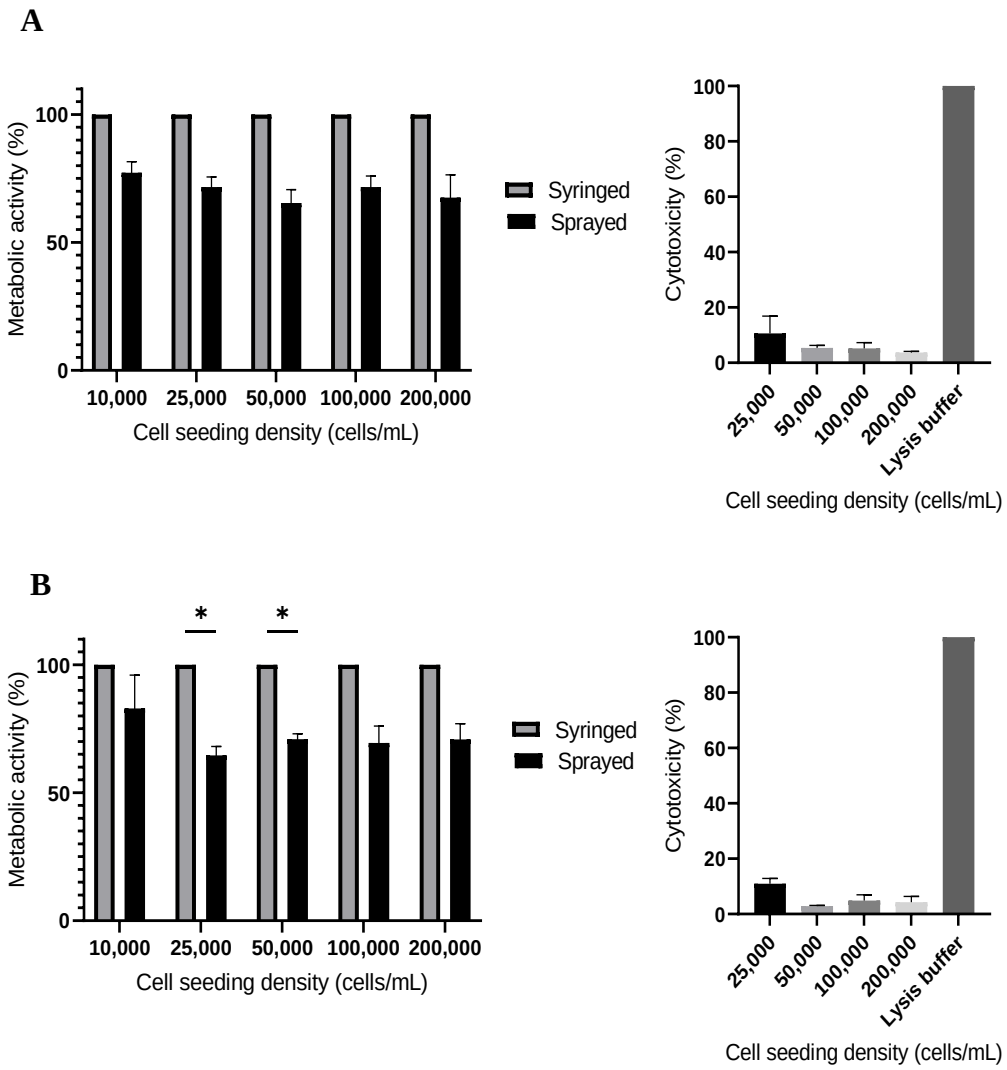


Figure 4.7 – Short-term assessment of the effect of spraying on the human SH-SY5Y cell line. Cells were added to 24-well plates by either spraying through the MAD, or via syringe (500 µL). PrestoBlue (left) and LDH (right) assay was carried after **A** 4- or **B** 24-hours to determine cytotoxicity of the spraying process. Three repeats were carried out in triplicate (N=3, n=3). Error bars show standard error of the mean. Multiple paired t-tests (normal distribution) were carried out to determine statistical significance between each syringe and spray conditions in the prestoBlue assay results. P value set to 0.05 with Holm-Šídák correction. * Shows $P \leq 0.05$.

In addition to the 3T3 mouse fibroblasts, SH-SY5Y cells were used. The LDH results shown in Figure 4.7 indicates the spraying process results in 3-10% cytotoxicity of the SH-SY5Y cells. The results of the prestoBlue assay indicate a reduction in metabolic activity in the sprayed conditions compared to the syringed, however only the seeding density 25,000 and 50,000 cells/mL at the

24-hour timepoint showed a statistically significant difference. These show the largest reduction in metabolic activity of all the densities and both timepoints tested, with a reduction of approximately 35% and 30% for the 25,000 cells/mL and 50,000 cells/mL densities respectively.

Figure 4.6 and Figure 4.7 show that the population of SH-SY5Y cells have a higher reduction in metabolic activity than the 3T3 cells. The 25,000 cells/mL seeding density was the only density to show a statistically significant reduction in metabolic activity in both cell lines. It also showed the highest release of LDH in the SH-SY5Y cells.

4.4.4. Viability of hMSCs after spraying

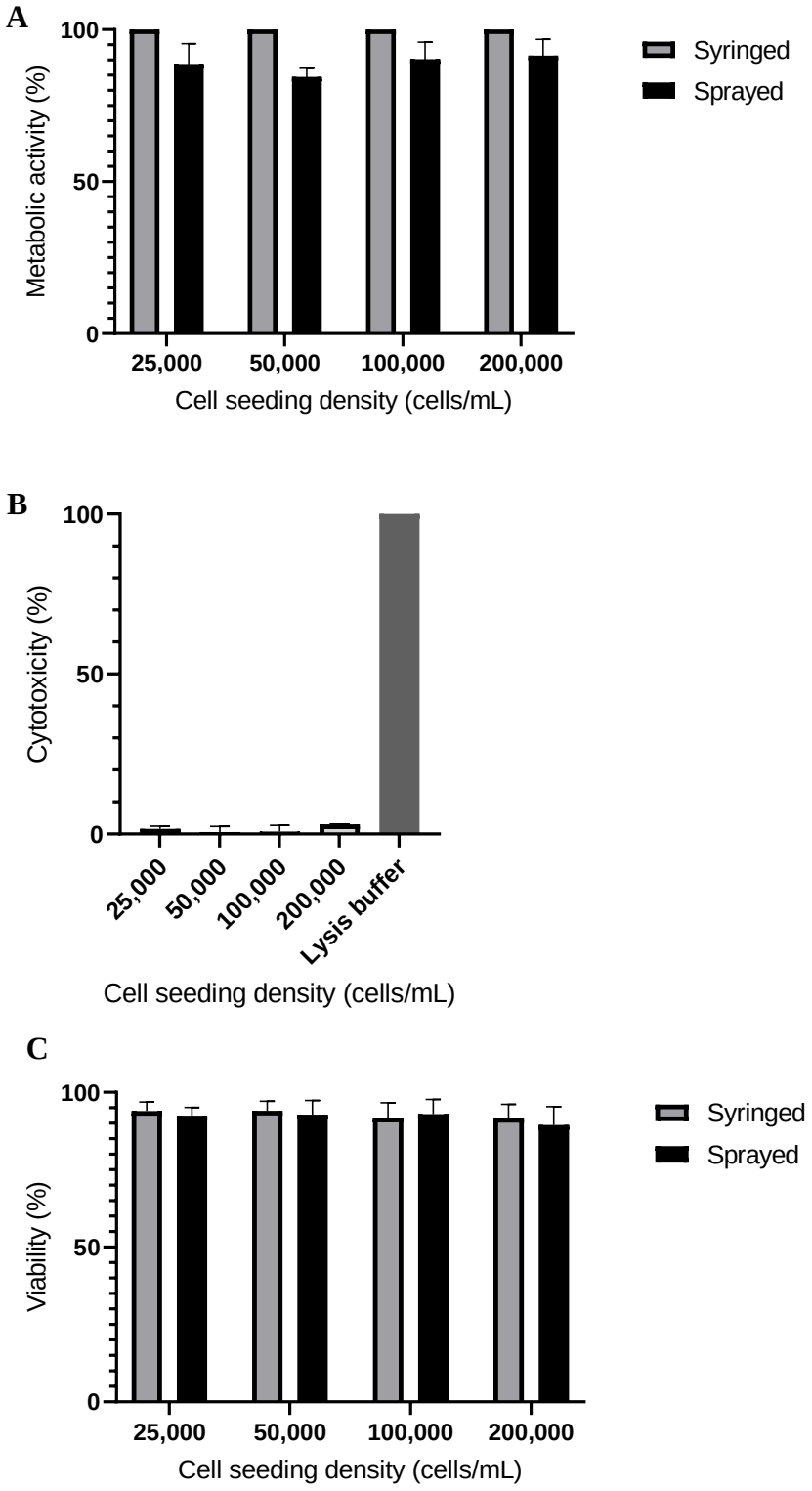


Figure 4.8 – Short-term assessment of the effect of spraying on human MSCs. Cells were added to 24-well plates by either spraying through the MAD, or by using a syringe (500 µL). After 24 hours, **A** PrestoBlue assay to determine metabolic activity, **B** LDH assay to measure LDH release, and **C** live/dead cell counts were carried out. Metabolic activity is as a percentage of each syringed

control at each seeding density. In both assays, three repeats using separate donors were carried out in triplicate (N=3, n=3). Error bars show + standard error of the mean. Multiple paired t-tests (normal distribution) were carried out to determine statistical significance between each syringe and spray conditions in the prestoBlue results. P value set to 0.05 with Holm-Šídák correction. For live/dead counting, hMSCs were stained using calcein to stain live cells, and ethidium homodimer-1 to stain dead cells, and counted in FIJI. Three repeats were carried out using separate cell donors. Error bars show + SEM.

After initial studies using 3T3 and SH-SY5Y cell lines showed that viable cells could be sprayed at a variety of cell densities, the viability of primary hMSCs after spraying was then assessed. The metabolic activity of the hMSC after spraying at the different densities shown in Figure 4.8 indicates there is a slight reduction in metabolic activity of sprayed cells after 24 hours (maximum of 15% in the 50,000 cells/mL density), however this difference is not statistically significant at any of the densities tested. In addition, the LDH release from hMSCs indicated very low levels of cytotoxicity in response to the spraying process at all densities tested, 24 hours after the cells were sprayed.

The results of the live/dead counts (Figure 4.8C) show >89% viability in all densities sprayed or syringed after 24 hours. There was very little difference between the syringed and sprayed conditions, indicating viability was maintained in hMSCs when sprayed through the MAD sprayer.

4.4.5. hMSC viability after spraying in pectin

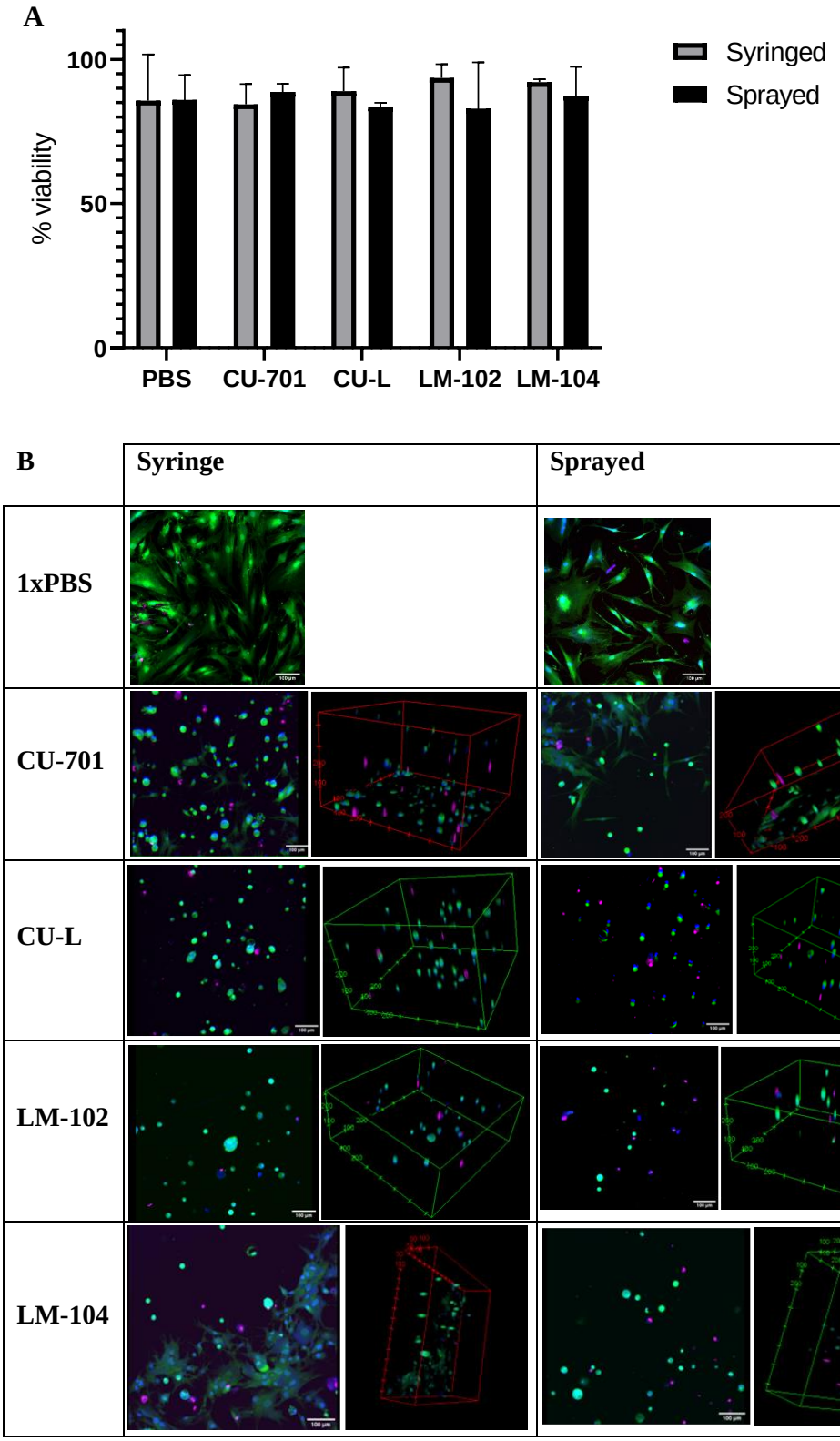


Figure 4.9 – Viability of hMSCs sprayed (MAD sprayer) or seeded by syringe within 1% w/v pectin solutions or 1xPBS. Cells were added to 24-well plates by either spraying through the MAD, or syringe (500 µL) at a density of 100,000 cells/mL. Pectin solutions were gelled with 50 µL of 100 mM $CaCl_2$, which was added to the wells before cells. Samples were incubated for 24-hours before

media was removed and Live/Dead (calcein/ethidium homodimer-1) and NucBlue Stains were added, and cells visualised using confocal microscopy, with **B** representative images shown. Images show the z stack composite (left) and 3D view (right). Green stain = live, blue = nuclei, and magenta = dead. Scale bar = 100 µm. FIJI analysis was used to calculate **A** percentage viability. Three biological replicates were carried out (N=3). Multiple paired t-tests (normal distribution) were carried out to determine statistical significance between each syringe and spray conditions. P value set to 0.05 with Holm-Šídák correction.

After establishing that viable hMSCs can be sprayed using the MAD sprayer, cells were suspended in the four pectin grades and the viability assessed using Live/Dead staining to calculate the viability of the cells. Figure 4.9 shows the viability of hMSCs when seeded by spraying or syringing in the four grades of pectin solutions or 1xPBS. The viability was determined from confocal images of the cells stained with calcein for live cells, ethidium homodimer-1 for dead cells, and NucBlue (Hoechst) to stain the nuclei (Figure 4.9B). These images show the morphology of cells within pectin gels, as well as the distribution of cells 24 hours after seeding. The morphology of the cells delivered to wells in 1xPBS appear more elongated as they are able to adhere to the surface at the bottom of the well. As there are no cell adherent sites within the pectin, all cells within the four pectin grades appear rounded, except where cells were able to adhere to the bottom of the wells as in the CU-701 sprayed and the LM-104 syringe conditions. Shown in Figure 4.9A, there is no statistical difference between the viability of the sprayed compared to the syringed cells in any of the pectin grades or 1xPBS, indicating the spraying process has little or no effect on the viability of cells 24 hours after spraying. All four grades of pectin demonstrated a very similar viability to the 1xPBS conditions.

4.4.6. Flow cytometry analysis on hMSCs after spray or syringe seeding

Following confirmation of viability, flow cytometry analysis was carried out on the hMSCs to determine whether the spraying process or the four different pectin grades affected the expression of the surface markers.

Table 4.3 – The percentage of positive cells and the standard deviation between donor repeats obtained from the flow cytometry analysis. hMSCs (500 µL at 100,000 cells/mL) were added to 24-well plates by syringe or spraying (MAD sprayer) in 1xPBS or 1% w/v pectin. 50 µL of 100 mM $CaCl_2$ were added to wells before cells to induce gelation. Samples were incubated for 24-hours before cells were extracted from pectin gels and removed from wells to form a single cell suspension. CD90, CD105, and CD73 were analysed using detection antibodies labelled with different fluorophores. The negative markers included antibodies specific to CD35, CD11b, CD19, CD45, and HLA-DR, all labelled with the PE fluorophore. Each sample was gated from the negative isotype control using PBS syringe hMSC, showing a population of cells negative for each detection fluorophore. The % positive shows the population of cells within the gate set for each sample and marker. The analysis was carried out using three separate donors. The standard deviation was calculated using the results for each donor.

% Positive cells ± standard deviation

Marker:	**PBS syringe**	**PBS spray**	**CU-701 syringe**	**CU-701 spray**	**CU-L syringe**	**CU-L spray**	**LM-102 syringe**	**LM-102 spray**	**LM-104 syringe**	**LM-104 spray**
CD90	98.08 ± 2.80	99.24 ± 1.05	97.94 ± 1.25	96.11 ± 3.67	96.71 ± 0.76	92.2 ± 5.75	93.55 ± 8.85	87.92 ± 17.77	88.71 ± 14.48	94.84 ± 3.86
CD105	83.52 ± 8.43	79.15 ± 8.89	77.84 ± 7.14	66.86 ± 16.83	75.51 ± 8.83	68.06 ± 15.50	68.16 ± 1.74	56.94 ± 19.73	53.66 ± 8.76	58.07 ± 20.69
CD73	99.31 ± 0.62	98.72 ± 1.56	98.51 ± 1.33	93.98 ± 7.71	96.11 ± 2.15	92.15 ± 5.92	98.15 ± 1.21	97.36 ± 1.79	89.71 ± 10.65	91.95 ± 8.30
Negative markers	0.15 ± 0.15	0.36 ± 0.25	0.43 ± 0.19	0.41 ± 0.25	8.81 ± 1.01	9 ± 3.48	6.1 ± 10.27	1.09 ± 1.15	2.45 ± 2.55	3.36 ± 0.93

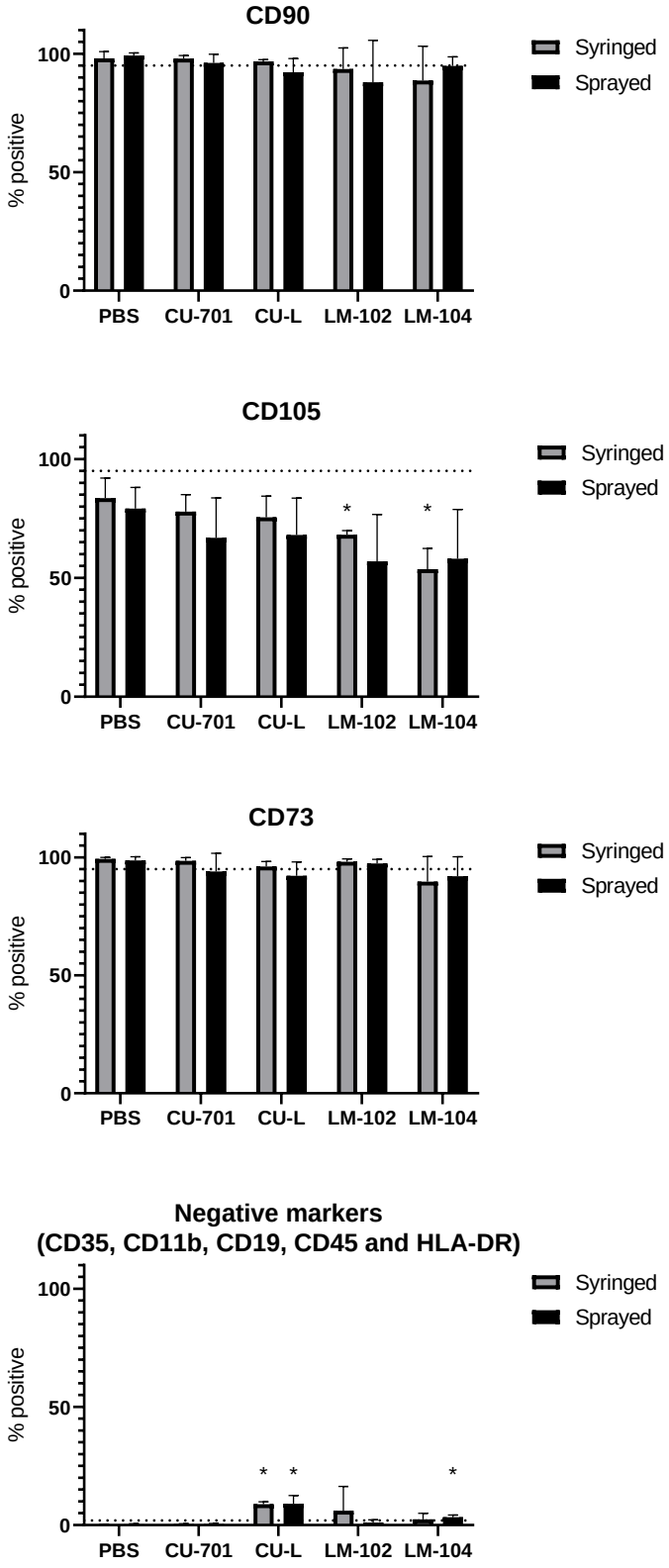


Figure 4.10 – Graphical representation of data shown in Table 4.3. hMSCs (500 µL at 100,000 cells/mL) were added to 24-well plates by syringing or spraying (MAD sprayer) in 1xPBS or 1% w/v pectin. 50 µL of 100 mM $CaCl_2$ were added to wells before cells to induce gelation. Samples were incubated for 24-hours before being extracted from pectin gels and removed from wells to form a single

cell suspension. CD90, CD105, and CD73 were analysed using detection antibodies labelled with different fluorophores. The negative markers included antibodies specific to CD35, CD11b, CD19, CD45, and HLA-DR, all labelled with the PE fluorophore. Each sample was gated from the negative isotype control using PBS syringe hMSC, showing a population of cells negative for each detection fluorophore. The dashed line in each graph shows the minimum expression level based on ISCT criteria. Three repeats were carried out on cells from different donors. Error bars show + SD. Student's paired T-test was carried out between PBS syringe condition and all other test conditions, * indicates statistically significant difference between test group and PBS syringe ($P<0.05$).

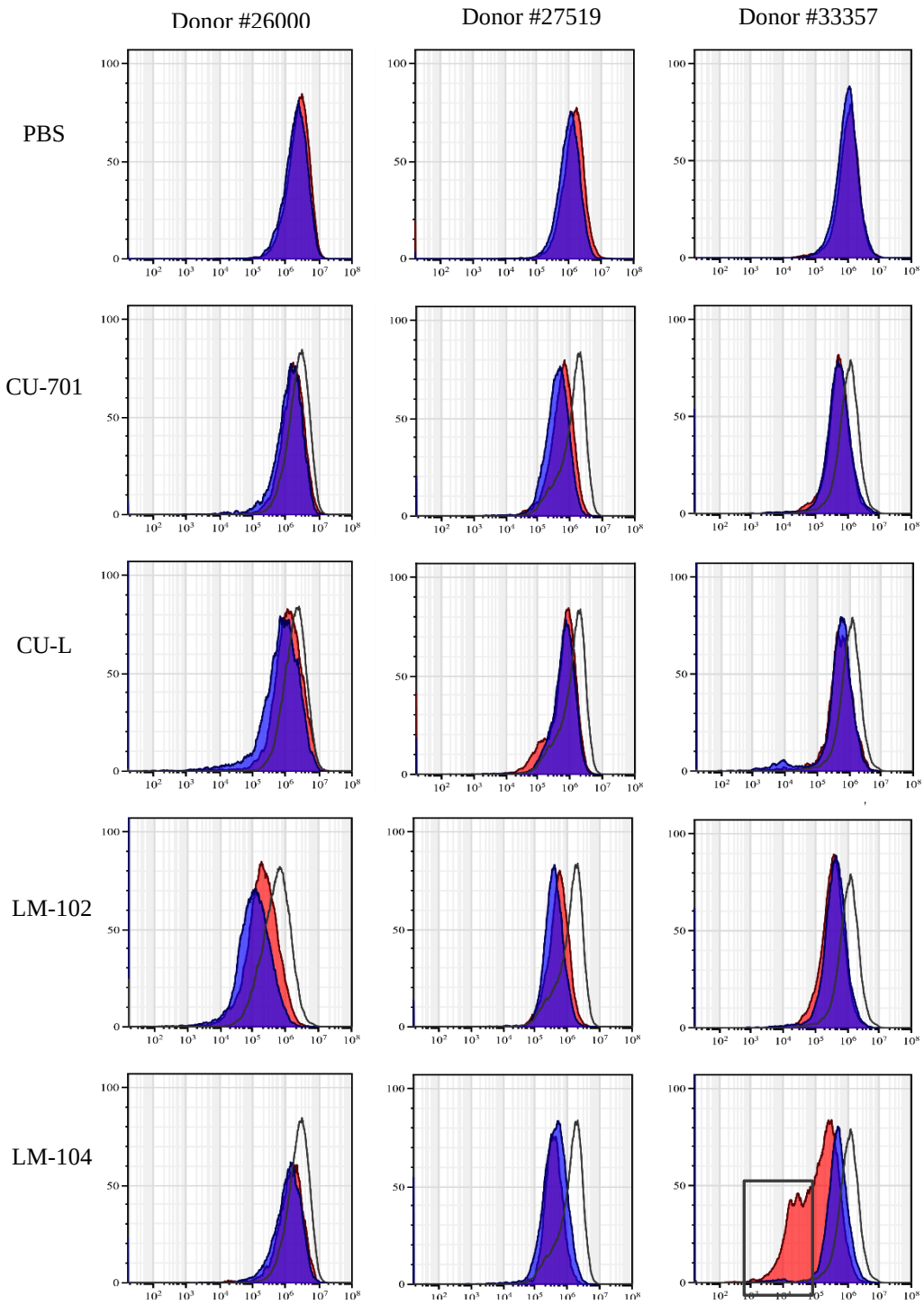


Figure 4.11 – CD90 FITC flow cytometry overlay analysis showing the histogram plots for each donor and pectin condition. hMSCs (500 µL at 100,000 cells/mL) were added to 24-well plates by syringing or spraying (MAD sprayer) in 1xPBS or 1% w/v pectin. 50 µL of 100 mM $CaCl_2$ were added to wells before cells to induce gelation. Samples were incubated for 24-hours before being extracted from pectin gels and removed from wells to form a single cell suspension. Histograms show cells from gates on the forward scatter-area (FSC-A) vs side scatter-area (SSC-A) plot to select for cells and disregard debris, then from gates set on the SSC-A vs SSC-H plot to select for single cell events. Black outline = PBS control, red = syringed samples, blue = sprayed samples. Green box highlights the negative population of cells in the LM-104 syringed condition using the #33357 donor.

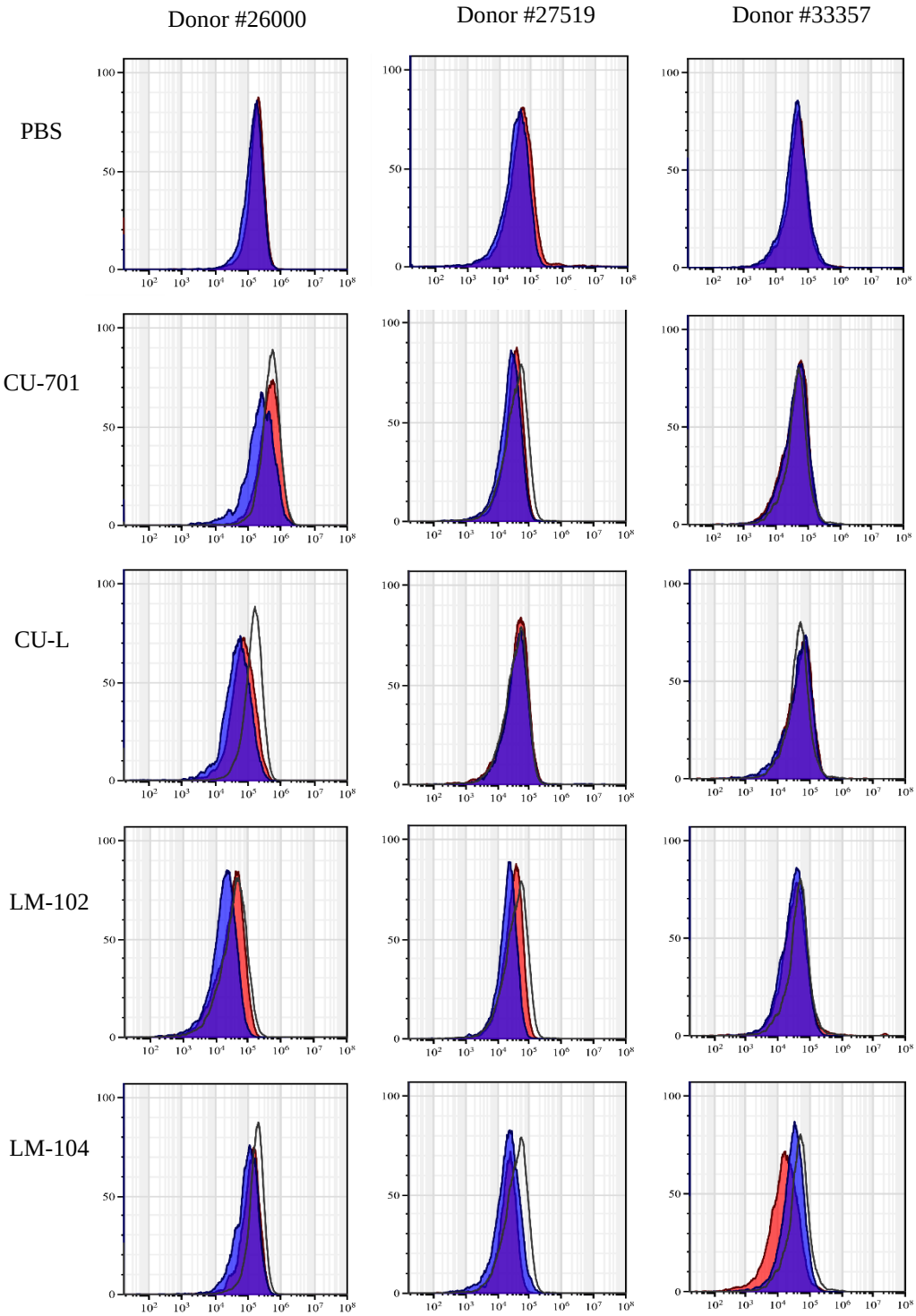


Figure 4.12 – CD105 PerCP-Cy5.5™ flow cytometry overlay analysis showing the histogram plots for each donor and pectin condition. hMSCs (500 µL at 100,000 cells/mL) were added to 24-well plates by syringing or spraying (MAD sprayer) in 1xPBS or 1% w/v pectin. 50 µL of 100 mM $CaCl_2$ were added to wells before cells to induce gelation. Samples were incubated for 24-hours before being extracted from pectin gels and removed from wells to form a single cell suspension. Histograms show cells from gates on the forward scatter-area (FSC-A) vs side scatter-area (SSC-A) plot to select for cells and disregard debris, then from gates set on the SSC-A vs SSC-H plot to select for single cell events. Black outline = PBS control, red = syringed samples, blue = sprayed samples.

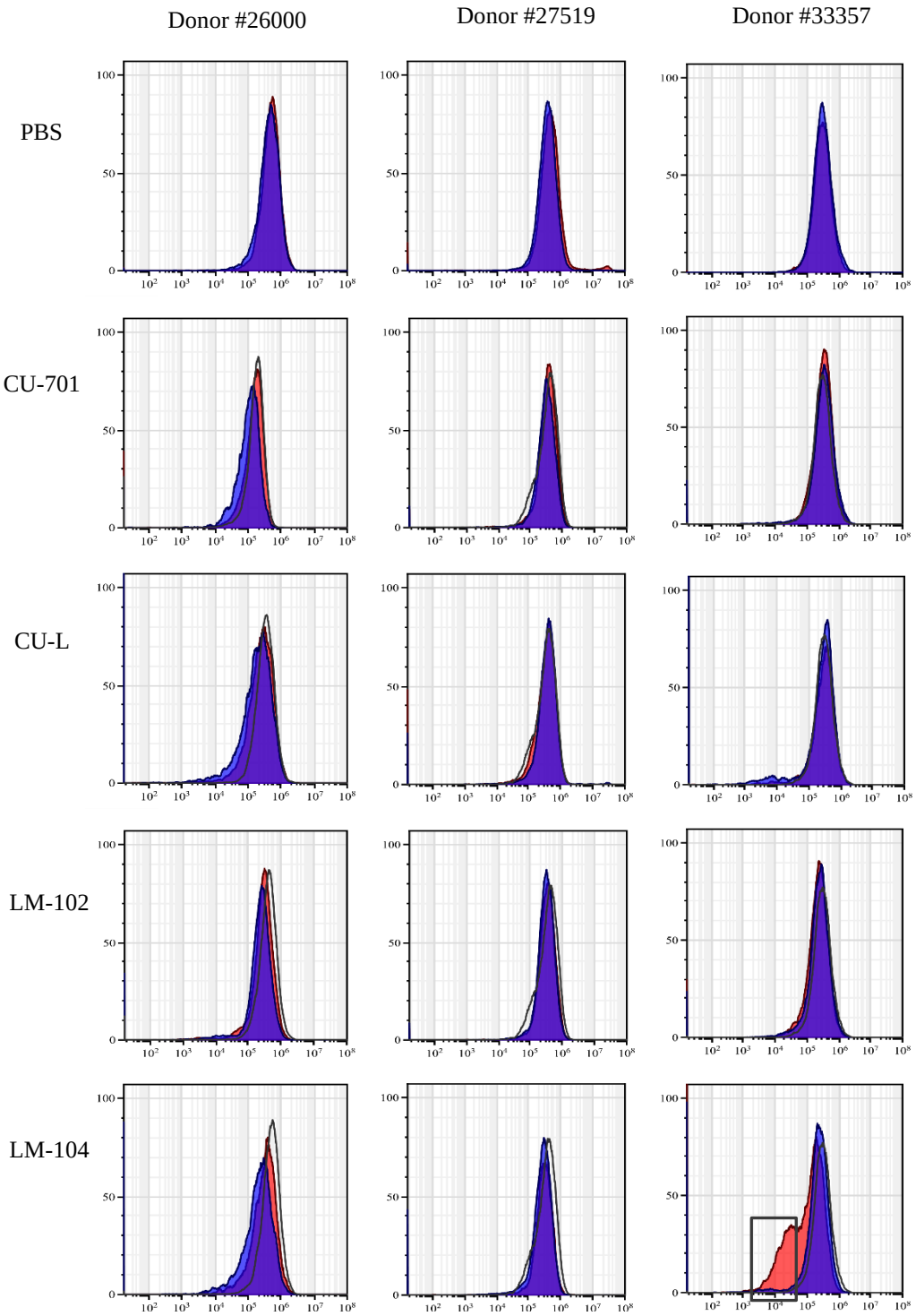


Figure 4.13 – CD73 APC flow cytometry overlay analysis showing the histogram plots for each donor and pectin condition. hMSCs (500 µL at 100,000 cells/mL) were added to 24-well plates by syringing or spraying (MAD sprayer) in 1xPBS or 1% w/v pectin. 50 µL of 100 mM $CaCl_2$ were added to wells before cells to induce gelation. Samples were incubated for 24-hours before being extracted from pectin gels and removed from wells to form a single cell suspension. Histograms show cells from gates on the forward scatter-area (FSC-A) vs side scatter-area (SSC-A) plot to select for cells and disregard debris, then from gates set on the SSC-A vs SSC-H plot to select for single cell events. Black outline = PBS control, red = syringed samples, blue = sprayed samples. Green box highlights the negative population of cells in the LM-104 syringed condition using the #33357 donor.

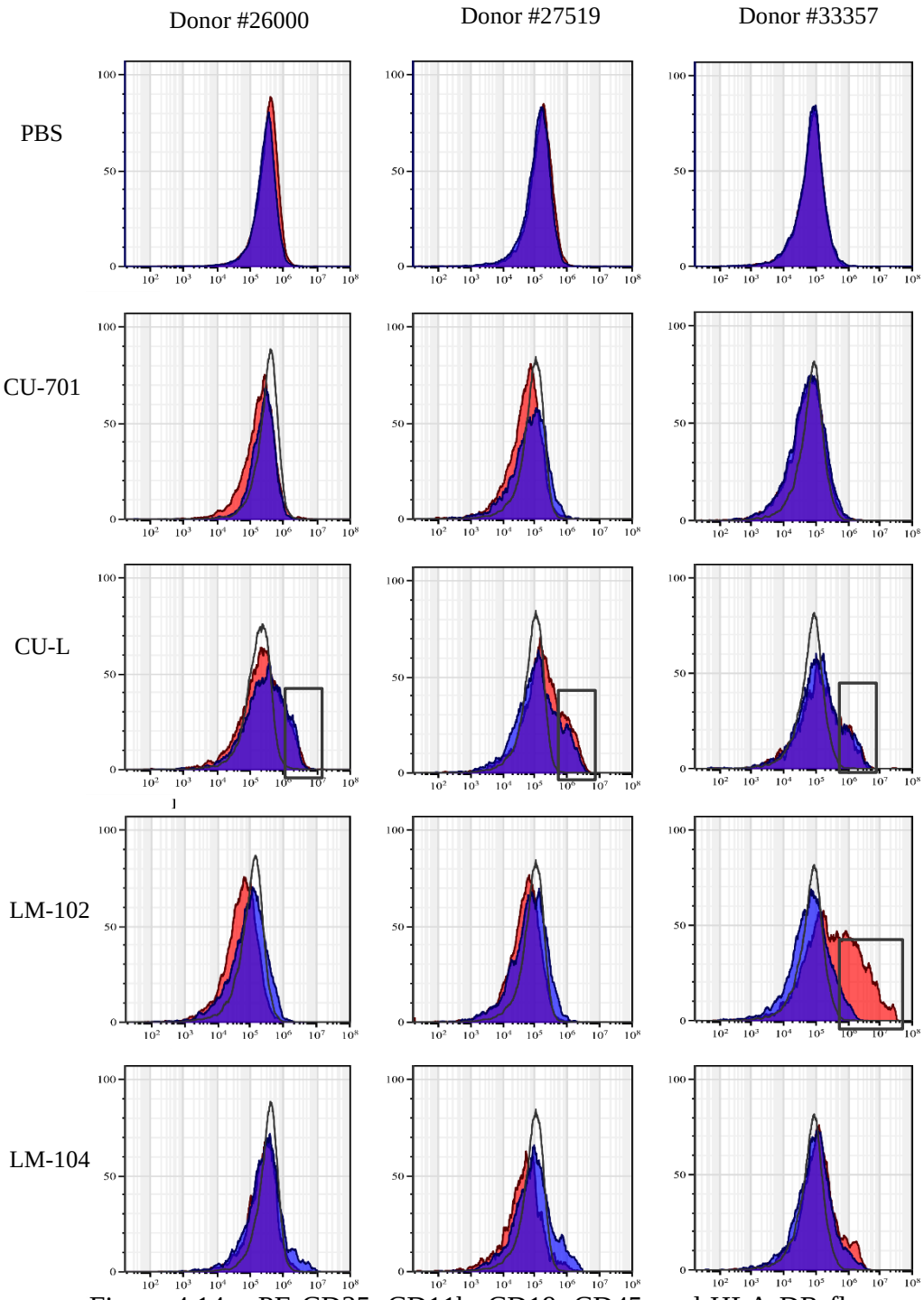


Figure 4.14 – PE CD35, CD11b, CD19, CD45, and HLA-DR flow cytometry overlay analysis showing the histogram plots for each donor and pectin condition. hMSCs (500 µL at 100,000 cells/mL) were added to 24-well plates by syringing or spraying (MAD sprayer) in 1xPBS or 1% w/v pectin. 50 µL of 100 mM $CaCl_2$ were added to wells before cells to induce gelation. Samples were incubated for 24-hours before being extracted from pectin gels and removed from wells to form a single cell suspension. Histograms show cells from gates on the forward scatter-area (FSC-A) vs side scatter-area (SSC-A) plot to select for cells and disregard debris, then from gates set on the SSC-A vs SSC-H plot to select for single cell events. Black outline = PBS control, red = syringed samples, blue = sprayed samples. Green box highlights the positive population of cells in the LM-102 syringed condition in #33357 donor, and in the CU-L conditions for all donors.

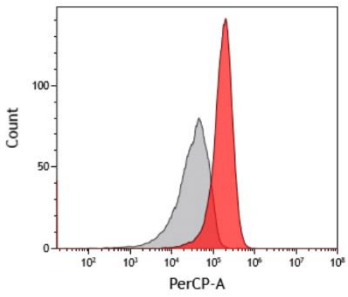


Figure 4.15 – CD105 PerCP-Cy5.5™ flow cytometry overlay analysis showing the histogram plots for the PBS syringe hMSCs with the CD105 detection antibodies (red) and the isotype antibodies (grey).

Table 4.3 shows the percentage positive cells and the standard deviation for each marker analysed in each condition determined by flow cytometry. Figure 4.10 is a graphical representation of these data. To be classed as hMSCs, cells should be >95% positive for CD90, CD105, and CD73, and <2% positive for CD35, CD11b, CD19, CD45, and HLA-DR (Dominici *et al.*, 2006). The mean value for all sprayed conditions is below 95% for all positive markers except for CU-701 with CD90, and LM-102 with CD73. All cell conditions, including the control cells are also below 95% for CD105. Only the controls and hMSCs in the CU-701 grade of pectin are below 2% for the negative markers in both the syringed and sprayed conditions. The sprayed, but not the syringed hMSCs in LM-102 are below 2% for the negative markers.

Figure 4.11, Figure 4.12, Figure 4.13, and Figure 4.14 show the overlaid histograms for each individual donor in each condition for each marker used in the flow cytometry. These show that donor #33357 tended to show a less MSC-like pattern of surface markers than the other two donors particularly for cells syringed in the LM-104 and LM-102 grades of pectin, resulting in the increased standard deviation. The markers MSCs should be negative for (CD35, CD11b, CD19, CD45, and HLA-DR) were detected using a cocktail of antibodies labelled with the PE fluorophore and histograms shown in Figure 4.14. CU-L has a positive population of cells in each donor, highlighted in the boxes on the figure, and a mean of 8.81% and 9% positive for syringe and sprayed respectively. The LM-104 condition also shows a shoulder on the PE histograms in Figure 4.14, although this is much smaller than CU-L and has a mean of 2.45% and 3.36% for syringed and sprayed respectively. LM-102 showed a large population (17.96%) of PE positive cells in the syringed condition for just one

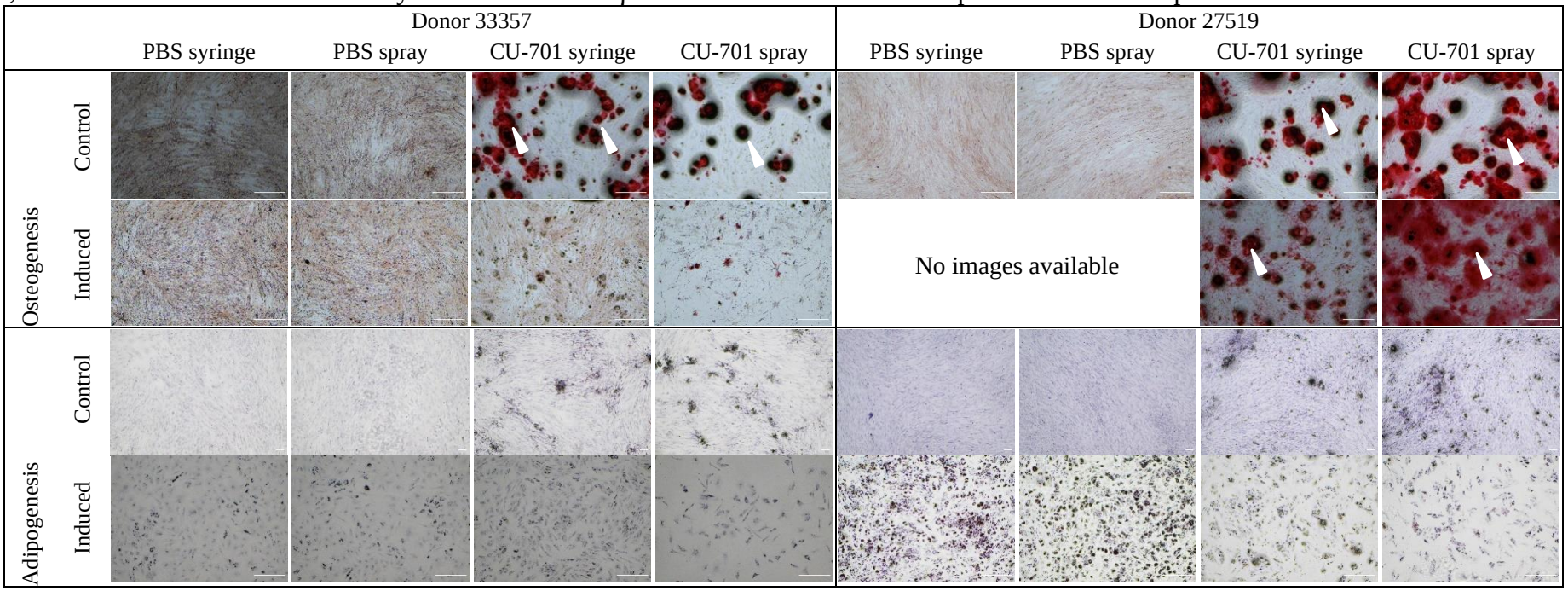
donor. Unfortunately, the PE marker is a mixed cocktail, therefore the particular surface marker that the positive cells express cannot be determined without further analysis.

The histograms shown in Figure 4.12 confirm that CD105 is consistently downregulated in all PBS and pectin samples, suggesting this downregulation is not just in response to the pectin or the spraying. Figure 4.15 shows the overlay of the PBS syringe hMSC histogram for the positive cocktail and the isotype control, highlighting the overlap between the two. This suggests there may be some non-specific binding and a requirement for an additional was step using this isotype control.

4.4.7. Differentiation of hMSCs

CU-701 was selected for the differentiation study as the only pectin grade not to have statistically significant changes in surface marker expression.

Table 4.4 – Images of hMSCs following incubation with basal growth media (control), osteogenic differentiation media, or adipogenic differentiation media. hMSCs (100,000 cells/mL) were syringed or sprayed (using the MAD sprayer) in 1xPBS or 1% w/v CU-701 pectin (gelled with 100 mM $CaCl_2$) into 12-well plates, incubated for 24-hours, then removed from wells and seeded (20,000 cells/well) in 24-well plates. Cells grew for 48-hours in basal growth media, before changing to differentiation media. Media was changed twice weekly. After 14-days, the osteogenic control and induced cells were stained with 1% Alizarin Red S solution. The adipogenic control and induced cells were stained with 0.5% Oil Red O, and counterstained with haematoxylin. Scale bar is 50 µm. White arrows indicate the presence of stained pectin debris.



The images in Table 4.4 show that none of the cells from either the 1xPBS, or the CU-701 pectin grade conditions spontaneously differentiated into cells of osteogenic or adipogenic lineage when cultured in basal growth media.

Detection of osteogenic differentiation was carried out using Alizarin Red to detect calcium deposits present in differentiated cells (Suvarna *et al.*, 2018). Pectin gelation was induced by calcium ions; therefore, the pectin debris still present in the wells containing hMSCs extracted from CU-701 pectin, was stained red. Some of the stained pectin debris is indicated by the presence of white arrows in the relevant images. The presence of calcium deposits was not obviously detected in the hMSCs from donor #33357 in any of the conditions tested with the osteogenic differentiation media, suggesting differentiation was not induced. As differentiation did not occur in the PBS syringe cells, used as the control without having been sprayed or in pectin, this suggests either the differentiation protocol was too short, or the cells from this donor no longer retained the capacity to differentiate down the osteogenic lineage. The length of time was based on the manufacturer's protocol (PromoCell, 2023), however others used longer time periods (Díez *et al.*, 2015).

Human MSCs from both PBS conditions from donor #27519 were lost before staining, therefore are not shown. hMSCs from the syringe and sprayed CU-701 pectin conditions appear to have calcium deposits following incubation with differentiation media, suggesting differentiation has been induced. However, these deposits are difficult to see due to the presence of the pectin debris.

Detection of adipogenic differentiation was carried out using Oil Red O to detect lipid vacuoles (Suvarna *et al.*, 2018). All hMSCs from both donors in the tested conditions show differentiation down the adipogenic lineage when incubated with adipogenic differentiation media, shown by the presence of stained vacuoles. This suggests the CU-701 pectin and the spraying process have not affected the ability of the hMSCs to differentiate down the adipogenic lineage.

4.4.8. Differential gene expression of hMSCs

Similar to the differentiation study, RNA-seq and differential gene expression was carried out using the CU-701 pectin as this was the only grade of pectin not to show a statistically significant change in expression of surface markers.

Table 4.5 – Differential gene expression analysis summary. hMSCs from three separate donors were syringed or sprayed (MAD sprayer) into 12-well plates (1 mL at 100,000 cells/mL) in 1xPBS or 1% w/v CU-701 pectin. After incubation for 24 hours, cells were removed from the wells, and RNA was extracted. This was submitted to the DeepSeq department in the Queens Medical Centre, University of Nottingham, for library preparation, sequencing, and data analysis. RNA samples from each donor were sequenced independently, and the counts used for differential expression analysis, which was carried out using DESeq2. DESeq2 was designed to normalise count data and carry out statistical analysis (Love *et al.*, 2014). The gene count for up and down regulated genes are those with a statistically significant (adjusted p-value <0.10) $\log_2$ fold change (LFC).

Contrast	Up regulated		Down regulated	
	Gene count	%	Gene count	%
PBS spray vs PBS syringe	53	0.18	51	0.17
CU-701 spray vs. CU-701 syringe	64	0.21	12	0.04
CU-701 syringe vs. PBS syringe	1942	6.50	1872	6.20
CU-701 spray vs. PBS spray	2142	7.10	2110	7.00

The differential gene expression analysis shown in Table 4.5 shows the number of significantly up and down regulated genes in the contrasts listed. The analysis was carried out by the DeepSeq department at the University of Nottingham using the DESeq2 package, which was designed to carry out statistical testing on the inputted count data. The statistical testing is designed to account for the small number of replicates (N=3) to provide stable estimates of fold-changes (Love *et al.*, 2014), which are summarised in Table 4.5. The analysis shows more genes were up and down regulated in hMSCs when comparing different materials for delivery (PBS vs CU-701 pectin) using the same delivery method (spray or syringe), than when comparing the same material and different delivery method.

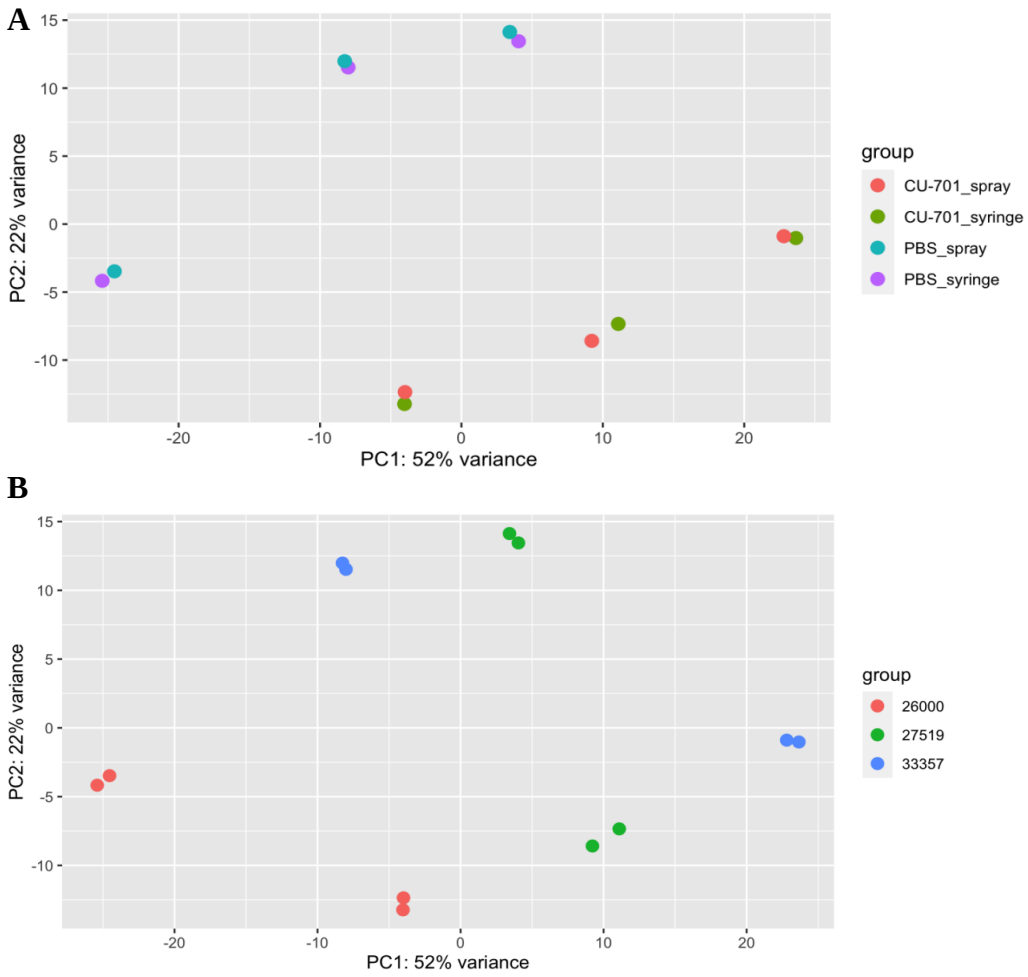


Figure 4.16 – Principal component analysis (PCA) showing the extent of clustering of treatments along the first two principal components. hMSCs from three separate donors were syringed or sprayed (MAD sprayer) into 12-well plates (1 mL at 100,000 cells/mL) in 1xPBS or 1% w/v CU-701 pectin. After incubation for 24 hours, cells were removed from the wells, and RNA was extracted. This was submitted to the DeepSeq department in the Queens Medical Centre, University of Nottingham, for library preparation, sequencing, and data analysis. The figures are coloured by condition in **A**, and by donor in **B**. The figures were generated by Dr Graeme Fox from the DeepSeq department.

Figure 4.16 shows the effect of the delivery method and the hMSC donor on the variance of the data. Figure 4.16A shows the CU-701 syringe and spray samples are clustered in pairs, and the PBS spray and syringe samples are also clustered in pairs. Figure 4.16B shows each of the donors are clustered in pairs which correspond to the pairs shown in Figure 4.16A. In combination, the two parts show that donor and delivery material have the largest effect on the variation in gene expression, and that spraying or syringing as a delivery method has a much smaller effect on gene expression difference.

Table 4.6 – Top 20 up and down regulated genes comparing PBS spray versus PBS syringe. hMSCs from three separate donors were syringed or sprayed (MAD sprayer) into 12-well plates (1 mL at 100,000 cells/mL) in 1xPBS or 1% w/v CU-701 pectin. After incubation for 24 hours, cells were removed from the wells, and RNA was extracted. This was submitted to the DeepSeq department in the Queens Medical Centre, University of Nottingham, for library preparation, sequencing, and data analysis. Novel transcripts are genes that have not been annotated/named yet.

Gene	Full name	LFC
PTCSC2	Papillary thyroid carcinoma susceptibility candidate 2	33.9543
ENSG00000286445	Novel transcript	27.9896
SVIL2P	Supervillin family member 2, pseudogene	27.9653
CPLX4	Complexin 4	27.3701
ENSG00000277991	Novel transcript	26.9588
ENSG00000256678	Novel transcript	26.6459
LINC02393	Long intergenic non-protein coding RNA 2393	26.6379
MIR4668	MicroRNA 4668	26.6379
ENSG00000230709	Novel transcript	25.7621
SYPL1P2	Synaptophysin like 1 pseudogene 2	25.7621
B4GALNT3	Beta-1,4-N-acetyl-galactosaminyltransferase 3	25.1969
ABCG4	ATP binding cassette subfamily G member 4	25.1969
HRG-AS1	HRG and FETUB antisense RNA 1	24.3118
ENSG00000271917	Novel transcript	24.3118
RNU6-419P	RNA, U6 small nuclear 419, pseudogene	24.3064
ILVBL-AS1	ILVBL antisense RNA 1	23.535
SNORD101	Small nucleolar RNA, C/D box 101	20.4117
ENSG00000253361	Novel transcript	19.9393
KRT32	Keatin 32	19.5725
ITGAM	Integrin subunit alpha M	19.5478
LINC00885	Long intergenic non-protein coding RNA 885	-34.97947
NIBAN3	Niban apoptosis regulator 3	-34.57871
TMSB4Y	Thymosin beta 4 Y-linked	-29.04706
ENSG00000279166	Novel transcript	-27.5566
SMG1P3	SMG1 pseudogene 3	-27.51592
ENSG00000273419	Novel transcript	-27.50339
MAP3K9	Mitogen-activated protein kinase kinase kinase 9	-27.34536
LINC01991	Long intergenic non-protein coding RNA 1991	-27.22668
RPL21P135	Ribosomal protein L21 pseudogene 135	-26.86598
ENSG00000272940	Novel transcript	-26.86598
ENSG00000260163	Novel transcript	-26.09151
ENSG00000284523	Novel transcript	-26.09151
HEATR4	HEAT repeat containing 4	-25.04184
ENSG00000286329	Novel transcript	-24.71403
CCDC63	Coiled-coil domain containing 63	-24.4844
ENSG00000270240	Novel transcript	-24.26666
FGL2	Fibrinogen like 2	-23.45979
PBX3-DT	PBX3 divergent transcript	-20.14107
KPNA7	Karyopherin subunit alpha 7	-19.88532
ENSG00000279827	Novel transcript	-19.7452

Table 4.7 – Top 20 up and down regulated genes comparing CU-701 spray versus CU-701 syringe. hMSCs from three separate donors were syringed or sprayed (MAD sprayer) into 12-well plates (1 mL at 100,000 cells/mL) in 1xPBS or 1% w/v CU-701 pectin. After incubation for 24 hours, cells were removed from the wells, and RNA was extracted. This was submitted to the DeepSeq department in the Queens Medical Centre, University of Nottingham, for library preparation, sequencing, and data analysis. Novel transcripts are genes that have not been annotated/named yet.

Gene	Full name	LFC
PTPRD-AS1	PTPRD antisense RNA 1	22.431
LINC02223	Long intergenic non-protein coding RNA 2223	22.0877
GRID2	Glutamate ionotropic receptor delta type subunit 2	20.6386
ENSG00000287902	Novel transcript	20.6173
ENSG00000278949	Novel transcript	20.4334
ENSG00000273090	Novel transcript	20.2425
PINCR	P53-induced noncoding RNA	20.1319
CDRT4	CMT1A duplicated region transcript 4	20.0568
ENSG00000278112	Novel transcript	20.0296
ENSG00000279827	Novel transcript	19.4383
C11orf97	Chromosome 11 open reading frame 97	19.4119
TEX26	Testis expressed 26	19.3558
SLC10A4	Solute carrier family 10 member 4	19.336
ENSG00000275676	Novel transcript	19.1674
ENSG00000283213	Novel transcript	19.1524
ENSG00000259126	Novel transcript	19.1319
TIAM1-AS1	TIAM1 antisense RNA 1	18.9979
ENSG00000289989	Novel transcript	18.9979
RPL17P15	Ribosomal protein L17 pseudogene 15	18.9494
ENSG00000286264	Novel transcript	18.9494
ENSG00000243243	Novel transcript	-18.96895
ENSG00000286728	Novel transcript	-18.674
TFEC	Transcription factor EC	-18.42526
ENSG00000286827	Novel transcript	-17.81088
PRICKLE2-DT	PRICKLE2 divergent transcript	-17.79822
TRPC3	Transient receptor potential cation channel subfamily C member 3	-17.72446
TRPM2	Transient receptor potential cation channel subfamily M member 2	-17.36333
SNORD111	Small nucleolar RNA, C/D box 111	-17.07568
TRPC6	Transient receptor potential cation channel subfamily C member 6	-16.76518
TMSB4Y	Thymosin beta 4 Y-linked	-16.06793
LINC00598	Long intergenic non-protein coding RNA 598	-14.65684
SPOPL-DT	SPOPL divergent transcript	-14.5148

Table 4.8 – Top 20 up and down regulated genes comparing CU-701 syringe versus PBS syringe. hMSCs from three separate donors were syringed or sprayed (MAD sprayer) into 12-well plates (1 mL at 100,000 cells/mL) in 1xPBS or 1% w/v CU-701 pectin. After incubation for 24 hours, cells were removed from the wells, and RNA was extracted. This was submitted to the DeepSeq department in the Queens Medical Centre, University of Nottingham, for library preparation, sequencing, and data analysis. Novel transcripts are genes that have not been annotated/named yet.

Gene	Full name	LFC
C2CD4A	C2 calcium dependent domain containing 4A	8.14078
RASD2	RASD family member 2	6.84971
MYBPH	Myosin binding protein H	6.78225
PDK4	Pyruvate dehydrogenase kinase 4	6.59666
IL24	Interleukin 24	6.11879
IGFBP5	Insulin like growth factor binding protein 5	5.84562
SEPTIN7P13	Septin 7 pseudogene 13	5.67524
A2M	Alpha-2-macroglobulin	5.57355
KCNK3	Potassium two pore domain channel subfamily K member 3	5.55444
GPR183	G protein-coupled receptor 183	5.28254
BMF	Bcl2 modifying factor	5.24859
SYT12	Synaptotagmin 12	5.14539
RNA5SP288	RNA, 5S ribosomal pseudogene 288	5.07822
SLC16A6	Solute carrier family 16 member 6	4.98302
PLXDC1	Plexin domain containing 1	4.98075
RNU6-1195P	RNA, U6 small nuclear 1195, pseudogene	4.95036
MEDAG	Mesenteric oestrogen dependent adipogenesis	4.85813
MUC13	Mucin 13, cell surface associated	4.84306
FAXDC2	Fatty acid hydroxylase domain containing 2	4.80279
DCSTAMP	Dendrocyte expressed seven transmembrane protein	4.80079
VLDLR-AS1	VLDLR antisense RNA 1	-4.948539
TICRR	TOPBP1 interacting checkpoint and replication regulator	-4.634575
SERPINB2	Serpin family B member 2	-4.568949
ENSG00000243802	Novel transcript	-3.819328
SPC25	SPC25 component of NSC80 kinetochore complex	-3.632166
PDCD1LG2	Programmed cell death 1 ligand 2	-3.551736
ENSG00000249379	Novel transcript	-3.463429
BHLHA15	Basic helix-loop-helix family member a15	-3.418996
ERCC6L	ERCC excision repair 6 like, spindle assembly checkpoint helicase	-3.405107
ODAPH	Odontogenesis associate phosphoprotein	-3.361555
ENSG00000267774	Novel transcript	-3.336418
ENSG00000250038	Novel transcript	-3.279635
ENSG00000279069	Novel transcript	-3.207962
CELSR1	Cadherin EGF LAG seven-pass G-type receptor 1	-3.095572
RPSAP54	Ribosomal protein SA pseudogene 54	-3.081426
L3MBTL2-AS1	L3MBTL2 antisense RNA 1	-3.056453
ORC1	Origin recognition complex subunit 1	-3.043862
ZSCAN31	Zinc finger and SCAN domain containing 31	-3.041534
KIF23	Kinesin family member 23	-3.010213
ENSG00000272599	Novel transcript	-2.941503

Table 4.9 – Top 20 up and down regulated genes comparing CU-701 spray versus PBS spray. hMSCs from three separate donors were syringed or sprayed (MAD sprayer) into 12-well plates (1 mL at 100,000 cells/mL) in 1xPBS or 1% w/v CU-701 pectin. After incubation for 24 hours, cells were removed from the wells, and RNA was extracted. This was submitted to the DeepSeq department in the Queens Medical Centre, University of Nottingham, for library preparation, sequencing, and data analysis. Novel transcripts are genes that have not been annotated/named yet.

Gene	Full name	LFC
PDK4	Pyruvate dehydrogenase kinase 4	7.51764
ENSG00000266538	Novel transcript	6.93331
KCNK3	Potassium two pore domain channel subfamily K member 3	6.85748
DCSTAMP	Dendrocyte expressed seven transmembrane protein	6.51433
SNORD83A	Small nucleolar RNA, C/D box 83A	6.45336
MYBPH	Myosin binding protein H	6.26424
RNA5SP288	RNA, 5S ribosomal pseudogene 288	6.15834
SNORD13E	Small nucleolar RNA, C/D box 13E	6.15232
SLC38A8	Solute carrier family 38 member 8	5.92789
LINC00869	Long intergenic non-protein coding RNA 869	5.89233
RNA5SP258	RNA, 5S ribosomal pseudogene 258	5.70178
IL24	Interleukin 24	5.61286
ENSG00000262877	Novel transcript	5.40996
BMF	Bcl2 modifying factor	5.29649
LGI4	Leucine rich repeat LGI family member 4	5.26806
C2CD4A	C2 calcium dependent domain containing 4A	5.26446
RNA5SP357	RNA, 5S ribosomal pseudogene 357	5.22517
MIAT	Myocardial infarction associated transcript	5.1914
IGFBP5	Insulin like growth factor binding protein 5	5.0932
NPTXR	Neuronal pentraxin receptor	5.05468
CAMSAP1-DT	CAMSAP1 divergent transcript	-5.647318
RPSAP54	Ribosomal protein SA pseudogene 54	-5.354408
APLN	Apelin	-5.185049
ZNF876P	Zinc finger protein 876, pseudogene	-5.147745
ENSG00000269176	Novel transcript	-4.876641
VIM-AS1	VIM antisense RNA 1	-4.864523
SHC3	SHC adaptor protein 3	-4.568773
MGAM	Maltase-glucoamylase	-4.523251
ENSG00000228714	Novel transcript	-4.507446
CCDC89	Coiled-coil domain containing 89	-4.466413
MYB	MYB proto-oncogene transcription factor	-4.402284
PDE11A	Phosphodiesterase 11A	-4.354362
ADGRG6	Adhesion G protein-coupled receptor G6	-4.324109
DIO3	Iodothyonine deiodinase 3	-4.273252
FAM111B	FAM111 trypsin like peptidase B	-4.208948
EME1	Essential meiotic structure-specific endonuclease 1	-4.0714
H3P43	H3 histone pseudogene 43	-3.95768
ENSG00000289357	Novel transcript	-3.930736
ZNF662	Zinc finger protein 662	-3.891114
DDIAS	DNA damage induced apoptosis suppressor	-3.841924

Table 4.10 – Log_2 fold change (LFC) and adjusted P-value (Padj) of selected genes in the listed contrasts. Genes were selected based on their implication in pro-regenerative and immunomodulation effect of the hMSC secretome. hMSCs from three separate donors were syringed or sprayed (MAD sprayer) into 12-well plates (1 mL at 100,000 cells/mL) in 1xPBS or 1% w/v CU-701 pectin. After incubation for 24 hours, cells were removed from the wells, and RNA was extracted. This was submitted to the DeepSeq department in the Queens Medical Centre, University of Nottingham, for library preparation, sequencing, and data analysis.

Contrast →	**PBS spray vs PBS syringe**		**CU-701 spray vs CU-701 syringe**		**CU-701 syringe vs PBS syringe**		**CU-701 spray vs PBS spray**	
Gene name ↓	LFC	Padj	LFC	Padj	LFC	Padj	LFC	Padj
TGFB1	-0.2797	1	-0.0137	1	0.7892	0.0073	1.0553	0.0001969
IGF1	0.5534	1	0.3661	1	1.5668	NA	1.3795	NA
VEGF	-0.2000	1	-0.0249	1	0.3784	0.1738	0.1535	0.6429
HGF	-0.1495	1	0.7421	1	0.7704	0.2423	1.6620	0.0037
GDNF	0.0960	1	-0.0248	1	-0.0195	0.9492	-0.1403	0.5705
BDNF	0.1162	1	0.0055	1	-0.6920	0.0391	-0.8027	0.0142
NGF	0.1619	1	-0.1298	1	-1.0920	0.1994	-1.3836	0.0935
IDO	-0.9741	NA	0.1675	NA	-0.7997	NA	0.3418	NA
IL1RN	0.2699	1	1.0089	1	-0.7768	NA	-0.0378	0.9926
Oct4	NA	NA	NA	NA	0.1521	NA	NA	NA
Sox2	0.9396	NA	-3.6005	1	2.1060	NA	0.3969	NA

Table 4.6, Table 4.7, Table 4.8, and Table 4.9 show the top 20 up and down regulated genes for the four conditions comparisons shown which were statistically significant (adjusted P-value <0.1). Table 4.10 shows the LFC for selected genes for the four condition comparisons based on identified growth factors and cytokines of the hMSC secretome. The adjusted P-value is shown for the selected genes in each condition comparison; values >0.1 are deemed not statistically significant. None of the selected genes were significantly differentially expressed in the comparisons where the delivery medium (1xPBS or CU-701 pectin) was kept the same, but the delivery method (syringe or spray) significantly changed expression of some genes. Specifically, TGF-B1 (TGF-β1) was significantly upregulated when comparing cells delivered in CU-701 pectin to 1xPBS in both syringe and spray contrasts. BDNF was significantly downregulated. Additionally, HGF was significantly upregulated, and NGF significantly downregulated when comparing CU-701 spray versus PBS spray. Whilst these changes were statistically significant, it is worth noting that the LFC change is much lower than the LFC of the top 20 up and down regulated genes.

Searches for the genes responsible for positive markers of hMSC CD90, CD105, and CD73 were also carried out. No significant LFC was found in any contrasts except for CD105 in CU-701 syringe versus PBS syringe. There was an LFC of 0.5767, adjusted P-value 0.0033.

4.5. Discussion

The results in this chapter aimed to assess the suitability of the MAD sprayer and pectin for local delivery of hMSCs. Studies began with the 3T3 and SH-SY5Y cell lines to evaluate whether cells were being retained in the device and to assess the effect of spraying at different cell densities on the LDH release and metabolic activity of cells. Studies then progressed to hMSCs, assessing the viability of cells after spraying in the four different grades of pectin (CU-701, CU-L, LM-102, and LM-104), as well as the phenotype, the differentiation capacity, and differential gene expression in response to spraying and the CU-701 grade of pectin.

Starting with the assessment of whether cell lines are retained in the device, the cell density was counted before and after spraying, syringing, and pipetting. At both densities tested, the cell count was equivalent to the seeding density in the sprayed condition, therefore cells do not appear to be retained within the device and the measured metabolic activity and LDH release should be a true reflection of the expected cell population based on seeding density. The data is in agreement with the patent claims for the spray device in having a small volume of dead space inside the device (Denton, 2022).

Having confirmed that cells were not retained in the device, the SH-SY5Y cells when sprayed had a larger reduction in metabolic activity than the 3T3 cells. The results of the LDH assay suggest a maximum cytotoxicity of 10% 24-hours following the spraying process, whereas the lowest metabolic activity is 65% after 24 hours. This indicated the cells were responding to stress, but not necessarily dead. It is expected that SH-SY5Y cells are more sensitive than 3T3 cells, as the data is in agreement with Connolly *et al.* (2021) who have shown SH-SY5Y cells to be sensitive to shear stress via the flow of fluid over the cells in culture (Connolly *et al.*, 2021). A link between smaller cell size and increased survival of cells after spraying has been suggested (Kardia *et al.*, 2014), but there was no correlation observed here between cell survival and cell size. Of the three cell types tested, hMSCs have the largest diameter (18-30 µm) (Ge *et al.*, 2014), compared to 12 µm and 15 µm for SH-SY5Ys and 3T3s respectively (Harvard, 2023), and hMSCs had the highest viability.

For both cell lines (3T3 and SH-SY5Y) and hMSC, there did not appear to be any correlation between cell density and the measured cell viability. This is consistent with a study investigating the use of a pump spray device with this U937 human monocyte-like cell line, whereby the two cell densities tested showed no difference in viability (Beneke *et al.*, 2018). Similarly, five hMSC densities tested with two different spray devices showed no difference in cell viability in either device used with a change in cell density (Thiebes *et al.*, 2021).

Having shown that hMSCs at different densities can be sprayed, the viability of the hMSCs after syringing or spraying in pectin was then carried out at a cell density of 100,000 cells/mL. This cell density was the highest that gave a cell number/cm^2 within the range of cell density obtained from hMSCs cultured in 2D at 80% confluency but that would not result in overcrowding in the PBS conditions (ThermoFisher, 2014, Bhat *et al.*, 2021). In all four grades of pectin, hMSC viability was not affected compared to the control in PBS, with no statistical differences shown between the conditions. hMSCs were added to pectin solutions of the four different grades, then seeded into wells by syringe or spraying. The distribution of the live and dead cells indicates cells suspended in the gel have enough nutrients to survive over the 24-hour time period tested. There does not appear to be a higher number of dead cells in the centre of, or underneath the pectin gels. These findings agree with previous studies encapsulating cells in pectin hydrogels, with viability of L929 mouse fibroblasts demonstrated over 7 days of culture (Gentilini *et al.*, 2018), and hMSCs remaining viable within pectin hydrogels for 14 days (Neves *et al.*, 2015).

Increased viscosity of the medium in which cells are sprayed has been correlated with a reduction in the viability of delivered cells, with viscosity measurements of 25 mPa·s (Pehlivaner Kara and Ekenseair, 2016) and 15 kPa·s (Hendriks *et al.*, 2015) leading to a significant reduction in viability, whereas even the most viscous pectin grade used here (CU-701 with viscosity of 11.1 mPa·s at 10,000 1/s shear rate shown in 3.4.5) demonstrated high viability. However, both the aforementioned studies used an airbrush-based device, unlike the syringe device used here.

Having shown that viable cells could be sprayed in all four grades of pectin, flow cytometry was then used to analyse what proportion of the cell populations were

positive for CD90, CD105, and CD73, and negative for a cocktail of CD34, CD11b, CD19, CD45, and HLA-DR, based on the minimal criteria for MSCs (Dominici *et al.*, 2006). Of all the hMSCs sprayed or syringed in 1xPBS or the four grades of pectin, only CU-701 did not have a statistically significant change in the level of expression of these markers compared to the 1xPBS syringe condition used as the control.

Cells obtained from donor #33357 showed a less MSC-like phenotype in response to the different pectin grades, highlighting donor variability. The use of different donors has been shown to affect expression levels of a variety of proteins, the differentiation potential, and the proliferation of the hMSCs (Siegel *et al.*, 2013). There were also trends observed by Siegel *et al.* (2013) between some of the changes and age, as well as sex differences. The three cell donors used in the study in this thesis (#26000, #27519, and #33357) were close in age, 20, 21, and 28, and donors were male, female, male. Three repeats are not enough to begin to spot trends in the differences related to age and sex of the donors, however, it does begin to support the overall findings of donor variability already published.

The percentage of hMSCs positive for CD105 was below the 95% threshold in all tested conditions, including the 1xPBS syringe condition used as the control. CD105, otherwise known as endoglin, functions as a co-receptor in the TGF-β family, has functions in angiogenesis, with expression responsive to TGF-β and hypoxia (Schoonderwoerd *et al.*, 2020). Reduced expression of CD105 has been linked to culture in serum free media, with expression levels down to approximately 50% when serum free media was used (Mark *et al.*, 2013). The hMSCs tested here were cultured for 24 hours in half media (as media is added in a 1:1 volume ration to 1xPBS/pectin), however this is a much shorter timeframe than Mark *et al.* (2013) used. The histograms in Figure 4.12 show a single population of cells in each condition, however this overlays the isotype control shown in Figure 4.15. This could result from a non-specific binding of the isotype antibodies shifting the fluorescence of the isotype samples to the right and interfering with the detection of the positive population of cells. Further investigation would be required to determine the cause of the measured reduction in CD105, such as additional wash steps to reduce the non-specific binding. An

additional control grown in basal growth media only could be run to understand whether the lower level of CD105 expression detected was due to a phenotype of the cells already present, or due to the 24-hour culture in half the amount of media.

Similar studies to understand the effect of scaffold materials on the surface marker expression of MSCs have been undertaken previously. Gasparotto *et al.* (2014) investigated the use of a fibrin sealant on the proliferation, viability, and CD34, CD44, and CD90 expression of rat MSCs. The fibrin sealant was shown not to affect the expression of CD90 (Gasparotto *et al.*, 2014), however CD105 and CD73 were not analysed.

It is known that the use of biomaterials with MSCs can act to induce differentiation of the cells (Zhao *et al.*, 2014). Factors including material chemistry, elasticity and stiffness, topography, and adhesion to the material, all affect cell response and differentiation (McMurray *et al.*, 2015). Increased stiffness of materials is associated with more osteogenic differentiation of MSCs (Mao *et al.*, 2016). In the context of using hMSCs as a treatment for TBI, the trophic effects of the hMSCs is primarily of interest (Baez-Jurado *et al.*, 2019). There is no need or desire to induce differentiation of the hMSCs down an adipogenic, osteogenic, or chondrogenic lineage, therefore spontaneous differentiation in the panel carried out using cells that had been syringed or sprayed in 1xPBS or CU-701 pectin was not desired. However, as differentiation potential down those three lineages is used as an identifier for MSCs (Dominici *et al.*, 2006), the ability to retain the differentiation potential was desired.

Typically, differentiation studies take place over 2-3 weeks for adipogenesis, osteogenesis, and chondrogenesis (Díez *et al.*, 2015). To maintain consistency with other studies carried out in this chapter, the cells were maintained in CU-701 pectin for 24 hours, before being removed and studied for their differentiation potential. As 24 hours is much shorter than the length of time hMSCs typically take to differentiate (Díez *et al.*, 2015), it was hypothesised that the pectin would not cause spontaneous differentiation. Using both donors, in all four conditions tested, spontaneous differentiation was not observed when cells were cultured in basal growth media and stained for osteogenic or adipogenic

differentiation. This is favourable for the use of pectin in the brain, as spontaneous differentiation is not desired.

Using differentiation media, osteogenic differentiation was not demonstrated in one of the donors (#33357), detected by the lack of calcium deposits being stained with Alizarin Red. The PromoCell protocol for differentiation instructs a 12-14-day incubation with osteogenic differentiation media (PromoCell, 2023), however many studies, including Díez *et al.* (2015) incubate for 21 days, therefore it is possible 14 days was not long enough for detectable calcium deposits to be formed. The PBS samples incubated in osteogenic differentiation media using donor #27519 were lost, so a donor comparison cannot be made between PBS samples, however, there does appear to be stained calcium deposits from hMSCs that were pre-incubated in CU-701 pectin (both syringed and sprayed). Adipogenic differentiation could be induced in all conditions using cells from both hMSC donors. Further work is required to complete the differentiation panel using a longer incubation for the osteogenic differentiation, and to include the chondrogenic condition, however the lack of spontaneous differentiation and the ability of the cells to differentiate down the adipogenic lineage is a positive initial result. The desire is for hMSCs to stimulate neurogenesis, angiogenesis, and downregulate inflammation in the brain following injury to aid recovery in patients via trophic effects (Andrzejewska *et al.*, 2021), not to differentiate in the brain.

As discussed, donor #33357 showed the most variable results in the flow cytometry analysis, and a lack of osteogenic differentiation. The PCA of the differential gene expression analysis showed that whilst spraying or syringing had very little effect on differential expression of genes, the presence of CU-701 pectin and the different cell donors caused variation in the expression of genes. The cells used throughout this thesis were derived from the bone marrow of three separate donors, and they varied in sex and age. Donor variability is a consideration often discussed in reviews on potential use of hMSCs in regenerative medicine (Wright *et al.*, 2021). Sex-specific differences in hMSC (derived from adipose tissue) gene expression have been highlighted in a meta-analysis study by Bianconi *et al.* (2020) which showed differences in the expression of numerous genes, including those related to inflammation

(Bianconi *et al.*, 2020). Age and sex have both been shown to affect protein expression in BM-hMSCs (Siegel *et al.*, 2013). The results of the PCA support this donor variability previously reported, however further gene analysis would be required to comment on any specific changes related to sex or age.

RNA-seq and differential gene expression analysis shows the large change in gene expression in response to different culture environments; transcriptome analysis of hMSCs treated with nanosilicates revealed over 4,000 genes were differentially expressed compared to untreated cells (Carrow *et al.*, 2018). MSCs cultured in alginate hydrogels of differing stiffness showed 1,637 differentially expressed genes in gels with 3 kPa stiffness compared to 30 kPa stiffness (Darnell *et al.*, 2018). These studies highlight the impact differences in material have on gene expression in MSCs. The contrasts carried out here between 1xPBS and CU-701 pectin showed 3,814 (syringe contrast) and 4,252 (spray contrast) were differentially expressed (adjusted P-value >0.1).

The genes that appear in both the CU-701 syringe versus PBS syringe, and CU-701 spray versus PBS spray contrasts are *C2CD4A, PDK4, IL24, IGFBP5*, and *BMF*. *C2CD4A* upregulation is likely to be in response to the calcium present in the pectin. *PDK4* is involved in switching cells from glucose utilisation to fatty acid utilisation (Zhang *et al.*, 2014), which may indicate the hMSCs within the pectin gels are not receiving as much of the glucose from the media as the hMSCs in the PBS condition if diffusion is slower to cells in the pectin gels. The upregulation of *PDK4* could also be linked to the presence of increased concentrations of calcium in those hMSC encapsulated in CU-701 pectin. *PDK4* is a mitochondrial gene involved in the regulation of metabolism (Thoudam *et al.*, 2022), and calcium influx and efflux from the mitochondria is also involved in the regulation of energy production (Finkel *et al.*, 2015), therefore it is also possible that *PDK4* expression levels is linked to calcium.

IL-24 has functions in inflammatory and apoptosis pathways, seemingly in connection with calcium signalling within cells (Persaud *et al.*, 2016). It is hypothesised that this is again linked to calcium within the pectin. *IGFBP5* has been found *in vitro* to inhibit osteogenesis by blocking the actions of IGF (Mukherjee and Rotwein, 2008), which could provide some explanation for the lack of differentiation of the cells from donor #33357 down an osteogenic

lineage, although only for those cells extracted from the CU-701 pectin. Bcl2 modifying factor (*BMF*), found in both contrasts, has been implicated in cytoskeleton damage and to signal cell death (Hausmann *et al.*, 2011). If CU-701 pectin is causing increased expression of genes related to damage and cell death, longer term studies into viability are required to establish whether pectin is inducing apoptosis.

The transcriptome analysis was carried out to understand whether any of the secreted proteins implicated in the regenerative and immunomodulatory properties of hMSCs (*TGFB1, IGF1, VEGF, HGF, GDNF, BDNF, NGF, IDO, IL1RN*) (Baez-Jurado *et al.*, 2019, Ferreira *et al.*, 2018) and stemness genes (sox2, oct4, and Nanog) (Pennock *et al.*, 2015) were differentially expressed in response to spraying or pectin. None of these were significantly differentially expressed in either of the contrasts evaluating spray versus syringe (PBS spray versus PBS syringe and CU-701 spray versus CU-701 syringe). However, *TGFB1* was significantly upregulated in both the CU-701 versus PBS contrasts (CU-701 syringe versus PBS syringe and CU-701 spray versus PBS spray), and *BDNF* significantly downregulated in both contrasts. Additionally, in the CU-701 spray versus PBS spray contrasts, *NGF* was significantly down regulated, and *HGF* up regulated, all based on an adjusted P-value <0.1. However, it is worth noting that none of the LFC were >2, therefore these changes were not large. This suggests the CU-701 pectin may have very little effect on the immunomodulatory and regenerative phenotype of the hMSCs.

As the genes highlighted in the differential gene expression in the CU-701 pectin versus 1xPBS contrasts were associated with calcium transport or increases in intracellular calcium, the use of exogenous calcium should be re-evaluated. Calcium was added to pectin to induce gelation in the cell culture wells to ensure hydrogels were formed and cells encapsulated, however gene expression changes within the hMSCs may have occurred as a consequence. This may require further investigation to unpick the changes in gene expression in response to the pectin and the calcium separately. If calcium is negatively affecting the hMSCs, the spraying within pectin process would require optimisation to understand the behaviour of 1% w/v pectin solutions when in contact with brain tissue to reduce or remove the need for additional calcium.

4.6. Future work

4.6.1. Spray device development

The MAD syringe spray device was assessed for delivering cells. As previously discussed, this reduces the amount of equipment required compared to air pressure devices and may be more appropriate when considering the use is for local brain delivery following TBI. Three pump bottle spray actuators were initially considered for spraying cells, shown in Figure 4.17.



Figure 4.17 – Three bottle pump spray actuators initially investigated for their suitability for spraying pectin and cells. All three were generously donated by AptarPharma. On the left is the APF+ device, the centre is the standard actuator, and the right is the nasal spray.

The use of these with cell suspensions was difficult, with an excess volume of approximately 1 mL required to fill the void space at the bottle of the bottle, and frequent occurrences of partial spraying resulting in inconsistent dosing. In addition, the nasal spray was ruled out due to the requirement to invert the device to spray, and observable variability in droplet size. The APF+ device was initially very interesting as the air intake used after each spraying event utilises a sterile valve, maintaining the sterility of the bottle contents. The idea of a syringe spray device originated from removing the standard actuator and attaching a syringe, shown below.

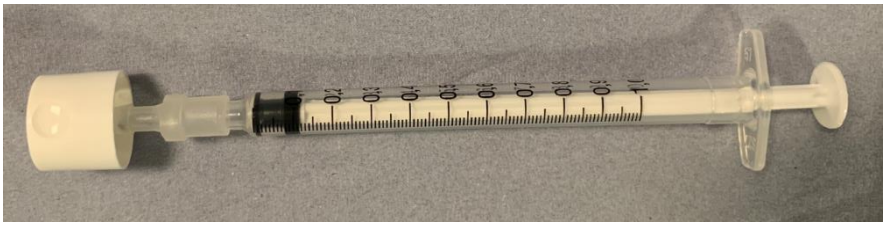


Figure 4.18 – The AptarPharma standard actuator attached to a syringe for spraying.

Better dose control, easier use, and less waste of cell suspensions were observed in initial experiments conducted using the spray device shown in Figure 4.18. Searches were then carried out, and the MAD sprayer chosen for subsequent cell spraying work due to the intended use as a syringe-based spray device. Good viability both with and without pectin were demonstrated, however the spray pattern using pectin was not ideal due to a very narrow droplet pattern.

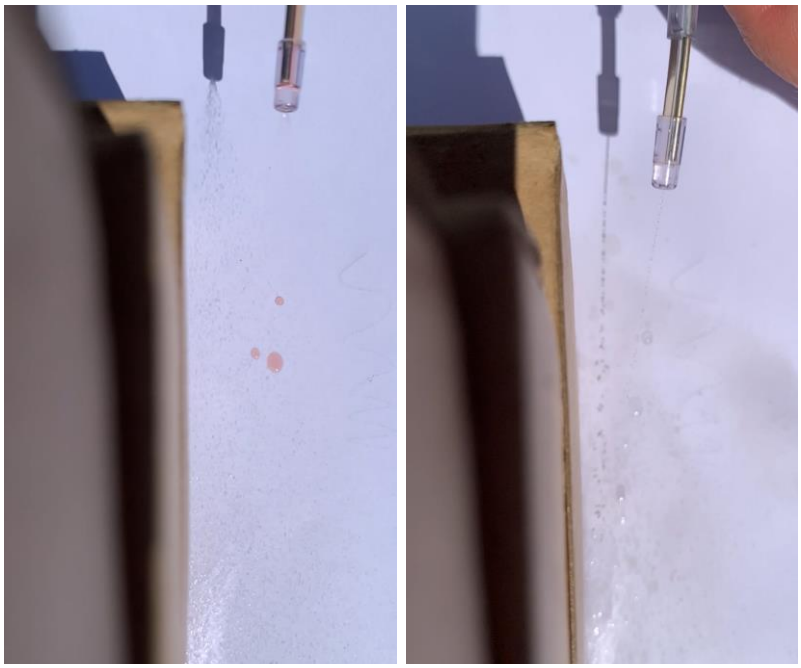


Figure 4.19 – Spray pattern of water and food dye on the left, and pectin on the right. Spray pattern is shown in the shadows.

Shown in Figure 4.19, a spray is still generated when using the more viscous pectin solution, however the droplets are ejected in a line, rather than a cone pattern seen on the left of the figure. With more time, more work would have been carried out to understand how to improve the spray pattern when using pectin. Some preliminary investigations and designs were carried out, but none of the designs were used with cells.

On initial inspection, it appeared the device was a simple liquid pressure device with a void space; therefore, this design was adapted, adjusting the size of the aperture liquid leaves through.

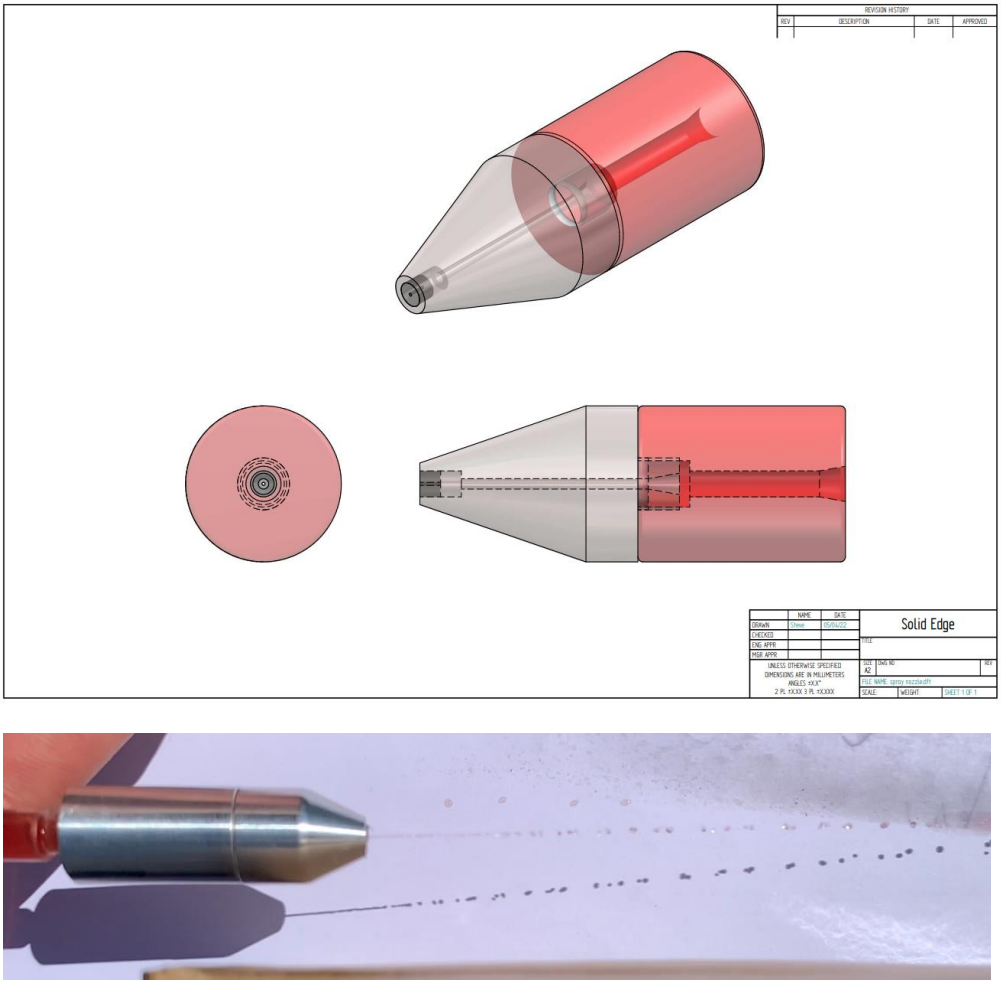


Figure 4.20 – Syringe device design (top). The inlet hole is designed to fit standard syringes. This lead to a 1.5 mm diameter channel, a 3 mm by 2 mm void space, and a 0.3 mm outlet hole. This device was manufactured (bottom) and tested with water and food dye, with the spray pattern shown.

The images in Figure 4.20 show a first draft at designing and manufacturing a spray device. Unfortunately, as seen in the lower image, the spray pattern was more of a jet than a spray, therefore no improvement on the purchased device. A V-notch was added to the ejection hole on the device which did improve the spray pattern, but only when high pressures were used. The spray can be seen in Figure 4.21.

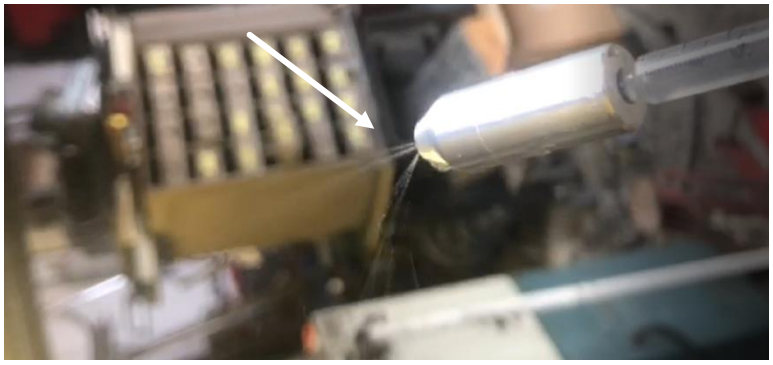


Figure 4.21 – The device from Figure 4.20, modified by the addition of a V-notch on the external side of the ejection hole. The arrow indicates the water leaving the device as a spray; however, this was only achieved using high pressure generated by the syringe.

Further work and development would be to test designs prior to manufacture using a programme such as the Ansys suite of software. It was hypothesised that a helical fluid flow within the device would create surface impingement and break up the liquid into droplets within the device before being ejected. A V-notch on the ejection hole could also be added to cause a fan or cone spray pattern. Both these design options are shown in Figure 4.22.

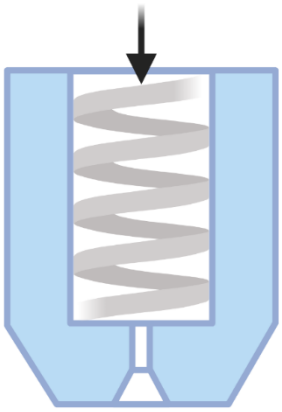


Figure 4.22 – A possible design option to optimise pectin and cell spraying.

Parameters such as the helix geometry, diameters, and fluid path length could be altered and modelled to understand and optimise the effects on droplet size and spraying pattern, and the pressure required to generate a spray. These could then be tested using similar methods discussed in this chapter to select the best design.

As discussed, the exogenous calcium concentration used requires further investigation and optimisation. During the gelation screen carried out in Chapter 3, it was shown that calcium concentrations found endogenously in the brain (1-

2 mM) were not high enough to cause gelation of pectin. The optimal concentration based on the work in Chapter 3 was 100 mM, therefore this was used. However, this was a compromise to use pectin as a hydrogel in a cell culture environment. In addition to gelation by calcium, pectin demonstrates strong mucoadhesive and bio adhesive properties. This has been shown in a variety of studies investigating pectin for a range of uses and indications, such as buccal (Wattanakorn *et al.*, 2010), intestinal (Thirawong *et al.*, 2008), and brain drug delivery (McCrorie *et al.*, 2020). Pectin is a hydrophilic polymer with groups available to form hydrogen bonds. It is thought this hydrophilicity and ability to hydrogen bond with water and other molecules is the reason for the adhesive properties of pectin (Sriamornsak *et al.*, 2008, Sriamornsak *et al.*, 2010). Adhesion of pectin gels to the brain surface has been demonstrated using a texture analyser to measure the force required to separate a pectin hydrogel from the surface of a rat brain slice (McCrorie *et al.*, 2020). Due to the mucoadhesive property of pectin, a reduced concentration of calcium may be required to achieve a hydrogel stable enough to retain hMSCs at the site of injury.

4.7. Conclusions

The results of the cell spraying with 3T3 cells, SH-SY5Y cells, and hMSCs indicate that the MAD sprayer is suitable for the spraying of cells. When moving on to the use of pectin within which to spray hMSCs, again cell viability was maintained, suggesting pectin is a suitable material for the delivery of hMSCs. Flow cytometry analysis enabled the selection of the CU-701 grade of pectin as this showed the smallest change in surface marker expression compared to the PBS syringe control condition. The differentiation study requires further work to include the hMSCs from donor #26000 and chondrocyte differentiation. Spontaneous differentiation is not a desired response to the pectin and spraying for use as a TBI treatment, however the potential of the cells to differentiate down an adipogenic, osteogenic, and chondrogenic lineage would demonstrate the cells remain MSCs after spraying in pectin. Results so far suggest the differentiation of hMSCs down the osteogenic lineage may be inhibited which may suggest the MSCs have lost some “stemness”, particularly when in combination with the result of the differential gene expression analysis showing

the upregulation of *IGFBP5* in response to CU-701 pectin. The results of the differential gene expression analysis suggested further optimisation of the pectin conditions may be required to minimise the response of the hMSCs to the calcium in the pectin.

Chapter 5 *In vitro* TBI modelling

5.1. Introduction

The results in Chapter 4 show that viable hMSCs can be sprayed in pectin, and that some grades are suitable for retaining the phenotype of those sprayed cells. This allows for progression to traumatic brain injury (TBI) models to understand the potential efficacy of the sprayed hMSCs in pectin. Ultimately, a comparative study would be undertaken using an animal TBI model to understand whether local hMSC delivery by spraying in pectin is superior to intravenous delivery in terms of improving recovery after injury. Jackson *et al.* (2010) has carried out a comparative study investigating how intracerebral injection compared to intravenous using a neuroinflammation model, finding superior transplanted cell number in the brain when delivered intracerebrally in rats (Jackson *et al.*, 2010). This study did not evaluate functional recovery, however, shows there are benefits to local delivery to improve the number of cells that reach the brain.

To better understand and optimise novel therapies, *in vitro* models are used before moving to animal models. There are numerous possible models for TBI, with varying complexity. Each TBI *in vitro* model published has advantages and disadvantages, and none completely model all the injury pathways (Kumaria and Tolias, 2008). *Ex vivo* tissue, primary cells, differentiated stem cells, and cell lines have all been used in published studies investigating TBI and are discussed in Chapter 1 (1.3.1).

Whilst cell lines have drawbacks in terms of their immortality and altered genotype compared to primary cells, they also have many advantages such as reduced population variation and reproducibility (Kaur, 2012). Many are easy to culture relative to primary and stem cells, with relatively low cost, so can be used for high-throughput modelling and to establish early *in vitro* models (Barbosa *et al.*, 2015).

The SH-SY5Y cell line is derived from human neuroblastoma and has been used in many studies investigating novel therapies for TBI. The cells grow with neurite-like outgrowths which can be used as a measure of response to injury and treatment (Kovalevich and Langford, 2013). As the SH-SY5Y cell line is

derived from human cells, the genes and proteins expressed are human. When considering the use of human MSCs as a therapy, testing on an *in vitro* model established also using human cells may offer an advantage in terms of translatability.

SH-SY5Y cells have been used to model many injury pathways observed in secondary TBI, including oxygen deprivation, glucose deprivation, both oxygen and glucose deprivation combined, oxidative stress using H_2O_2, and excitotoxicity using glutamate (Liu *et al.*, 2018). The therapeutic benefits of MSCs are largely mediated via the secretome (Vizoso *et al.*, 2017). This includes various growth factors and anti-inflammatory factors, discussed in Chapter 4 (4.1.5). One in particular is GDNF, secreted by MSCs and shown to be neuroprotective (Neff *et al.*, 2002, Baez-Jurado *et al.*, 2019), which SH-SY5Y cells are sensitive to. GDNF functions to promote survival and proliferation of cells (Hansford and Marshall, 2005), and has been used in SH-SY5Y models of damage (Wang *et al.*, 2016).

Oxidative stress in TBI causes damage via reactive oxygen species, including H_2O_2, and is a component of the neuroinflammatory process causing cell further cell death following the primary injury (Fesharaki-Zadeh, 2022). Glutamate excitotoxicity also causes cell death via overstimulation of the NMDA receptors causing the influx of Ca^{2+}, which activates catabolic enzymes, damages the cell and leads to cell death (Ladak *et al.*, 2019). MSCs have demonstrated protection against excitotoxicity mediated by glutamate, both *in vitro* and *in vivo* (Papazian *et al.*, 2018), and they have demonstrated immunomodulatory effects (Baez-Jurado *et al.*, 2019). Therefore, testing an MSC based therapy on both a glutamate damage model, and oxidative stress damage model to imitate a component of inflammation, is reasonable to understand possible therapeutic benefits. SH-SY5Y cells, being of human origin, and sensitive to both damage types, are a suitable cell line for *in vitro* modelling of these secondary injury pathways for early testing.

Table 5.1 summarises studies investigating SH-SY5Y response to glutamate injury. Hydrogen peroxide has been used in combination with SH-SY5Y cells to

model oxidative stress and the effect of novel therapies in oxidative stress models. Table 5.2 summarises the parameters of some of the published models.

Table 5.1 – Glutamate model conditions as reported in current literature. Metabolic activity was measured by MTT assay in all studies.

SH-SY5Y conditions	Damage conditions	Metabolic activity reduction	Reference
10,000 cells/well, 96-well plate, cultured in DMEM.	8 mM glutamate for 30 minutes, followed by a 12-hour incubation	30%	(Hu *et al.*, 2012)
Cells cultured in MEM:F12 media. Cell seeding density not stated.	10 mM glutamate for 24 hours.	45%	(Wang *et al.*, 2016)
Cell seeding density not stated. Cells cultured in DMEM and seeded 24-48 hours prior to damaging.	80 mM glutamate for 24 hours.	45%	(Sun *et al.*, 2010)
50,000 cells/well, 96-well plates, seeded 24-hours prior to damaging, cultured in DMEM.	100 mM glutamate for 3 hours.	50%	(Lee *et al.*, 2019)

Table 5.2 – H_2O_2 model conditions as reported in current literature. Metabolic activity was measured by MTT assay in all studies.

SH-SY5Y conditions	Damage conditions	Metabolic activity reduction	Reference
6-8,000 cells/well in 96-well plate. Cultured in DMEM.	Cells were cultured in reduced serum media for 24 hours (1% FBS, reduced from 10%), before adding 600 µM H_2O_2 for 24 hours.	40%	(Zhao *et al.*, 2019)
Unknown seeding density. Cultured in MEM:F12.	450 µM H_2O_2 for 24 hours.	45%	(Chen *et al.*, 2020b)
40,000 cell/well in 96-well plate. Cultured in DMEM.	400 µM H_2O_2 for 24 hours.	50%	(Feng *et al.*, 2016)
10,000 cells/well in 96-well plate. Cultured in EMEM:F12.	300 µM H_2O_2 for 24 hours.	40%	(Tian *et al.*, 2021)
100,000 cells/well in 96-well plate. Cultured in DMEM:F12.	100 µM H_2O_2 for 24 hours.	50%	(Nirmaladevi *et al.*, 2014)

The different protocols used by research groups when establishing SH-SY5Y cell damage models is highlighted in Table 5.1 looking at glutamate damage, and Table 5.2 looking at H_2O_2 damage. The seeding density, culture media, incubation time, concentration of glutamate or H_2O_2, and measured outcomes are listed where known. In both models, there is a range of concentrations of

glutamate and H_2O_2 used to establish cell death, with the chosen endpoint resulting in a 30-50% reduction in metabolic activity, used as an indicator of cell viability. These studies were used to inform the conditions used to optimise models described in the Section 5.4.

5.2. Hypothesis, aims, and objectives

5.2.1. Hypothesis:

- Sprayed hMSCs in pectin offer therapeutic potential in an *in vitro* damage model of excitotoxicity and oxidative stress.

5.2.2. Aims

- Determine the effect of pectin hydrogels on the SH-SY5Y damage models.
- Determine the effect of sprayed hMSCs in pectin on the SH-SY5Y damage models.

5.2.3. Objectives

- Establish models of excitotoxicity and oxidative stress using the SH-SY5Y cell line. Measure the metabolic activity of SH-SY5Y cell population after the addition of different concentrations of glutamate or H_2O_2 to find a concentration that leads to approximately 50% reduction in metabolic activity. Metabolic activity is used as an indicator of cell viability in all experiments.
- Measure the metabolic activity of damaged SH-SY5Y cells after incubation with pectin hydrogels.
- Measure the metabolic activity of damaged SH-SY5Y cells after co-culture with sprayed hMSCs in pectin.

5.3. Method design

The SH-SY5Y cell line was chosen due to the popularity of the cell line for early brain research and previously published protocols discussed in section 5.1. The glutamate excitotoxicity model and oxidative stress model were chosen as both damage types are present in secondary injury in TBI (Prins *et al.*, 2013). As previously discussed in Chapter 4, one of the therapeutic benefits of hMSCs is the secretion of factors able to support regeneration and repair (Baez-Jurado *et al.*, 2019). Therefore, SH-SY5Y co-culture models to investigate the recovery of the cells after damage with either glutamate or H_2O_2 were established to understand whether the presence of pectin and hMSCs could enhance the recovery.

SH-SY5Y cell culture, hMSC culture, and damage model protocols were carried out as described in Chapter 2 (Cell culture: 2.4.2. and 2.4.3, models: 2.13, 2.14, 2.15, and 2.16) The recommended seeding density for the SH-SY5Y cell line is $3x10^3$ to $1x10^5$ cells/cm^2, with a saturation density of approximately $1x10^6$ cells/cm^2 (Kovalevich and Langford, 2013), which is a broad range, within which all the quoted seeding densities in Table 5.1 and Table 5.2 fall. Cells in this study were seeded at a density of 5,000 cells/well in a 96-well plate, to give approximately 15,700 cells/cm^2. This density was kept consistent when optimising the model for use with 24-well plates. This density was lower than many of the studies summarised in Table 5.1 and Table 5.2, however it was chosen as it gave approximately 70-80% confluency after 24-hours of culture. Glutamate concentrations ranging from 10-1000 mM were used to both incorporate and exceed the range of concentrations described in Table 5.1, in order to choose a concentration resulting in 50% reduction of viability, indicated by a loss of metabolic activity from the cell population. H_2O_2 concentrations ranging from 10 – 400 µM were used in the model optimisation to select a concentration resulting in 50% reduction in viability, indicated by a loss of metabolic activity from the cell population.

Three models were established: (i) glutamate model; (ii) 1-hour H_2O_2 model and (iii) the 24-hour H_2O_2 model. In the glutamate model cells were damaged for 1 hour with glutamate, then the media changed. Treatments were added with the media change, and this model was used to understand the effect of the treatments

on the recovery of the cells after damage. In the 1-hour H_2O_2 model cells were damaged for 1 hour with H_2O_2, then media changed. Treatments were added with the media change, and this model was also used to understand the effect of the treatments on the recovery of the cells after damage. In the 24-hour H_2O_2 model cells were damaged for 24 hours with H_2O_2. Treatments were added at the same time as H_2O_2. As the H_2O_2 was present throughout the 24 hours, this model was used to understand the effect of the treatments on protecting the cells from damage. A PrestoBlue assay was carried out after 24 hours to maintain consistency with reported literature, and with the timeframe used in Chapter 4. Full method description in Chapter 2 (2.16).

5.4. Results

5.4.1. SH-SY5Y damage model development

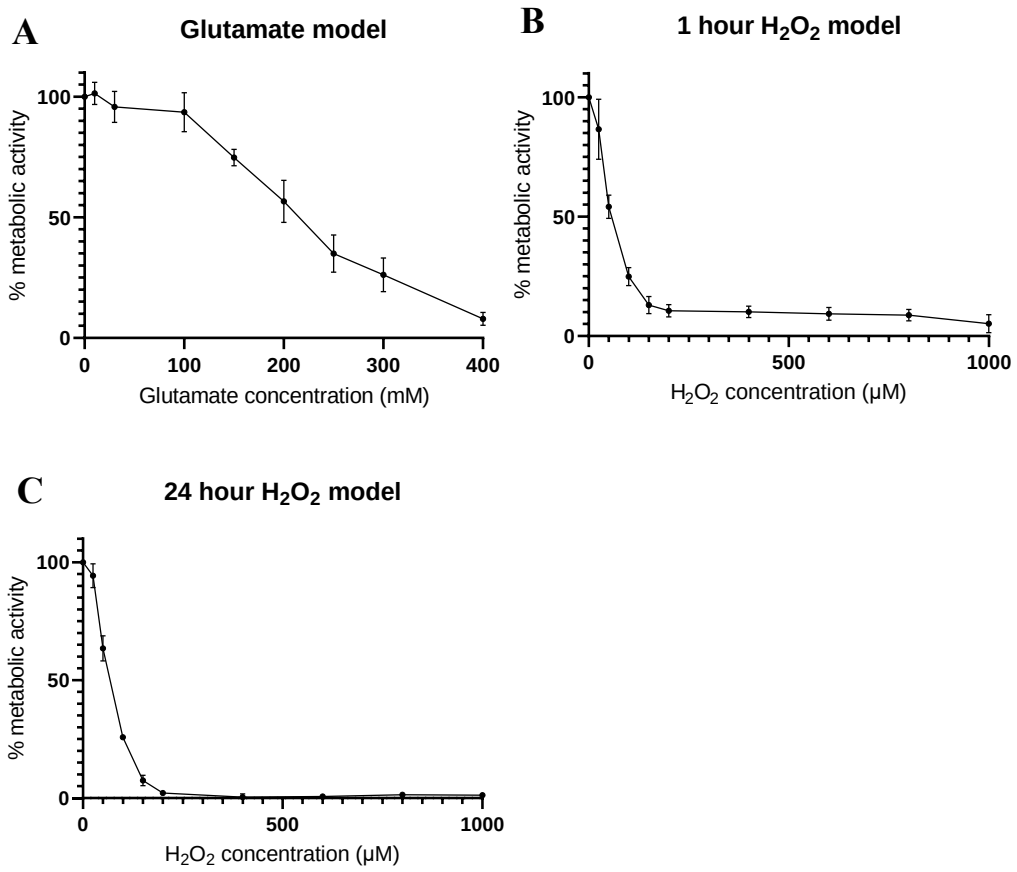


Figure 5.1 – Metabolic activity of SH-SY5Y cells following damage by the addition of **A** glutamate for 1 hour, **B** hydrogen peroxide for 1 hour, or **C** hydrogen peroxide for 24 hours. In the 24-hour model, hydrogen peroxide was added and left on the cells for 24 hours before carrying out the PrestoBlue assay. In the 1-hour models, cells were washed after 1 hour and fresh media added. PrestoBlue metabolic assays were carried out 24 hours after the addition of the damaging media. Results were calculated as a percentage of the undamaged control. Tests were carried out in triplicate on four separate occasions (N=4, n=3) and error bars show the standard error of the mean.

Figure 5.1 shows the results of the 96-well plate damage model optimisation. Overall, as the concentration of glutamate or H_2O_2 in the media increases, the metabolic activity (used to indicated viability) of the cell population decreases. Each data point was normalised to an undamaged condition undergoing media changes at the same time. In the glutamate model, a concentration of 400 mM resulted in a metabolic activity close to 0%. Concentrations of glutamate ranging from 10 – 100 mM resulted in only slight reductions in metabolic activity (down to 94% for 100 mM).

In the 1-hour H_2O_2 model, concentrations of 150 – 800 µM resulted in a reduction of metabolic activity to approximately 10%, with 1000 µM resulting in 5% metabolic activity. In the 24-hour model, 150 µM H_2O_2 resulted in only 7% metabolic activity, and concentrations ranging from 200 – 1000 µM lead to 0% metabolic activity.

The concentrations required to achieve approximately a 50% reduction in metabolic activity for the glutamate model was 200 mM, and for both H_2O_2 models, 50 µM was required.

5.4.2. SH-SY5Y damage model development in 24-well tissue culture plates

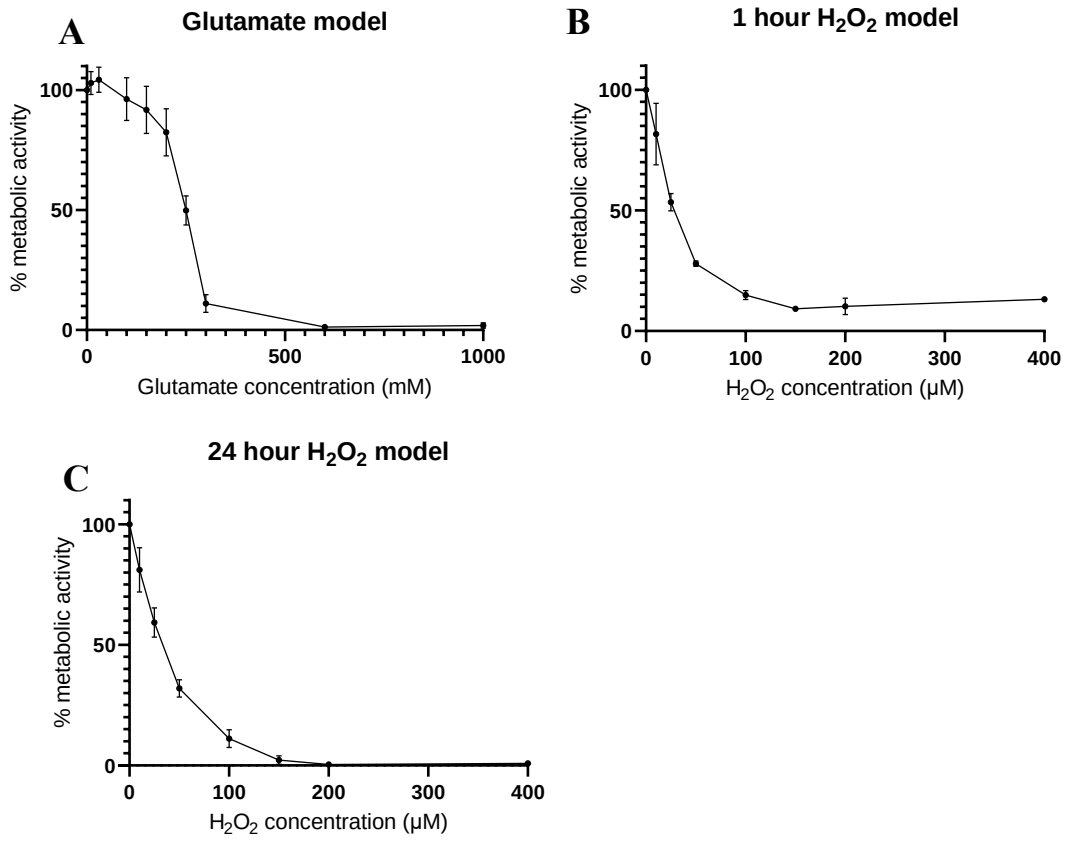


Figure 5.2 – Metabolic activity of SH-SY5Y cells following damage by the addition of **A** glutamate for 1 hour, **B** hydrogen peroxide for 1 hour, or **C** hydrogen peroxide for 24 hours. In the 24-hour model, hydrogen peroxide was added and left on the cells for 24 hours before carrying out the PrestoBlue assay. In the 1-hour models, cells were washed after 1 hour and fresh media added. PrestoBlue metabolic assays were carried out 24 hours after the addition of the damaging media, and results were calculated as a percentage of the undamaged control. Tests were carried out in triplicate on three separate occasions (N=3, n=3) and error bars show the standard error of the mean.

After initial method development and optimisation experiments were carried out in 96-well, optimisation was then continued in 24-well plates due to the well inserts (used for the co-culture model) requiring the use of 24-well plates. Figure 5.2 shows the result of the 24-well plate damage model optimisation. As in the 96-well plate model optimisation, overall, as the concentration of glutamate or H_2O_2 in the media increases, the metabolic activity (used as an indicator of viability) of the cell population decreases. In the glutamate model, the concentration range was increased to include 600 and 1000 mM due to metabolic

activity in the 96-well plate model not quite reaching 0%. At both these concentrations in the 24-well plate, metabolic activity was reduced to approximately 1%. A concentration of 250 mM gave the desired reduction of 50% metabolic activity.

In the 1-hour H_2O_2 model, 0% metabolic activity is not reached, but the metabolic activity is reduced to <15% from 100 µM onwards. The 24-hour model resulted in 0% metabolic activity when H_2O_2 concentrations were greater than 150 µM. In both the 1-hour and 24-hour models, 25 µM H_2O_2 have approximately 50% reduction in the metabolic activity of the population of cells.

Comparing the concentrations required to reduce the metabolic activity by 50% in the 96-well plates compared to the 24-well plates, a higher concentration of glutamate was required in the 24-well plate (200 mM increased to 250 mM). In the H_2O_2 models, a lower concentration was required in the 24-well plates (50 µM decreased to 25 µM). These results show the well plate size does seem to affect the response of the cells to damage.

5.4.3. Pectin hydrogel addition to SH-SY5Y damage models

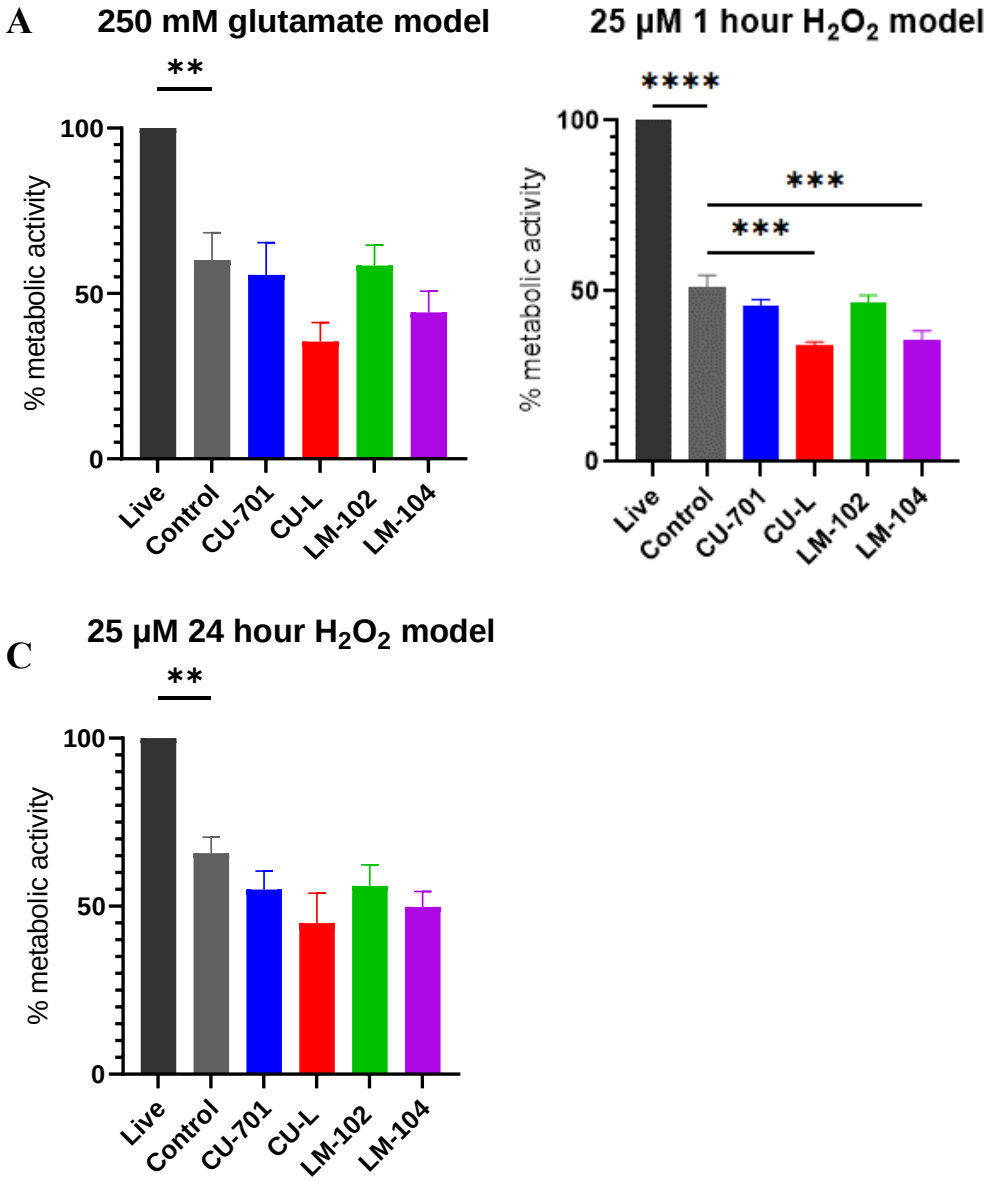


Figure 5.3 – Metabolic activity of SH-SY5Y cells in 24-well plates with or without pectin hydrogels, following damage by the addition of **A** 250 mM glutamate for 1 hour, **B** 25 µM H_2O_2 for 1 hour, or **C** 25 µM H_2O_2 for 24 hours. In the 1-hour models, cells were washed after 1 hour and fresh media added, then 1% w/v pectin hydrogels added. In the 24-hour model, 1% w/v pectin hydrogels were added immediately after the addition of H_2O_2 media. PrestoBlue metabolic assays were carried out after 24 hours. Results were calculated as a percentage of the undamaged control, which had media changes at the same time as damaged cells, but never had glutamate or H_2O_2 added. Tests were carried out in triplicate on three occasions (N=3, n=3). Error bars show standard error of the mean. One-way ANOVA with a Dunnett's post-test was carried out to determine statistical significance between the damage control cells and all other conditions. ** shows P<0.01, *** shows P<0.001, **** shows P<0.0001.

Based on the results of the 24-well plate model optimisation, 250 mM glutamate, and 25 µM H_2O_2 were used to give approximately 50% reduction in the metabolic activity of the cell population. Figure 5.3 shows the result of the damage models following the addition of pectin hydrogels formed using the four different grades of pectin. All three models showed a statistically significant difference in metabolic activity between the damaged condition and the live control cells. The trends across the three models were similar: CU-701 and LM-102 had the highest metabolic activity of the four pectin grades, and CU-L and LM-104 had the lowest. This reduction was statistically significant in the 1-hour H_2O_2 model when compared to the damaged cells with no pectin.

When comparing the damage controls in the 1-hour H_2O_2 model and the 24-hour H_2O_2 model, there is a less significant reduction (based on P-value) in the 24-hour model. This may be due to the 1-hour model having a media change/wash step which could remove any loosely adhered cells which would not be lost in the 24-hour model which does not have any wash steps before the PrestoBlue assay. This could be the cause of the lower metabolic activity in the 1-hour model.

5.4.4. hMSC in PBS/pectin co-culture SH-SY5Y damage models

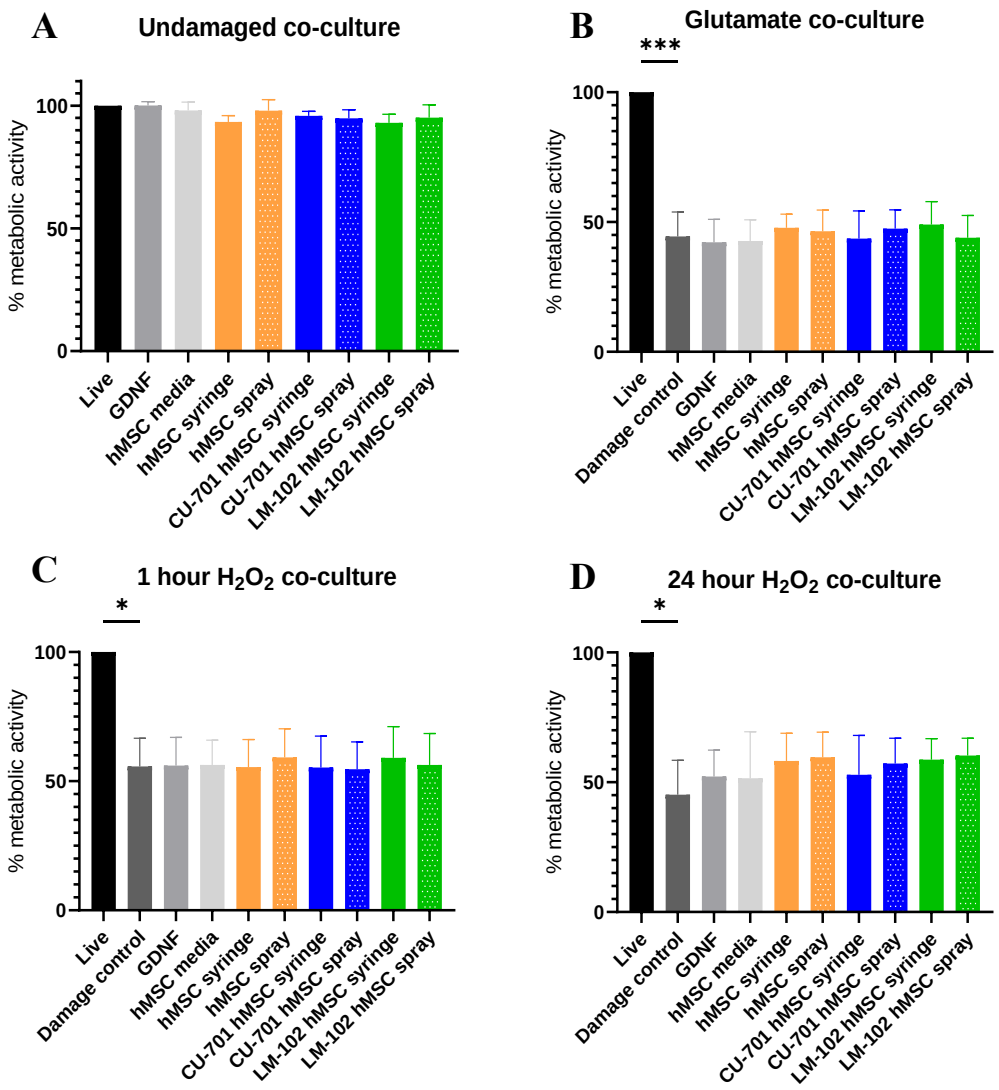


Figure 5.4 – Metabolic activity of SH-SY5Y damage co-culture model with hMSCs in PBS or pectin seeded into 24-well well inserts by syringe or spraying. SH-SY5Y cells were **A** undamaged, **B** damaged with 250 mM glutamate for 1 hour, **C** damaged with 25 µM H_2O_2 for 1 hour, or **D** damaged with 25 µM H_2O_2 for 24 hours. In 1- hour models, cells were washed after 1-hour, fresh media added, followed by well inserts. In the 24-hour model, well inserts were added immediately after H_2O_2 media. PrestoBlue metabolic assays were carried out after 24 hours. Results were calculated as a percentage of the undamaged control, which had media changes at the same time as damaged cells, but never had glutamate or H_2O_2 added. Tests were carried out in duplicate using three hMSC donors (N=3, n=2). Error bars show the standard error of the mean. One-way ANOVA with a Dunnett's post-test was carried out to determine statistical significance between the damage control cells and all other conditions. * shows $P<0.05$ and *** shows $P<0.001$.

Figure 5.4 shows the results of the co-culture damage model. All three models showed a statistically significant difference in metabolic activity between the damaged condition and the live control. All of the treatment conditions gave very similar metabolic activity to the untreated damaged cells, with no statistically significant differences observed.

The damage controls for both the H_2O_2 models in the co-culture showed more similar reductions in metabolic activity than the models used for the pectin hydrogels (Figure 5.3), but more variation between repeats (shown by the larger error bars). This is possibly due the well inserts increasing the protocol time and therefore increasing the length of time the cells are not in the incubator. Figure 5.3 also showed a higher metabolic activity in the damage control wells in the 24-hour model, however this is not seen in Figure 5.4.

5.5. Discussion

The aim of this chapter was to determine whether the pectin hydrogels and the hMSCs had a positive on models of excitotoxicity or oxidative stress, measured by an increase in metabolic activity of the population of cells. Cell lines were selected over primary cell cultures and other *in vitro* models for this study due to advantages for ease of use and lower cost when carrying out larger studies (Kumaria, 2017). All four grades of pectin were tested, and multiple damage pathways modelled. Therefore, due to the multiple conditions being modelled, cell lines are more suitable for high-throughput screening (Kaur, 2012). There is a selection of cell lines commonly used to model TBI *in vitro* due to their relevance to brain cells and the ease of use for larger, high-throughput screening studies (Morrison *et al.*, 2011). These are described in (Table 1.1) and include the PC-12, SH-SY5Y, NG108-15, bEnd.3, BV-2, and HT22 cell lines.

The bEnd.3 cell line is derived from endothelial cells and used to model the BBB (Berrout *et al.*, 2012). MSCs have been shown to positively affect the BBB stability both following injury *in vivo* and using the bEnd.3 in a co-culture model (same study) (Park *et al.*, 2015), and it would be interesting to confirm this therapeutic effect is still observed following the delivery of MSCs in pectin. However, for the purposes of the experiments in this chapter, the neuroprotective and neurorestorative effects of hMSCs on neuron-like cells were under investigation, therefore the bEnd.3 cell line was not used as it is endothelial and used for BBB modelling.

The PC-12, SH-SY5Y, NG108-15, and HT22 cells all demonstrate neurite-like extensions from the cell body and can be used to model neurons (Wiatrak *et al.*, 2020, Shipley *et al.*, 2016, Daniels, 1974, Liu *et al.*, 2009). All but the SH-SY5Y cells are derived from rodents. Proteins found in the secretome of hMSCs will be derived from human genes, and as SH-SY5Y cells were derived from humans, these also express the human versions of genes (Kovalevich and Langford, 2013). For this reason, the human SH-SY5Y cells were chosen over the others.

When modelling excitotoxicity and oxidative stress using the SH-SY5Y cell line, metabolic activity is commonly used as an indirect measure of cell viability (Liu *et al.*, 2018). To establish the concentration of glutamate and H_2O_2 required

to achieve a 50% reduction in the metabolic activity of the cell population, optimisation was carried out using a range of concentrations, and PrestoBlue used to measure metabolic activity. Similar to MTT, PrestoBlue measures metabolic activity of the cells, but is more sensitive and has an easier to use protocol than MTT, more amenable to high-throughput screening assays (Xu *et al.*, 2015). The cell density per cm^2 and volume to cell ratio was kept consistent for the change from the 96-well plate to 24-well plate. The concentration required to reduce the metabolic activity of the cell population by 50% did change with the change in well size. In the glutamate model, the concentration changed from 200 mM in the 96-well plate, to 250 mM in the 24-well plate. This concentration was more than 10x higher than some values used in past studies (Wang *et al.*, 2016). For the H_2O_2 models, the concentration changed from 50 µM in the 96-well plate, to 25 µM in the 24-well plate, lower than the concentrations used in the past studies listed in Table 5.2. These results show that well size caused variability in the cell response.

The studies detailed in Table 5.2 all left H_2O_2 on the cells for 24 hours, whereas one model used in this study only left the H_2O_2 on for 1 hour to be comparable to the glutamate damage model. The concentration required for a 50% reduction in metabolic activity was similar for both models (1-hour and 24-hour), which suggests most of the damage occurs within the first hour. This correlates with a meta-analysis investigating the use of H_2O_2 in oxidative stress, which demonstrated conversion of H_2O_2 to O_2 by catalase within a few minutes (Ransy *et al.*, 2020).

In the 1-hour H_2O_2 model, CU-L and LM-104 pectin grades demonstrated a statistically significant reduction compared to the damage control cell population. As a result, only CU-701 and LM-102 were taken forward into the co-culture models. The reason for this difference in metabolic activity is unclear, however one trend observed is those two grades of pectin gel did not dissolve during the 24-hour test period, whereas the CU-701 and LM-102 grades did. Pectin can be broken down enzymatically (by bacterial enzymes), by hydrolysis, or by loss of Ca^{2+} (Liu *et al.*, 2003). This lack of degradation could suggest the gels may block the effective flow of nutrients, however SH-SY5Y cells demonstrated biocompatibility in Chapter 3 (Figure 3.11), and hMSCs

demonstrated high viability when encapsulated in all grades of pectin gel for 24-hours (Figure 4.9). The CU-L and LM-104 grades have the lowest DM of the four grades; 28% and 27% respectively. A lower DM is correlated with a higher sensitivity to gelation by Ca^{2+} (Gawkowska *et al.*, 2018), therefore this factor may influence cell survival. Little is known about how different pectin grades may affect the SH-SY5Y cells following damage directly, however depletion of intracellular calcium stores have been linked to SH-SY5Y cell death (Nguyen *et al.*, 2002). Future work to image the SH-SY5Y cells at the gel-cell interface could provide insight into whether there are any interactions between the damaged cells and the pectin hydrogel. Carrying out a calcium assay could provide insight into whether the different DM of the pectin grades is affecting the availability of calcium in the media and assess whether this correlates with cell viability.

The co-culture model showed no significant differences between the damage control cells and the treatments in all models, including no significant difference with GDNF. GDNF functions to promote survival, proliferation, maturation, differentiation, and neurite outgrowth in neurons (Cortés *et al.*, 2017), and acts to promote viability and proliferation in SH-SY5Y cells following treatment (Mu *et al.*, 2020). 50 ng/mL of GDNF was used on glutamate damaged SH-SY5Y cells by Mu *et al.* (2020) showing increased cell proliferation in response to GDNF. Wang *et al.* (2016) also an SH-SY5Y glutamate damage model and showed higher viability of cells treated with 50 ng/mL GDNF. The concentration of glutamate used to damage cells in that study was 10 mM (Wang *et al.*, 2016), which is much lower than the 250 mM used here. The cell seeding density used by Wang *et al.* (2016) was not stated; both these factors could influence how the cells respond to the presence of GDNF following damage and could explain the lack of promotion of proliferation/viability. The metabolic activity was also not increased when GDNF was added to undamaged cells, suggesting the concentration of GDNF used was too low.

The co-culture models used in this chapter using the well-inserts investigated the effect of the hMSC secretome from hMSCs in co-culture on the damaged SH-SY5Y cells. The secretome has demonstrated efficacy in rat models of TBI (Zhang *et al.*, 2015), and glutamate induced damage models using SH-SY5Y

cells where increased cell survival was seen with the addition on rat and human MSC conditioned media (Karagyaur *et al.*, 2021). In all the tested co-culture conditions in this chapter, no statistically significant changes were seen. The 24-hour H_2O_2 model showed slight increases in metabolic activity in the treatment wells, however these were small and not statistically significant. Due to the presence of H_2O_2 throughout the 24-hour test period, the 24-hour H_2O_2 model was more aimed at any protective effects of the treatment conditions. An additional hypothesis for possible protective effects in the 24-hour H_2O_2 model (in addition to the protective effects of the secretome) is the presence of additional cells in the well inserts containing hMSCs may have aided the conversion of H_2O_2 into O_2 by catalase (Ransy *et al.*, 2020), however as no significant changes were seen, this was not shown in the co-culture model.

When adding a soluble test molecule, it is available to the cells immediately, whereas the co-culture models rely on the hMSCs secreting those protein and extracellular vesicles before a positive effect can be seen. 24 hours may not have been enough time for the hMSCs to have an impact on the recovery of the SH-SY5Y cells in the damage model. If time had allowed, further work using a longer time period, or testing media conditioned with hMSCs in pectin could have been carried out. In addition, the density of hMSCs used may have been insufficient, therefore further work could have investigated the effect of an increase in hMSC density.

Protection against oxidative stress by MSCs has been demonstrated *in vitro* through transfer of mitochondria from MSCs to primary cortical neurons (Tseng *et al.*, 2021). This mechanism was not modelled here due to the use of well-inserts but could be an interesting avenue for further work to understand whether this would occur in damaged SH-SY5Y cells.

There are many TBI models available and hMSCs secrete many factors that are therapeutically active via many different pathways (Eleuteri and Fierabracci, 2019). The response to the secretome of hMSCs *in vivo* involves many cell types and research is ongoing to develop and enhance the regenerative potential of hMSCs and the secretome (Pischiutta *et al.*, 2022). Other cell types found in the brain, such as astrocytes, microglia, and oligodendrocytes, have been implicated

in the response to hMSCs in TBI (Adugna *et al.*, 2022)., therefore co-culture models incorporating these cell types could be used in future work.

Down regulation of neuroinflammation is an additional mechanism of action by which hMSCs are therapeutically active in the treatment of TBI. Pectin has also demonstrated reduced inflammation when delivered both orally (Lim *et al.*, 2003), and as a capsule surrounding alginate beads containing pancreatic islet cells for transplant to diabetic mice (Hu *et al.*, 2020b, Hu *et al.*, 2020a). Therefore, an organotypic model investigating inflammatory damage could provide insight into possible protection against neuroinflammation. Stucky *et al.* (2015) used rat organotypic hippocampal slices to model inflammation induced by the administration of lipopolysaccharide. They were looking at the possible modulation of neuroinflammation by hMSCs encapsulated in alginate beads. The study showed that encapsulated hMSCs reduced the expression of the pro-inflammatory cytokine TNF-α, and the encapsulated hMSCs themselves increased the expression of prostaglandin E_2 (Stucky *et al.*, 2015). Future work using this model to establish dose responses, pectin grade responses, and the effect of spraying vs syringing the therapy could provide insight into immunomodulatory effects. The use of an organotypic culture could also be used to understand the effect of the mucoadhesive properties of pectin for cell delivery to the brain.

Animal models ultimately demonstrate efficacy and safety prior to human trials; however, it can be difficult to pick apart the mechanisms of action due to a higher level of complexity, which is where *in vitro* models have merit (Morrison *et al.*, 2011). Following further work and characterisation using alternative *in vitro* models described above, progression to animal models of TBI to compare spray delivery of cells in pectin to intravenous delivery could be carried out. Efficacy in immunomodulation has been demonstrated following intravenous delivery of MSCs to rats injured using a weight-drop model (Zhang *et al.*, 2013), therefore, this may be a suitable starting place when considering the design of a comparative animal study.

5.6. Conclusions

The results of the model optimisation demonstrate that model of excitotoxicity and oxidative stress were established, but differences were seen when scaling the model up to larger well sizes, therefore this is an important variable to consider. Concentrations of glutamate and H_2O_2 were established to give a 50% reduction in the metabolic activity of the population of SH-SY5Y cells. The models were used in combination with the four grades of pectin hydrogels. The result of these, in combination with results from Chapter 4, led to the identification of two potentially unsuitable pectin grades which were not taken forward to the co-culture model.

The results of the three co-culture SH-SY5Y damage models showed that the hMSCs in pectin, delivered by any either syringe or spray, did not have efficacy in recovering/protecting cells damaged by glutamate or H_2O_2. This indicates that the secretome from the hMSCs, over the 24-hour test period, was insufficient in promoting survival or proliferation of the SH-SY5Y cells. The use of alternative *in vitro* models, using other injury mechanisms, would further add to the understanding of whether delivery of hMSCs in pectin, by spraying, is a viable treatment option for TBI patients.

Chapter 6 Discussion, future work, and conclusions

6.1. Discussion

MSCs have demonstrated efficacy in aiding repair following TBI in numerous animal models due to the immunomodulatory and regenerative effects of secreted proteins and extracellular vesicles (Chen *et al.*, 2022, Anbari *et al.*, 2014, Zanier *et al.*, 2011), and in human clinical trials (Wang *et al.*, 2013, Wang *et al.*, 2017). Intravenous delivery is often the delivery method of choice for therapeutic cells, however poor migration to the brain has been demonstrated (Harting *et al.*, 2009, Jackson *et al.*, 2010). Intrathecal delivery has been investigated in human trials, however topical delivery to the brain will result in the highest proportion of cells delivered being at the site of injury, and the use of a material to retain cells at the delivery site could enhance this further (Lam *et al.*, 2014).

Hence, to enhance the number of cells delivered, the overarching aim of this work was to evaluate the effect of spraying within pectin solutions on human MSCs to determine whether this may be an appropriate method for topical delivery to the brain. To date topical delivery of therapeutic cells by spraying has been principally investigated for wound care (Wood *et al.*, 2012, Zhang *et al.*, 2022, Pehlivaner Kara and Ekenseair, 2016) and lung delivery (Beneke *et al.*, 2018, Thiebes *et al.*, 2021). These studies have identified some key features of spraying to enhance viability, such as low pressure (Schwartz *et al.*, 2017), large nozzle size (Veazey *et al.*, 2005), and low viscosity (Hendriks *et al.*, 2015).

To aid topical delivery, materials for cell delivery can be used to prevent cells running away from the delivery site and aid delivery to uneven topographies (Moakes *et al.*, 2022). For spraying, a material must have a low enough viscosity at the point of spraying to pass through the spray device used. This could include materials with shear-thinning properties, thermo-responsive gels, or materials which will gel *in situ*. This study aimed to evaluate the use of pectin for cell spraying as it has shown biocompatibility (Hartman, 1943, McCrorie *et al.*, 2020), mucoadhesive properties (Sriamornsak *et al.*, 2010), including to brain tissue (McCrorie *et al.*, 2020), and will form a gel in the presence of Ca^{2+} (Grant, 1973), which is found in the brain (Egelman and Read Montague, 1999). The

DM and DA have been shown to affect the gelation properties (Gawkowska *et al.*, 2018), therefore four different grades were selected to determine whether there was a more suitable grade of pectin for the application in spraying hMSCs. The spray device selected for evaluation was the mucosal atomisation device (MAD) syringe sprayer, due to ease-of-use, with few parts for sterilisation and simple spray set-up.

The thesis hypothesis was that pectin would have suitable mechanical and biocompatibility properties for spraying hMSCs, and that when spayed in pectin, hMSCs would remain viable. Four grades of pectin (CU-701, CU-L, LM-102, and LM-104), each with different degrees of methylation (DM) and amidation (DA), were assessed for mechanical properties such as viscosity and gelation, for cytotoxicity. Next, the pectin grade suitability for spraying hMSCs was assessed by determining the viability, morphology, phenotype, and differential gene expression following spraying in pectin. *In vitro* models of TBI were then established to evaluate the efficacy of the sprayed pectin and hMSCs .

6.1.1. Pectin characterisation

In Chapter 3, an activated charcoal pectin purification method was evaluated based on a method developed for alginate (Bender, 2013), and subsequently used for the CU-701 grade of pectin (Neves *et al.*, 2015). The purification method was evaluated with the four grades of pectin (CU-701, CU-L, LM-102, and LM-104) by BCA protein assay and FTIR; however, the comparison to the work by Neves *et al.* (2015) was limited due to being unable to repeat the evaluation of polyphenol and LPS content. The protein content reduction in each grade of pectin tested was lower than that achieved by Neves *et al.* (2015). The FTIR spectra of the purified pectin assessed in this thesis appeared to have fewer peaks not associated with the bonds within pectin, indicating the removal of non-pectin contaminants.

The gelation properties of the different grades of purified pectin dissolved in different diluents were assessed as the presence of monovalent cations, such as Na^+ found in 1xPBS and NaCl, can prevent the pectin chains cross-linking by Ca^{2+} (Fan *et al.*, 2021). It was found that changing the diluent and adjusting the pH of the pectin solutions to 7.4 did not prevent the gelation of pectin by Ca^{2+}. In the 1% w/v pectin dissolved in 1xPBS at pH 7.4, the pectin gel strength at

each calcium concentration was equal or greater that the 1% w/v pectin in water condition, except with LM-102 which had a slightly reduced gel strength in the 1xPBS condition. Pectin solutions at 1% w/v dissolved 1xPBS pH 7.4 were used for all subsequent experiments in all chapters.

The viscosity of the 1% w/v pectin solutions were assessed at shear rates relevant to the spraying process, calculated based on the MAD sprayer dimensions. The four pectin grades showed Newtonian or slight shear thinning properties, which was greatest for the CU-701 pectin grade. This is consistent with published data using low pectin concentration (around 1% w/v) (Chen *et al.*, 2020a, Peighambardoust *et al.*, 2021). At the calculated maximum shear rate of 7,958 1/s within the MAD, CU-701 pectin (the most viscous) had a viscosity of approximately 12 mPa·s.

A lower DM has been shown to lead to higher Ca^{2+} sensitivity and stronger gel formation (Gawkowska *et al.*, 2018), a trend that was also observed in the results of the amplitude sweep and Young's modulus testing. A higher DA had been reported to stabilise gels formed when the pectin was at a low pH (Fraeye *et al.*, 2010), however the pectin gels tested here were formed at pH 7.4 therefore this may be why the result was not in agreement with published data.

All grades of pectin demonstrated biocompatibility in cytotoxicity testing based on ISO 10993-5 using both the direct and elution method. There was a trend towards a lower metabolic activity (used as the indicator for viability) when the lower concentration of Ca^{2+} (25 mM) was used to cause gelation. McCrorie *et al.* (2020) hypothesised this was due to Ca^{2+} sequestration from the media. 100 mM pectin was selected as this showed the lowest cytotoxicity and as compromise to ensure handling of the pectin gels for use with cells in tissue culture, however it is possible due to the mucoadhesive properties (Sriamornsak *et al.*, 2010) particularly to the brain (McCrorie *et al.*, 2020), this could have been reduced if the pectin was used *in vivo* or on *ex vivo* tissue.

6.1.2. Optimisation of cell spraying in pectin

Chapter 4 aimed to optimise the parameters for cell spraying, and to compare the effect of spraying in pectin on primary human MSCs derived from bone marrow with those sprayed or syringed in 1xPBS. The MAD syringe sprayer was

evaluated, which had been designed for use in nasal drug delivery (Denton, 2022). The patent claimed a small void space within the device which minimised drug loss (Denton, 2022), and this was also true of SH-SY5Y cells when the cell density after spraying was tested as the cell number was approximately equivalent before and after spraying.

It was determined that the concentration at which cells were sprayed did not affect the measured viability using the 3T3 cell line, the SH-SY5Y cell line, or the hMSCs. This result was supported by published data using the U937 human monocyte-like cell line at two concentrations (Beneke *et al.*, 2018) and hMSCs (Thiebes *et al.*, 2021) using five cell concentrations ($1x10^5$ – $4x10^6$ cells/mL) with no differences in viability. The viscosity of the highest viscosity of pectin measured at the shear rate relevant to the MAD was 12 mPa·s, which based on work by Hendriks *et al.* (2015) suggested viability may be as low as 30%. However, their work used an airbrush device which uses pressurised air to generate a spray (Hendriks *et al.*, 2015), whereas here the MAD was used and viability of the hMSCs was not significantly affected when they were sprayed in any of the 1% w/v pectin solutions.

The CU-701 pectin grade was selected for further characterisation based on the result of the flow cytometry surface marker analysis as the only grade not to result in a significant up regulation in CD34, CD11b, CD19, CD45, and HLA-DR, or down regulation in CD90, CD105, or CD73 when compared to the PBS syringe control condition. The differentiation potential was also assessed as hMSCs should be able to differentiate down an adipogenic, osteogenic, and chondrogenic lineage (Dominici *et al.*, 2006). Material stiffness, chemistry, and topography are all known to influence cell differentiation (McMurray *et al.*, 2015), however it was hypothesised that as the cells were only in the CU-701 pectin for 24 hours before being removed and seeded for the differentiation study, this would not be long enough to induce differentiation alone. Using two of the three donors, none of the cell conditions (PBS syringe, PBS spray, CU-701 syringe, and CU-701 spray) induced spontaneous differentiation. All of the conditions for both donors were able to differentiate down the adipogenic lineage, however the cells from donor #33357 did not differentiate down an osteogenic lineage. The cells were allowed 14 days in differentiation media, as

per the manufacturer's protocol, but this was not as long as other studies (Díez *et al.*, 2015) therefore this may be the reason for the lack of differentiation.

The differential gene expression analysis was carried out using the contrasts PBS spray versus PBS syringe, CU-701 spray versus CU-701 syringe, CU-701 syringe versus PBS syringe, and CU-701 spray versus PBS spray. When material (PBS or CU-701) was kept the same, but the delivery method differed (spray versus syringe), there was a relatively small number of differentially expressed genes (0.35% and 0.25% for PBS and CU-701 respectively). However, when the delivery method was kept the same, and the material differed, 12.7% and 14.1% of genes (for syringe and spray conditions respectively) were differentially expressed. The PCA confirmed this, and also highlighted the variation in gene expression caused by the different donors. Both these results agree with published data showing the presence of nanosilicate material results in around 4000 genes being differentially expressed (Carrow *et al.*, 2018), and that variation in the sex of MSC donors affect the expression of key genes implicated in the pathways involved in inflammation (Bianconi *et al.*, 2020). Of the top 20 up regulated genes, a number of those found in both material contrasts (CU-701 versus PBS) were implicated in calcium transport or signalling. This is likely due to the Ca^{2+} used to induce gelation and highlights a possible limitation with using the higher concentrations of Ca^{2+} required to be able to form gels for use in cell culture wells.

6.1.3. In vitro modelling of TBI

The SH-SY5Y human neuroblastoma cell line was selected to establish models of excitotoxicity and oxidative stress, two key features of secondary injury (Kaur and Sharma, 2018). The cell line is human, therefore expresses human versions of genes on which the human secretome from the MSCs may act (Kovalevich and Langford, 2013). Previously published studies using the SH-SY5Y cell line to model both excitotoxicity and oxidative stress have shown variability in cell seeding density, concentration of glutamate or H_2O_2 used, and measured metabolic activity. Glutamate concentrations ranged from 8 mM (Hu *et al.*, 2012) to 100 mM (Lee *et al.*, 2019) therefore, a range of concentrations were used to optimise the model and establish a concentration resulting in a 50% reduction in the metabolic activity (used as an indicator of viability) of the cell

population. 250 mM glutamate was selected as this showed 50% metabolic activity in both 96-well and 24-well plates. This was higher than published literature, however the cell seeding density and duration the glutamate was on the cells for also differed, which could have affected how the cells responded to damage.

The oxidative stress models published are similarly variable, using concentrations of H_2O_2 ranging from 100 µM (Nirmaladevi *et al.*, 2014) to 600 µM (Zhao *et al.*, 2019). Again, a range of H_2O_2 concentrations were tested to establish a concentration resulting in 50% metabolic activity from the cell populations. 25 µM was selected for both the 1-hour and 24-hour models, and this concentration also scaled between the 96-well and the 24-well plates.

The different grades of pectin were then tested on the different models, with CU-L and LM-104 demonstrating a significant reduction in metabolic activity of the cell population in the 1-hour oxidative stress model. These two grades had the lowest DM of the four grades, which may have led to calcium sequestration from the cell culture media as a lower DM correlated with higher Ca^{2+} sensitivity (Gawkowska *et al.*, 2018). Depletion of intracellular calcium in SH-SY5Y cells is linked to increased cell death (Nguyen *et al.*, 2002), therefore if the lower DM pectin grades are sequestering calcium from the media, this may be the cause of the lower metabolic activity.

Based on the results of testing the different pectin grades on the models, LM-102 and CU-701 were taken forward into the co-culture models. For these, hMSCs in 1xPBS, LM-102 pectin, or CU-701 pectin were syringed or sprayed into well inserts to test the effect on the damaged SH-SY5Y cells. There were no significant changes observed, including hMSCs in 1xPBS. hMSCs are known to have a positive effect in recovery in TBI models (Hasan *et al.*, 2017), so based on the results in Chapter 5, the hMSC treatment required further optimisation, or has therapeutic effects via pathways other than the excitotoxicity and oxidative stress modelled in isolation here.

6.1.4. Summary

In summary, the work completed in this thesis has demonstrated that pectin has suitable mechanical and biocompatibility properties for spraying viable hMSCs.

The MAD syringe sprayer can be used to deliver viable hMSCs, with the retention of the MSC surface markers, shown by flow cytometry. The process of spraying appears to have little effect on the gene expression of the hMSCs, highlighting that the use of syringe spray devices may be an appropriate local or topical cell delivery method.

6.2. Future work

Whilst the work completed in this thesis presents a promising start for the use of pectin for the spray delivery of hMSCs, there are some areas where further optimisation and experimentation could be carried out. The spray device used (MAD) showed good viability with the hMSCs, however the spray pattern with pectin could be improved. Additionally, to ensure gelation in the cell culture conditions, additional calcium had to be added to the pectin. The differential gene expression analysis highlighted the effect of this on the gene expression, therefore further optimisation using *ex vivo* tissue to reduce this calcium concentration is required.

The *in vitro* models used in Chapter 5 demonstrated robust responses to oxidative stress and excitotoxicity, however improvements in metabolic activity of the SH-SY5Y cells in response to treatment were not demonstrated using the co-culture models. Additional *in vitro* modelling of alternative pathways, including neuroinflammation, could further elucidate the pathways by which the pectin and hMSC therapy may have a therapeutic effect. MSCs encapsulated in alginate have demonstrated modulation of neuroinflammation in an organotypic model (Stucky *et al.*, 2015). Replicating this model could provide insight into both the mucoadhesion of sprayed hMSCs in pectin and whether MSCs encapsulated in pectin could also reduce neuroinflammation.

Animal models would be used to compare local spray delivery of cells in pectin to other MSC delivery pathways to evaluate whether the spray delivery in pectin may be a viable delivery route of hMSCs for TBI patients. To determine whether spraying of MSCs in pectin offers a superior delivery route to intravenous or intrathecal delivery, a comparison would need to be made in animal models. The use of pectin in the delivery method is to aid the retention at the delivery site, rather than to be used as a scaffold for lesion repair. For this reason, an animal model with large lesions (such as those in penetrating or blast models) would be

less appropriate. The fluid percussion, controlled cortical impact, or the weight drop models all cause diffuse injuries which have injury characteristics similar to those seen in human TBIs resulting from road traffic collisions and falls, which cause the largest proportion of TBIs (Hyder *et al.*, 2007, Dewan *et al.*, 2019). In addition, MSCs delivered to rats injured via these three models have shown improvements in neurological outcomes (Chen *et al.*, 2022, Zanier *et al.*, 2011, Anbari *et al.*, 2014), therefore there is a rationale for testing the sprayed pectin delivery method in one of these models.

Longer term, consideration must be given to the translation of spraying MSCs in pectin as a delivery method to the clinic. For use in the brain, validation of the activated charcoal purification method would be required to confirm consistent removal of LPS. For use as a medical device, LPS levels are required to be <0.06 EU/mL (FDA, 2012). The spray device evaluated here was the MAD spray device, however as discussed, spraying may be optimised by designing a device specifically for the purpose of spraying pectin and hMSCs. The design process should include consultation with clinicians to optimise the spray device based on their requirements. The device must be easily sterilised, made from an inexpensive and easy to manufacture material, generate a suitable spray pattern with the retention of cell viability, and be simple to use in a surgical setting.

MSCs can be obtained from an allogeneic source for therapeutic use, making an "off-the-shelf" therapy more achievable (Oliva *et al.*, 2019). However, shown in this thesis and in published work, donor variability requires consideration to ensure the MSC are maximally efficacious as a treatment (Bianconi *et al.*, 2020). Scalability is another factor to consider when aiming for translation to the clinic. The cell density used throughout this thesis was chosen to compare to 2D cultures, however the cell number required for animal models, then for humans, would be much higher. Although there was no correlation seen between cell concentration and viability when spraying the cells, validation of higher cell concentrations would be required. Prior to any clinical trials involving humans, both efficacy and safety must be demonstrated in animal models. The use of hMSCs have demonstrated safety in humans, however pectin has not been delivered to human brains, therefore thorough safety testing must be demonstrated. MSCs, pectin, and the spray device would need to satisfy

regulatory requirements prior to human use. Processes including pectin purification and sterilisation, and MSCs culture would need to be carried out according to good manufacturing processes. Future work should aim to incorporate these factors into workflows to ensure translation to humans is possible and feasible.

6.3. Conclusions

This thesis has aimed to test the hypothesis that spraying within pectin is suitable for hMSC delivery, with cells retaining their viability and phenotype as hMSCs. This was the first time the MAD sprayer and pectin has been investigated for use in spray delivery of cells. The viability of the hMSCs was retained after spraying, suggesting pectin has suitable mechanical and biocompatibility properties for spray delivery. For the retention of hMSC phenotype, the CU-701 grade of pectin was deemed to be the most suitable and was therefore taken forward into further testing. The differential gene expression analysis has highlighted some key factors for further optimisation and demonstrated that process of spraying has little effect on the gene expression of hMSCs. Models of excitotoxicity and oxidative stress were developed and tested in co-culture. The results indicate that hMSCs may have limited effects on these injury pathways in isolation, however there are many additional models of TBI pathways which could be tested. This thesis has provided some key information to inform further development of spraying in pectin as a method of local hMSC delivery.

References

[ISO], I. O. F. S. 2009. ISO 10993 Biological evaluation of medical devices. *Part 5: Tests for in vitro toxicity.*

[ISO], I. O. F. S. 2012. ISO 10993 Biological evaluation of medical devices. *Part 12: Sample preparation and reference materials.*

ADAMS, H., KOLIAS, A. G. & HUTCHINSON, P. J. 2016. The Role of Surgical Intervention in Traumatic Brain Injury. *Neurosurgery Clinics of North America,* 27**,** 519-528.

ADATIA, K., NEWCOMBE, V. F. J. & MENON, D. K. 2021. Contusion Progression Following Traumatic Brain Injury: A Review of Clinical and Radiological Predictors, and Influence on Outcome. *Neurocritical Care,* 34**,** 312-324.

ADUGNA, D. G., ARAGIE, H., KIBRET, A. A. & BELAY, D. G. 2022. Therapeutic Application of Stem Cells in the Repair of Traumatic Brain Injury. *Stem Cells and Cloning: Advances and Applications,* Volume 15**,** 53-61.

AHMED, E. M. 2015. Hydrogel: Preparation, characterization, and applications: A review. *Journal of Advanced Research,* 6**,** 105-121.

AHN, S., LEE, H., BONASSAR, L. J. & KIM, G. 2012. Cells (MC3T3-E1)-Laden Alginate Scaffolds Fabricated by a Modified Solid-Freeform Fabrication Process Supplemented with an Aerosol Spraying. *Biomacromolecules,* 13**,** 2997-3003.

ANBARI, F., KHALILI, M. A., BAHRAMI, A. R., KHORADMEHR, A., SADEGHIAN, F., FESAHAT, F. & NABI, A. 2014. Intravenous transplantation of bone marrow mesenchymal stem cells promotes neural regeneration after traumatic brain injury. *Neural Regen Res,* 9**,** 919-23.

ANDERSEN, T., AUK-EMBLEM, P. & DORNISH, M. 2015. 3D Cell Culture in Alginate Hydrogels. *Microarrays,* 4**,** 133-161.

ANDRADE, R. D., SKURTYS, O. & OSORIO, F. A. 2012. Atomizing Spray Systems for Application of Edible Coatings. *Comprehensive Reviews in Food Science and Food Safety,* 11**,** 323-337.

ANDREWS, P. J. D., SINCLAIR, H. L., RODRIGUEZ, A., HARRIS, B. A., BATTISON, C. G., RHODES, J. K. J. & MURRAY, G. D. 2015. Hypothermia for Intracranial Hypertension after Traumatic Brain Injury. *New England Journal of Medicine,* 373**,** 2403-2412.

ANDRZEJEWSKA, A., DABROWSKA, S., LUKOMSKA, B. & JANOWSKI, M. 2021. Mesenchymal Stem Cells for Neurological Disorders. *Advanced Science,* 8**,** 2002944.

ARANGO, M., QUINTERO-RONDEROS, P. & CASTIBLANCO, J. 2013. Cell culture and cell analysis. *In:* ANAYA JM, S. Y., ROJAS-VILLARRAGA A (ed.) *Autoimmunity: From Bench to Bedside.* El Rosario University Press.

ARNOLD, E. 2000a. Chapter 2 Molecular Biology and basic techniques. *In:* WALKER, K. W. A. J. (ed.) *Principles and Techniques of Practical Biochemistry.* Cambridge University Press.

ARNOLD, E. 2000b. Chapter 4 Immunochemical techniques. *In:* WALKER, K. W. A. J. (ed.) *Principles and Techniques of Practical Biochemistry.* Cambridge University Press.

ARUN, P., SPADARO, J., JOHN, J., GHARAVI, R. B., BENTLEY, T. B. & NAMBIAR, M. P. 2011. Studies on blast traumatic brain injury using in-vitro model with shock tube. *NeuroReport,* 22.

ATCC. 2023a. *bEnd.3*

CRL-2299™ [Online]. Available: https://www.atcc.org/products/crl-2299#:~:text=CRL%2D2299%E2%84%A2-,bEnd.,Applications%20include%20neuroscience%20research. [Accessed 13/03/2023 2023].

ATCC. 2023b. *SH-SY5Y*

CRL-2266™ [Online]. ATCC: ATCC. Available: https://www.atcc.org/products/crl-2266 [Accessed 12/03/2023 2023].

BABERG, F., GEYH, S., WALDERA-LUPA, D., STEFANSKI, A., ZILKENS, C., HAAS, R., SCHROEDER, T. & STÜHLER, K. 2019. Secretome analysis of human bone marrow derived mesenchymal stromal cells. *Biochimica et Biophysica Acta (BBA) - Proteins and Proteomics,* 1867**,** 434-441.

BAEZ-JURADO, E., HIDALGO-LANUSSA, O., BARRERA-BAILÓN, B., SAHEBKAR, A., ASHRAF, G. M., ECHEVERRIA, V. & BARRETO, G. E. 2019. Secretome of Mesenchymal Stem Cells and Its Potential Protective Effects on Brain Pathologies. *Molecular Neurobiology,* 56**,** 6902-6927.

BAIROCH, A. 2018. The Cellosaurus, a Cell-Line Knowledge Resource. *J Biomol Tech,* 29**,** 25-38.

BAKER, G. L. 1935. Pectin in Nature and Industry. *The Scientific Monthly,* 40**,** 48-54.

BAR-KOCHBA, E., SCIMONE, M. T., ESTRADA, J. B. & FRANCK, C. 2016. Strain and rate-dependent neuronal injury in a 3D in vitro compression model of traumatic brain injury. *Scientific Reports,* 6**,** 30550.

BAR-PELED, M., URBANOWICZ, B. & O'NEILL, M. 2012. The Synthesis and Origin of the Pectic Polysaccharide Rhamnogalacturonan II – Insights from Nucleotide Sugar Formation and Diversity. *Frontiers in Plant Science,* 3.

BARBOSA, D. J., CAPELA, J. P., DE LOURDES BASTOS, M. & CARVALHO, F. 2015. In vitro models for neurotoxicology research. *Toxicology Research,* 4**,** 801-842.

BELKHEIRI, A., FOROUHAR, A., URSU, A. V., DUBESSAY, P., PIERRE, G., DELATTRE, C., DJELVEH, G., ABDELKAFI, S., HAMDAMI, N. & MICHAUD, P. 2021. Extraction, Characterization, and Applications of Pectins from Plant By-Products. *Applied Sciences,* 11**,** 6596.

BENDER, J. C. M. E. V., PIETER SEBASTIAAN. 2013. *Method for removing impurities from biopolymer material*. United States patent application 12/999,565.

BENEKE, V., KÜSTER, F., NEEHUS, A.-L., HESSE, C., LOPEZ-RODRIGUEZ, E., HAAKE, K., RAFIEI HASHTCHIN, A., SCHOTT, J. W., WALTER, D., BRAUN, A., WOLKERS, W. F., ACKERMANN, M. & LACHMANN, N. 2018. An immune cell spray (ICS) formulation allows for the delivery of functional monocyte/macrophages. *Scientific Reports,* 8.

BERGER PELLETIER, E., ÉMOND, M., LAUZIER, F., SAVARD, M. & TURGEON, A. F. 2014. Hyperosmolar Therapy in Severe Traumatic Brain Injury: A Survey of Emergency Physicians from a Large Canadian Province. *PLoS ONE,* 9**,** e95778.

BERROUT, J., JIN, M. & O'NEIL, R. G. 2012. Critical role of TRPP2 and TRPC1 channels in stretch-induced injury of blood–brain barrier endothelial cells. *Brain Research,* 1436**,** 1-12.

BHAT, S., VISWANATHAN, P., CHANDANALA, S., PRASANNA, S. J. & SEETHARAM, R. N. 2021. Expansion and characterization of bone marrow derived human mesenchymal stromal cells in serum-free conditions. *Scientific Reports,* 11.

BIANCONI, E., CASADEI, R., FRABETTI, F., VENTURA, C., FACCHIN, F. & CANAIDER, S. 2020. Sex-Specific Transcriptome Differences in Human Adipose Mesenchymal Stem Cells. *Genes,* 11**,** 909.

BIRCH, N. P., BARNEY, L. E., PANDRES, E., PEYTON, S. R. & SCHIFFMAN, J. D. 2015. Thermal-Responsive Behavior of a Cell Compatible Chitosan/Pectin Hydrogel. *Biomacromolecules,* 16**,** 1837-1843.

BLUMENBERG, M. 2019. Introductory Chapter: Transcriptome Analysis. IntechOpen.

BOLTZE, J. 2015. The dark side of the force – constraints and complications of cell therapies for stroke. 6.

BRADL, M. & LASSMANN, H. 2010. Oligodendrocytes: biology and pathology. *Acta Neuropathologica,* 119**,** 37-53.

BRITANNICA, E. 2022. *Young's modulus* [Online]. Britannica: Encyclopedia Britannica. Available: https://www.britannica.com/science/Youngs-modulus [Accessed 14 December 2022].

BRYDEN, D. W., TILGHMAN, J. I. & HINDS, S. R. 2019. Blast-Related Traumatic Brain Injury: Current Concepts and Research Considerations. *Journal of Experimental Neuroscience,* 13**,** 117906951987221.

BULLOCK, M. R., CHESNUT, R., GHAJAR, J., GORDON, D., HARTL, R., NEWELL, D. W., SERVADEI, F., WALTERS, B. C. & WILBERGER, J. E. 2006. Surgical Management of Acute Subdural Hematomas. *Neurosurgery,* 58**,** S2-16-S2-24.

CAMPOS-PIRES, R., KOZIAKOVA, M., YONIS, A., PAU, A., MACDONALD, W., HARRIS, K., EDGE, C. J., FRANKS, N. P., MAHONEY, P. F. & DICKINSON, R. 2018. Xenon Protects against Blast-Induced Traumatic Brain Injury in an in Vitro Model. *Journal of Neurotrauma,* 35**,** 1037-1044.

CANFIELD, S. G., STEBBINS, M. J., MORALES, B. S., ASAI, S. W., VATINE, G. D., SVENDSEN, C. N., PALECEK, S. P. & SHUSTA, E. V. 2017. An isogenic blood-brain barrier model comprising brain endothelial cells, astrocytes, and neurons derived from human induced pluripotent stem cells. *Journal of Neurochemistry,* 140**,** 874-888.

CAO, L., LU, W., MATA, A., NISHINARI, K. & FANG, Y. 2020. Egg-box model-based gelation of alginate and pectin: A review. *Carbohydrate Polymers,* 242**,** 116389.

CAO, N., CHEN, X. & SCHREYER, D. 2012. Influence of calcium ions on cell survival and proliferation in the context of an alginate hydrogel. *International Scholarly Research Notices,* 2012.

CARROW, J. K., CROSS, L. M., REESE, R. W., JAISWAL, M. K., GREGORY, C. A., KAUNAS, R., SINGH, I. & GAHARWAR, A. K. 2018. Widespread changes in transcriptome profile of human mesenchymal stem cells induced by two-dimensional nanosilicates. *Proceedings of the National Academy of Sciences,* 115**,** E3905-E3913.

CELORRIO, M., SHUMILOV, K., PAYNE, C., VADIVELU, S. & FRIESS, S. H. 2022. Acute minocycline administration reduces brain injury and improves long-term functional outcomes after delayed hypoxemia following traumatic brain injury. *Acta Neuropathologica Communications,* 10.

CHARTOFF, E. H., DAMEZ-WERNO, D., SONNTAG, K. C., HASSINGER, L., KAUFMANN, D. E., PETERSON, J., MCPHIE, D., CATALDO, A. M. & COHEN, B. M. 2011. Detection of Intranasally Delivered Bone Marrow-Derived Mesenchymal Stromal Cells in the Lesioned Mouse Brain: A Cautionary Report. *Stem Cells International,* 2011**,** 1-12.

CHEN, C., HU, N., WANG, J., XU, L., JIA, X.-L., FAN, X., SHI, J.-X., CHEN, F., TU, Y., WANG, Y.-W. & LI, X.-H. 2022. Umbilical cord mesenchymal stem cells promote neurological repair after traumatic brain injury through regulating Treg/Th17 balance. *Brain Research,* 1775**,** 147711.

CHEN, Q., XUE, G., NI, Q., WANG, Y., GAO, Q., ZHANG, Y. & XU, G. 2020a. Physicochemical and rheological characterization of pectin‐rich polysaccharides from Gardenia jasminoides J. Ellis flower. *Food Science & Nutrition,* 8**,** 3335-3345.

CHEN, W.-T., KUO, Y.-Y., LIN, G.-B., LU, C.-H., HSU, H.-P., SUN, Y.-K. & CHAO, C.-Y. 2020b. Thermal cycling protects SH-SY5Y cells against hydrogen peroxide and β-amyloid-induced cell injury through stress response mechanisms involving Akt pathway. *PLOS ONE,* 15**,** e0240022.

CHENG, N.-C., WANG, S. & YOUNG, T.-H. 2012. The influence of spheroid formation of human adipose-derived stem cells on chitosan films on stemness and differentiation capabilities. *Biomaterials,* 33**,** 1748-1758.

CLAUDE H. HILLS, C. L. O., RUDOLPH SPEISER 1945. Determination of Methyl Ester Content of Pectin. *industrial and Engineering Chemistry,* 17**,** 507-510.

COLLINS, M. N., ZAMBONI, F., SERAFIN, A., ESCOBAR, A., STEPANIAN, R., CULEBRAS, M., REIS, R. L. & OLIVEIRA, J. M. 2022. Emerging scaffold- and cellular-based strategies for brain tissue regeneration and imaging. *In vitro models,* 1**,** 129-150.

COLONNA, M. B., O. 2017. Microglia Function in the Central Nervous System During Health and Neurodegeneration. *Annu Rev Immunol,* 35**,** 441-468.

COMMISSION, T. E. 2012. Commission Regulation (EU) No 231/2012. *In:* COMMISSION, T. E. (ed.). European Union.

CONNOLLY, S., NEWPORT, D. & MCGOURTY, K. 2021. Cell specific variation in viability in suspension in in vitro Poiseuille flow conditions. *Scientific Reports,* 11.

CORTÉS, D., CARBALLO-MOLINA, O. A., CASTELLANOS-MONTIEL, M. J. & VELASCO, I. 2017. The Non-Survival Effects of Glial Cell Line-Derived Neurotrophic Factor on Neural Cells. *Front Mol Neurosci,* 10**,** 258.

COX, C. S. 2023. A Clinical Trial to Determine the Safety and Efficacy of Hope Biosciences Autologous Mesenchymal Stem Cell Therapy for the Treatment of Traumatic Brain Injury and Hypoxic-Ischemic Encephalopathy. https://ClinicalTrials.gov/show/NCT04063215.

CRUPI, R., CORDARO, M., CUZZOCREA, S. & IMPELLIZZERI, D. 2020. Management of Traumatic Brain Injury: From Present to Future. *Antioxidants,* 9**,** 297.

D. MAY, C. 1990. Industrial pectins: Sources, production and applications. *Carbohydrate Polymers,* 12**,** 79-99.

DANEMAN, R. P., ALEXANDRE 2015. The Blood–Brain Barrier. *Cold Spring Harbor Perspectives in Biology,* 7**,** a020412.

DANIELS, M. P. H., BERND 1974. THE ULTRASTRUCTURE OF NEUROBLASTOMA GLIOMA SOMATIC CELL HYBRIDS. *Journal of Cell Biology,* 63**,** 691-699.

DANIELYAN, L., SCHÄFER, R., VON AMELN-MAYERHOFER, A., BUADZE, M., GEISLER, J., KLOPFER, T., BURKHARDT, U., PROKSCH, B., VERLEYSDONK, S. & AYTURAN, M. 2009. Intranasal delivery of cells to the brain. 88**,** 315-324.

DARNELL, M., GU, L. & MOONEY, D. 2018. RNA-seq reveals diverse effects of substrate stiffness on mesenchymal stem cells. *Biomaterials,* 181**,** 182-188.

DASH, H. H. & CHAVALI, S. 2018. Management of traumatic brain injury patients. *Korean Journal of Anesthesiology,* 71**,** 12.

DE WINDT, T. S., VONK, L. A., BUSKERMOLEN, J. K., VISSER, J., KARPERIEN, M., BLEYS, R. L. A. W., DHERT, W. J. A. & SARIS, D. B. F. 2015. Arthroscopic airbrush assisted cell implantation for cartilage repair in the knee: a controlled laboratory and human cadaveric study. *Osteoarthritis and Cartilage,* 23**,** 143-150.

DENTON, M. T. C., PERRY W; CHRISTENSEN, MARK A; WOLFE, TIMOTHY R; J. MICHAEL BROWN. 2022. *Atomizer for Nasal Therapy*. United States patent application 17 / 666,099.

DEWAN, M. C., RATTANI, A., GUPTA, S., BATICULON, R. E., HUNG, Y.-C., PUNCHAK, M., AGRAWAL, A., ADELEYE, A. O., SHRIME, M. G., RUBIANO, A. M., ROSENFELD, J. V. & PARK, K. B. 2019. Estimating the global incidence of traumatic brain injury. *Journal of Neurosurgery,* 130**,** 1080-1097.

DI GASPERO, G., RADOVIC, S., DE LUCA, E., SPADOTTO, A., MAGRIS, G., FALGINELLA, L., CATTONARO, F. & MARRONI, F. 2022. Evaluation of sensitivity and specificity in RNA-Seq-based detection of grapevine viral pathogens. *Journal of Virological Methods,* 300**,** 114383.

DIAZ, J. V., ANTHON, G. E. & BARRETT, D. M. 2007. Nonenzymatic Degradation of Citrus Pectin and Pectate during Prolonged Heating: Effects of pH, Temperature, and Degree of Methyl Esterification. *Journal of Agricultural and Food Chemistry,* 55**,** 5131-5136.

DÍEZ, J. M., BAUMAN, E., GAJARDO, R. & JORQUERA, J. I. 2015. Culture of human mesenchymal stem cells using a candidate pharmaceutical grade xeno-free cell culture supplement derived from industrial human plasma pools. *Stem Cell Research & Therapy,* 6.

DISCHER, D. E. 2005. Tissue Cells Feel and Respond to the Stiffness of Their Substrate. *Science,* 310**,** 1139-1143.

DOBIN, A., DAVIS, C. A., SCHLESINGER, F., DRENKOW, J., ZALESKI, C., JHA, S., BATUT, P., CHAISSON, M. & GINGERAS, T. R. 2013. STAR: ultrafast universal RNA-seq aligner. *Bioinformatics,* 29**,** 15-21.

DOHERTY, J. & JACKSON, A. A. 1992. The effect of dietary pectin on rapid catch-up weight gain and urea kinetics in children recovering from severe undernutrition. *Acta Paediatrica,* 81**,** 514-517.

DOMINICI, M., LE BLANC, K., MUELLER, I., SLAPER-CORTENBACH, I., MARINI, F., KRAUSE, D., DEANS, R., KEATING, A., PROCKOP, D. & HORWITZ, E. 2006. Minimal criteria for defining multipotent mesenchymal stromal cells. The International Society for Cellular Therapy position statement. *Cytotherapy,* 8**,** 315-7.

DOSS, B. L., PAN, M., GUPTA, M., GRENCI, G., MÈGE, R.-M., LIM, C. T., SHEETZ, M. P., VOITURIEZ, R. & LADOUX, B. 2020. Cell response to substrate rigidity is regulated by active and passive cytoskeletal stress. *Proceedings of the National Academy of Sciences,* 117**,** 12817-12825.

DRANCA, F. & OROIAN, M. 2018. Extraction, purification and characterization of pectin from alternative sources with potential technological applications. *Food Research International,* 113**,** 327-350.

DUMONT, J., EUWART, D., MEI, B., ESTES, S. & KSHIRSAGAR, R. 2016. Human cell lines for biopharmaceutical manufacturing: history, status, and future perspectives. *Critical Reviews in Biotechnology,* 36**,** 1110-1122.

DUVAL, K., GROVER, H., HAN, L.-H., MOU, Y., PEGORARO, A. F., FREDBERG, J. & CHEN, Z. 2017. Modeling Physiological Events in 2D vs. 3D Cell Culture. *Physiology,* 32**,** 266-277.

EAKIN, K., LI, Y., CHIANG, Y.-H., HOFFER, B. J., ROSENHEIM, H., GREIG, N. H. & MILLER, J. P. 2013. Exendin-4 Ameliorates Traumatic Brain Injury-Induced Cognitive Impairment in Rats. *PLoS ONE,* 8**,** e82016.

EGELMAN, D. M. & READ MONTAGUE, P. 1999. Calcium Dynamics in the Extracellular Space of Mammalian Neural Tissue. *Biophysical Journal,* 76**,** 1856-1867.

EL SAYED, T., MOTA, A., FRATERNALI, F. & ORTIZ, M. 2008. Biomechanics of traumatic brain injury. *Computer Methods in Applied Mechanics and Engineering,* 197**,** 4692-4701.

ELEUTERI, S. & FIERABRACCI, A. 2019. Insights into the Secretome of Mesenchymal Stem Cells and Its Potential Applications. *International Journal of Molecular Sciences,* 20**,** 4597.

ENGLISH, K. 2013. Mechanisms of mesenchymal stromal cell immunomodulation. *Immunology & Cell Biology,* 91**,** 19-26.

EUROPEAN MEDICINES AGENCY, E. 2018. *Alofisel* [Online]. Available: https://www.ema.europa.eu/en/medicines/human/EPAR/alofisel [Accessed 24/01/2023 2023].

EVANGELISTA, M. B., HSIONG, S. X., FERNANDES, R., SAMPAIO, P., KONG, H.-J., BARRIAS, C. C., SALEMA, R., BARBOSA, M. A., MOONEY, D. J. & GRANJA, P. L. 2007. Upregulation of bone cell differentiation through immobilization within a synthetic extracellular matrix. *Biomaterials,* 28**,** 3644-3655.

FALANGA, V., IWAMOTO, S., CHARTIER, M., YUFIT, T., BUTMARC, J., KOUTTAB, N., SHRAYER, D. & CARSON, P. 2007. Autologous Bone

Marrow–Derived Cultured Mesenchymal Stem Cells Delivered in a Fibrin Spray Accelerate Healing in Murine and Human Cutaneous Wounds. *Tissue Engineering,* 13**,** 1299-1312.

FAN, S., FANG, F., LEI, A., ZHENG, J. & ZHANG, F. 2021. Effects of Salts on Structural, Physicochemical and Rheological Properties of Low-Methoxyl Pectin/Sodium Caseinate Complex. *Foods,* 10**,** 2009.

FDA, U. 2012. Guidance for Industry Pyrogen and Endotoxins Testing: Questions and Answers. *In:* FDA, U. (ed.). https://www.fda.gov/media/83477/download: FDA.

FEENEY, D. M., BOYESON, M. G., LINN, R. T., MURRAY, H. M. & DAIL, W. G. 1981. Responses to cortical injury: I. Methodology and local effects of contusions in the rat. *Brain Research,* 211**,** 67-77.

FENG, C., LUO, T., ZHANG, S., LIU, K., ZHANG, Y., LUO, Y. & GE, P. 2016. Lycopene protects human SH-SY5Y neuroblastoma cells against hydrogen peroxide-induced death via inhibition of oxidative stress and mitochondria-associated apoptotic pathways. *Molecular Medicine Reports,* 13**,** 4205-4214.

FERNANDO, R. H., XING, L. L. & GLASS, J. E. 2000. Rheology parameters controlling spray atomization and roll misting behavior of waterborne coatings. *Progress in Organic Coatings,* 40**,** 35-38.

FERREIRA, J. R., TEIXEIRA, G. Q., SANTOS, S. G., BARBOSA, M. A., ALMEIDA-PORADA, G. & GONÇALVES, R. M. 2018. Mesenchymal Stromal Cell Secretome: Influencing Therapeutic Potential by Cellular Pre-conditioning. *Frontiers in Immunology,* 9.

FESHARAKI-ZADEH, A. 2022. Oxidative Stress in Traumatic Brain Injury. *International Journal of Molecular Sciences,* 23**,** 13000.

FINKEL, T., MENAZZA, S., HOLMSTRÖM, K. M., PARKS, R. J., LIU, J., SUN, J., LIU, J., PAN, X. & MURPHY, E. 2015. The Ins and Outs of Mitochondrial Calcium. *Circulation Research,* 116**,** 1810-1819.

FLIERL, M. A., STAHEL, P. F., BEAUCHAMP, K. M., MORGAN, S. J., SMITH, W. R. & SHOHAMI, E. 2009. Mouse closed head injury model induced by a weight-drop device. *Nature Protocols,* 4**,** 1328-1337.

FON, E. A., EDWARDS, R. H. & . 2001. Molecular mechanisms of neurotransmitter release. *Muscle & Nerve,* 24**,** 581-601.

FONG, R., KONAKONDLA, S., SCHIRMER, C. M. & LACROIX, M. 2017. Surgical Interventions for Severe Traumatic Brain Injury. 1.

FONTAINE, M. J., SHIH, H., SCHÄFER, R. & PITTENGER, M. F. 2016. Unraveling the Mesenchymal Stromal Cells' Paracrine Immunomodulatory Effects. *Transfusion Medicine Reviews,* 30**,** 37-43.

FRAEYE, I., DUVETTER, T., DOUNGLA, E., VAN LOEY, A. & HENDRICKX, M. 2010. Fine-tuning the properties of pectin–calcium gels by control of pectin fine structure, gel composition and environmental conditions. *Trends in Food Science & Technology,* 21**,** 219-228.

FRATI, A., CERRETANI, D., FIASCHI, A., FRATI, P., GATTO, V., LA RUSSA, R., PESCE, A., PINCHI, E., SANTURRO, A., FRASCHETTI, F. & FINESCHI, V. 2017. Diffuse Axonal Injury and Oxidative Stress: A Comprehensive Review. *International Journal of Molecular Sciences,* 18**,** 2600.

FREMY, E. 1840. Untersuchungen über das Pectin und die Pectinsäure. *Annalen der Chemie und Pharmacie,* 35**,** 318-342.

GALGANO, M., TOSHKEZI, G., QIU, X., RUSSELL, T., CHIN, L. & ZHAO, L. R. 2017. Traumatic Brain Injury: Current Treatment Strategies and Future Endeavors. *Cell Transplant,* 26**,** 1118-1130.

GASPAROTTO, V. P. O., LANDIM-ALVARENGA, F. C., OLIVEIRA, A. L. R., SIMÕES, G. F., LIMA-NETO, J. F., BARRAVIERA, B. & FERREIRA, R. S. 2014. A new fibrin sealant as a three-dimensional scaffold candidate for mesenchymal stem cells. *Stem Cell Research & Therapy,* 5**,** 78.

GAWKOWSKA, D., CYBULSKA, J. & ZDUNEK, A. 2018. Structure-Related Gelling of Pectins and Linking with Other Natural Compounds: A Review. *Polymers,* 10**,** 762.

GE, J., GUO, L., WANG, S., ZHANG, Y., CAI, T., ZHAO, R. C. H. & WU, Y. 2014. The Size of Mesenchymal Stem Cells is a Significant Cause of Vascular Obstructions and Stroke. *Stem Cell Reviews and Reports,* 10**,** 295-303.

GENTILINI, R., MUNARIN, F. & BLOISE, N. 2018. Polysaccharide-based hydrogels with tunable composition as 3D cell culture systems. *International Journal of Artificial Organs,* 41**,** 213-222.

GHALAENOVI, H., FATTAHI, A., KOOHPAYEHZADEH, J., KHODADOST, M., FATAHI, N., TAHERI, M., AZIMI, A., ROHANI, S. & RAHATLOU, H. 2018. The effects of amantadine on traumatic brain injury outcome: a double-blind, randomized, controlled, clinical trial. *Brain Injury,* 32**,** 1050-1055.

GONZÁLEZ-GONZÁLEZ, A., GARCÍA-SÁNCHEZ, D., DOTTA, M., RODRÍGUEZ-REY, J. C. & PÉREZ-CAMPO, F. M. 2020. Mesenchymal stem cells secretome: The cornerstone of cell-free regenerative medicine. *World Journal of Stem Cells,* 12**,** 1529-1552.

GOSHI, N., MORGAN, R. K., LEIN, P. J. & SEKER, E. 2020. A primary neural cell culture model to study neuron, astrocyte, and microglia interactions in neuroinflammation. *Journal of Neuroinflammation,* 17.

GRANT, G. T., MORRIS, EDWIN R., REES, DAVID A., SMITH, PETER J.C. AND THOM, DAVID 1973. Biological interactions between polysaccharides and divalent cations: The egg-box model. *FEBS Letters*.

GRAPHPAD, P. 2023a. *Options for multiple t tests* [Online]. Available: https://www.graphpad.com/guides/prism/latest/statistics/stat_options_for_multiple_t_tests.htm [Accessed 28/02/2023 2023].

GRAPHPAD, P. 2023b. *Tukey and Dunnett method* [Online]. Available: https://www.graphpad.com/guides/prism/latest/statistics/stat_the_methods_of_tukey_and_dunne.htm [Accessed 28/02/2023 2023].

GREVE, M. W., ZINK, B. J. & . 2009. Pathophysiology of traumatic brain injury. *Mount Sinai Journal of Medicine: A Journal of Translational and Personalized Medicine,* 76**,** 97-104.

GUAN, J., ZHU, Z., ZHAO, R. C., XIAO, Z., WU, C., HAN, Q., CHEN, L., TONG, W., ZHANG, J., HAN, Q., GAO, J., FENG, M., BAO, X., DAI, J. & WANG, R. 2013. Transplantation of human mesenchymal stem cells loaded on collagen scaffolds for the treatment of traumatic brain injury in rats. *Biomaterials,* 34**,** 5937-5946.

GUILLOTIN, S. E., BAKX, E. J., BOULENGUER, P., SCHOLS, H. A. & VORAGEN, A. G. J. 2007. Determination of the degree of substitution, degree of amidation and degree of blockiness of commercial pectins by using capillary electrophoresis. *Food Hydrocolloids,* 21**,** 444-451.

HAMILTON, K. A. & SANTHAKUMAR, V. 2020. Current ex Vivo and in Vitro Approaches to Uncovering Mechanisms of Neurological Dysfunction after Traumatic Brain Injury. *Curr Opin Biomed Eng,* 14**,** 18-24.

HAN, Y., LI, X., ZHANG, Y., HAN, Y., CHANG, F. & DING, J. 2019. Mesenchymal Stem Cells for Regenerative Medicine. *Cells,* 8**,** 886.

HAN, Y., YANG, J., FANG, J., ZHOU, Y., CANDI, E., WANG, J., HUA, D., SHAO, C. & SHI, Y. 2022. The secretion profile of mesenchymal stem cells and potential applications in treating human diseases. *Signal Transduction and Targeted Therapy,* 7.

HANNA, M. E. & PFISTER, B. J. 2023. Advancements in in vitro models of traumatic brain injury. *Current Opinion in Biomedical Engineering,* 25**,** 100430.

HANSFORD, L. M. & MARSHALL, G. M. 2005. Glial cell line-derived neurotrophic factor (GDNF) family ligands reduce the sensitivity of neuroblastoma cells to pharmacologically induced cell death, growth arrest and differentiation. *Neuroscience Letters,* 389**,** 77-82.

HARKIN, D. G., DAWSON, R. A. & UPTON, Z. 2006. Optimized delivery of skin keratinocytes by aerosolization and suspension in fibrin tissue adhesive. *Wound Repair Regen,* 14**,** 354-63.

HARTING, M. T., JIMENEZ, F., XUE, H., FISCHER, U. M., BAUMGARTNER, J., DASH, P. K. & COX, C. S. 2009. Intravenous mesenchymal stem cell therapy for traumatic brain injury. *Journal of neurosurgery,* 110**,** 1189-1197.

HARTMAN, F. W. 1951. Tissue changes following the use of plasma substitutes. *Archives of Surgery,* 63.

HARTMAN, F. W., SCHELLING, V., HARKINS, H. & BRUSCH, B. 1941. Pectin Solution As a Blood Substitute. *Annals of Surgery,* 114**,** 212-225.

HARTMAN, F. W., SCHELLING, V., BRUSH, B., & WARREN, K. W. 1943. The relative value of pectin solution in shock. *Journal of the American Medical Association,* 121.

HARVARD. 2023. BioNumbers. Available: https://bionumbers.hms.harvard.edu/files/Sizes%20of%20various%20cells.pdf [Accessed 27/02/23 2023].

HASAN, A., DEEB, G., RAHAL, R., ATWI, K., MONDELLO, S., MAREI MADY, H. E. S., GALI, A. & SLEIMAN, E. 2017. Mesenchymal Stem Cells in the Treatment of Traumatic Brain Injury. *Frontiers in Neurology,* 8.

HAUS, D. L., LÓPEZ-VELÁZQUEZ, L., GOLD, E. M., CUNNINGHAM, K. M., PEREZ, H., ANDERSON, A. J. & CUMMINGS, B. J. 2016. Transplantation of human neural stem cells restores cognition in an immunodeficient rodent model of traumatic brain injury. *Experimental Neurology,* 281**,** 1-16.

HAUSMANN, M., LEUCHT, K., PLONER, C., KIESSLING, S., VILLUNGER, A., BECKER, H., HOFMANN, C., FALK, W., KREBS, M., KELLERMEIER, S., FRIED, M., SCHÖLMERICH, J.,

OBERMEIER, F. & ROGLER, G. 2011. BCL-2 Modifying Factor (BMF) Is a Central Regulator of Anoikis in Human Intestinal Epithelial Cells. *Journal of Biological Chemistry,* 286**,** 26533-26540.

HAYMAN, E., KALEDJIAN, K., GERZANICH, V. & SIMARD, J. M. 2018. Development of a Rodent Model of Closed Head Injury: The Maryland Model. Springer New York.

HENDRIKS, J., WILLEM VISSER, C., HENKE, S., LEIJTEN, J., SARIS, D. B. F., SUN, C., LOHSE, D. & KARPERIEN, M. 2015. Optimizing cell viability in droplet-based cell deposition. *Scientific Reports,* 5**,** 11304.

HERTZEL SALMAN, MICHAEL BERGMAN, MEIR DJALDETTI, JEROME ORLIN & HANNA BESSLER 2008. Citrus pectin affects cytokine production by human peripheral blood mononuclear cells. *Biomedicine & Pharmacotherapy,* 62**,** 579-582.

HIPP, J. A., ANTHONY 2008. Sources of Stem Cells for Regenerative Medicine. *Stem Cell Reviews,* 4**,** 3-11.

HRDLICKOVA, R., TOLOUE, M. & TIAN, B. 2017. <scp>RNA</scp> ‐Seq methods for transcriptome analysis. *WIREs RNA,* 8**,** e1364.

HU, S., KUWABARA, R., BEUKEMA, M., FERRARI, M., DE HAAN, B. J., WALVOORT, M. T. C., DE VOS, P. & SMINK, A. M. 2020a. Low methyl-esterified pectin protects pancreatic β-cells against diabetes-induced oxidative and inflammatory stress via galectin-3. *Carbohydrate Polymers,* 249**,** 116863.

HU, S., KUWABARA, R., NAVARRO CHICA, C. E., SMINK, A. M., KOSTER, T., MEDINA, J. D., DE HAAN, B. J., BEUKEMA, M., LAKEY, J. R. T., GARCÍA, A. J. & DE VOS, P. 2020b. Toll-like receptor 2-modulating pectin-polymers in alginate-based microcapsules attenuate immune responses and support islet-xenograft survival. *Biomaterials***,** 120460.

HU, Y., LI, J., LIU, P., CHEN, X., GUO, D.-H., LI, Q.-S. & RAHMAN, K. 2012. Protection of SH-SY5Y Neuronal Cells from Glutamate-Induced Apoptosis by 3,6′ -Disinapoyl Sucrose, a Bioactive Compound Isolated from Radix Polygala. *Journal of Biomedicine and Biotechnology,* 2012**,** 1-5.

HUMPEL, C. 2015. Organotypic brain slice cultures: A review. *Neuroscience,* 305**,** 86-98.

HYDER, A. A., WUNDERLICH, C. A., PUVANACHANDRA, P., GURURAJ, G. & KOBUSINGYE, O. C. 2007. The impact of traumatic brain injuries: A global perspective. *NeuroRehabilitation,* 22**,** 341-353.

INVITROGEN. 2023. *Product information sheet - CyQUANT™ LDH Cytotoxicity Assay Kit* [Online]. ThermoFisher Scientific. Available: https://www.thermofisher.com/document-connect/document-connect.html?url=https://assets.thermofisher.com/TFS-Assets%2FLSG%2Fmanuals%2FMAN0018500_CyQUANT-LDH-Cytotoxicity-Assay-Kit_PI.pdf [Accessed 14/03.2023 2023].

JACKSON, J. S., GOLDING, J. P., CHAPON, C., JONES, W. A. & BHAKOO, K. K. 2010. Homing of stem cells to sites of inflammatory brain injury after intracerebral and intravenous administration: a longitudinal imaging study. *Stem Cell Research & Therapy,* 1**,** 17.

JAIN, S. & IVERSON, L. M. 2020. Glasgow Coma Scale. *StatPearls.* Treasure Island (FL).

JÄKEL, S., DIMOU, L. & . 2017. Glial Cells and Their Function in the Adult Brain: A Journey through the History of Their Ablation. *Frontiers in Cellular Neuroscience,* 11.

JALLOH, I., CARPENTER, K. L. H., HELMY, A., CARPENTER, T. A., MENON, D. K. & HUTCHINSON, P. J. 2015. Glucose metabolism following human traumatic brain injury: methods of assessment and pathophysiological findings. *Metabolic Brain Disease,* 30**,** 615-632.

JANG, S. E., QIU, L., CHAN, L. L., TAN, E. K. & ZENG, L. 2020. Current Status of Stem Cell-Derived Therapies for Parkinson's Disease: From Cell Assessment and Imaging Modalities to Clinical Trials. *Front Neurosci,* 14**,** 558532.

JANMEY, P. A., FLETCHER, D. A. & REINHART-KING, C. A. 2019. Stiffness Sensing by Cells. *Physiological Reviews,* 100**,** 695-724.

JAVED, K. R. V., LUI F. 2022. Neuroanatomy, Cerebral Cortex. StatPearls [Internet]: Treasure Island (FL): StatPearls Publishing.

JHA, K., PENTECOST, M., LENIN, R., KLAIC, L., ELSHAER, S., GENTRY, J., RUSSELL, J., BELAND, A., REINER, A., JOTTERAND, V., SOHL, N. & GANGARAJU, R. 2018. Concentrated Conditioned Media from Adipose Tissue Derived Mesenchymal Stem Cells Mitigates Visual Deficits and Retinal Inflammation Following Mild Traumatic Brain Injury. *International Journal of Molecular Sciences,* 19**,** 2016.

JOSEPH, I. 1995. Indomethacin sustained release from alginate-gelatin or pectin-gelatin coacervates. *International Journal of Pharmaceutics,* 126**,** 161-168.

JOVIC, D., YU, Y., WANG, D., WANG, K., LI, H., XU, F., LIU, C., LIU, J. & LUO, Y. 2022. A Brief Overview of Global Trends in MSC-Based Cell Therapy. *Stem Cell Reviews and Reports,* 18**,** 1525-1545.

KABADI, S. V., HILTON, G. D., STOICA, B. A., ZAPPLE, D. N. & FADEN, A. I. 2010. Fluid-percussion–induced traumatic brain injury model in rats. *Nature Protocols,* 5**,** 1552-1563.

KABU, S., GAO, Y., KWON, B. K. & LABHASETWAR, V. 2015. Drug delivery, cell-based therapies, and tissue engineering approaches for spinal cord injury. 219**,** 141-154.

KARAGYAUR, M., DZHAUARI, S., BASALOVA, N., ALEKSANDRUSHKINA, N., SAGARADZE, G., DANILOVA, N., MALKOV, P., POPOV, V., SKRYABINA, M., EFIMENKO, A. & TKACHUK, V. 2021. MSC Secretome as a Promising Tool for Neuroprotection and Neuroregeneration in a Model of Intracerebral Hemorrhage. *Pharmaceutics,* 13**,** 2031.

KARDIA, E., CH'NG, E. S. & YAHAYA, B. H. 2018. Aerosol-based airway epithelial cell delivery improves airway regeneration and repair. *Journal of Tissue Engineering and Regenerative Medicine,* 12**,** e995-e1007.

KARDIA, E., YUSOFF, N. M., ZAKARIA, Z. & YAHAYA, B. 2014. Aerosol-Based Delivery of Fibroblast Cells for Treatment of Lung Diseases. *Journal of Aerosol Medicine and Pulmonary Drug Delivery,* 27**,** 30-34.

KAUR, G. D., JANNETTE M. 2012. Cell lines. *Spermatogenesis,* 2**,** 1-5.

KAUR, P. & SHARMA, S. 2018. Recent Advances in Pathophysiology of Traumatic Brain Injury. *Current Neuropharmacology,* 16**,** 1224-1238.

KHALIN, I., JAMARI, N. L., RAZAK, N. B., HASAIN, Z. B., NOR, M. A., ZAINUDIN, M. H., OMAR, A. B. & ALYAUTDIN, R. 2016. A mouse

model of weight-drop closed head injury: emphasis on cognitive and neurological deficiency. *Neural Regen Res,* 11**,** 630-5.

KHELLAF, A., KHAN, D. Z. & HELMY, A. 2019. Recent advances in traumatic brain injury. *Journal of Neurology,* 266**,** 2878-2889.

KIM, S. U. D. V., JEAN 2009. Stem cell-based cell therapy in neurological diseases: A review. *Journal of Neuroscience Research,* 87**,** 2183-2200.

KIM, S. Y., BURGESS, J. K., WANG, Y., KABLE, E. P. W., WEISS, D. J., CHAN, H.-K. & CHRZANOWSKI, W. 2016. Atomized Human Amniotic Mesenchymal Stromal Cells for Direct Delivery to the Airway for Treatment of Lung Injury. *Journal of Aerosol Medicine and Pulmonary Drug Delivery,* 29**,** 514-524.

KIM, Y., PARK, J. & CHOI, Y. K. 2019. The Role of Astrocytes in the Central Nervous System Focused on BK Channel and Heme Oxygenase Metabolites: A Review. *Antioxidants,* 8**,** 121.

KIMURA, K., BREITBACH, M., SCHILDBERG, F. A., HESSE, M. & FLEISCHMANN, B. K. 2021. Bone marrow CD73+ mesenchymal stem cells display increased stemness in vitro and promote fracture healing in vivo. *Bone Reports,* 15**,** 101133.

KISSELBACH, L., MERGES, M., BOSSIE, A. & BOYD, A. 2009. CD90 Expression on human primary cells and elimination of contaminating fibroblasts from cell cultures. *Cytotechnology,* 59**,** 31-44.

KLOUDA, L., MIKOS, A. & G 2008. Thermoresponsive hydrogels in biomedical applications. *European Journal of Pharmaceutics and Biopharmaceutics,* 68**,** 34-45.

KÖHLER, S., WINKLER, U. & HIRRLINGER, J. 2021. Heterogeneity of Astrocytes in Grey and White Matter. *Neurochemical Research,* 46**,** 3-14.

KOVALEVICH, J. & LANGFORD, D. 2013. Considerations for the Use of SH-SY5Y Neuroblastoma Cells in Neurobiology. Humana Press.

KOZIOŁ, A., ŚRODA-POMIANEK, K., GÓRNIAK, A., WIKIERA, A., CYPRYCH, K. & MALIK, M. 2022. Structural Determination of Pectins by Spectroscopy Methods. *Coatings,* 12**,** 546.

KUHN, N. Z. & TUAN, R. S. 2010. Regulation of stemness and stem cell niche of mesenchymal stem cells: Implications in tumorigenesis and metastasis. *Journal of Cellular Physiology,* 222**,** 268-277.

KUMAR, A., STOICA, B. A., LOANE, D. J., YANG, M., ABULWERDI, G., KHAN, N., KUMAR, A., THOM, S. R. & FADEN, A. I. 2017. Microglial-derived microparticles mediate neuroinflammation after traumatic brain injury. *Journal of Neuroinflammation,* 14.

KUMARIA, A. 2017. In Vitro Models as a Platform to Investigate Traumatic Brain Injury. *Alternatives to Laboratory Animals,* 45**,** 201-211.

KUMARIA, A. & TOLIAS, C. M. 2008. In vitromodels of neurotrauma. *British Journal of Neurosurgery,* 22**,** 200-206.

LADAK, A. A., ENAM, S. A. & IBRAHIM, M. T. 2019. A Review of the Molecular Mechanisms of Traumatic Brain Injury. *World Neurosurgery,* 131**,** 126-132.

LAM, J., LOWRY, W. E., CARMICHAEL, S. T. & SEGURA, T. 2014. Delivery of iPS-NPCs to the Stroke Cavity within a Hyaluronic Acid Matrix Promotes the Differentiation of Transplanted Cells. *Advanced Functional Materials,* 24**,** 7053-7062.

LAM, P. K., LO, A. W. I., WANG, K. K. W., LAU, H. C. H., LEUNG, K. K. C., LI, K. T. C., LAI, P. B. S. & POON, W. S. 2013. Transplantation of mesenchymal stem cells to the brain by topical application in an experimental traumatic brain injury model. 20**,** 306-309.

LARA-ESPINOZA, C., CARVAJAL-MILLAN, E., BALANDRAN-QUINTANA, R., LOPEZ-FRANCO, Y. & RASCON-CHU, A. 2018. Pectin and Pectin-Based Composite Materials: Beyond Food Texture. *Molecules,* 23.

LASKOWITZ, D. & GRANT, G. 2016. *Translational Research in Traumatic Brain Injury*, CRC Press.

LEE, H., SPANDIDOS, D., TSATSAKIS, A., MARGINA, D., IZOTOV, B. & YANG, S. 2019. Neuroprotective effects of Scrophularia buergeriana extract against glutamate-induced toxicity in SH-SY5Y cells. *International Journal of Molecular Medicine*.

LI, J. & MOONEY, D. J. 2016. Designing hydrogels for controlled drug delivery. *Nature Reviews Materials,* 1**,** 16071.

LI, L., JIANG, Q., DING, G., ZHANG, L., ZHANG, Z. G., LI, Q., PANDA, S., LU, M., EWING, J. R. & CHOPP, M. 2010a. Effects of administration route on migration and distribution of neural progenitor cells transplanted into rats with focal cerebral ischemia, an MRI study. 30**,** 653-662.

LI, L. M., TIMOFEEV, I., CZOSNYKA, M. & HUTCHINSON, P. J. 2010b. The Surgical Approach to the Management of Increased Intracranial Pressure After Traumatic Brain Injury. *Anesthesia & Analgesia,* 111.

LI, Q., QU, M., WANG, N., WANG, L., FAN, G. & YANG, C. 2022. Betaine protects rats against ischemia/reperfusion injury-induced brain damage. *Journal of Neurophysiology,* 127**,** 444-451.

LI, W., ZHOU, J. & XU, Y. 2015. Study of the in vitro cytotoxicity testing of medical devices. *Biomedical Reports,* 3**,** 617-620.

LI, Y. & BORASCHI, D. 2016. Endotoxin contamination: a key element in the interpretation of nanosafety studies. *Nanomedicine,* 11**,** 269-287.

LIAO, Y., SMYTH, G. K. & SHI, W. 2014. featureCounts: an efficient general purpose program for assigning sequence reads to genomic features. *Bioinformatics,* 30**,** 923-930.

LIFSHITZ, J. 2009. Fluid Percussion Injury Model. Humana Press.

LIM, B. O., LEE, S. H., PARK, D. K. & CHOUE, R. W. 2003. Effect of Dietary Pectin on the Production of Immunoglobulins and Cytokines by Mesenteric Lymph Node Lymphocytes in Mouse Colitis Induced with Dextran Sulfate Sodium. *Bioscience, Biotechnology, and Biochemistry,* 67**,** 1706-1712.

LIU, J., LI, L. & SUO, W. Z. 2009. HT22 hippocampal neuronal cell line possesses functional cholinergic properties. *Life Sciences,* 84**,** 267-271.

LIU, J., TU, H., ZHANG, D., ZHENG, H. & LI, Y.-L. 2012. Voltage-gated sodium channel expression and action potential generation in differentiated NG108-15 cells. *BMC Neuroscience,* 13**,** 129.

LIU, L., FISHMAN, M. L., KOST, J. & HICKS, K. B. 2003. Pectin-based systems for colon-specific drug delivery via oral route. *Biomaterials,* 24**,** 3333-3343.

LIU, Y., EATON, E. D., WILLS, T. E., MCCANN, S. K., ANTONIC, A. & HOWELLS, D. W. 2018. Human Ischaemic Cascade Studies Using SH-

SY5Y Cells: a Systematic Review and Meta-Analysis. *Translational Stroke Research,* 9**,** 564-574.

LOVE, M. I., HUBER, W. & ANDERS, S. 2014. Moderated estimation of fold change and dispersion for RNA-seq data with DESeq2. *Genome Biology,* 15.

LOZANO, D., SCHIMMEL, S. & ACOSTA, S. 2017. Neuroinflammation in traumatic brain injury: A chronic response to an acute injury. *Brain Circulation,* 3**,** 135.

LU, D., MAHMOOD, A., WANG, L., LI, Y., LU, M. & CHOPP, M. 2001. Adult bone marrow stromal cells administered intravenously to rats after traumatic brain injury migrate into brain and improve neurological outcome. *Neuroreport,* 12**,** 559-63.

LUDWIG, P. E., THANKAM, F. G., PATIL, A. A., CHAMCZUK, A. J. & AGRAWAL, D. K. 2018. Brain injury and neural stem cells. *Neural Regen Res,* 13**,** 7-18.

LUO, H., XU, C., LIU, Z., YANG, L., HONG, Y., LIU, G., ZHONG, H., CAI, X., LIN, X., CHEN, X., WANG, C., NANWEN, Z. & XU, W. 2019. Neural differentiation of bone marrow mesenchymal stem cells with human brain-derived neurotrophic factor gene-modified in functionalized self-assembling peptide hydrogel in vitro. *Journal of Cellular Biochemistry,* 120**,** 2828-2835.

LYETH, B. G. 2016. Historical Review of the Fluid-Percussion TBI Model. *Frontiers in Neurology,* 7.

MA, F., FUQUA, B. K., HASIN, Y., YUKHTMAN, C., VULPE, C. D., LUSIS, A. J. & PELLEGRINI, M. 2019. A comparison between whole transcript and 3' RNA sequencing methods using Kapa and Lexogen library preparation methods. *BMC Genomics,* 20.

MACGILLIVRAY, T. E. 2003. Fibrin Sealants and Glues. *Journal of Cardiac Surgery,* 18**,** 480-485.

MACKENZIE, C. G., MACKENZIE, J. B. & BECK, P. 1961. THE EFFECT OF pH ON GROWTH, PROTEIN SYNTHESIS, AND LIPID-RICH PARTICLES OF CULTURED MAMMALIAN CELLS. *The Journal of Biophysical and Biochemical Cytology,* 9**,** 141-156.

MACLAY, W. D., SHEPHERD, A. & LOTZKAR, H. 1944. Use of pectin in pharmaceutical pastes and ointments. *Journals of the American Pharmaceutical Association Science Edition,* 33**,** 113-116.

MADRIGAL, M., RAO, K. S. & RIORDAN, N. H. 2014. A review of therapeutic effects of mesenchymal stem cell secretions and induction of secretory modification by different culture methods. *Journal of Translational Medicine,* 12.

MAHMOOD, A., LU, D., LU, M. & CHOPP, M. 2003. Treatment of Traumatic Brain Injury in Adult Rats with Intravenous Administration of Human Bone Marrow Stromal Cells. *Neurosurgery,* 53.

MANNING, L., FERREIRA, I. B., GITTINGS, P., HIEW, J., RYAN, E., BABA, M., RABY, E., CARVILLE, K., NORMAN, P. E., DAVIS, W. A., WOOD, F., HAMILTON, E. J. & RITTER, J. C. 2022. Wound healing with " spray - on " autologous skin grafting (<scp>ReCell</scp>) compared with standard care in patients with large diabetes - related foot wounds: an open - label randomised controlled trial. *International Wound Journal,* 19**,** 470-481.

MAO, A. S., SHIN, J.-W. & MOONEY, D. J. 2016. Effects of substrate stiffness and cell-cell contact on mesenchymal stem cell differentiation. *Biomaterials,* 98**,** 184-191.

MARGIANA, R., MARKOV, A., ZEKIY, A. O., HAMZA, M. U., AL-DABBAGH, K. A., AL-ZUBAIDI, S. H., HAMEED, N. M., AHMAD, I., SIVARAMAN, R., KZAR, H. H., AL-GAZALLY, M. E., MUSTAFA, Y. F. & SIAHMANSOURI, H. 2022. Clinical application of mesenchymal stem cell in regenerative medicine: a narrative review. *Stem Cell Research & Therapy,* 13.

MARK, P., KLEINSORGE, M., GAEBEL, R., LUX, C. A., TOELK, A., PITTERMANN, E., DAVID, R., STEINHOFF, G. & MA, N. 2013. Human Mesenchymal Stem Cells Display Reduced Expression of CD105 after Culture in Serum-Free Medium. *Stem Cells International,* 2013**,** 1-8.

MARMAROU, C. R., PRIETO, R., TAYA, K., YOUNG, H. F. & MARMAROU, A. 2009. Marmarou Weight Drop Injury Model. Humana Press.

MARTIN, M. 2011. Cutadapt removes adapter sequences from high-throughput sequencing reads. *EMBnet.journal,* 17**,** 10.

MASHKOURI, S., CROWLEY, M. G., LISKA, M. G., COREY, S. & BORLONGAN, C. V. 2016. Utilizing pharmacotherapy and mesenchymal stem cell therapy to reduce inflammation following traumatic brain injury. *Neural Regen Res,* 11**,** 1379-1384.

MAYS, R. W. 2023a. MultiStem® Administration for Stroke Treatment and Enhanced Recovery Study. https://ClinicalTrials.gov/show/NCT03545607.

MAYS, R. W. 2023b. Study to Examine the Effects of MultiStem in Ischemic Stroke. https://ClinicalTrials.gov/show/NCT01436487.

MCCRORIE, P., MISTRY, J., TARESCO, V., LOVATO, T., FAY, M., WARD, I., RITCHIE, A. A., CLARKE, P. A., SMITH, S. J., MARLOW, M. & RAHMAN, R. 2020. Etoposide and olaparib polymer-coated nanoparticles within a bioadhesive sprayable hydrogel for post-surgical localised delivery to brain tumours. *European Journal of Pharmaceutics and Biopharmaceutics,* 157.

MCKEE, A. C. & DANESHVAR, D. H. 2015. The neuropathology of traumatic brain injury. Elsevier.

MCMURRAY, R. J., DALBY, M. J. & TSIMBOURI, P. M. 2015. Using biomaterials to study stem cell mechanotransduction, growth and differentiation. *Journal of Tissue Engineering and Regenerative Medicine,* 9**,** 528-539.

MENDES FILHO, D., RIBEIRO, P. D. C., OLIVEIRA, L. F., DE PAULA, D. R. M., CAPUANO, V., DE ASSUNÇÃO, T. S. F. & DA SILVA, V. J. D. 2018. Therapy With Mesenchymal Stem Cells in Parkinson Disease: History and Perspectives. *The Neurologist,* 23.

MERCK. 2023. *NG108-15* [Online]. Sigma Aldrich. Available: https://www.sigmaaldrich.com/GB/en/product/sigma/cb_88112302 [Accessed 12/03/2023 2023].

MEZGER, T. G. 2014. *The Rheology Handbook,* Hanover, Germany, Vincentz Network GmbH & Co.

MICHINAGA, S., INOUE, A., SONODA, K., MIZUGUCHI, H. & KOYAMA, Y. 2021. Down-regulation of astrocytic sonic hedgehog by activation of endothelin ETB receptors: Involvement in traumatic brain injury-induced disruption of blood brain barrier in a mouse model. *Neurochemistry International,* 146**,** 105042.

MINOR, M., ALCEDO, K. P., BATTAGLIA, R. A. & SNIDER, N. T. 2019. Cell type- and tissue-specific functions of ecto-5′ -nucleotidase (CD73). *American Journal of Physiology-Cell Physiology,* 317**,** C1079-C1092.

MINZANOVA, S., MIRONOV, V., ARKHIPOVA, D., KHABIBULLINA, A., MIRONOVA, L., ZAKIROVA, Y. & MILYUKOV, V. 2018. Biological Activity and Pharmacological Application of Pectic Polysaccharides: A Review. *Polymers,* 10**,** 1407.

MOAKES, R. J. A., GROVER, L. M. & ROBINSON, T. E. 2022. Can We Structure Biomaterials to Spray Well Whilst Maintaining Functionality? *Bioengineering,* 10**,** 3.

MOORE, S., MESCHKAT, M., RUHWEDEL, T., TREVISIOL, A., TZVETANOVA, I. D., BATTEFELD, A., KUSCH, K., KOLE, M. H. P., STRENZKE, N., MÖBIUS, W., DE HOZ, L. & NAVE, K.-A. 2020. A role of oligodendrocytes in information processing. *Nature Communications,* 11.

MORRISON, B., CATER, H. L., BENHAM, C. D. & SUNDSTROM, L. E. 2006. An in vitro model of traumatic brain injury utilising two-dimensional stretch of organotypic hippocampal slice cultures. *Journal of Neuroscience Methods,* 150**,** 192-201.

MORRISON, B., ELKIN, B. S., DOLLÉ, J.-P. & YARMUSH, M. L. 2011. In Vitro Models of Traumatic Brain Injury. *Annual Review of Biomedical Engineering,* 13**,** 91-126.

MU, P., LIU, Y., JIANG, S., GAO, J., SUN, S., LI, L. & GAO, D. 2020. Glial cell line ‐ derived neurotrophic factor alters lipid composition and protein distribution in MPP+ ‐ injured differentiated SH ‐ SY5Y cells. *Journal of Cellular Physiology,* 235**,** 9347-9360.

MUKHERJEE, A. & ROTWEIN, P. 2008. Insulin-Like Growth Factor-Binding Protein-5 Inhibits Osteoblast Differentiation and Skeletal Growth by Blocking Insulin-Like Growth Factor Actions. *Molecular Endocrinology,* 22**,** 1238-1250.

MUNARIN, F., GUERREIRO, S. G., GRELLIER, M. A., TANZI, M. C., BARBOSA, M. A., PETRINI, P. & GRANJA, P. L. 2011. Pectin-based injectable biomaterials for bone tissue engineering. *Biomacromolecules,* 12**,** 568-77.

MUNARIN, F., PETRINI, P., TANZI, M., BARBOSA, M. & GRANJA, P. 2012a. Biofunctional chemically modified pectin for cell delivery. *Soft Matter,* 8**,** 4731-4739.

MUNARIN, F., PETRINI, P., TANZI, M. C., BARBOSA, M. A. & GRANJA, P. L. 2012b. Biofunctional chemically modified pectin for cell delivery. *Soft Matter,* 8**,** 4731-4739.

MUNJERI, O., COLLETT, J. H. & FELL, J. T. 1997. Amidated Pectin Hydrogel Beads for Colonic Drug Delivery-An in vitro Study. *Drug Delivery,* 4**,** 207-211.

MURUGAN SUMATHRA, DHARMAN GOVINDARAJ, MURUGARAJ JEYARAJ, ARFAJ, ABDULLA A., A. MUNUSAMY,

M., SURESH KUMAR, S. & MARIAPPAN RAJAN 2017. Sustainable pectin fascinating hydroxyapatite nanocomposite scaffolds to enhance tissue regeneration. *Sustainable Chemistry and Pharmacy,* 5**,** 46-53.

NAMJOSHI, D. R., GOOD, C., CHENG, W. H., PANENKA, W., RICHARDS, D., CRIPTON, P. A. & WELLINGTON, C. L. 2013. Towards clinical management of traumatic brain injury: a review of models and mechanisms from a biomechanical perspective. *Disease Models & Mechanisms,* 6**,** 1325-1338.

NAPHADE, S., BHATNAGAR, R., HANSON-SMITH, V., CHOI, I. & ZHANG, A. 2022. Systematic comparative analysis of strand-specific RNA-seq library preparation methods for low input samples. *Scientific Reports,* 12.

NEFF, F., NOELKER, C., EGGERT, K. & SCHLEGEL, J. 2002. Signaling Pathways Mediate the Neuroprotective Effects of GDNF. *Annals of the New York Academy of Sciences,* 973**,** 70-74.

NEVES, S., GOMES, D., SOUSA, A., BIDARRA, S., PETRINI, P., MORONI, L., BARRIAS, C. & GRANJA, P. 2015. Biofunctionalized pectin hydrogels as 3D cellular microenvironments. 3**,** 2096-2108.

NGUYEN, H. N., WANG, C. & PERRY, D. C. 2002. Depletion of intracellular calcium stores is toxic to SH-SY5Y neuronal cells. *Brain Research,* 924**,** 159-166.

NIRMALADEVI, D., VENKATARAMANA, M., CHANDRANAYAKA, S., RAMESHA, A., JAMEEL, N. M. & SRINIVAS, C. 2014. Neuroprotective Effects of Bikaverin on H2O2-Induced Oxidative Stress Mediated Neuronal Damage in SH-SY5Y Cell Line. *Cellular and Molecular Neurobiology,* 34**,** 973-985.

NISHIMURA, O. 2023. *Flowchart: choosing a test by the data* [Online]. Colorado State University. Available: https://onishlab.colostate.edu/wp-content/uploads/2019/07/which_test_flowchart.png [Accessed 28/02/2023 2023].

NOREEN, A., NAZLI, Z.-I. H., AKRAM, J., RASUL, I., MANSHA, A., YAQOOB, N., IQBAL, R., TABASUM, S., ZUBER, M. & ZIA, K. M. 2017. Pectins functionalized biomaterials; a new viable approach for biomedical applications: A review. *International Journal of Biological Macromolecules,* 101**,** 254-272.

OLIVA, A. A., MCCLAIN‐MOSS, L., PENA, A., DROUILLARD, A. & HARE, J. M. 2019. Allogeneic mesenchymal stem cell therapy: A regenerative medicine approach to geroscience. *AGING MEDICINE,* 2**,** 142-146.

OLSEN, A. G. 1933. Pectin Studies I: Citrus Pectin. *Industrial and Engineering Chemistry,* 25**,** 699-703.

OLSEN, A. G. 1940. Pectin therapy and pectin types. *American Journal of Digestive Diseases,* 7**,** 515-519.

OLSEN, A. G., STUEWER, R. F., FEHLBERG, E. R., AND BEACH, N. M 1939. Pectin studies. Relation of combining weight to other properties of commercial pectins. *Industrial and Engineering Chemistry,* 31**,** 1015-1030.

OSIER, N. D. & DIXON, C. E. 2016. The Controlled Cortical Impact Model: Applications, Considerations for Researchers, and Future Directions. *Frontiers in Neurology,* 7.

OSIER, N. D., KORPON, J. R. & DIXON, C. E. 2015. Controlled Cortical Impact Model. CRC Press/Taylor & Francis, Boca Raton (FL).

PAAR, A. 2023. *Amplitude sweeps* [Online]. Anton Paar Wiki. Available: https://wiki.anton-paar.com/uk-en/amplitude-sweeps/ [Accessed 24/03/2023 2023].

PAPAZIAN, I., KYRARGYRI, V., EVANGELIDOU, M., VOULGARI-KOKOTA, A. & PROBERT, L. 2018. Mesenchymal Stem Cell Protection of Neurons against Glutamate Excitotoxicity Involves Reduction of NMDA-Triggered Calcium Responses and Surface GluR1, and Is Partly Mediated by TNF. *International Journal of Molecular Sciences,* 19**,** 651.

PARIKH, S., KOCH, M. & NARAYAN, R. K. 2007. Traumatic Brain Injury. *International Anesthesiology Clinics,* 45.

PARK, H. J., SHIN, J. Y., KIM, H. N., OH, S. H., SONG, S. K. & LEE, P. H. 2015. Mesenchymal stem cells stabilize the blood–brain barrier through regulation of astrocytes. *Stem Cell Research & Therapy,* 6.

PARK, I.-H., LEROU, P. H., ZHAO, R., HUO, H. & DALEY, G. Q. 2008. Generation of human-induced pluripotent stem cells. *Nature Protocols,* 3**,** 1180-1186.

PEARN, M. L., NIESMAN, I. R., EGAWA, J., SAWADA, A., ALMENAR-QUERALT, A., SHAH, S. B., DUCKWORTH, J. L. & HEAD, B. P. 2017. Pathophysiology Associated with Traumatic Brain Injury: Current Treatments and Potential Novel Therapeutics. *Cellular and Molecular Neurobiology,* 37**,** 571-585.

PEHLIVANER KARA, M. O. & EKENSEAIR, A. K. 2016. In situ spray deposition of cell-loaded, thermally and chemically gelling hydrogel coatings for tissue regeneration. *Journal of Biomedical Materials Research Part A,* 104**,** 2383-2393.

PEIGHAMBARDOUST, S. H., JAFARZADEH-MOGHADDAM, M., PATEIRO, M., LORENZO, J. M. & DOMÍNGUEZ, R. 2021. Physicochemical, Thermal and Rheological Properties of Pectin Extracted from Sugar Beet Pulp Using Subcritical Water Extraction Process. *Molecules,* 26**,** 1413.

PEIRCE, S. C. & CAROLAN-REES, G. 2019. ReCell® Spray-On Skin System for Treating Skin Loss, Scarring and Depigmentation after Burn Injury: A NICE Medical Technology Guidance. *Applied Health Economics and Health Policy,* 17**,** 131-141.

PENNOCK, R., BRAY, E., PRYOR, P., JAMES, S., MCKEEGAN, P., STURMEY, R. & GENEVER, P. 2015. Human cell dedifferentiation in mesenchymal condensates through controlled autophagy. *Scientific Reports,* 5**,** 13113.

PERSAUD, L., DE JESUS, D., BRANNIGAN, O., RICHIEZ-PAREDES, M., HUAMAN, J., ALVARADO, G., RIKER, L., MENDEZ, G., DEJOIE, J. & SAUANE, M. 2016. Mechanism of Action and Applications of Interleukin 24 in Immunotherapy. *International Journal of Molecular Sciences,* 17**,** 869.

PICCIRILLO, S., CASTALDO, P., MACRÌ, M. L., AMOROSO, S. & MAGI, S. 2018. Glutamate as a potential "survival factor" in an in vitro model of neuronal hypoxia/reoxygenation injury: leading role of the Na+/Ca2+ exchanger. *Cell Death & Disease,* 9.

PIERSCHBACHER, M. D. & RUOSLAHTI, E. 1984. Cell attachment activity of fibronectin can be duplicated by small synthetic fragments of the molecule. *Nature,* 309**,** 30-33.

PISCHIUTTA, F., CARUSO, E., CAVALEIRO, H., SALGADO, A. J., LOANE, D. J. & ZANIER, E. R. 2022. Mesenchymal stromal cell secretome for traumatic brain injury: Focus on immunomodulatory action. *Experimental Neurology,* 357**,** 114199.

PONSFORD, J., WILLMOTT, C., ROTHWELL, A., CAMERON, P., KELLY, A.-M., NELMS, R., CURRAN, C. & NG, K. I. M. 2000. Factors influencing outcome following mild traumatic brain injury in adults. *Journal of the International Neuropsychological Society,* 6**,** 568-579.

POPOV, S. V., MARKOV, P. A., POPOVA, G. Y., NIKITINA, I. R., EFIMOVA, L. & OVODOV, Y. S. 2013. Anti-inflammatory activity of low and high methoxylated citrus pectins. *Biomedicine & Preventive Nutrition,* 3**,** 59-63.

POPPER, H. 1945. Evaluation of gelatin and pectin solutions as substitutes for plasma in the treatment of shock. *Archives of Surgery,* 51**,** 34-45.

PRASANNA MALLICK, S., NARAYAN SINGH, B., AMIT RASTOGI & PRADEEP SRIVASTAVA 2018. Design and evaluation of chitosan/poly(l-lactide)/pectin based composite scaffolds for cartilage tissue regeneration. *International Journal of Biological Macromolecules,* 112**,** 909-920.

PRINS, M., GRECO, T., ALEXANDER, D. & GIZA, C. C. 2013. The pathophysiology of traumatic brain injury at a glance. *Disease Models & Mechanisms,* 6**,** 1307-1315.

PRODROMOS, C. 2023. Safety of Cultured Allogeneic Adult Umbilical Cord Derived Mesenchymal Stem Cell Intravenous Infusion for TBI. https://ClinicalTrials.gov/show/NCT05018832.

PROMOCELL. 2023. *Mesenchymal Stem Cell Osteogenic Differentiation Medium* [Online]. Available: https://promocell.com/product/mesenchymal-stem-cell-osteogenic-differentiation-medium/ [Accessed 12/01/2023 2023].

RACHMANY, L., TWEEDIE, D., RUBOVITCH, V., LI, Y., HOLLOWAY, H. W., KIM, D. S., RATLIFF, W. A., SAYKALLY, J. N., CITRON, B. A., HOFFER, B. J., GREIG, N. H. & PICK, C. G. 2017. Exendin-4 attenuates blast traumatic brain injury induced cognitive impairments, losses of synaptophysin and in vitro TBI-induced hippocampal cellular degeneration. *Scientific Reports,* 7.

RAGHAVAN, S. R. & CIPRIANO, B. H. 2006. Gel Formation: Phase Diagrams Using Tabletop Rheology and Calorimetry. *In:* WEISS, R. G. & TERECH, P. (eds.) *Molecular Gels: Materials with Self-Assembled Fibrillar Networks.* Dordrecht: Springer Netherlands.

RAMIREZ, S., MUKHERJEE, A., SEPULVEDA, S., BECERRA-CALIXTO, A., BRAVO-VASQUEZ, N., GHERARDELLI, C., CHAVEZ, M. & SOTO, C. 2021. Modeling Traumatic Brain Injury in Human Cerebral Organoids. *Cells,* 10**,** 2683.

RANSY, C., VAZ, C., LOMBÈS, A. & BOUILLAUD, F. 2020. Use of H2O2 to Cause Oxidative Stress, the Catalase Issue. *International Journal of Molecular Sciences,* 21**,** 9149.

ROBERT, S. 2020. Traumatic brain injury and mood disorders. *Ment Health Clin,* 10**,** 335-345.

RODRIGUEZ, L. A., MOHAMMADIPOOR, A., ALVARADO, L., KAMUCHEKA, R. M., ASHER, A. M., CANCIO, L. C. & ANTEBI, B. 2019. Preconditioning in an Inflammatory Milieu Augments the Immunotherapeutic Function of Mesenchymal Stromal Cells. *Cells,* 8**,** 462.

RODRÍGUEZ ROBLEDO, V. & CASTRO VÁZQUEZ, L. I. 2020. Pectin - Extraction, Purification, Characterization and Applications. IntechOpen.

ROEDERER, M. 2002. Compensation in flow cytometry. *Curr Protoc Cytom,* Chapter 1**,** Unit 1.14.

ROWLEY, J. A., MADLAMBAYAN, G. & MOONEY, D. J. 1999. Alginate hydrogels as synthetic extracellular matrix materials. *Biomaterials,* 20**,** 45-53.

SAHA, K., KEUNG, A. J., IRWIN, E. F., LI, Y., LITTLE, L., SCHAFFER, D. V. & HEALY, K. E. 2008. Substrate Modulus Directs Neural Stem Cell Behavior. *Biophysical Journal,* 95**,** 4426-4438.

SARNTIVIJAI, S., LIN, Y., XIANG, Z., MEEHAN, T. F., DIEHL, A. D., VEMPATI, U. D., SCHÜRER, S. C., PANG, C., MALONE, J., PARKINSON, H., LIU, Y., TAKATSUKI, T., SAIJO, K., MASUYA, H., NAKAMURA, Y., BRUSH, M. H., HAENDEL, M. A., ZHENG, J., STOECKERT, C. J., PETERS, B., MUNGALL, C. J., CAREY, T. E., STATES, D. J., ATHEY, B. D. & HE, Y. 2014. CLO: The cell line ontology. *Journal of Biomedical Semantics,* 5**,** 37.

SCHEPICI, G., SILVESTRO, S., BRAMANTI, P. & MAZZON, E. 2020. Traumatic Brain Injury and Stem Cells: An Overview of Clinical Trials, the Current Treatments and Future Therapeutic Approaches. *Medicina,* 56**,** 137.

SCHINDELIN, J., ARGANDA-CARRERAS, I., FRISE, E., KAYNIG, V., LONGAIR, M., PIETZSCH, T., PREIBISCH, S., RUEDEN, C., SAALFELD, S., SCHMID, B., TINEVEZ, J.-Y., WHITE, D. J., HARTENSTEIN, V., ELICEIRI, K., TOMANCAK, P. & CARDONA, A. 2012. Fiji: an open-source platform for biological-image analysis. *Nature Methods,* 9**,** 676-682.

SCHOONDERWOERD, M. J. A., GOUMANS, M.-J. T. H. & HAWINKELS, L. J. A. C. 2020. Endoglin: Beyond the Endothelium. *Biomolecules,* 10**,** 289.

SCHUSTER, S. C. 2008. Next-generation sequencing transforms today's biology. *Nature Methods,* 5**,** 16-18.

SCHWARTZ, D. M., PEHLIVANER KARA, M. O., GOLDSTEIN, A. M., OTT, H. C. & EKENSEAIR, A. K. 2017. Spray Delivery of Intestinal Organoids to Reconstitute Epithelium on Decellularized Native Extracellular Matrix. *Tissue Engineering Part C: Methods,* 23**,** 565-573.

SEDAGHAT, A. 2017. A novel and robust model for determining rheological properties of Newtonian and non-Newtonian fluids in a marsh funnel. *Journal of Petroleum Science and Engineering,* 156**,** 896-916.

SERRA-PREZ, A., VERDAGUER, E., PLANAS, A. M. & SANTALUCA, T. 2008. Glucose promotes caspase-dependent delayed cell death after a transient episode of oxygen and glucose deprivation in SH-SY5Y cells. *Journal of Neurochemistry,* 106**,** 1237-1247.

SHERMAN, S. A., PHILLIPS, J. K., COSTA, J. T., CHO, F. S., OUNGOULIAN, S. R. & FINAN, J. D. 2016. Stretch Injury of Human Induced Pluripotent Stem Cell Derived Neurons in a 96 Well Format. *Scientific Reports,* 6**,** 34097.

SHIPLEY, M. M., MANGOLD, C. A. & SZPARA, M. L. 2016. Differentiation of the SH-SY5Y Human Neuroblastoma Cell Line. *Journal of visualized experiments : JoVE***,** 53193-53193.

SIEGEL, G., KLUBA, T., HERMANUTZ-KLEIN, U., BIEBACK, K., NORTHOFF, H. & SCHÄFER, R. 2013. Phenotype, donor age and gender affect function of human bone marrow-derived mesenchymal stromal cells. *BMC Medicine,* 11**,** 146.

SIRACUSA, R., FUSCO, R. & CUZZOCREA, S. 2019. Astrocytes: Role and Functions in Brain Pathologies. *Frontiers in Pharmacology,* 10.

SIVANATHAN, K. N., ROJAS-CANALES, D., GREY, S. T., GRONTHOS, S. & COATES, P. T. 2017. Transcriptome Profiling of IL-17A Preactivated Mesenchymal Stem Cells: A Comparative Study to Unmodified and IFN-γModified Mesenchymal Stem Cells. *Stem Cells International,* 2017**,** 1-16.

SKOTAK, M., WANG, F. & CHANDRA, N. 2012. An in vitro injury model for SH-SY5Y neuroblastoma cells: Effect of strain and strain rate. *Journal of Neuroscience Methods,* 205**,** 159-168.

SOHNI, A. & VERFAILLIE, C. M. 2013. Mesenchymal Stem Cells Migration Homing and Tracking. *Stem Cells International,* 2013**,** 1-8.

SPURLOCK, M. S., AHMED, A. I., RIVERA, K. N., YOKOBORI, S., LEE, S. W., SAM, P. N., SHEAR, D. A., HEFFERAN, M. P., HAZEL, T. G., JOHE, K. K., GAJAVELLI, S., TORTELLA, F. C. & BULLOCK, R. M. 2017. Amelioration of Penetrating Ballistic-Like Brain Injury Induced Cognitive Deficits after Neuronal Differentiation of Transplanted Human Neural Stem Cells. *Journal of Neurotrauma,* 34**,** 1981-1995.

SRIAMORNSAK, P. 2003. Chemistry of pectin and its pharmaceutical uses: A review. *Silpakorn University International Journal,* 3**,** 206-228.

SRIAMORNSAK, P., WATTANAKORN, N., NUNTHANID, J. & PUTTIPIPATKHACHORN, S. 2008. Mucoadhesion of pectin as evidence by wettability and chain interpenetration. *Carbohydrate Polymers,* 74**,** 458-467.

SRIAMORNSAK, P., WATTANAKORN, N. & TAKEUCHI, H. 2010. Study on the mucoadhesion mechanism of pectin by atomic force microscopy and mucin-particle method. *Carbohydrate Polymers,* 79**,** 54-59.

STOJKOV, G., NIYAZOV, Z., PICCHIONI, F. & BOSE, R. K. 2021. Relationship between Structure and Rheology of Hydrogels for Various Applications. *Gels,* 7**,** 255.

STUCKY, E. C., SCHLOSS, R. S., YARMUSH, M. L. & SHREIBER, D. I. 2015. Alginate micro-encapsulation of mesenchymal stromal cells enhances modulation of the neuro-inflammatory response. *Cytotherapy,* 17**,** 1353-1364.

SUN, Z.-W., ZHANG, L., ZHU, S.-J., CHEN, W.-C. & MEI, B. 2010. Excitotoxicity effects of glutamate on human neuroblastoma SH-SY5Y cells via oxidative damage. *Neuroscience Bulletin,* 26**,** 8-16.

SUVARNA, K. S., LAYTON, C. & BANCROFT, J. D. 2018. *Bancroft's Theory and Practice of Histological Techniques E-Book*, Philadelphia, UNITED KINGDOM, Elsevier.

SZEKALSKA, M., PUCIŁOWSKA, A., SZYMAŃSKA, E., CIOSEK, P. & WINNICKA, K. 2016. Alginate: Current Use and Future Perspectives in Pharmaceutical and Biomedical Applications. *International Journal of Polymer Science,* 2016**,** 1-17.

TAKEI, T., SATO, M., IJIMA, H. & KAWAKAMI, K. 2010. In situ gellable oxidized citrus pectin for localized delivery of anticancer drugs and prevention of homotypic cancer cell aggregation. *Biomacromolecules,* 11**,** 3525-30.

TENNY, S. T. W. 2022. Intracranial Hemorrhage. *StatPearls [Internet]*. StatPearls Publishing.

TER HORST, B., MOAKES, R. J. A., CHOUHAN, G., WILLIAMS, R. L., MOIEMEN, N. S. & GROVER, L. M. 2019. A gellan-based fluid gel carrier to enhance topical spray delivery. *Acta Biomaterialia,* 89**,** 166-179.

THERMOFISHER. 2014. *Culturing Human Mesenchymal Stem Cells (MSCs) under Serum-Free and Xeno-Free Conditions* [Online]. Available: https://www.thermofisher.com/uk/en/home/references/protocols/cell-culture/stem-cell-protocols/ipsc-protocols/culturing-human-mesenchymal-stem-cells-mscs-under-serum-free-and-xeno-free-conditions.html#:~:text=While%20human%20MSCs%20grown%20in,2%20(see%20Appendix%20A). [Accessed 27/03/2023 2023].

THERMOSCIENTIFIC 2015. FTIR Basic Organic Functional Group Reference Chart.

THIEBES, A. L., UHL, F. E., HAUSER, M., CORNELISSEN, C. G., JOCKENHOEVEL, S. & WEISS, D. J. 2021. Endoscopic atomization of mesenchymal stromal cells: in vitro study for local cell therapy of the lungs. *Cytotherapy,* 23**,** 293-300.

THIRAWONG, N., THONGBORISUTE, J., TAKEUCHI, H. & SRIAMORNSAK, P. 2008. Improved intestinal absorption of calcitonin by mucoadhesive delivery of novel pectin–liposome nanocomplexes. *Journal of Controlled Release,* 125**,** 236-245.

THOUDAM, T., CHANDA, D., SINAM, I. S., KIM, B.-G., KIM, M.-J., OH, C. J., LEE, J. Y., KIM, M.-J., PARK, S. Y., LEE, S. Y., JUNG, M.-K., MUN, J. Y., HARRIS, R. A., ISHIHARA, N., JEON, J.-H. & LEE, I.-K. 2022. Noncanonical PDK4 action alters mitochondrial dynamics to affect the cellular respiratory status. *Proceedings of the National Academy of Sciences,* 119.

TIAN, W., HEO, S., KIM, D.-W., KIM, I.-S., AHN, D., TAE, H.-J., KIM, M.-K. & PARK, B.-Y. 2021. Ethanol Extract of Maclura tricuspidata Fruit Protects SH-SY5Y Neuroblastoma Cells against H2O2-Induced Oxidative Damage via Inhibiting MAPK and NF-κB Signaling. *International Journal of Molecular Sciences,* 22**,** 6946.

TIMMERMAN, R., BURM, S. M. & BAJRAMOVIC, J. J. 2018. An Overview of in vitro Methods to Study Microglia. *Frontiers in Cellular Neuroscience,* 12.

TIWARY, C. M., WARD, J. A. & JACKSON, B. A. 1997. Effect of pectin on satiety in healthy US Army adults. *Journal of the American College of Nutrition,* 16**,** 423-428.

TSENG, N., LAMBIE, S. C., HUYNH, C. Q., SANFORD, B., PATEL, M., HERSON, P. S. & ORMOND, D. R. 2021. Mitochondrial transfer from mesenchymal stem cells improves neuronal metabolism after oxidant injury in vitro: The role of Miro1. *J Cereb Blood Flow Metab,* 41**,** 761-770.

ULLAH, F., OTHMAN, M. B., JAVED, F., AHMAD, Z. & MD AKIL, H. 2015a. Classification, processing and application of hydrogels: A review. *Mater Sci Eng C Mater Biol Appl,* 57**,** 414-33.

ULLAH, I., SUBBARAO, R. B. & RHO, G. J. 2015b. Human mesenchymal stem cells - current trends and future prospective. *Biosci Rep,* 35.

ULLAH, M., LIU, D. D. & THAKOR, A. S. 2019. Mesenchymal Stromal Cell Homing: Mechanisms and Strategies for Improvement. *iScience,* 15**,** 421-438.

URA, H., TOGI, S. & NIIDA, Y. 2022. A comparison of mRNA sequencing (RNA-Seq) library preparation methods for transcriptome analysis. *BMC Genomics,* 23.

VEAZEY, W. S., ANUSAVICE, K. J. & MOORE, K. 2005. Mammalian cell delivery via aerosol deposition. *Journal of Biomedical Materials Research Part B: Applied Biomaterials,* 72B**,** 334-338.

VIZOSO, F., EIRO, N., CID, S., SCHNEIDER, J. & PEREZ-FERNANDEZ, R. 2017. Mesenchymal Stem Cell Secretome: Toward Cell-Free Therapeutic Strategies in Regenerative Medicine. *International Journal of Molecular Sciences,* 18**,** 1852.

VOLKMAN, R. O., DANIEL 2017. Concise Review: Mesenchymal Stem Cells in Neurodegenerative Diseases. *STEM CELLS,* 35**,** 1867-1880.

VORAGEN, A. G. J., COENEN, G.-J., VERHOEF, R. P. & SCHOLS, H. A. 2009. Pectin, a versatile polysaccharide present in plant cell walls. *Structural Chemistry,* 20**,** 263-275.

WALKER, P. A., SHAH, S. K., HARTING, M. T. & COX, C. S. 2009. Progenitor cell therapies for traumatic brain injury: barriers and opportunities in translation. *Disease Models & Mechanisms,* 2**,** 23-38.

WANG, K., ZHU, X., ZHANG, K., ZHOU, F. & ZHU, L. 2016. Gas1 Knockdown Increases the Neuroprotective Effect of Glial Cell-Derived Neurotrophic Factor Against Glutamate-Induced Cell Injury in Human SH-SY5Y Neuroblastoma Cells. *Cellular and Molecular Neurobiology,* 36**,** 603-611.

WANG, S., CHENG, H., DAI, G., WANG, X., HUA, R., LIU, X., WANG, P., CHEN, G., YUE, W. & AN, Y. 2013. Umbilical cord mesenchymal stem cell transplantation significantly improves neurological function in patients with sequelae of traumatic brain injury. *Brain Research,* 1532**,** 76-84.

WANG, Z., GERSTEIN, M. & SNYDER, M. 2009. RNA-Seq: a revolutionary tool for transcriptomics. *Nature Reviews Genetics,* 10**,** 57-63.

WANG, Z., LUO, Y., CHEN, L. & LIANG, W. 2017. Safety of neural stem cell transplantation in patients with severe traumatic brain injury. *Experimental and Therapeutic Medicine*.

WAT, R., MAMMI, M., PAREDES, J., HAINES, J., ALASMARI, M., LIEW, A., LU, V. M., ARNAOUT, O., SMITH, T. R., GORMLEY, W. B., AGLIO, L. S., MEKARY, R. A. & ZAIDI, H. 2019. The Effectiveness of Antiepileptic Medications as Prophylaxis of Early Seizure in Patients with Traumatic Brain Injury Compared with Placebo or No Treatment: A Systematic Review and Meta-Analysis. *World Neurosurgery,* 122**,** 433-440.

WATTANAKORN, N., ASAVAPICHAYONT, P., NUNTHANID, J., LIMMATVAPIRAT, S., SUNGTHONGJEEN, S., CHANTASART, D. & SRIAMORNSAK, P. 2010. Pectin-Based Bioadhesive Delivery of Carbenoxolone Sodium for Aphthous Ulcers in Oral Cavity. *AAPS PharmSciTech,* 11**,** 743-751.

WATTS, P. & SMITH, A. 2009. PecSys: in situ gelling system for optimised nasal drug delivery. *Expert Opin Drug Deliv,* 6**,** 543-52.

WEI, X., YANG, X., HAN, Z.-P., QU, F.-F., SHAO, L. & SHI, Y.-F. 2013. Mesenchymal stem cells: a new trend for cell therapy. *Acta Pharmacologica Sinica,* 34**,** 747-754.

WEISS, J. & BARKER, J. 2018. Diverse pro-inflammatory endotoxin recognition systems of mammalian innate immunity. *F1000Research,* 7**,** 516.

WERNER, C. E., K 2007. Pathophysiology of traumatic brain injury. *British Journal of Anaesthesia,* 99**,** 4-9.

WIATRAK, B., KUBIS-KUBIAK, A., PIWOWAR, A. & BARG, E. 2020. PC12 Cell Line: Cell Types, Coating of Culture Vessels, Differentiation and Other Culture Conditions. *Cells,* 9**,** 958.

WILLATS, W. G. T., MCCARTNEY, L., MACKIE, W. & KNOX, P. J. 2001. Pectin: Cell biology and prospects for functional analysis. *Plant Molecular Biology,* 47**,** 9-27.

WILLIAMS, A. J., LING, G. S. F. & TORTELLA, F. C. 2006. Severity level and injury track determine outcome following a penetrating ballistic-like brain injury in the rat. *Neuroscience Letters,* 408**,** 183-188.

WILSON, L., STEWART, W., DAMS-O'CONNOR, K., DIAZ-ARRASTIA, R., HORTON, L., MENON, D. K. & POLINDER, S. 2017. The chronic and evolving neurological consequences of traumatic brain injury. *The Lancet Neurology,* 16**,** 813-825.

WINTERS, M., TOMPKINS, C. A., & CROOK, G. W. 1939. Pectin-agar diets in the treatment of bacillary dysentery of infants and children. , 14(6), 788–797. *The Journal of Pediatrics,* 14**,** 788-797.

WOBMA, H. M., LIU, D. & VUNJAK-NOVAKOVIC, G. 2018. Paracrine Effects of Mesenchymal Stromal Cells Cultured in Three-Dimensional Settings on Tissue Repair. *ACS Biomaterials Science & Engineering,* 4**,** 1162-1175.

WOOD, F. M., GILES, N., STEVENSON, A., REA, S. & FEAR, M. 2012. Characterisation of the cell suspension harvested from the dermal epidermal junction using a ReCell® kit. *Burns,* 38**,** 44-51.

WRIGHT, A., ARTHAUD-DAY, M. L. & WEISS, M. L. 2021. Therapeutic Use of Mesenchymal Stromal Cells: The Need for Inclusive Characterization Guidelines to Accommodate All Tissue Sources and Species. *Frontiers in Cell and Developmental Biology,* 9.

WU, S. 2013. Intranasal Delivery of Neural Stem Cells: A CNS-specific, Non-invasive Cell-based Therapy for Experimental Autoimmune Encephalomyelitis. *Journal of Clinical & Cellular Immunology,* 04.

XIONG, L.-L., HU, Y., ZHANG, P., ZHANG, Z., LI, L.-H., GAO, G.-D., ZHOU, X.-F. & WANG, T.-H. 2018a. Neural Stem Cell Transplantation Promotes Functional Recovery from Traumatic Brain Injury via Brain Derived Neurotrophic Factor-Mediated Neuroplasticity. *Molecular Neurobiology,* 55**,** 2696-2711.

XIONG, Y., MAHMOOD, A. & CHOPP, M. 2018b. Current understanding of neuroinflammation after traumatic brain injury and cell-based therapeutic opportunities. *Chinese Journal of Traumatology,* 21**,** 137-151.

XIONG, Y. ASIM M. MICHAEL C. 2013. Animal models of traumatic brain injury. *Nature Reviews Neuroscience,* 14**,** 128-142.

XU, M., MCCANNA, D. J. & SIVAK, J. G. 2015. Use of the viability reagent PrestoBlue in comparison with alamarBlue and MTT to assess the viability of human corneal epithelial cells. *Journal of Pharmacological and Toxicological Methods,* 71**,** 1-7.

YAMANAKA, S. 2020. Pluripotent Stem Cell-Based Cell Therapy—Promise and Challenges. *Cell Stem Cell,* 27**,** 523-531.

YOON, J.-K., PARK, B.-N., SHIM, W.-Y., SHIN, J. Y., LEE, G. & AHN, Y. H. 2010. In vivo tracking of 111In-labeled bone marrow mesenchymal stem cells in acute brain trauma model. *Nuclear Medicine and Biology,* 37**,** 381-388.

YU, H., CAO, B., FENG, M., ZHOU, Q., SUN, X., WU, S., JIN, S., LIU, H. & LIANHONG, J. 2010. Combinated Transplantation of Neural Stem Cells and Collagen Type I Promote Functional Recovery After Cerebral Ischemia in Rats. *The Anatomical Record: Advances in Integrative Anatomy and Evolutionary Biology,* 293**,** 911-917.

YUE, B. 2014. Biology of the extracellular matrix: an overview. *J Glaucoma,* 23**,** S20-3.

ZANDER, N. E., PIEHLER, T., BANTON, R. & BOGGS, M. 2016. The effect of explosive blast loading on human neuroblastoma cells. *Analytical Biochemistry,* 504**,** 4-6.

ZANDER, N. E., PIEHLER, T., BOGGS, M. E., BANTON, R. & BENJAMIN, R. 2015. In vitro studies of primary explosive blast loading on neurons. *Journal of Neuroscience Research,* 93**,** 1353-1363.

ZANIER, E. R., MONTINARO, M., VIGANO, M., VILLA, P., FUMAGALLI, S., PISCHIUTTA, F., LONGHI, L., LEONI, M. L., REBULLA, P., STOCCHETTI, N., LAZZARI, L. & DE SIMONI, M.-G. 2011. Human umbilical cord blood mesenchymal stem cells protect mice brain after trauma*. *Critical Care Medicine,* 39.

ZHANG, B., HU, B., NAKAUMA, M., FUNAMI, T., NISHINARI, K., DRAGET, K. I., PHILLIPS, G. O. & FANG, Y. 2019. Modulation of calcium-induced gelation of pectin by oligoguluronate as compared to alginate. *Food Research International,* 116**,** 232-240.

ZHANG, J., WANG, X., LI, J., HUANG, R., YU, X., DONG, C., LIU, P., ZHANG, F., HU, J., QI, Y., ZHANG, J., LI, Q. & YAN, B. 2016. The Preclinical Research Progress of Stem Cells Therapy in Parkinson's Disease. 2016**,** 1-6.

ZHANG, K., SHI, Z., ZHOU, J., XING, Q., MA, S., LI, Q., ZHANG, Y., YAO, M., WANG, X., LI, Q., LI, J. & GUAN, F. 2018. Potential application of an injectable hydrogel scaffold loaded with mesenchymal stem cells for treating traumatic brain injury. *Journal of Materials Chemistry B,* 6**,** 2982-2992.

ZHANG, L., YAN, X., AN, L., WANG, M., XU, X., MA, Z., NIE, M., DU, F., ZHANG, J. & YU, S. 2022. Novel pneumatically assisted atomization device for living cell delivery: application of sprayed mesenchymal stem cells for skin regeneration. *Bio-Design and Manufacturing,* 5**,** 220-232.

ZHANG, R., LIU, Y., YAN, K., CHEN, L., CHEN, X.-R., LI, P., CHEN, F.-F. & JIANG, X.-D. 2013. Anti-inflammatory and immunomodulatory mechanisms of mesenchymal stem cell transplantation in experimental traumatic brain injury. *Journal of Neuroinflammation,* 10**,** 106.

ZHANG, S., HULVER, M. W., MCMILLAN, R. P., CLINE, M. A. & GILBERT, E. R. 2014. The pivotal role of pyruvate dehydrogenase kinases in metabolic flexibility. *Nutrition & Metabolism,* 11**,** 10.

ZHANG, S., LACHANCE, B. B., MOIZ, B. & JIA, X. 2020. Optimizing Stem Cell Therapy after Ischemic Brain Injury. *Journal of Stroke,* 22**,** 286-305.

ZHANG, X., MEDOW, J. E., ISKANDAR, B. J., WANG, F., SHOKOUEINEJAD, M., KOUEIK, J. & WEBSTER, J. G. 2017. Invasive and noninvasive means of measuring intracranial pressure: a review. *Physiological Measurement,* 38**,** R143-R182.

ZHANG, Y., CHOPP, M., MENG, Y., KATAKOWSKI, M., XIN, H., MAHMOOD, A. & XIONG, Y. 2015. Effect of exosomes derived from multipluripotent mesenchymal stromal cells on functional recovery and neurovascular plasticity in rats after traumatic brain injury. *Journal of Neurosurgery,* 122**,** 856-867.

ZHAO, L. L., JUNJIE; ZHANG, LIANG; WANG, YU; WANG, JIEXIN; GU, BIN; CHEN, JIANFENG; HAO, TONG; WANG, CHANGYONG; WEN, NING 2016. Preparation and characterization of calcium phosphate/pectin scaffolds for bone tissue engineering. *RSC Advances,* 6**,** 62071-62082.

ZHAO, W., LI, X., LIU, X., ZHANG, N. & WEN, X. 2014. Effects of substrate stiffness on adipogenic and osteogenic differentiation of human mesenchymal stem cells. *Materials Science and Engineering: C,* 40**,** 316-323.

ZHAO, X., FANG, J., LI, S., GAUR, U., XING, X., WANG, H. & ZHENG, W. 2019. Artemisinin Attenuated Hydrogen Peroxide (H2O2)-Induced Oxidative Injury in SH-SY5Y and Hippocampal Neurons via the Activation of AMPK Pathway. *International Journal of Molecular Sciences,* 20**,** 2680.

ZHENG, W.-X., WANG, F., CAO, X.-L., PAN, H.-Y., LIU, X.-Y., HU, X.-M. & SUN, Y.-Y. 2014. Baicalin protects PC-12 cells from oxidative stress induced by hydrogen peroxide via anti-apoptotic effects. *Brain Injury,* 28**,** 227-234.

ZHONG, J., CHAN, A., MORAD, L., KORNBLUM, H. I., GUOPING, F. & CARMICHAEL, S. T. 2010. Hydrogel Matrix to Support Stem Cell Survival After Brain Transplantation in Stroke. *Neurorehabilitation and Neural Repair,* 24**,** 636-644.

ZIMMERLIN, L., RUBIN, J. P., PFEIFER, M. E., MOORE, L. R., DONNENBERG, V. S. & DONNENBERG, A. D. 2013. Human adipose stromal vascular cell delivery in a fibrin spray. *Cytotherapy,* 15**,** 102-108.